MODELLING GLACIER AND RUNOFF CHANGES IN THE ALPS & HIMALAYA

James Stephen Douglas

Department of Geography

University of Sheffield

June 2018

Thesis submitted for the degree of Doctor of Philosophy

ABSTRACT

Glacier melt within alpine catchments provides a vital component of runoff that constitutes an important water resource for downstream populations. With future climate changes, it is expected that glacier volume change will be considerable in the coming decades, with associated implications for runoff. Estimation of future changes in glacier volume and catchment runoff is therefore essential for understanding future water resource implications in alpine environments.

This thesis focuses on glacier volume and runoff changes predicted using the statistical model GERM (Glacier Evolution and Runoff Model; Huss et al., 2008a) and has three novel aims. Firstly, to provide more robust assessments of the modelling uncertainty associated with predicted glacier and runoff changes from alpine catchments than previous studies, by challenging the model to reproduce historic changes in glacier volume and evolution over 120 year periods, and comparing predicted and measured runoff. Secondly, to use this assessment of uncertainty to contextualise and understand the precision of future (to 2100 AD) runoff projections for alpine catchments under a wide range of possible climate changes scenarios. Thirdly, to develop the model so that it can be applied to a debris-covered, downwasting glacier in the Himalaya. Two further novel aspects of this thesis are the development of a more systematic and robust calibration procedure for GERM, and the application of climate data downscaling techniques that are more sophisticated than have hitherto been applied in glacio-hydrological studies.

To achieve aim 1, GERM was used to forward model glacier volume and runoff for the Griesgletscher and Rhonegletscher catchments in the European Alps from 1884-2004. As a statistical model that requires catchment-specific calibration, GERM was first calibrated to each catchment using contemporary glacier volume and catchment runoff measurements (as is standard when using the model for future projections). Digital elevation models were then used to obtain the initial glacier geometry required to begin each model run, and each completed model run was subsequently used to estimate the accumulated uncertainty associated with the predicted glacier volume/runoff changes by comparing modelled with observed glacier volume/runoff change at the end of the simulation.

To achieve aim 2, future model runs (2010-2100) were conducted for the same two catchments and the glacier volume/runoff uncertainty calculated from model performance in the past (aim 1) applied to future projections. Future simulations were driven by a wide-range of climate inputs to allow quantification of the uncertainty associated with climate scenarios/models. The combination of these two sources of uncertainty (GERM and climate) provides future

projections with greater awareness and better quantification of uncertainties than previous studies.

Finally, to achieve aim 3, GERM was applied to the debris-covered Khumbu Glacier by adjusting the mass redistribution process of GERM (Δh-parameterisation) to reflect the downwasting behaviour of the debris-covered glacier tongue, based on observed thinning rates at Khumbu Glacier. Additionally, to account for the insulating effect of debris on ice, the modelled melt rate was reduced in proportion to debris thickness on a spatially distributed basis (i.e. debris thickness was not uniform) using observations of reduced melt at glaciers close to Khumbu.

Improvements to the calibration procedure used when applying GERM were made and applied throughout this thesis by developing an automated calibration which systematically adjusts the parameters, calculates a combined goodness-of-fit statistic that allows comparison to observations of both glacier volume and runoff, and selects the optimal parameter set. Improved downscaling methods were also used and applied to all future volume and runoff change projections made during this thesis. Specifically, state-of-the-art General Circulation Model simulations were dynamically-statistically downscaled using Regional Climate Model simulations and quantile mapping, and were used to drive future model runs at all three sites. Finally, the novel adjustments made to the mass redistribution process and the inclusion of reduced melt beneath debris indicate that GERM can now be applied to debris-covered glaciers. A recommendation for future research is that GERM is further tested on additional debris-covered glaciers and applied to additional catchments in the larger Everest region.

The results of the uncertainty analyses (aim 1) show that glacio-hydrological model uncertainty amounts to annual runoff errors of ±0.04 $10^6 m^3 yr^{-1}$ (±0.15 % yr^{-1}), and glacier volume errors of ±0.16 % yr^{-1}, over time periods of 120 years at Griesgletscher. At Rhonegletscher, the uncertainty assessment resulted in annual runoff errors of ±0.16 $10^6 m^3 yr^{-1}$ (±0.2 % yr^{-1}) and glacier volume errors of ±0.13 % yr^{-1}, over time periods of 120 years. Nonetheless, the key finding is that the main sources of future uncertainty relate to emissions scenarios and GCM-RCM (General Circulation Model - Regional Climate Model), combinations which lead to variations in predicted future runoff in 2100 of ±36 % at Griesgletscher and ±20 % at Rhonegletscher. The results of the future simulations (aims 2 and 3) indicate that all three glaciers that form the focus of this thesis will lose considerable volume. Specifically, by 2100, Griesgletscher is likely to have become an ice-free catchment (87-100 % ice loss); Rhonegletscher will have lost 70-90 % of ice; and Khumbu Glacier will have lost 61-92 % of ice. The results further show that mass losses will cause an initial increase in annual river discharge followed by a decline in discharge levels, such that annual discharge by 2100 will be considerably lower than present, with peak discharge at Griesgletscher occurring in 2020, at Rhonegletscher in 2075, and at Khumbu Glacier in 2045.

DEDICATION

Dedicated to my Grandma

ACKNOWLEDGEMENTS

Throughout the course of my PhD, I have been fortunate to receive help, support, inspiration, and motivation from many individuals, without whom the enjoyment and success of this PhD would not have been assured.

Firstly, I would like to express my gratitude to my supervisors, Julie Jones and Darrel Swift, whose guidance and insight throughout has been essential to fulfilling the aims of this project. In particular, Julie's assistance (and patience!) when I was trying to understand and programme bias-correction methodologies was invaluable; and Darrel's in-depth knowledge of glaciology and awareness of the 'bigger picture' has been crucial to shaping this thesis.

The successful completion of this project also owes much to Matthias Huss who, during an intensely hard-working visit to Fribourg, taught me how to use the Glacier Evolution and Runoff Model and has continued to provide enthusiasm and expertise through my PhD. Ann Rowan is also thanked for bringing me up-to-speed and providing many interesting discussions on debris-covered glaciers, as are Duncan Quincey and David Rounce for use of figures and data. For help with climate data and downscaling, Franco Salerno, Martin Widmann, Sven Kotlarski, and Nicolas Guyennon all provided valuable assistance. Eleanor Stillman is also thanked for her assistance and statistics-expertise when devising the calibration methodology.

Fellow A-floor PhD students, I would like to thank all those who have provided help, distraction, pub visits, and coffee breaks, over the past four years: Kate (also thanked for proof-reading), Tom Parker, Amy, Ernesto (also thanked for downscaling help), Hannah, Tom Wilkes, Tom Pering, Johnny, Rich, Jez, Ingun, Vaibhav, and Rob. Also from the department, the members of the 5-a-side football team provided many good memories and a welcome distraction. Thanks to all those in the department for all the help over the last decade or so, particularly those in the ICERS research group, for interesting seminars, discussions, and feedback. International friends, mostly the UNIS Glaciology group and those at Fribourg, thanks for sharing some great memories in the Arctic, Switzerland, and Himalaya. The funding for this project was provided by the E-Futures DTC (EPSRC).

Finally, a huge thank you to my parents, brother and sister, and to George for your love, support, proof-reading skills, and constant reassurance, particularly during the final weeks of writing when the end seemed a very long way away!

TABLE OF CONTENTS

LIST OF FIGURES

LIST OF TABLES

LIST OF ACRONYMS

AAR	Accumulation Area Ratio
ASTER	Advanced Spaceborne Thermal Emission and Reflection Radiometer
BC	Bias Correction
CDF	Cumulative Distribution Function
CMIP5	Coupled Model Intercomparison Project Phase 5
CORDEX	Coordinated Regional climate Downscaling Experiment
DDF	Degree day factor
DEM	Digital Elevation Model
DOY	Day Of Year
EB	Energy Balance
ELA	Equilibrium Line Altitude
ENSO	El Nino Southern Oscillation
ESGF	Earth System Grid Federation
ET	Evapotranspiration
ETI	Enhanced Temperature Index
GCM	General Circulation Model
GERM	Glacier Evolution and Runoff Model
GIS	Geographic Information System
GPR	Ground Penetrating Radar
GPS	Global Positioning System
HBV	Hydrologiska Byråns Vattenbalansavdelning
HKH	Hindu Kush-Himalaya
HTI	Hock Temperature Index
LW	Longwave
MF	Melt Factor
NAO	North Atlantic Oscillation
NAST	Nepal Academy of Science and Technology
NSE	Nash Sutcliffe Efficiency
PET	Potential Evapotranspiration
RCM	Regional Climate Model
RCP	Representative Climate Pathway
RGI	Randolph Glacier Inventory
RMSE	Root Mean Square Error
SEB	Simplified Energy Balance
SHARE	Stations at High Altitude for Research on the Environment
SRM	Snowmelt Runoff Model
SRTM	Shuttle Radar Topography Mission
SW	Shortwave
TAS	Surface Temperature
TI	Temperature Index
TOPKAPI	Topographic Kinematic Approximation and Integration Model
UBCWM	University of British Columbia Watershed Model
VE	Volume Change Error
WGMS	World Glacier Monitoring Service

1. INTRODUCTION.

Future changes in runoff volume from alpine catchments due to climate-driven glacier retreat could have considerable impacts on downstream water resources. This thesis focuses on the simulation of both glacier volume and runoff changes in high-alpine catchments using the statistical model GERM (Glacier Evolution and Runoff Model; Huss et al., 2008a). This chapter introduces the wider context of this work (Section 1.1) and reviews relevant glacio-hydrological modelling approaches (Section 1.2), including GERM. Section 1.3 then introduces the current state of knowledge concerning glaciated catchment responses to past and likely future climate changes, and, finally, Sections 1.5 and 1.6 sets out the aims, objectives and structure of this thesis.

1.1. Research Context.

Mountainous regions have been referred to as water towers that provide water resources to the surrounding region (EEA, 2009; Vivroli et al., 2007). Mountains form barriers to the movement of air, promoting uplift and therefore cooling and condensation of water vapour held within air masses, leading to cloud formation and precipitation. Consequently, the level of precipitation in mountain regions is consistently higher than neighbouring low-level regions (Viviroli & Messerli, 2003; Viviroli et al., 2011). Further, the high topography of mountainous areas encourages precipitation to fall as snow and provides conditions suitable for the year-round persistence of snow and its transformation into glacier ice. These glaciers are important freshwater reservoirs due to the relatively long residence time of precipitation within the glacier system (20 to 100 years; Pidwirny, 2006) relative to that in the atmosphere or in rivers (Oki, 2006). As a result, mountain glaciers represent one of the most important freshwater resources on Earth.

The storage of water as snow and ice means highly glacierised catchments exhibit a unique seasonal pattern of discharge characterised by minimal winter discharge contrasted with very high spring and summer discharges due to melt of snow and ice. Further, ice melt in summer provides a “compensation effect” during periods of low or zero precipitation (Zhang et al., 2016) that in many situations provides the only source of water to the drier lowlands (Singh et al., 2008; Bradley et al., 2006; Bradley et al., 2009). However, this resource is under threat because temperatures are expected to warm more rapidly at high altitudes than at low altitudes (Bradley et al., 2004; Bradley et al., 2006; Bradley et al., 2009; Diaz et al., 2006; Shrestha et al., 2000; Immerzeel, 2008), with observations showing significant warming in recent decades (e.g. Auer et al., 2007; Xu et al., 2009), implying reductions in solid precipitation and glacier volume. Indeed, glaciers have shown significant recent change, with the vast majority of global mountain

glaciers exhibiting recent mass loss (WGMS, 2015; Gardner et al., 2013), and global glacier volume is expected by 2100 to decrease by between 15-55 % (Representative Concentration Pathway- RCP 2.6) and 35-85 % (RCP 8.5) (IPCC5 WGII, 2014). Glacier wastage at present rates implies that, following a temporary increase in discharge that reflects increased initial melting of ice stores, the annual discharge regime will change from ice melt to snowmelt domination (Horton et al., 2006) and the compensation effect provided by the ice cover will diminish or disappear completely (Zhang et al., 2016).

The wider impacts of glacier loss in terms of changes to annual and seasonal discharge are predicted to be extensive. For example, alpine catchments (defined as high mountain, i.e. not specific to the European Alps) are essential sources of water for large regions (Arnell, 1999) and provide a range of essential services including drinking water (Bradley et al., 2006; Barnett et al., 2005; Bookhagen & Burbank, 2010), agriculture (Piao et al., 2010; Bradley et al., 2006; Immerzeel et al., 2010; Zierl & Bugmann, 2005), tourism (Koenig & Abegg, 1997; Elsasser & Bürki, 2002; Wang et al., 2010), hydropower (Sternberg, 2008; Sternberg, 2010; Finger et al., 2012; Schaefli et al., 2007; Vergara et al., 2007), and ecosystem support (Cannone et al., 2008; Wohlfarth et al., 2008). Another impact of the melting of mountain glaciers is their potential contribution to sea-level rise because the small size of mountain glaciers (in comparison to ice sheets and ice caps) means their climatic response is faster (Pidwirny, 2006). The potential contribution of mountain glaciers to sea level rise is estimated to be 0.59 m sea level equivalent (Radić & Hock, 2011).

Mitigation and adaptation strategies that are required to address the runoff implications of climate driven high-mountain catchment changes require robust methods of future runoff prediction, meaning models must accurately predict many independent runoff components, including precipitation, snow melt, and glacier melt. Of these components, precipitation and snow melt respond to temperature changes relatively simply and can largely be accounted for using climate model outputs (Chen et al., 2017), particularly in relation to the seasonal and annual changes that are of concern to future mitigation studies. However, glacier change, which is anticipated to alter considerably both the seasonal runoff pattern and the annual total runoff volume, cannot be derived directly from climate model outputs due to the long residence time of precipitation within the glacier system and the complexities of glacier response to warming climates (Huss et al., 2017). Recent work in this field has therefore focused on glacier runoff modelling, and has responded to the challenge posed by the remote nature of alpine catchments and the corresponding lack of abundant *in-situ* data by developing simple non-physical glacier evolution models, such as GERM, that require minimal input or calibration data and are easily "portable" between glaciated regions. These non-physical models are based upon statistical

correlations that govern the glacier response to climatic drivers, for example the relationship between temperature and melt, and attempt to calculate glacier mass balance and represent the dynamics of ice motion without explicitly representing the complexities of glacier dynamics.

It is within the context of requiring robust glacier melt projections to support mitigation and adaptation strategies that this thesis aims to make its key contribution to this field. Specifically, this thesis seeks to contribute to the understanding of how reliably models that have minimal data demands, such as GERM, can be applied successfully in catchments in different regions and how the full uncertainty of their catchment runoff projections can be accounted for and understood. In doing so, it is necessary that, for future projections, the uncertainties introduced by different climate models and emissions scenarios, are also included in such estimates.

1.2. Review of Glacio-Hydrological Modelling of Mountain Glaciers.

Glacio-hydrological models that seek to project future glacier and runoff evolution over 90-100 years must: (1) estimate (ideally daily) ablation and accumulation totals for snow and ice sources for each individual year; (2) account for differences in the timing of runoff from these sources due to their routing through the catchment and particularly the glacier system; and (3) redistribute the net glacier balance (the sum of all ablation and accumulation estimates) at the end of each hydrological year so that the glacier geometry evolves appropriately from year-to-year. In this review, the mechanisms of glacier melt are reviewed and specific melt models are described. Following this, accumulation, retreat, and hydrological routing processes are reviewed, with specific reference to the GERM model used in this thesis.

1.2.1. Glacier Ablation.

1.2.1.1. Mechanisms of Glacier Melt.

Numerical simulation of glacier melt requires representation of the energy balance at the interface between the glacier and atmosphere, which determines how much energy is available for ice and snow melt. Hock (2005) provides the most thorough review of glacier melt processes and should be considered as reference throughout this section. The key controls over the surface energy balance are the meteorological conditions and the physical properties of the ice surface, which interact creating feedbacks between the atmosphere and glacier surface. The energy available for melting, Q_M, can be defined as:

$$Q_M = Q_N + Q_H + Q_L + Q_P + Q_G \quad [1.1]$$

where Q_N is net radiation, Q_H is the sensible heat flux, Q_L is the latent heat flux, Q_P is the energy from rain, and Q_G is the ground heat flux, energy from heat conduction in the snow.

Net radiation is a function of:

$$Q_N = G + R + L\downarrow + L\uparrow \quad [1.2]$$

where G is shortwave radiation, R is reflected shortwave radiation, which is a function of albedo, $L\downarrow$ is incoming longwave radiation and $L\uparrow$ is outgoing longwave radiation. The typical albedos of ice, firn and snow range from 0.2-0.4, 0.4-0.6, and 0.7-0.9, respectively (Cuffey & Paterson, 2010), meaning that ice absorbs more shortwave radiation than firn and snow, providing more energy available for melt. Meteorological conditions, specifically air temperature and humidity, determine the amount of incoming longwave radiation emitted by the atmosphere. Finally, the temperature of the glacier surface determines the amount of outgoing longwave radiation emitted.

Sensible heat flux is the transfer of heat energy between the ice/snow surface and the atmosphere, and is a function of both wind speed and the temperature difference between the glacier surface and the air over the surface. Because the surface temperature of glaciers cannot exceed 0°C, temperature inversions are common with a thin layer of cool air surrounding the ice. This stable atmospheric stratification reduces the energy contribution of sensible heat. However, high wind-speeds can create turbulence thus removing the cold air at the interface between the glacier and the air, providing warm air that can contribute to melt.

Latent heat flux comprises the energy consumed or released during the phase change of water to or from vapour and ice. This varies according to the wind speed and vapour pressure. For example, air near saturation point (high vapour pressure) will condense when the air is cooled by the glacier surface, resulting in condensation on the glacier surface contributing energy for melting. Conversely, if the air vapour pressure is lower than that of the surface, evaporation or sublimation can occur, contributing to ablation but significantly reducing the energy available for melting (e.g. Francou et al., 2003).

Wet precipitation provides energy to the glacier surface depending on the rain intensity and rain temperature, and directly contributes only a small proportion of the energy available for melt. However, indirectly, rain may reduce the albedo of snow by increasing the water content, thus increasing the absorption of incoming shortwave radiation causing more melt (Hock, 2005).

The relative importance of these components, in terms of providing energy for melt, varies with location and altitude. However, the main contributor to energy for melt is incoming shortwave radiation during the day, although incoming longwave radiation can be dominant during cloudy

periods and at night (Ohmura, 2001; Pellicciotti et al., 2005). Net radiation is a particularly important melt energy contributor at high altitudes due to the enhanced radiation and cooler air. The turbulent heat fluxes are particularly important in maritime regions providing over 50 % of energy, and are important over sub-daily periods (Hock, 2005). Additionally, latent heat flux is important at high altitude where sublimation can be the main source of ablation (Francou et al., 2003). If the sum of the aforementioned components of the surface energy balance is positive, this energy will be used to heat up the ice/snow surface, and if the energy is enough to heat it to 0°C, it will then melt.

1.2.1.2. A Review of the Types of Melt Model.

There are several different approaches to the representation of the surface energy balance of ice in mass balance melt models. The simplest model is the classical temperature index (TI) approach whereas the most complex is the Energy Balance (EB) model, with a continuum of models of varying complexity in-between. The physical basis and data requirements of each type of model vary significantly. Here, the key different model types will be described in order of increasing complexity, with examples of their implementation in the Swiss Alps and Himalaya included.

1.2.1.2.1. Temperature-Index (TI) Models.

All variations of the classical-TI model assume a relationship between temperature and many components of the glacier surface energy balance, and therefore melt. Specifically, the turbulent heat fluxes, rain heat flux (if the temperature is positive during precipitation events), and incoming longwave radiation are highly temperature dependent, and global radiation affects temperature (Ohmura, 2001). The crucial relationship here is between temperature and incoming radiation which is the most dominant energy source for melt, and is highly correlated with temperature. For example, Ohmura (2001) found that, in clear-sky conditions, up to 60 % of longwave radiation is emitted by the 100 m of atmosphere closest to the surface, and 90 % from the first 1 km of atmosphere. With cloudy skies, the lowest 1 km of atmosphere emits between 70-90 % of longwave radiation received at the surface, with air temperature observed at the surface being the most influential factor (Ohmura, 2001; Hock, 2003). Although temperature index melt models are sometimes considered to have limited physical basis, this strong correlation between air temperature and several important components of the energy balance, is sufficient for most practical purposes (Ohmura, 2001). This relationship is the fundamental component of all the models reviewed in this chapter, with the exception of the Simplified EB Model and EB Model.

The classical-TI model calculates melt, *M*, as:

$$M = DDF_{ice/snow} \cdot T \qquad : T > 0°C$$
$$M = 0 \qquad : T < 0°C \tag{1.3}$$

where *DDF* is the degree day factor in mm d^{-1} K^{-1} for ice or snow, and *T* is the daily mean air temperature (°C). When below 0°C, melt equals 0. DDF varies between snow and ice due to the higher albedo of snow resulting in differing melt rates.

Since temperature is relatively easy to measure, extrapolate, and forecast (Begert et al., 2005), TI models have been widely used to estimate snow and ice melt in operational hydrological models (Hock, 2005), for example the HBV model (Hydrologiska Byråns Vattenbalansavdelning; Bergstroem, 1976), the SRM (Snowmelt Runoff Model; Martinec & Rango, 1986), the UBCWM (University of British Columbia Watershed Model; Quick & Pipes, 1977) and the HyMet model (Tangborn, 1984). TI models have also been used to provide the mass balance forcing of dynamical ice models (e.g. Johannesson, 1997; Oerlemans et al., 1998; Schäfer et al., 2015). Additionally, a common application of TI models is glacier melt simulation over large regions, where their simplicity is beneficial both in terms of computational efficiency and limited data requirements. For example, Huss and Hock (2015) use the TI approach to calculate ablation in their global-scale mass balance analysis.

In terms of glacio-hydrological models, the TI approach has been widely used (e.g. Horton et al., 2006; Schaefli and Huss, 2011; Schaefli et al., 2005; Uhlmann et al., 2013a, 2013b). For example, the study of Horton et al. (2006) applied a precipitation-runoff model (GSM-SOCONT) to 11 glaciated catchments in Switzerland, calculating glacier melt using the classical-TI approach and calculating changes in glacier surface using the Accumulation Area Ratio (AAR; see Section 1.2.3 for details).

Despite widespread application, the classical-TI model has considerable limitations. Firstly, the use of spatially constant DDFs in the classical-TI model means the model cannot adequately account for spatial variations in melt caused by topographic shading (Hock, 1999). Secondly, the relationship between air temperature and melt only correlates well over long periods of several days to weeks (Hock, 1999; Ohmura, 2001). As a result, DDF calculated on an hourly time-scale vary significantly due to diurnal radiation changes suggesting that classical-TI models are inadequate for hourly resolution modelling (Hock, 2005). Moreover, DDFs vary seasonally due to changes in clear-sky direct radiation and snow metamorphism causing decreased albedo (Pellicciotti et al., 2005). Additionally, assuming that melt cannot occur below 0°C, and always occurs above 0°C, is a simplification of reality. Specifically, penetration of incoming short-wave radiation to depths below the surface can provide the energy for subsurface melt despite the

surface energy balance ensuring the surface remains below 0°C (Liston et al., 1999). Equally, a cold ice or snow surface requires considerable energy input for heating to melt point before melt can occur (Irvine-Fynn, 2008). However, such factors are rarely accounted for in glacio-hydrological studies because in-situ data on the surface energy balance are required, rarely the case over long periods or large spatial scales. Despite shortcomings, the classical-TI model adequately simulates glacier melt as long as temperature is adjusted accordingly for elevation (Hock, 2003; Braithwaite & Zhang, 2000).

1.2.1.2.2. Hock Temperature-Index (HTI) Model.

Because of the aforementioned issues with the classical-TI model, attempts have been made to provide a stronger physical basis and to represent sub-daily melt and spatial variability. The HTI model proposed in Hock (1999) includes a term for clear-sky potential solar radiation that accounts for atmospheric conditions, slope, and topographic shading:

$$M = (MF + a_{snow/ice} \,.\, I) \,.\, T \tag{1.4}$$

where *MF* is the melt factor, *a* is the radiation coefficient to differentiate between snow and ice, and *I* is the potential clear sky incoming solar radiation. *I* is calculated as a function of the solar constant, atmospheric transmission, solar incidence angle, and topographic shading, therefore allowing spatial variation in the receipt of energy. These modifications improve the diurnal and spatial melt rate variability (e.g. Hock, 1999; Schneeberger et al., 2001) yet do not increase the data requirements since clear-sky potential radiation, sun angle, and azimuth can be calculated using only a Digital Elevation Model (DEM).

Despite a substantial increase in performance over the classical-TI model, there remain limitations in the HTI model. For example, the combination of *MF + a* prevents separation of the degree day factor from the radiation factor and dictates that the differing albedo between ice, firn and snow is crudely accounted for by calibrating a_{snow} and a_{ice} separately. Additionally, Pellicciotti et al. (2005) noted that the multiplication of *I* and *T* contradicts the energy balance equation (Eq. 1.1) in which the components remain independent (Greuell & Genthon 2004; Irvine-Fynn, 2008). Konya et al. (2004) demonstrated that multiplying *I* and *T* leads to overestimation of melt at peak daily temperatures when simulations at hourly resolution are conducted. Despite these limitations, the HTI models have been shown to perform well in a range of catchments. For example, Hock (1999) compared the performance to an EB model finding only slightly reduced accuracy in terms of catchment discharge simulation.

The combination of comparable performance to EB models and very limited data requirements mean that the HTI model is perhaps the mostly widely applied ablation model in glacio-

hydrological studies (e.g. Scandinavia: Schneeberger et al., 2001; Alps: Gabbi et al., 2012; Huss and Farinotti, 2012; Huss et al., 2008a; Huss et al., 2008b). For example, the model used throughout this thesis, GERM, was devised by Huss et al. (2008a) who created a fully distributed variant of the HTI model, capable of simulating melt at hourly or daily resolution and a spatial resolution of 25 m. GERM also incorporates all components of the water balance and glacier volume changes, without additional data requirements, and will be fully described in Chapter 2. The limited data requirements of GERM mean that the model is very portable and application of GERM is widespread in the Swiss Alps. For example, Farinotti et al. (2012) used GERM to simulate the evolution of glacier changes and runoff in nine Swiss catchments from 2010-2100. Similarly, Gabbi et al. (2012) applied GERM to the Mauvoisin catchment in Switzerland. Huss et al. (2010) used GERM to reconstruct the mass balance of 30 glaciers in the Swiss Alps, building on the work of Huss et al. (2008b) and Huss et al. (2009a), examples of using glacio-runoff models to reconstruct glacio-hydrological changes, as well as simulate future changes.

1.2.1.2.3. Enhanced Temperature-Index (ETI) Model.

The ETI model, developed in Pellicciotti et al. (2005), includes the shortwave radiation balance and accounts for cloud cover, therefore further extending the physical basis of the HTI model:

$$M = TF.T + SRF\,(1-\alpha)\,I_c \tag{1.5}$$

where *TF* is the temperature factor, *SRF* the shortwave radiation factor, α is the surface albedo and I_c is the incoming shortwave radiation corrected for cloudiness. I_c is estimated as the product of clear-sky incoming shortwave radiation with a factor to reduce radiation to account for cloudiness. The advantage of this approach is that melt due to temperature and turbulent fluxes and melt due to short-wave radiation are separated, more accurately reproducing the surface energy balance. The inclusion of cloud cover in the ETI model was further developed in Pellicciotti et al. (2011) who proposed a parameterisation based on the relationship between cloud cover and the diurnal temperature range, showing improvements over the HTI model in hourly resolution simulation of melt. However, the inclusion of cloud cover in future simulations is uncertain due to a lack of understanding of cloud processes over mountains (Barry, 1992) and the limited ability of climate models to estimate future changes in cloud cover (e.g. Wild and Schmucki, 2011). Therefore, local calibration of the relationship between cloud cover and temperature enhances performance. Thus, although the ETI model can be applied with the same data as the TI and HTI models, the ETI model is ideally suited to short-term studies with detailed in-situ datasets (e.g. cloud cover, net radiation etc.).

Examples of studies applying the ETI model have been limited to short-term or point scale modelling (e.g. Carenzo et al., 2009; Pellicciotti et al., 2005) with continuous studies relatively

limited because the ETI model has only recently been developed for application in continuous mass balance modelling (e.g. Carenzo et al., 2009; Pellicciotti et al., 2005). An example of the implementation of the ETI model in the Alps is Finger et al. (2012), who modified the TOPKAPI (Topographic Kinematic Approximation and Integration Model; Liu and Todini, 2002) to include the HTI method of calculating ablation, applying their model to the Vispa catchment in Switzerland.

1.2.1.2.4. Simplified Energy Balance (SEB) Model.

Oerlemans (2001) developed the SEB model as a simplified formulation of the energy balance equation (1), and calculates the energy available for melt, Q_M, as:

$$Q_M = (1 - \alpha).\, I + k_0 + k_1 T \tag{1.6}$$

where I is the global incoming shortwave radiation, $k_0+k_1.T$ is the sum of the radiation balance and the turbulent heat exchange linearised around the melting point. Melt rates are then obtained by dividing Q_M by the latent heat of fusion, L_f and density of water, $\rho_{w,}$:

$$M = \frac{Q_M}{\rho_w L_f} \tag{1.7}$$

This approach is similar to the ETI model; however, the melt energy is calculated and converted to melt rates by the latent heat of fusion, rather than using a temperature threshold. An advantage of this is the reduced sensitivity of melt to temperature; however, this approach can lead to an oversensitivity of melt to incoming radiation. Examples of this approach in existing studies are relatively limited with examples including Huss et al. (2014), who applied the SEB model in an assessment of glacier runoff uncertainty at Findelgletscher in the Swiss Alps, and Machguth et al. (2012; 2009) who used the SEB approach to reconstruct mass balance in the Swiss Alps from 1970-1985.

1.2.1.2.5. Energy Balance (EB) Model.

The most advanced and physically based melt models include all components of the surface energy balance (Eq. 1.1) to calculate the energy available for melt, and then calculate melt as described in Eq. 1.6. Although the EB model explicitly represents the physical processes of the glacier surface, considerable meteorological measurements are required including temperature, humidity, wind speed, short-wave radiation, reflected short-wave radiation, and cloud cover. Variables such as wind speed and humidity, which are highly temporally and spatially variable and form complex fields, are typically assumed to be spatially constant (e.g. Gabbi et al., 2014). Moreover, calculation of turbulent heat fluxes is problematic since surface roughness and wind fields are difficult to measure over large areas so must be parameterised. For example, the bulk

aerodynamic method (Munro, 1989) uses air temperature, wind speed and humidity to estimate turbulent heat fluxes and is applied in several energy balance models (e.g. Carenzo, 2012; Pellicciotti et al., 2005). However, for application in this thesis, where a model that can be applied to data-poor catchments is essential, the EB model is inappropriate.

1.2.1.3. Summary of the Types of Melt Model.

Clearly, as the physical basis of glacier melt models increases, the complexity and data requirements of the models increases. Thus, the choice of a glacier melt model is often dictated by data availability as well as the aims of the study. The ability of the simplest TI models to reproduce melt using only the correlation between temperature and melt is encouraging and sufficient for many applications, and the addition of a radiation term (HTI and ETI models) offers performance comparable with EB models. The increasing complexity does not necessarily improve performance unless high spatial and temporal resolution is essential to the study. For this thesis, it is essential that the model can be applied in a data-poor catchment, which rules out the use of the EB model. Therefore, GERM, which is based on the HTI approach, is well-proven, shows comparable performance to the EB model, and requires minimal data input, is ideal for this thesis in that it can be applied over long time-scales (for long-term validation) and in data-poor catchments.

1.2.2. Modelling Glacier Accumulation.

Modelling of snow accumulation on a glacier's surface is crucial for accurate mass balance modelling. For example, the timing and spatial distribution of precipitation in the catchment will affect when ice is exposed in spring, when the ice melt season ends, and the contribution of snow redistribution to accumulation (e.g. avalanches; Sailer et al., 2008). However, precipitation in mountain regions is complicated by avalanche redistribution of snow and wind-induced redistribution and preferential deposition (Lehning et al., 2008), which can strongly contribute to glacier accumulation (e.g. Benn and Lehmkuhl, 2000). Therefore, accounting for the redistribution of snow is important in glacio-hydrological modelling.

Despite the large range of methods to calculate ice and snow ablation (Section 1.2.1), accumulation is typically simulated using the same principle in all mass balance models, where accumulation is calculated based on the air temperature with a threshold defining the transition from solid to liquid precipitation. Full details of accumulation calculations are provided in Chapter 2. To account for the redistribution of snow through avalanching and wind-fields, glacio-hydrological models typically either neglect to include these (e.g. Machguth et al., 2009; Paul and Kotlarski, 2010; Salzmann et al., 2012) or use simple empirical methods. For example, the method applied in the GERM model (Blöschl et al., 1991; Huss et al., 2008a) is representative of

many glacio-hydrological models and uses surface slope and curvature to estimate areas of preferential deposition and potential avalanche redistribution. Precipitation in the centre of the catchment is then modified spatially according the calculated redistribution and according to precipitation lapse rates. These methods are also applied in this thesis and are fully described in Section 2.2.

1.2.3. Modelling Glacier Retreat.

The changing size and volume of glaciers over time is important in glacio-hydrological studies over long time-periods. For example, substantial glacier retreat has been shown to change the seasonal pattern of discharge, with more water in early spring and reduced water in mid-to-late summer (e.g. Farinotti et al., 2012; Horton et al., 2006). Furthermore, changes to glacier hypsometry partially determine the climatic-sensitivity of the glacier in the future (Huss et al., 2008a). However, many hydrological models employ inadequate methods to simulate retreat. For example, glaciers are treated as constant surfaces throughout simulations of future changes, or simplistic linear retreat is applied (Bergstrom, 1955; Schaefli et al., 2007). Although these models may yield good agreement between calculated and observed runoff for calibration periods (e.g. Klok et al., 2001), accurate representation of future glacier retreat and awareness of uncertainties is essential to ensure the best possible simulations of future discharge.

Methods to calculate changes in glacier volume range from the simple Accumulation Area Ratio (AAR) approach to complex 3D dynamic ice flow models. The aforementioned study of Horton et al. (2006) used the AAR method to calculate changes in glacier geometry in simulations running up to 2100. The AAR is the ratio between the accumulation area and the total area glacier area. This ratio is used to calculate total glacier area based on the assumption that the multi-year mean accumulation area occupies a fixed proportion of total ice area (Benn & Evans, 2010) and that the glacier is in equilibrium with the climate, a situation rarely encountered in practice (Cuffey & Paterson, 2010). Although this method has been widely used, particularly in palaeo-climatic reconstructions (e.g. Benn and Lehmkuhl, 2000; Porter, 1975), its implementation in runoff models is limited because it is not mass-conserving, i.e. changes in glacier volume can occur with no change in discharge, and it does not allow accurate simulation of the glacier hypsometry (e.g. Huss et al., 2008a), therefore not capturing changes in the sensitivity of the glacier to climate.

In order to assess glacial changes as accurately as possible, a dynamical glacier flow model, coupled to a mass-balance model, is required. For example, the study of Jouvet et al. (2011) combines the GERM model (i.e. uses the HTI approach to calculate melt) with a 3D full-Stokes ice-flow model, representing one of the only glacio-hydrological studies to use dynamical ice

flow models. However, examples of dynamic ice flow models are rare in glacio-hydrological modelling due to their complexity, data requirements, and computational burden, which limit the efficiency of multiple calibration simulations, for example.

Thus, an alternative method of simulating realistic glacier change that is computationally efficient, yet still accounts for changes in ice volume in a mass-conserving way, was proposed by Huss et al. (2010) and incorporated into GERM. Their method, used throughout this thesis and hereafter referred to as the Δh parameterisation, takes the calculated mass change from a mass balance model and redistributes the mass over the glacier surface according to observed patterns of glacier response to climate changes at 34 glaciers in the Alps. Specifically, surface elevation changes are larger at the terminus and decrease with elevation. The study of Huss et al. (2010) compared the glacier retreat determined by the Δh parameterisation to that of a dynamic ice flow model (Jouvet et al., 2009) at Rhonegletscher, showing similar performance. A drawback of this parameterisation is that it cannot be used to model glacier advance (see Section 2.2.2.2 for details). Although this method is mass-conserving, with volume changes contributing to discharge, it is designed for typical valley glaciers in the European Alps and its validity elsewhere is unproven. Therefore, this thesis will be the first to test this parameterisation in a Himalayan catchment. Section 2.2.2.2 will describe the Δh parameterisation in detail.

1.2.4. Modelling Catchment Hydrology.

The aforementioned components of glacio-hydrological models determine the glacier mass balance, melt, and changes in the ice surface elevation. However, a key part of hydrological models concerns the delivery of water from the components of catchment runoff (e.g. snow melt, liquid precipitation) to the discharge station at the catchment boundary. Although the hydrological approach has minimal impact on the overall annual runoff, it exerts a control on the seasonal evolution of discharge and timing of peak summer discharge.

Hydrological models range from simple approaches, such as input-output black-box models (e.g. Artificial Neural Networks; see Dawson and Wilby, 2001), to semi-lumped conceptual models, to physically based fully distributed models. Physically based models are rarely applied to larger-scale glacio-hydrological studies due to their intensive data requirements (Todini, 2011), limiting their use to small basins. Instead, lumped or semi-lumped conceptual models based on the concept of linear-reservoirs are commonly applied in almost all glacio-hydrological studies. One of the first linear-reservoir models used in glacier studies was that of Baker and Oerter (1982), who divided the drainage system into three reservoirs to account for ice, snow, and firn, and a

constant used to account for groundwater storage. Their three-reservoir approach has since been applied in numerous studies (e.g. Hock and Noetzli, 1997; Verbunt et al., 2003).

The study of Huss et al. (2008a) used a fast and a slow reservoir to simulate runoff in the development of the GERM model in Valais, Switzerland. This approach was improved in Farinotti et al. (2012) by introducing surface-type (e.g. snow, ice, rock, low and high vegetation) dependent interaction between fast, slow, and interception reservoirs, with variable storage potential depending on the surface. The scheme of Farinotti et al. (2012) is used in GERM and throughout this thesis, with more details provided in Section 2.2.2.4.

1.2.5. The Selection of GERM for this Thesis.

The glacio-hydrological model GERM (Huss et al., 2008a) is used throughout this thesis. As outlined above, GERM combines the HTI ablation approach with the Δh parameterisation of glacier retreat, both of which have been well proven in comparison to more data-intensive approaches, yet require minimal data requirements (DEM, daily temperature and precipitation). Additionally, the lack of extensive input data requirements mean that GERM simulations can run for the full duration of meteorological observations, as opposed to when glaciological observations began. This is advantageous because meteorological observations, particularly temperature and precipitation, typically have longer records (e.g. 1880-present day in the Alps) than glaciological observations (e.g. mass balance records began around 1900-1930 for some glaciers in the Alps, but many records are much shorter; Farinotti et al., 2012). Such long-term glacio-hydrological simulations allow rigorous validation of model performance by comparing modelled variables to observed variables, adding to a more complete understanding of how accurately the model reproduces observed changes. Furthermore, the version of GERM used in this thesis also includes the runoff routing module of Farinotti et al. (2012; Section 2.2.2.4), as well as snow-redistribution (see Section 2.2.2). The inclusion of the runoff routing module allows non-glacial sources of runoff: precipitation and snow-melt, to be modelled realistically. This is important since, even in alpine catchments, glacier cover rarely exceeds 50 % of total catchment area (Huss et al., 2017) so precipitation and snow-melt make up a considerable proportion of overall runoff. In summary, the combination of these components equates to a well-proven glacio-hydrological model that is applicable to a wide range of catchments, and is designed to be computationally simple enough to run on desktop computers. Implementation of the model was undertaken with the assistance of the model author, Matthias Huss.

1.3. Impacts of Climate Changes on Glacier and Runoff Evolution in the Alps and Himalaya.

1.3.1. Future Climate Changes.

Simulating the hydrological and glaciological response of glaciated catchments to climate change requires estimates of potential future changes in temperature and precipitation, often provided by General Circulation Models (GCMs). GCM simulations of future climate are increasing in number and complexity, with the CMIP5 (Coupled Model Intercomparison Project Phase 5; Taylor et al., 2007) containing simulations from 61 different GCMs, each for a range of emissions scenarios, resulting in a very large number of simulations of future climate, and hence a large range of simulated future climate changes. Although advances in climate model developments are significant, for example improved representation of monsoons between CMIP3 and CMIP5 (Sperber et al., 2013), GCMs are designed for global scale simulations and are not sufficiently high resolution for catchment-scale studies (<200 km^2; Guyennon et al., 2013). Moreover, due to the highly complex nature of the climate system, it is fundamentally impossible for a GCM to describe all processes precisely, regardless of model complexity (Tebaldi & Knutti, 2007). Therefore, different GCMs may be designed for different applications, resulting in a large range of GCMs each replicating the various components of the climate system with varying accuracy. Thus, GCM ensembles are often used to provide a range of possible futures.

GCMs are required to simulate the global response to two types of variability in the climate. Firstly, external forcings, which include greenhouse gas concentrations, solar irradiance and volcanic eruptions, and cause changes to the climate on decadal timescales from multiannual (volcanic) to decadal or longer (Forster et al., 2007), with variations in the orbit of the Earth around the Sun (Milankovitch Cycles) operating on timescales of tens to hundreds of thousands of years. In terms of this thesis, it is external forcings (excluding volcanic) that will cause changes to the climate between 2010 and 2100 and lead to glacio-hydrological changes. However, a second source of climate fluctuations, internal variability, is also important to consider. Internal climate variability occurs due to the different components of the climate system (e.g. atmosphere, ocean, cryosphere) interacting on different time-scales (Deser et al., 2012). The complex, non-linear, interactions between these components mean that they are never in equilibrium, resulting in climate phenomena such as the El Nino Southern Oscillation (ENSO) and the North Atlantic Oscillation (NAO). Internal variability causes changes on time-scales of days to several years (Deser et al., 2012). It should be noted however that modes of internal variability such as ENSO and the NAO can be influenced by external forcing.

In addition to the ability of GCMs to simulate climate changes, the actions and choices made by humanity in the coming decades will have a significant impact on the climate in 2100, and are realised in CMIP5 GCMs through Representative Concentration Pathways (RCPs) fully described in van Vuuren et al. (2011b). RCPs, which are each based on a set of socioeconomic assumptions (e.g. emissions, population, energy sources, and farming) are shown in Figure 1.1 and Table 1.1, and will be described in turn with the exception of RCP 6 which is not used in this thesis. RCP 2.6 represents considerable efforts to limit the increase in global mean temperature to 2°C with a peak in radiative of 3.1 W/m^2 in the mid-century, after which radiative forcing drops and stabilises at 2.6 W/m^2. Achieving such levels of radiative forcing will require widespread, rapid adaptation of energy efficient technologies and considerable reduction of CO_2 emissions combined with significant carbon capture and storage (van Vuuren et al., 2011a). RCP 4.5 represents a radiative forcing of 4.5 W/m^2 that stabilises in 2100, representing a low-emissions scenario that causes stable CO_2 concentrations from 2060-2100 and a global population peak of 9 billion in 2065 before decline to 8.7 billion in 2100 (Thomson et al., 2011). Finally, RCP 8.5 represents increasing greenhouse gas emissions over time reflecting no changes to climate and energy policy regarding emissions reductions. The radiative forcing of 8.5 W/m^2 in 2100 is based on a population of 12 billion by 2100 and unabated emissions increases (Riahi et al., 2011).

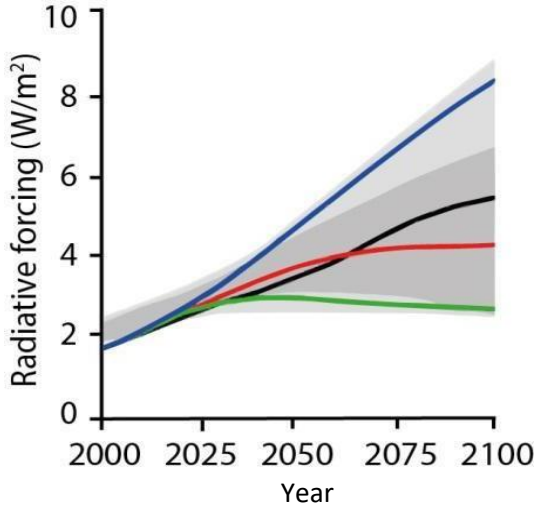

Figure 1.1: Trends in radiative forcing under four RCP scenarios: blue is RCP 8.5, black is RCP 6, red is RCP 4.5, and green is RCP 2.6. Figure from van Vuuren et al. (2011b). Note that RCP 6 is not used in this thesis.

Table 1.1: Summary of the radiative forcing and equivalent CO_2 concentrations for the three RCPs used in this thesis (Moss et al. 2010).

RCP	Radiative Forcing (Wm^{-2})	Peak CO_2 equivalent (p.p.m.)
2.6	Peak of 3.1 in 2050 declining to 2.6 in 2100	490
4.5	4.5 stabilising after 2100	650
8.5	8.5 in 2100	1370

Although GCMs are required to simulate future changes in climate, their coarse spatial resolution (typically 1 to >3° / 111 to >333 km^2) means that they cannot be applied directly to smaller scale impact studies, so downscaling is commonly applied to obtain local-scale climate. The two types of downscaling are dynamical downscaling and statistical downscaling. Dynamical downscaling is the nesting of a Regional Climate Model (RCM) within a GCM, which increases the spatial resolution (typical RCM resolution: <0.5°/10-50 km^2). Statistical downscaling is the process of statistically translating GCM or RCM outputs onto fine scale or point scale observations (Maraun et al., 2010), and applying this relationship to future RCM or GCM data to obtain local variables. A review of both dynamical and statistical downscaling will be described in detail in Section 3.1.2.

In many glaciological studies, the consideration of future climate changes and downscaling are somewhat limited. For example, several glaciological studies elected not to use simulations of future climate, instead applying simple approaches that demonstrate the effect of climate changes without explicitly incorporating a time series from climate model output. For example, Rowan et al. (2015) simulated future glacier changes at Khumbu Glacier by shifting the ELA (Equilibrium Line Altitude) by a height equivalent to 1.6°C warming. Similarly, Huss et al. (2008a) applied future climate changes to a glacier mass balance model using the mean changes in temperature and precipitation from a separate modelling study (Frei, 2007), but imposed random variability on these mean changes based on observations from 1980-2000. Although these approaches provide an indication of the future response of glaciers to climate changes, they do not include temporal variability or decadal-scale climate variability. Furthermore, studies that do apply GCM data to drive glacio-hydrological models typically apply statistical downscaling methods that are not as sophisticated as those applied in other areas of impact studies (e.g. agriculture: Robertson et al., 2007; hydrology: Chen et al., 2013). For example, the delta-change approach (see Section 3.1.2 for details) is applied in many glacio-hydrological studies (e.g. Akhtar et al., 2008; Huss and Farinotti, 2012), but does not adequately correct for errors in climate model outputs (Fowler et al., 2007). Therefore, a key aim of this thesis is to improve on existing downscaling approaches applied in glacio-hydrological studies by applying a more advanced dynamical-statistical downscaling technique. These issues will be discussed further in Chapter 3.

1.3.2. European Alps.

The monitoring of glacier changes in the European Alps (note, all following references to the 'Alps' refers to the European Alps) has produced some of the most detailed and longest records in the world. Thus, Alpine glaciers are some of the most heavily investigated with an extensive

range of studies, particularly in Switzerland (e.g. Pellicciotti et al., 2014), which will form the basis of this review.

Glaciers in the Swiss Alps have shown well documented recession. For example, Paul et al. (2004) used remote-sensing methods to assess the changes to 930 glaciers in the Alps, with results suggesting 18 % of ice area was lost between 1985 and 1999. Similarly, Bauder et al. (2007) used DEM-differencing to assess geodetic changes of 19 Swiss glaciers from 1860 to 1999, finding a negative trend in ice mass interrupted by short periods of mass gain, with rates of ice loss accelerating since 1980. However, because these studies are based on remote-sensing, the temporal resolution is limited to the time between successive DEMs.

To increase the temporal resolution of mass balance estimates, modelling studies have been applied to reconstruct mass balance in the periods between DEMs. For example, the studies of Huss et al. (2008b; 2010) used GERM to calculate the mass balance of 30 glaciers in the Swiss Alps from 1908-2008. Their reconstructions revealed strongly negative trends since 1908 with overall mass losses at all glaciers, interrupted by short periods of mass gain in 1912-1920 and 1974-1981, as well as periods of extensive mass loss in 1942-1950 and 1998-2006. The authors attributed periods of mass gain to less negative summer balances, likely due to decreased summer temperatures. The first period of considerable mass loss was attributed to strongly enhanced solar radiation (Huss et al., 2009b) and the recent period of substantial mass loss due to warming atmospheric temperatures. Such widespread glacier mass loss is in line with global glacier changes (WGMS, 2015; Gardner et al., 2013), and reiterates the importance of estimating future glacier and runoff changes, which requires models.

Modelling studies of future changes in glacial catchments in the Swiss Alps are numerous. For example, the aforementioned study of Horton et al. (2006) applied their TI-based precipitation-runoff model to 11 glaciated catchments using climate projections from nine RCMs forced by three GCMs to drive their model. Using the AAR method to calculate glacier changes, they projected that runoff in 2079-2100 will be lower than current levels and that the onset of the melt season will occur earlier in spring. However, Horton et al. (2006) also found that runoff estimates are sensitive to different climate model inputs.

The GERM model was used by Farinotti et al. (2012) to simulate the evolution of glacier changes and runoff in nine Swiss catchments from 2010-2100, using 10 GCM-RCM combinations all forced by the same scenario (A1B - Van der Linden and Mitchell, 2009) to project glacier and runoff changes. They found that an initial increase, followed by an overall decrease in discharge is projected, with considerable mass loss of glaciers throughout Switzerland. Similarly, Gabbi et

al., (2012) applied GERM to the Mauvoisin catchment in Switzerland, finding a similar increase in runoff in the next two decades followed by a decrease.

In a study that used the ETI approach to calculating ablation, Finger et al. (2012), focussed on assessing how changes in runoff will impact the hydropower industry in the Vispa catchment in Switzerland. Their study did not explicitly simulate glacier evolution, instead changes in glacier area were prescribed based on the results of the aforementioned study of Farinotti et al. (2012). Their study corroborated results from other studies, projecting a decrease in runoff of up to 33 % in 2100 combined with earlier onset of the melt season and a strong reduction in later summer discharge.

1.3.3. Himalaya.

The availability of long-term (e.g. decadal or more) field-data in Himalayan catchments is very limited. Therefore, assessing the glacial changes is reliant upon remote-sensing data. For example, Bolch et al. (2011), Gardelle et al. (2013), Kääb et al. (2012), and Nuimura et al. (2012) all used satellite remote sensing to calculate the geodetic mass balance (e.g. photogrammetry and DEM differencing using multi-temporal DEMs) of glaciers over large regions, finding strongly negative mass balances with the exception of the Karakoram range. Such limited in-situ data are problematic for glacio-hydrological modelling, as the lack of data limits the potential for model calibration and validation. Therefore, studies in the Himalayan region typically focus on specific glaciers for which glaciological data are available (e.g. Langtang and Khumbu Glaciers), with the majority of Himalayan catchments not studied. Until recent years, glacio-hydrological modelling of Himalayan Glaciers was extremely limited. However, there has been a recent surge in interest in the region resulting in a range of recent studies. This section will briefly introduce the key differences between glaciers in the European Alps and the Himalaya, before reviewing key glacio-hydrological studies.

A full explanation of the differences between typical glaciers in the Alps and Himalaya is provided in Section 6.1.2 so will be only briefly described here. Two significant traits of Himalayan glaciers are the high proportion of debris-covered glaciers in the Himalaya (36 % in the Everest region; Thakuri et al., 2014), and the resulting manifestation of mass losses through downwasting rather than frontal retreat. The impact of debris cover on glacier melt is considerable (e.g. Benn et al., 2012; Hambrey et al., 2009; Reid and Brock, 2010), something glacio-hydrological models have only very recently attempted to include. Similarly, the loss of mass through downwasting (e.g. Scherler et al., 2011) means that the spatial pattern of retreat needs to be considered in glacio-hydrological models.

Existing studies in the Himalaya can be categorised into regional scale and local scale. Of the regional scale studies, Shea et al. (2015) conducted a study into the future evolution of all glaciers in the Everest region, projecting that remaining ice volume in 2100 will be between 4-27 % of ice volume in 2010. To incorporate the influence of debris cover, their study used a different degree-day factor for clean ice and debris-covered ice. This approach is typical in much of the literature (e.g. Immerzeel et al., 2013) and, although this does reduce melt beneath debris, it does not consider the strong spatial variability of debris thickness. Immerzeel et al. (2013) applied a glacio-hydrological model to the Langtang catchment in Nepal and the Baltoro catchment in the Karakoram. Their model estimated ablation using a TI model that accounted for different degree day factors on debris-covered ice as well as north and south facing ice. They used four GCMs to force their glacio-hydrological model, finding reductions in glacier area but overall consistent increases in runoff at both catchments. The increases in runoff were attributed to the Indian Monsoon which they suggested will continue to sustain increasing water demands in the region in catchments dominated by monsoon rainfall, regardless of glacier changes. These results were corroborated by the study of Lutz et al. (2014) who assessed changing glacier melt and runoff over the Greater Himalayan region, finding increases in runoff until 2050 when their simulation ended. Further discussion of the Indian Monsoon and its representation in climate models is included in Section 3.5.2 and 8.1.1.1.

Studies at a more local scale typically apply glacio-hydrological models that are heavily calibrated to field-studies (e.g. Nicholson and Benn, 2006; Ragettli et al., 2015). Due to the difficulties in accessing Himalayan catchments, many such studies are centred on the Langtang catchment (e.g. Ragettli et al., 2016, 2015; Shrestha and Aryal, 2011) or the Khumbu catchment (e.g. Shrestha and Aryal, 2011; Soncini et al., 2016). However, these studies use data-intensive approaches. For example, Soncini et al. (2016) assessed the future evolution of Khumbu Glacier, employing an ETI model (Pellicciotti et al., 2005) coupled to a dynamical ice-flow model at Khumbu. Ablation stake measurements were used to calibrate ablation on bare ice, debris-covered ice, and to measure debris depth, rendering their approach inapplicable to other catchments for which equivalent field-data are not available. They forced their model with three GCM outputs, each forced with RCPs 2.6, 4.5, and 8.5, and statistically downscaled using the delta-change approach for temperature and a weather generator approach for precipitation (see Section 3.1.2 for details on downscaling approaches). Their study projected a 26 % reduction in discharge in 2100, compared to the discharge in 2011-2013 with at least 50 % loss of ice mass, contrasting the projections of the aforementioned regional scale studies. Although the data-intensive approach is suitable for short-term simulations at the few glaciers with data, the stationarity of surface conditions over time is uncertain (Fujita & Sakai, 2014), as is behaviour of the debris surface in the future.

In summary, the state of Himalayan glacio-hydrological modelling is relatively limited in comparison to the Alps, with the limited long-term field-data a considerable barrier. Regional scale studies typically apply TI approaches to calculating ablation, with variations in debris thickness not considered. However, the data-intensive approaches are not applicable on wider scales, limiting a comprehensive spatial assessment of future water resources.

1.4. Summary and Knowledge Gaps.

The review of literature in the Alps and Himalaya points to several areas that have not been fully addressed in existing studies.

Firstly, although several studies have attempted to investigate the uncertainty related to long-term glacio-hydrological modelling, this is yet to be fully constrained. For example, the studies of Horton et al. (2006) and Farinotti et al. (2012) both evaluated part of the uncertainty relating to climate model data inputs but neglected the uncertainty associated with the model itself, in terms of its ability to accurately predict glacier and runoff changes. The study of Huss et al. (2014) attempted to include all sources of uncertainty resulting from glacio-hydrological models by conducting a series of sensitivity analyses from 2010-2100 and comparing the extent to which different factors (e.g. initial ice volume, calibration strategy, method to calculate melt and glacier retreat, etc.) impact upon runoff projections. However, to the best of the author's knowledge, no study has explicitly calculated the uncertainty associated with *long-term* glacio-hydrological simulations by comparing simulated changes in glacier and runoff evolution to observed changes over timescales of 120 years. Using short "validation" periods is clearly unsatisfactory given that the response time of small mountain glaciers is typically 15-60 years (Cuffey & Paterson, 2010). Further, the length of validation periods used in this thesis (120 years) is similar to the length of period of future projections (typically 90 years). This is important because the non-physical, statistical basis of models such as GERM will introduce uncertainties as glacier retreat causes glacio-hydro-climatological process changes (such as transitions from melt-dominated ablation to calving-dominated ablation as a terminus retreats through an overdeepening). Moreover, the statistical basis of such models, which relies on establishing melt factors for snow and ice by calibrating the model to observed volume and runoff changes over a defined "calibration" period, is unlikely to be stable on such timescales. For example, the relationship between the surface energy balance of ice and the air temperature, which governs melt in mass balance models, is known not to be constant (Huss et al., 2008b). Finally, by comparing modelled changes to observed changes, all components of the model structure are integrated into the uncertainty analysis and the quantified uncertainty can be applied to future projections, thus improving the robustness of future projections.

Secondly, in much of the glacio-hydrological literature, the treatment of climate model data is typically not considered with equal importance compared to other aspects of glacio-hydrological modelling. Since climate model data are an essential part of the modelling chain, it is important that they are considered equally to glacier models. Crucially, the coarse resolution of climate model outputs cannot be applied directly to catchment-scale studies, necessitating the use of downscaling. Therefore, this thesis will improve upon the approaches of many glacio-hydrological studies by implementing an advanced dynamical-statistical downscaling procedure. This will complement the aforementioned assessment of GERM uncertainty by allowing both the uncertainty associated with GERM, and the uncertainty associated with the climate model/scenario, to be applied to future glacier and runoff projections, thereby providing more robust and contextualised future projections than previous studies.

Thirdly, an area of glacio-hydrological modelling that requires further development relates to the application of glacio-hydrological models to regions outside the Alps, where previous work is much more limited. For example, compared to the Alps, there are considerably fewer studies of Himalayan catchment runoff, where the considerable supra-glacial debris cover, combined with observations of widespread downwasting rather than frontal recession, means that glacio-hydrological models cannot be applied without modifications. Existing modelling attempts in the Himalaya are typically regional scale simulations that inadequately incorporate debris cover, or data-intensive approaches that are only applicable in very few catchments due to the very limited field-data in this region. This thesis will incorporate fully distributed debris-cover, and downwasting ice into GERM and develop and test the model in a Himalayan catchment.

In summary, this thesis will focus on improving the quantification of uncertainties relating to long-term glacio-hydrological studies; applying these uncertainties to future projections of glacier and runoff evolution using an advanced downscaling methodology to correct climate model data; and adapting a GERM such that key characteristics of Himalayan glaciers can be incorporated. The wider context of this research is to provide robust projections of future changes in catchment runoff that can be used in adaptation and mitigation studies to assess the impact of changing water resources on downstream populations.

1.5. Research Aims and Objectives.

This section will outline the three key aims (numbered) and objectives (lettered) of this thesis.

1) Assess the skill of GERM to recreate long-term (120 years) glacio-hydrological changes in alpine catchments, and assess the associated modelling uncertainty.

a. The calibration methodology of GERM is improved so that it is systematic, automated and repeatable, and produces a statistical goodness-of-fit assessment over the full parameter space. This new calibration procedure is used to calibrate GERM at the Griesgletscher and Rhonegletscher catchments in the European Alps (from 1998-2004), using contemporary glacier volume and catchment runoff measurements to identify optimum parameter sets.

b. Digital elevation models are used to obtain the initial glacier geometry required to begin each model run, and GERM is run from 1884-2004.

c. Each completed model run is used to estimate the accumulated uncertainty associated with the simulated glacier/runoff changes by comparing modelled with observed glacier/runoff change at the end of the simulation.

2) Use this assessment of uncertainty to contextualise and understand the precision of future (to 2100 AD) runoff projections for alpine catchments under a wide range of possible climate changes scenarios.

a. Identify suitable Global Climate Models (GCMs) and address the problem of scale differences between GCM grid resolution and the catchment scale using downscaling.

b. Develop and test these downscaling methodologies before applying them to GCM/RCM simulations forced by scenarios of future greenhouse gas emissions, to provide input to GERM.

c. Using the results from (1) and (2a/b), simulate the future response of Griesgletscher and Rhonegletscher and calculate the uncertainty related to future simulations in terms of both GERM uncertainty and climate model/scenario uncertainty, therefore providing runoff projections that can be used in adaption and mitigation studies.

3) Apply GERM to a debris-covered glacier in the Himalaya in order to identify the challenges of widespread model application, and incorporate modifications to the model such that it can be used for future projections in this region.

a. Review the limitations of glacio-hydrological modelling in the Himalayas, and modify GERM to account for the influence of debris cover on ice melt and the influence of downwasting on glacier evolution, so that GERM can be applied to the Khumbu Glacier in Nepal.

b. Use these modifications to simulate the future response of the Khumbu Glacier when driving the model with a range of climate models and scenarios.

1.6. Thesis Structure.

The aims and objectives listed above will be addressed sequentially throughout this thesis.

Chapter 2 will explain how GERM works and provide examples of previous applications of GERM, in order to provide an overview of the methodology used in subsequent chapters.

Chapter 3 will review and identify the current state-of-the-art in simulations of future climate change, and the necessary downscaling techniques to overcome the gap between climate model grid resolution (GCMs: typically 1 to >3°; RCMs: typically <0.5°) and the catchment scale, thus providing estimates of future climate (temperature and precipitation) for different scenarios of future climate change to drive future simulations of GERM (Objective **2a**).

Chapter 4 will apply GERM from 1884-2004 at Griesgletscher and Rhonegletscher in the European Alps, for which detailed, long-term, glacial observations are available. Simulations for these catchments will be used to evaluate the performance of the model in simulating glacier and hydrological changes in comparison to observations over 120 years, therefore satisfying Aim **1**.

Chapter 5 will apply the downscaled climate model outputs (Objective **2a**) to future simulations at Griesgletscher and Rhonegletscher until 2100. This will use the range of climate inputs for different future scenarios to drive GERM and constrain climatic uncertainty, as well as use the long-term validation (Aim **1**) to constrain the modelling uncertainty, associated with future projections (Aim **2**).

Chapters 6 and 7 will develop GERM to incorporate downwasting dynamics and debris-covered ice. These modifications will then be applied to conduct future simulations at the Khumbu catchment (Aim **3**).

Chapters 8 & 9 will synthesise and discuss the results of the previous chapters, comparing the results of the differing glacio-hydrological changes in each catchment. Moreover, this section will critically analyse the key findings of this thesis by comparing the results to those in the literature, before making recommendations on the suggested direction of future research

2. INTRODUCTION TO THE GLACIER EVOLUTION AND RUNOFF MODEL.

This chapter introduces GERM and details the general method of applying the GERM model that is employed in following chapters. The following chapters contain additional methodology sections when it is necessary to expand the detail provided here.

2.1. Introduction to GERM.

GERM is a statistically based (i.e. non-physical) HTI mass balance model that also includes a fully distributed hydrological model. Parameterisation of the model is determined by statistical calibration to a set of observed data (one or more years of discharge and glacier volume change data) for a given catchment. Its design and prior applications are to simulate runoff from glacierised catchments for future runoff projection and incorporates changes in glacier volume. GERM is designed for use on desktop computers and the limited input data requirements (DEM data and daily temperature and precipitation) allow GERM to be applied to a range of catchments without the collection of detailed glaciological data that would be required for energy-balance melt models or dynamical ice flow models.

2.2. Methodology.

2.2.1. Overview of GERM.

GERM is both a glacier mass balance model and a hydrological model, and consists of modules which simulate accumulation, ablation, glacier evolution (volume and area change), evapotranspiration, and runoff routing, all in a spatially distributed model. GERM is designed to run at high spatial resolutions (25-50 m) and to produce outputs at a daily time-step, with representation of six surface types (ice, snow, rock, low vegetation, high vegetation and open water). The module structure is shown schematically in Figure 2.1. The original GERM model presented in Huss et al. (2008a) was modified in Huss et al. (2010a) and subsequently in Farinotti et al. (2012) and these publications should be considered as the key references for this section.

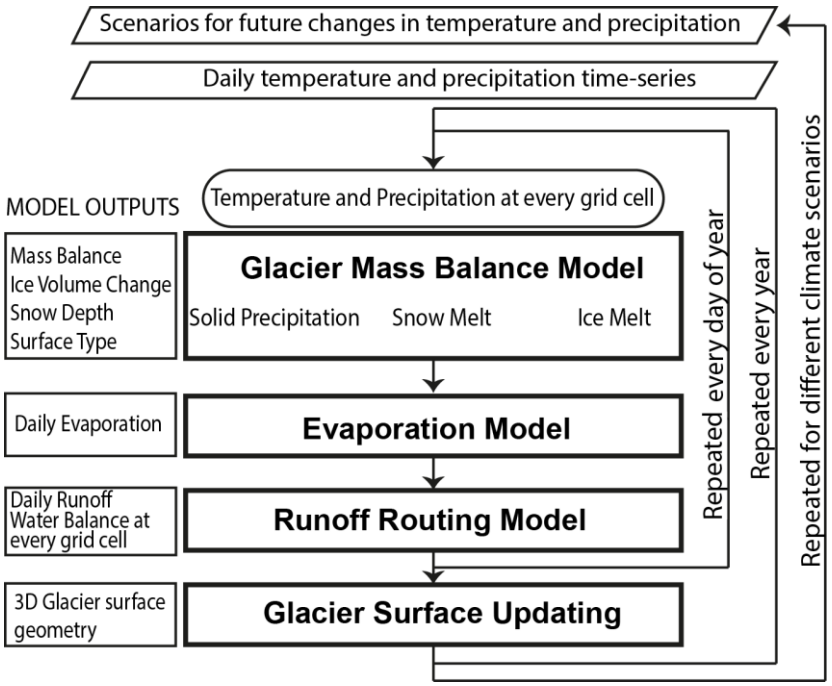

Figure 2.1: Schematic representation of the modules, data and outputs of GERM, modified from Huss et al. (2008a).

2.2.2. Initial Ice Thickness.

GERM requires an initial ice thickness distribution from which to begin each simulation. Although ground-penetrating radar thickness estimates are available for some glaciers (e.g. Dowdeswell et al., 2002; Gades et al., 2000; Moribayashi, 1978; Nolan et al., 1995), the spatial distribution of these estimates is incomplete, due to crevassing or inaccessibility (see, e.g., Plewes & Hubbard, 2001). Thus, GERM uses a glacier surface inversion technique to find the be topography, which requires only a DEM and glacier outline as inputs, as originally proposed in Farinotti et al. (2009) and developed further in Huss and Farinotti (2012).

The glacier outlines used in this thesis are provided by the Randolph Glacier Inventory version 3.2 (RGI; Pfeffer et al., 2014) and the Shuttle Radar Topography Mission (SRTM; Jarvis et al., 2008) provides elevation data at a 90 m resolution. Although the RGI has been updated in subsequent versions 4 and 5, version 3.2 was the most recent inventory available when this work was undertaken. For all glaciers considered in this thesis, outlines of the RGI 3.2 were visually checked for errors and modified where necessary, ensuring a reasonable estimation of ice extent. SRTM DEMs, freely available from srtm.csi.cgiar.org, are used throughout this thesis. SRTM is used in preference to ASTER DEMs (Advanced Spaceborne Thermal Emission and Reflection Radiometer) since studies have shown both products produce similar performance in mountain areas (root-mean-square errors of c. ±11 m; Fujita et al., 2008) but ASTER contain more gaps in data in extreme topography (Kaab et al. 2002; Huss & Farinotti, 2012).

The glacier thickness distribution is calculated as a function of surface slope, glacier width, and the steady state flux.

The first step is to interpolate the DEM to a regular grid over the glacier, using the glacier outline to intersect the DEM and divide the glacier into 10 m elevation bands. Surface slope and area is then calculated for each band. The surface shape of the ice is then simplified by estimating the width depending on the original DEM width, area, slope and shape, to produce a simplified 2D glacier.

An integrated form of Glen's ice flow law (Glen, 1955; Cuffey & Paterson, 2010) is then solved to calculate ice thickness *h* along the central flow line:

$$h = \sqrt[5]{\frac{q}{\frac{2}{5} A \left(S_f \rho g \sin\bar{\alpha}\right)^3}} \qquad (2.1)$$

where q is the ice flux, normalised to glacier width, g the acceleration due to gravity, A the temperature-dependent rate factor of the ice flow law, S_f a factor accounting for valley shape, ρ is the density of ice and α is equal to the mean slope along the flow-line.

The ice thickness is interpolated spatially assuming a parabolic valley shape and a boundary condition of h=0 at the glacier margin. Finally, corrections are applied to spatially distributed values of h to account for the local surface slope. The results of the ice-thickness calculation in this thesis for Griesgletscher are shown in Figure 2.2

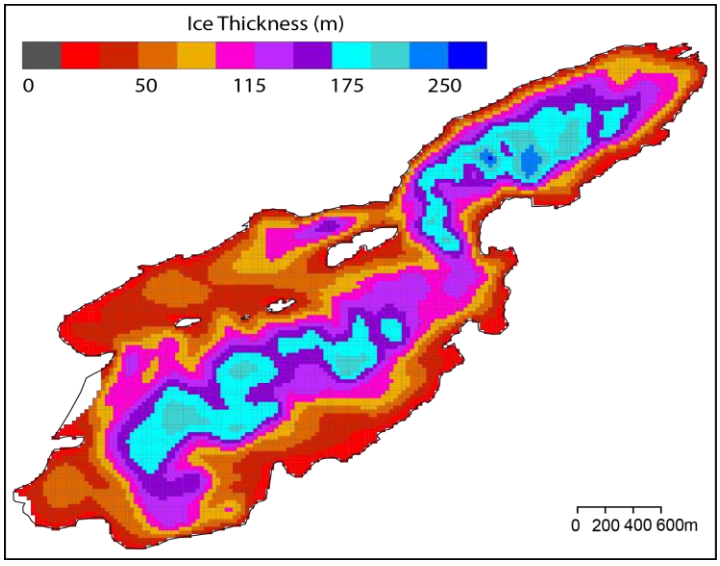

Figure 2.2: Ice thickness of Griesgletscher calculated using only a DEM from 2003 and a glacier boundary.

Huss et al. (2008a) and Huss & Farinotti (2012) describe the thickness calculation in full and validate results against radio-echo sounding at Glacier de Zinal, Grosser Aletschgletscher, and

Rhonegletscher, finding a correlation of measured and calculated ice thickness of r^2=0.72 and a mean relative error of 26 % when all results were combined, showing that this method produces reasonable results for glaciers without thickness measurements. Huss & Farinotti (2012) tested this method further for glaciers in different regions, again finding reasonable reproduction of observed thicknesses (Figure 2.3). Specifically, Huss and Farinotti (2012) compared the ice thickness estimates to observations at 21 glaciers in the Swiss Alps that had GPR (Ground Penetrating Radar) measurements available, finding an average point thickness bias of 10 m and an average mean thickness bias of 0 m. A full uncertainty analysis, including ice thickness modelling, DEM error, glacier inventory error, and glacier field data error, produced an RMSE (Root Mean Square Error) of 30 % for single glaciers.

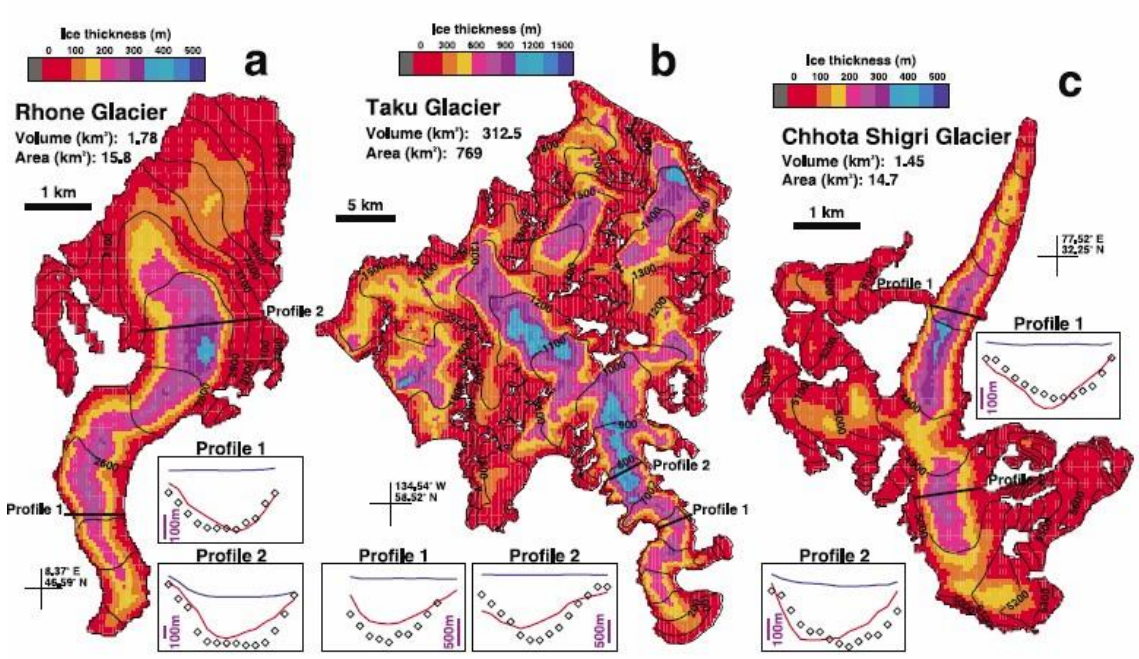

Figure 2.3: Calculated ice thickness of: (a) Rhone glacier (European Alps), (b) Taku Glacier (Alaska) and (c) Chhota Shigri glacier (Himalaya). Inserts show GPR surveys of thickness (diamonds) plotted against simulated (red line). Figure from Huss and Farinotti (2012).

The previous applications of GERM, and the use of the aforementioned method outside of GERM, have shown that the ice thickness estimation method works relatively well (e.g. Andreassen et al., 2015; Farinotti et al., 2009a, 2009b; Huss and Farinotti, 2014, 2012; Huss, 2012; Li et al., 2015). However, there remain potential limitations concerning the processes of mass turnover, which may be different to the 'typical' alpine glaciers for which this method was developed. For example, many Himalayan glaciers develop debris cover due to low flow rates on the glacier tongue, regular rock avalanching, relatively low snow fall in comparison to the potential of strong, near-equatorial incoming solar irradiance (Hambrey et al., 2009). This debris cover increases with proximity to the glacier terminus, thus causing a reduction of surface slope

due to preferential melting and thinning under thin debris (Benn et al., 2012). Therefore, the tongues of many debris-covered glaciers are almost flat and show very low dynamic activity and minimal redistribution of mass from the accumulation zones (Quincey et al., 2009). The current glacier thickness measurement is therefore likely to overestimate thickness in the glacier tongue since it will predict a higher mass turnover than reality, since it does not incorporate characteristics such as debris cover. The performance of the ice thickness estimation for a Himalayan Glacier will be tested in Section 6.2.

The application of this thickness estimation method has already been well proven at the catchments of Griesgletscher (Farinotti, 2010) and Rhonegletscher (Huss and Farinotti, 2012) that are modelled in this thesis. At Khumbu Glacier, potential issues mentioned above are mitigated by the incorporation of ice thickness observations from Gades et al. (2000), as described in full in Section 6.2.

2.2.3. GERM Operation.

This section will introduce the various modules that form GERM.

2.2.3.1. Mass Balance Module.

2.2.3.1.1. Accumulation.

The accumulation component of GERM forms part of the mass balance module. For each grid cell *i*, accumulation P_{sol} is calculated by:

$$P_{sol,i} = P_{ref} \cdot (1 + c_{prec}) \cdot \left[1 + z_i - z_{ref}\right) \cdot \frac{dP}{dz}\right] \cdot D_{snow,i} \cdot r_s \quad (2.2)$$

where P_{ref} is precipitation, c_{prec} is a correction factor which allows for correction of precipitation gauge-under catch (Bruce & Clark 1981), z_i-z_{ref} is the elevation difference between the reference location (precipitation gauge or centre of RCM grid) and the considered grid, *dP/dz* is the precipitation-elevation lapse rate (Peck & Brown 1962), $D_{snow,i}$ is a factor which accounts for spatial snow redistribution based on a DEM and r_s is the proportion of solid precipitation which increases linearly from 1 to 0 in the temperature range -1 °C to 1 °C (Hock, 1999), with the inverse of this representing liquid precipitation.

This methodology for calculating accumulation is similar in many glacio-hydrological models (e.g. Finger et al., 2012; Immerzeel et al., 2013; Pellicciotti et al., 2005; Shea et al., 2015) and should produce a good estimation of accumulation. However, this approach still represents a simplification of reality so care is needed in its application. For example, although there is a correction factor for precipitation gauge-undercatch, a more rigorous undercatch correction can be implemented outside the model to incorporate the type and height of gauge, wind speed and

the phase of precipitation (snow or rain), if data are available. Thus, the undercatch correction factor should only be used where no information on gauge-type and wind-speed are available, or when a non-gauge-based observation is being used (e.g. gridded reanalysis dataset). Additionally, the inclusion of snow redistribution through wind or avalanche (Lehning et al., 2008) is a significant simplification of reality (results at Griesgletscher shown in Figure 2.4), albeit typical of glacio-hydrological models (e.g. Gabbi et al., 2012), some of which neglect redistribution of snow completely (e.g. Koboltschnig et al., 2008; MacHguth et al., 2012; Machguth et al., 2009; Mott et al., 2008; Paul and Kotlarski, 2010; Salzmann et al., 2012). Specifically, where DEM surface slopes are between 30° and 60°, snow accumulation is decreased linearly from 100 % at 30°, to 0 % at 60°, and redistributed to less steep adjacent cells, mimicking the influence of avalanching and wind-blown snow. The curvature of groups of grid-squares is also included, with convex shaped cells receiving up to 50 % less accumulation than convex shaped grid-cells, since curvature is a good indicator of areas of wind-based snow redistribution and snow erosion (Blöschl et al., 1991). These factors influence how snow is accumulated both inside and outside of the glacier mask, as well as potentially redistributing snow from outside to inside the glacier mask. While this redistribution scheme may be appropriate for relatively small glaciers in the Alps, large Himalayan glaciers receive a higher proportion of accumulation from avalanching (Hambrey et al., 2009) and may require a more sophisticated redistribution model to fully capture the processes.

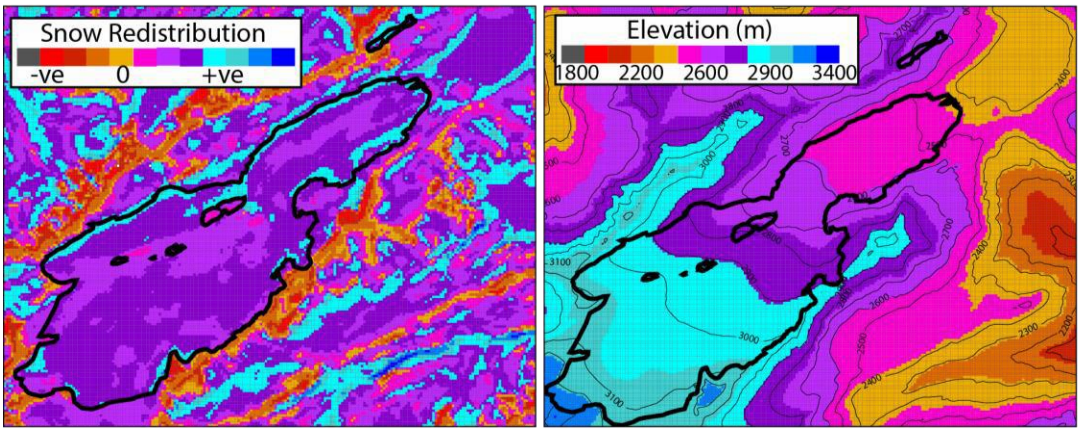

Figure 2.4: The snow-redistribution outputs at Griesgletscher with the DEM on which this is calculated. –ve refers to removal of snow from the surface, +ve refers to the addition of snow to the surface.

2.2.3.1.2. Ablation.

A distributed temperature index model is used for ablation but the effect of direct solar radiation is also incorporated (HTI; Hock, 1999; Huss et al., 2008a), as described in Section 1.2. This component of GERM is applied to ice, snow on the glacier, as well as snow outside of the glacier

boundary. Melt, *M*, is calculated through the following equation which is the same for ice, snow on the glacier, and snow outside of the glacier:

$$\begin{aligned} &\text{T} > 0°\text{C:} \quad && M = (f_M + r_{ice/snow} \cdot I_{pot,i}) \cdot T_i \\ &\text{T} \leq 0°\text{C:} \quad && M = 0 \end{aligned} \tag{2.3}$$

where f_M is a degree day factor, $r_{ice/snow}$ are separate radiation factors for snow and ice, $I_{pot,i}$ is the potential direct clear-sky radiation at grid cell *i*, and T_i is the mean daily air temperature at the same location. *T* is interpolated using a constant lapse rate and the average of snow and ice radiation factors are used for exposed firn areas. Initial firn area is calculated as a factor of the mean elevation of the firn line, potential radiation, and effects of snow-redistribution. The firn area is transiently updated according to the areas with positive mass balances in the previous hydrological year. The parameters f_M and $r_{ice/snow}$ should be calibrated specifically for each catchment using available observations. Although this thesis aims to use a model that requires minimal data, catchment specific calibration is essential when using all types of model reviewed in Section 1.2 and GERM requires less input data than EB, fully dynamical, and ETI model approaches, so represents one of the least data-demanding glacio-hydrological models.

Glacier surface mass balance is calculated as the sum of solid precipitation and melt at the end of the hydrological year and is integrated over every grid cell that contains ice to yield an annual ice volume change which is used to update glacier surface geometry (see following section). Potential direct clear-sky radiation is calculated based on slope, aspect, effective horizon, and position of the sun, according to Hock (1999), and was provided for this thesis by Matthias Huss.

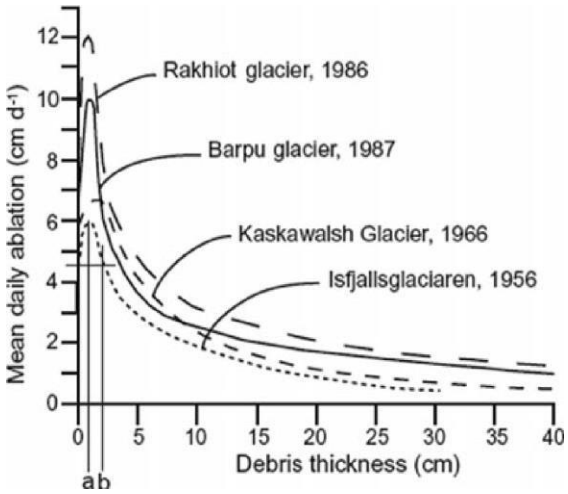

Figure 2.5: Measurements of debris thickness and ice ablation rate from glaciers in several regions. Figure from Nicholson and Benn (2006).

The influence of debris cover is incorporated into GERM but strongly oversimplifies its influence on melt rates and excludes dynamical changes that the debris cover causes. For application to the Khumbu Glacier, this has required modifications to the model that are described in Chapter 6. Here, however, it is only necessary to describe how the standard GERM model used in previous studies considers debris cover. Supraglacial debris cover can greatly modify the melt rate of ice. Debris reduces the albedo of the bare ice or snow surface from typical values of 0.25-0.5 or 0.4-0.97 respectively to values of 0.1 (Cuffey & Paterson, 2010) significantly increasing the absorption of incoming radiation. If the debris layer is sufficiently thin (<2 cm), this energy flux will be conducted to the ice surface causing enhanced surface melting. Conversely, a thicker layer of debris (>2 cm) will insulate the ice beneath the debris from incoming radiation, resulting in reduced melt compared to a bare-ice surface. In GERM, debris cover is accounted for by simply introducing a constant reduction factor f_{debris} for ablation:

While this method to incorporate debris cover into models is typical of many glacio-hydrological models (e.g. Immerzeel et al., 2013, 2012; Jouvet et al., 2011; Ragettli et al., 2013), the use of a constant reduction factor ignores considerable variations in melt rates of debris-covered ice shown in the Østrem curve (Figure 2.5). This part of GERM will be further discussed in Chapter 6.

2.2.3.2. Glacier Evolution.

Glacier geometry and volume changes need to be predicted as accurately as possible because of their influence on future runoff volumes. In GERM, glacier evolution is updated annually using an approach originally devised in Huss et al. (2008a) and improved in Huss et al. (2010b). This method uses an elevation-dependent function, Δh, to redistribute the simulated annual change in mass. Δh is based on records of geometry change from many glaciers and is divided into retreat patterns for small, medium and large glaciers, each of which will respond differently to

T > 0°C: $$M = ((f_M + r_{ice/snow} \cdot I_{pot,i}) \cdot T_i) \cdot f_{debris} \quad (2.4)$$

climate forcing (Figure 2.6). The Δh function dictates that the most pronounced changes will occur in the tongue region with accumulation zone changes relatively minor. If observations of mass losses are available for the glacier, a glacier-specific redistribution curve may be implemented, ensuring model results reproduce observed mass redistribution.

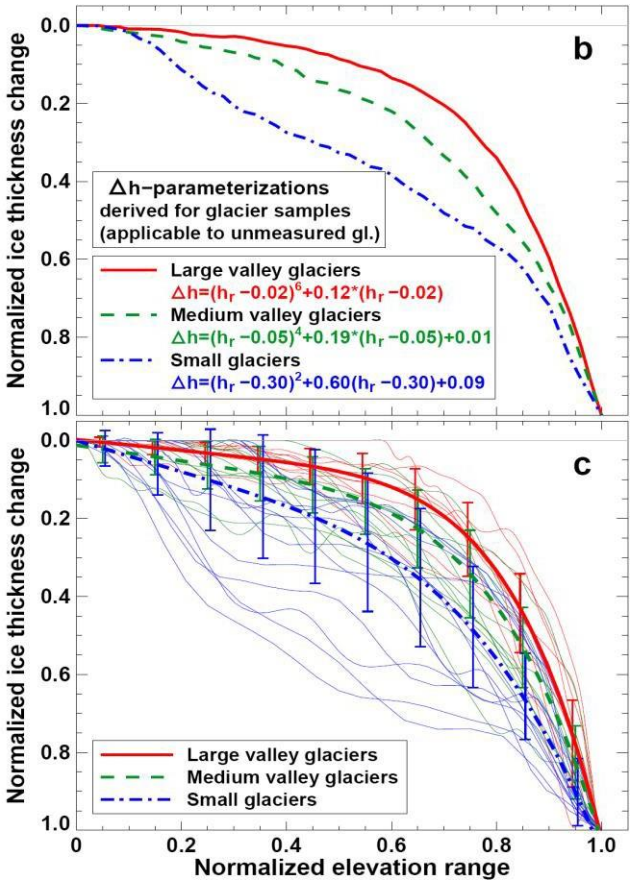

Figure 2.6: Ice thickness change relative to ice elevation for (B) average values from all observed glaciers split into categories dependent on size, and (C) 34 measured glaciers showing variability with each size class. Figure from Huss et al. (2010b).

A full description of this method can be found in Huss et al. (2010b) where the results of the *Δh* approach are compared to the results of a 3D dynamical ice flow model (Jouvet et al., 2011; Figure 2.7). Huss et al. (2010b) shows that the performance of the *Δh* is comparable to the ice-flow model during periods of retreat from 2008-2100. However, during short periods of advance, the *Δh* method cannot accurately simulate changes in ice extent. This because GERM cannot currently reproduce glacier advance since the module to update glacier geometry is only capable of increasing ice volume through thickening, rather than changes in area. Thus, glaciers can increase in volume, but cannot extend spatially. However, since glacier advances are limited to very few regions under current climatic conditions (Gardner et al., 2013; WGMS, 2015; IPCC5 WGII, 2014), the lack of glacier-advancement is not a major limitation and the fundamental aspect of the *Δh* method is its proven ability to reproduce glacier retreat (e.g. Farinotti et al., 2012; Huss and Hock, 2015; Li et al., 2015). Incorporating a glacier advance scheme is a potential improvement one could make in order to perform extremely long model runs where advances are possible. However, since this thesis is concerned with glacier changes from 1900-2100 where

retreat is dominant, this is outside the aims of this thesis but is encouraged in future model development.

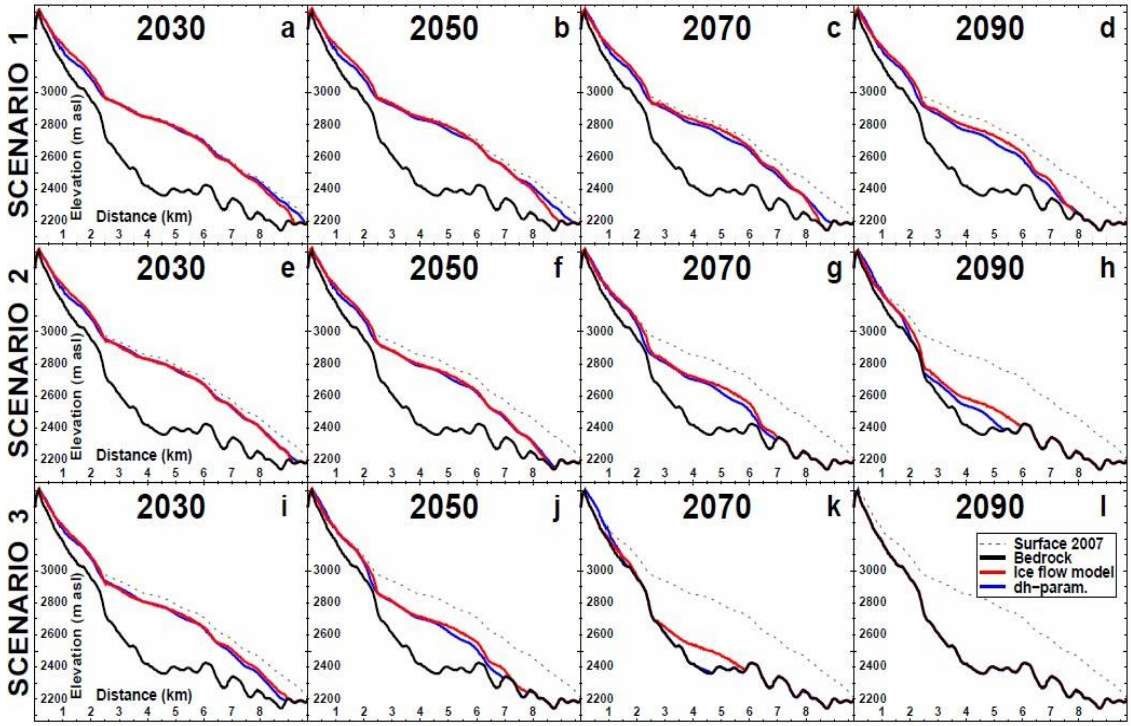

Figure 2.7: Comparison of glacier elevation profiles during 21st century retreat for Rhonegletscher in the Swiss Alps, under three different climate scenarios. Scenario 1: cold and wet; scenario 2: median, most probable scenario; scenario 3: warm and dry. The red profile is calculated by a 3D ice flow model (Jouvet et al., 2008) and the blue profile using the *Δh* parameterisation in GERM. Note the generally close agreement between the two profiles. Figure from Huss et al. (2010b).

2.2.3.3. Evapotranspiration.

Estimating evaporation in mountain catchments is difficult due to the lack of widespread observations. In GERM, an empirical model is used based on the approach of Hamon (1960), with modifications accounting for different surface types. For each grid cell *i*, actual evapotranspiration $ET_{act,i}$ is computed by reducing the potential evapotranspiration by a constant factor that can be defined for each of the six surface types $ET_{p,j}$ according to:

$$ET_{act,i} = \frac{35.77 \cdot DL \cdot e_s}{T_i + 273.3} \cdot S_j \int ETp,j \qquad (2.5)$$

where *DL* is the potential daily daylight (dependent on time of year), e_s is the saturation vapour pressure, T_i is the mean daily temperature (°C) and S_j an empirical factor which describes the properties of the surface type *j*.

The calibration of this module is difficult due to limited observations at high-altitude. For this reason, the parameters are calibrated only once for this thesis, using values from the literature taken close to Rhonegletscher (Bernath, 1991). This is a reasonable assumption for this thesis since seasonal and annual changes, the outputs of interest, are negligibly impacted by changes to the runoff routing module, which has a greater impact at daily timescales.

The understanding of future evapotranspiration changes is very limited (Hagg et al., 2006). For example, although potential evapotranspiration will increase with rising temperatures, actual evapotranspiration is constrained by soil moisture which is influenced by the rate and frequency of precipitation, the future response of which is not clear and regionally variable (Collins et al., 2013). Moreover, the ongoing deglaciation of high-Alpine catchments combined with potentially rising vegetation-lines (Theurillat & Guisan, 2001), may increase the importance of evapotranspiration, further complicating future changes in evapotranspiration.

The method applied in GERM is an oversimplification of real-world processes, and reflects the typical approach taken in many glacio-hydrological models (e.g. Hagg et al., 2007; Horton et al., 2006; Immerzeel et al., 2013, 2012; Ragettli et al., 2015; Stahl and Moore, 2006). However, for high-alpine catchments, this simplification is justified for two reasons. Firstly, the current importance of evapotranspiration is negligible (Huss et al., 2008a) due to the limited vegetated surfaces in high-alpine catchments (Braun et al., 1994). Secondly, the very limited observations restrict the implementation of more advanced evapotranspiration schemes (Gurtz et al., 1999). In summary, future simulation of evapotranspiration in this thesis is necessarily simplistic but the implications of such simplicity are likely to be negligible for current conditions.

2.2.3.4. Runoff Routing.

This module represents the hydrological component of GERM that distributes water throughout glacial and non-glacial parts of the catchment. The runoff routing module, originally proposed in Huss et al. (2008), was developed further in Farinotti et al. (2012) and is based on linear reservoirs (e.g. Jansson et al., 2003; Langbein, 1958) incorporating the following surface types: ice, snow, rock, low vegetation (pasture), high vegetation (forest) and open water. The most detailed description of this module can be found in Farinotti et al. (2012), with a brief summary provided below, and a schematic in Figure 2.8.

The local water balance is solved at all grid cells:

$$Q_i = P_{liq,i} + M_i - ET_i - \sum_r \Delta v_{r,i} \tag{2.6}$$

where Q_i is the runoff at grid cell i, P_{liq} is liquid precipitation, M is melt from the ablation module, ET is evapotranspiration and ΔV is the storage change of the reservoir, r.

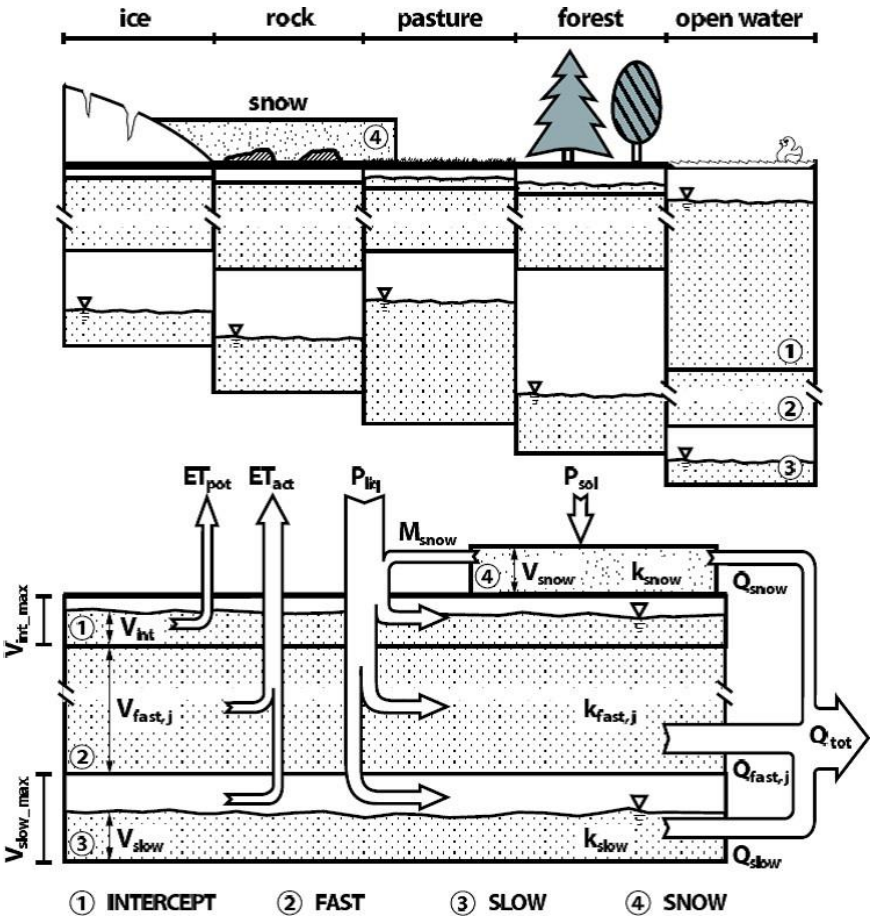

Figure 2.8: Schematic of the runoff routing module showing the different surface types in the top panel and the different reservoirs in the lower panel. Figure from Farinotti et al. (2012).

This module allows a hydrograph to be generated both for the entire catchment and for each individual surface type. There are four different types of storage included: interception reservoir, slow reservoir (groundwater), fast reservoir (soil-water discharge) and a separate reservoir for snow covered grid cells. The retention capacity of each surface type is adjustable and affects the fast reservoir. When snow is not present, three reservoirs (interception, fast and slow) are active. The interception reservoir represents the liquid precipitation and has a surface-type dependent capacity. If liquid precipitation exceeds the storage limit of the interception reservoir for a given storage type, the slow reservoir is filled depending on the filling rate of the slow reservoir. Any water not added to the slow reservoir is added to the fast reservoir representing direct and near-surface runoff components. The interception reservoir does not contribute to runoff but instead represents water that is available for evapotranspiration (ET), thus is emptied at the rate of potential evapotranspiration (PET). If the fill level of the interception reservoir is insufficient to satisfy the calculated PET, the difference is reduced to actual ET for that surface type and is subtracted from the fast reservoir. Solid precipitation is

treated separately to allow the build-up of snow when temperatures are below the melt-threshold temperature, with the snow reservoir only active once melting begins.

Emptying of the snow, fast and slow reservoirs uses a reservoir-dependent retention constant $k_{snow/fast/slow}$, which is surface type dependent for the fast reservoir. Thus, the contribution of grid cell *i* to discharge (Q_i) is calculated by:

$$Q_i = \sum_r V_{r,i}/k_r \tag{2.7}$$

where $V_{r,i}$ is the filling level of reservoir *r* at grid cell *i*. Open water is represented by grid cells with very large maximum capacities which corresponds to storing water in the cells and evaporating it with the potential evapotranspiration rate until the cell overflows. Finally, the total discharge from the catchment is computed by adding *Qi* for all grid cells.

Farinotti et al. (2012) developed this runoff routing module and tested the ability of the model to reproduce daily observed discharge in nine catchments in the Swiss Alps. The results (Figure 2.9) show that daily discharge is simulated well, with a Nash-Sutcliffe Efficiency (NSE; see Section 2.2.4.3 for details) of 0.78 ±0.21. Farinotti et al. (2012) also state that model performance improves with increased catchment glacierisation, suggesting that processes in less-glacierised catchments, for example groundwater storage, may less well represented. However, since this thesis will apply GERM to catchments with high levels (>30 %) of glacierisation, this limitation is minimal. Moreover, the reduced performance of GERM in less-glacierised catchments is limited to daily runoff, with monthly and annual discharge not affected. Since this thesis mainly concerns long time-scales, adequate performance on monthly time-scales is sufficient.

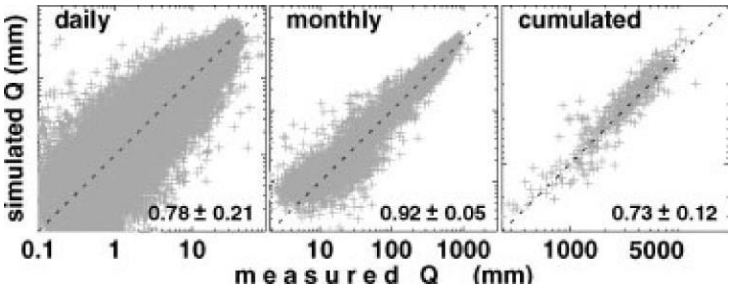

Figure 2.9: Observed vs. Simulated discharge in GERM for nine catchments in the Swiss Alps in the study of Farinotti et al. (2012). "Cumulated" discharge is calculated as the annual sum of daily discharge. Note, the y-scale is the same as x-scale. The lower-right corner of each plot shows the Nash-Sutcliffe Efficiency. Figure from Farinotti et al. (2012).

In terms of monthly and annual discharge, the studies employing GERM have consistently shown good representation of discharge during calibration and validation periods. For example,

simulated monthly discharge in Huss et al. (2014) produced a NSE of 0.89, Huss et al. (2008a) a NSE of 0.90, and Farinotti et al. (2012) a mean NSE of 0.92 across nine glaciers.

2.2.4. Application of GERM.

2.2.4.1. Calibration.

Statistically based temperature Index models, as for all empirical models, need to be calibrated to individual catchments in order to accurately simulate melt. The purpose of calibration is to identify the best fit between the parameters of the model and the observed glacier volume and runoff changes. This is no different in GERM, for which runoff and volume change data are used to obtain GERM's melt (f_m, r_{ice} *and* r_{snow}) and accumulation (c_{prec}, dP/dz) parameters.

Catchment specific calibration and validation are dictated by the availability of glaciological and hydrological data. In areas of abundant data, it is always recommended to use more than one data source for calibration (Huss et al., 2008; Schaefli & Huss, 2011). Model performance is maximised by applying multiple independent sources of calibration data, in this case glacier volume change and catchment runoff. The use of multiple independent datasets, obtained by different methods, minimises the likelihood of introduction of bias resulting from the sampling or measurement method (Pellicciotti et al., 2012; Huss et al., 2014). In addition, the use of volume change and runoff is more effective at calibrating the accumulation and ablation components of the model, as well as discharge from the non-glacial catchment, than either volume change or runoff alone (Ragettli & Pellicciotti, 2012).

In this thesis, the largely manual calibration methodology of Huss et al. (2008a), which has been implemented in all previous publications utilising GERM, is rejected in favour of an automated calibration procedure that systematically searches the parameter space and evaluates the results to find the optimum parameter set by combining the calculated error of glacier volume change and catchment runoff indicated by each set. This new, more repeatable and systematic method, which evaluates the performance of parameter combinations across a large parameter space, retains the model's portability but increases the transparency of the parameter choice method. The calibration procedure is explained in detail in 4.3.2 using Griesgletscher as an example.

This duration of calibration period used in this thesis (8-10 years) is typical of much of the literature (e.g. Gabbi et al., 2014; Horton et al., 2006), although some studies use shorter calibration periods (e.g. Finger et al., 2012). The duration of calibration has been shown to have an effect of the robustness of model parameterisation. For example, Huss et al. (2014) showed how longer calibration periods better constrain the relationship between temperature and glacier melt. Therefore, very long-term calibration periods appear to be the best option.

However, computational efficiency decreases with the number and duration of calibration simulations required. Therefore, the computational efficiency resulting from using the calibration periods in this thesis (8-10 years) allowed many repeat model runs thus ensuring calibration was rigorous.

2.2.4.2. Validation.

After GERM is calibrated to a specific catchment over a defined period, previous studies typically test the optimum parameter set by simulating a different period in the past. This process is hereafter referred to as "validation" and is vital to assess whether the calibrated parameters are representative of glacier and catchment behaviour, outside of the calibration period. As identified in the literature review (Section 1.2), many studies use a validation period that is of a similar length to calibration (e.g. Immerzeel et al., 2013; Finger et al., 2012; Schaefli et al., 2007). It has been argued that, while this is appropriate for short-term (e.g. 10 year) simulations, it will not adequately test the performance of the model if long-term future simulations (e.g. 2010-2100) that are the typical aim of most applications of GERM.

In this thesis, longer validation periods than any previous studies are used to test GERM in the past and assess the uncertainty of the simulations results. The rationale behind this is to assign this uncertainty to future simulations so that projections of future changes in glacier volume and catchment discharge are more realistic than existing studies.

2.2.4.3. Model Performance Indices.

To test the strength of the calibration parameters and to analyse results in the following chapters, a selection of statistical measures are employed alongside graphical measures (e.g. a hydrograph). A summary of the measures used in this thesis are provided here, while a full review of each measure and alternatives can be found in Krause et al. (2005).

Firstly, the coefficient of determination for multivariate scenarios, or R^2, is commonly employed in a large range of studies. It returns a dimensionless value between 0 and 1 where 1 represents optimum model performance. And can be calculated as:

$$\mathrm{r}^2 = \left(\frac{\sum_{t=1}^{T} (Q_o^t - \bar{Q}_o)(Q_m^t - \bar{Q}_m)}{\sqrt{\sum_{t=1}^{T} (Q_o^t - \bar{Q}_o)^2} \sqrt{\sum_{t=1}^{T} (Q_m^t - \bar{Q}_m)^2}} \right)^2 \quad (2.8)$$

where Q_o is observed discharge, Q_m is modelled discharge, Q_o^t is observed discharge at time t, and over-bars represent the mean of the respective variable. This measure can describe the proportion of variance within the observed data that is explained by the model. However, the main disadvantage is that it does not consider differences in the observed and simulated means so a model that produces the correct variance but a hugely incorrect mean can still produce an

r^2 of 1. In addition, r^2 is sensitive to outliers. Therefore, use of this measure for model validation should only be considered alongside other measures that can assess the accuracy of the mean.

The Nash-Sutcliffe Efficiency value, *NSE*, may be used to compare simulated and measured catchment discharge (Nash & Sutcliffe 1970) and is used in the calibration procedure of this thesis. This is commonly used to test the performance of hydrological models (e.g. Chen et al., 2011; Farinotti et al., 2012; Finger et al., 2012; Hock, 1999; Pellicciotti et al., 2005) and assesses the efficiency of models by comparing the modelled Q_m and observed Q_o discharge:

$$\mathrm{NSE} = 1 - \frac{\sum_{t=1}^{T}(Q_o^t - Q_m^t)^2}{\sum_{t=1}^{T}(Q_o^t - \overline{Q_o})^2} \tag{2.9}$$

where Q_o^t is the observed discharge at time *t.* This produces a dimensionless value where 1 represents perfect model performance. Compared to the commonly used or R^2, the NSE has advantages in that errors in both the simulated mean and variance will be penalised. However, the differences between simulated and observed values are calculated as squared values, leading to increased sensitivity to outlying data (Krause et al., 2005; Legates & McCabe Jr., 1999).

The Root Mean Square Error (RMSE) reveals the mean difference between modelled Q_m and observed Q_o discharge:

$$\mathrm{RMSE} = \sqrt{\frac{\sum_{t=1}^{n}(Q_m^t - Q_o^t)^2}{n}} \tag{2.10}$$

This is advantageous in that it retains the units of the original data so can be used to compare the magnitude of errors rather than only the model performance. Thus, RMSE values approaching zero represent better agreement between observations and predictions. However, similarly to R^2, a limitation is the large bias to outliers (Willmott et al., 2009). Finally, the absolute error is simply the difference between simulated and observed which is useful when the direction (i.e. positive or negative) of the bias is important.

Volume change error (VE), is used to assess the calibration of GERM throughout this thesis. Volume change is assessed according to the following equation, where VE is volume error, ΔV_{sim} is simulated volume change, and ΔV_{obs} is observed volume change over the simulation period:

$$\mathrm{VE} = 1 - \sqrt{\left(\frac{\Delta V_{sim} - \Delta V_{obs}}{\Delta V_{obs}}\right)^2} \tag{2.11}$$

2.3. Previous Applications of GERM.

It is clear that GERM can accurately reproduce runoff from highly glacierised basins of the European Alps, with Table 2.1 summarising examples of GERM in existing literature. The glaciers to which GERM has typically been applied are small to medium (length of 5–25 km) size mountain glaciers, generally debris-free, with abundant observations allowing accurate calibration. To date, Sorg et al. (2014), by applying GERM to the Tien Shen Mountains, Central Asia, represents the only application of GERM outside of the European Alps. The Δh method of glacier mass redistribution has several advantages over alternatives such as treating the glacier as static (e.g. HBV (Hydrologiska Byråns Vattenbalansavdelning) model: Akhtar et al., 2009; Hagg et al., 2007) or the AAR (Accumulation Area Ratio) method which is not mass-conserving (e.g. Horton et al., 2006, Paul et al., 2007). The main advantage is the accurate reproduction of ice volume changes and thus the amount of ice available for melt, without significantly increasing computation time compared to the HBV model or AAR method. Other methods may overestimate future runoff if glacier surfaces are treated as static (Junghans et al., 2015). Moreover the AAR method is not mass conserving so ice loss can occur without contributing to discharge. Further, Huss et al. (2014) demonstrated that the AAR method of Paul et al. (2007) systematically underestimates discharge by up to 30 % compared to the Δh approach, due to underestimated glacial area, likely related to the assumption of equilibrium with climate in the AAR method. However, there remain numerous shortcomings that can be grouped into application issues and model issues, which are outlined below.

Table 2.1: Previous studies that have used GERM.

Study	Glacier(s)	Calibration Data	Calibration Period	Validation Period	NSE (monthly)	NSE (annual)
Huss et al., 2008a	Zinal, CH	Volume Change, ELA, Discharge	1979-2006	1998-2006	0.9	not stated
Huss et al., 2008b	Various Swiss	Volume Change *2	NA	NA	NA	NA
Huss et al., 2010a	Rhone, Silvretta, CH	Volume change, MB	1957-2006	1957-2006	0.96	0.58
Huss et al., 2010b	20 in CH.	Volume change *2	NA	NA	0.88	not stated
Farinotti et al., 2012	9 in CH	Volume change, Winter MB	various	various	0.92	0.73
Finger et al., 2013	Plaine Morte, CH	Volume change	1956-2005	2010-2012	NA	NA
Huss et al., 2014*1	Findel, CH	Volume change, Winter MB	1982-2012		0.89	not stated
Sorg et al., 2014	Central Asia	Discharge, MB	1957-1998	not stated	NA	NA
Junghans et al., 2015	Silvretta, Rhone, CH	Discharge, MB	1975-2005	1975-2005	0.84	not stated

*1 Huss et al. (2014) use a variation of GERM that calculated melt according to the SEB model.
*2 GERM is re-calibrated for each DEM-period, thus reproducing observed MB.

2.3.1. Application Issues.

Firstly, although many studies run simulations from present to 2100, there remain very few studies that use equally long simulations in the past, for example, from 1900 to 2000. Where calibration and validation periods are very short, it is unlikely that the validation of the model is sufficient to fully cover the range of uncertainty associated with long-term future simulations. A key aim of this thesis is to address this omission and provide a thorough and realistic assessment of uncertainties, which can then be applied to future simulations and compared to other sources of uncertainty.

Secondly, GERM and similar models are mostly applied in areas with abundant data and understanding of glacier processes, e.g. the European Alps. There are significantly fewer studies of this type in regions where water resources are arguably more important, such as the Himalaya (Akhtar et al., 2008; Kehrwald et al., 2008; Bolch et al., 2012) and South American Andes (Bradley et al., 2006; Vuille et al., 2008). Due to climatological and glaciological differences in such other areas, it remains to be seen whether GERM can be applied elsewhere with similar competence. Therefore, this thesis will implement GERM in the Himalaya to assess its performance with limited data, its portability in application to different glaciological and climatological scenarios, and will implement modifications where necessary (see Chapter 6)

2.3.2. Model Issues.

Additionally, there are numerous methodological aspects of GERM that could be improved.

Firstly, the Δh parameterisation of glacier evolution is designed to reproduce patterns of glacier retreat according to observed glaciers of various sizes, without the computational and data intensive demands of fully dynamic ice flow models. Although the Δh parameterisation compares well to flow models, it cannot reproduce growth in glacier surface area limiting the models' application to areas of receding glaciers. Short term mass gains can be contained in a mass conserving way through glacier thickening, however, long-term advances would produce unrealistic thicknesses since surface area cannot increase. However, this limitation should not negatively impact model simulations of receding glaciers, and the Δh parameterisation has been shown to compare well to ice flow models during recession, therefore it is not addressed in this thesis.

Secondly, debris-covered ice is simply incorporated using a constant reduction factor to reduce ice melt. This does not account for varying thicknesses of debris or features of debris-covered ice such as ice cliffs and supraglacial lakes, both of which complicate the rate of ice melt (Miles et al., 2016; Steiner et al., 2015). Moreover, significant areas of debris cover on glaciers are often

manifestations of a reduction in ice dynamics preventing debris transport to the proglacial area (Quincey et al., 2009). Therefore, it is unlikely the Δh parameterisation would be as effective as for clean-ice glaciers since the patterns of mass loss can be very different. The impact of debris cover on glaciers and its incorporation into melt models is discussed in detail in Chapter 6, and modifications to the model are presented, in order to more accurately represent debris cover and its associated processes in to GERM.

Thirdly, evapotranspiration in GERM is based on simple empirical relations which remain relatively un-validated due to the difficulties of reliably measuring evaporation and how these will change in time (Hagg et al., 2006). However, evapotranspiration in highly glacierised catchments is not considered to be critically important, due to the relatively limited evaporation taking place at high altitudes (Braun et al., 1994) and the potential for net condensation on bare ice surfaces in summer (Lang et al., 1977; Bernath, 1991). Although warming temperatures, deglaciation and increasing vegetated surfaces in alpine catchments may increase the importance of evapotranspiration, this limitation of the model is not addressed in this thesis because it is considered of minor importance and little is known about future changes to evapotranspiration.

The lack of time-evolving parameters in GERM and temperature-index models in general, remains a considerable limitation. For example, the melt factor applicable under current climatic conditions at current ice extents is unlikely to be applicable in the future, if climatic conditions and the hypsometry of ice has changed (Hock, 2003). However, the temporal variability in melt-factors remain a major uncertainty in the use of temperature-index melt models due to the difficulty of prescribing a changing melt factor with any physical basis.

2.4. Summary and Relevance.

This chapter has described how GERM calculates glacio-hydrological changes in alpine catchments, as well as a selection of its previous applications. Clearly, GERM is a capable model that has been implemented successfully in many studies. However, opportunities for further development of GERM that would enable more repeatable, robust, transparent and portable applications of GERM were identified in Chapter 1. Many of these developments will be addressed in later chapters:

Chapter 3 will identify and apply a state-of-the-art dynamical-statistical downscaling methodology to climate model data, to provide a wide range of inputs for future simulations of GERM.

Chapters 4 and 5 will apply GERM to catchments in the European Alps, challenging model performance and quantifying uncertainties by using longer validation periods than previous studies, before applying this uncertainty to future simulations, using a range of climate scenarios and more sophisticated climate downscaling approaches than previous studies. This will enable both the uncertainty associated with GERM, and the climate input uncertainty, to be evaluated.

Chapters 6 and 7 will then apply the model in another region, the Nepalese Himalaya, developing modifications that allow the unique glaciological setting of the Khumbu Glacier to be modelled in GERM, thus enhancing the portable nature of GERM and identifying where future research should focus.

3. BIAS CORRECTION AND FUTURE CLIMATE PROJECTIONS.

This chapter introduces the methods for downscaling climate model outputs that are required to provide future projections of temperature and precipitation for sites in the European Alps and Himalaya. These projections will be used to drive GERM simulations of future glacier and runoff evolution in Chapters 5 and 7. Climate model data are compared with observations of temperature and precipitation in the past and bias-correction is applied. These estimates will be used to drive GERM in the following chapters to simulate the *future* glacier and runoff evolution of the Griesgletscher, Rhonegletscher and Khumbu catchments. This chapter addresses Aim 2a/b.

3.1 Introduction.

The literature review provided background information on climate models, emissions scenarios, external forcings, and internal forcings (Section 1.3.1), so these are not repeated here. The literature review also highlighted the scale mismatch between GCMs, RCMs, and catchment scale studies, which means further downscaling of climate model outputs is essential. Therefore, this section will focus on the downscaling.

3.1.1 The Necessity for Downscaling GCM Simulations of Temperature and Precipitation.

Direct utilisation of GCM outputs without prior correction in impact studies introduces significant errors and biases (Sharma et al., 2007; Piani et al., 2010; Kotlarski et al., 2014; Jakob Themeßl et al., 2011; Themeßl et al., 2012). Typical errors include a bias in the temperature and precipitation mean, underestimation of the number of dry days which lead to an overestimation of 'drizzle' days, and underestimation of high precipitation events (Boberg et al., 2007), thus impacting the full range of variability of both temperature and precipitation in the simulations (Piani et al., 2010). These errors are mainly caused by inadequate spatial resolution which prevents representation of sub-grid scale processes (Hay et al., 2000). This is particularly true in mountainous regions where the complex orography leads to highly heterogeneous climate phenomena (Whiteman, 2000). Moreover, the orography of GCM and RCM simulations is also limited by grid-size so it is important to ensure that model grid elevation is considered as part of the correction process. For example, Kotlarski et al. (2010) found that the maximum elevation of the RCM surface representing the Alps was 2870 m, only marginally higher than the mean ELA for glaciers in the Alps of 2700 m (WGMS, 2015) and considerable lower than the highest peak, Mont Blanc, at 4809 m. Therefore, it is essential that both GCM and RCM outputs are compared

to in-situ data and downscaling applied where necessary. This chapter will discuss downscaling approaches before describing how bias-correction (the method of downscaling chosen for this thesis) was undertaken, and the challenges associated with bias-correction in this thesis.

3.1.2 Review of Downscaling Methodologies.

The purpose of this section is to provide a brief outline of the most common downscaling techniques applied to climate data for use in glacier melt and runoff studies. There are several reviews of downscaling techniques in the climatology literature, for example, Maraun et al. (2010), Fowler et al. (2007), Teutschbein and Seibert (2012) and Salathe et al. (2007). Downscaling methodologies can be divided into dynamical downscaling and statistical downscaling.

3.1.2.1 Dynamical Downscaling.

Dynamical Downscaling is the process of nesting a RCM inside a GCM, to try to resolve the issue of coarse GCM spatial resolution (typically 1° to >3°). The GCM is used to provide boundary conditions for the RCM (typical resolution of <0.5°), thus better capturing the complex atmospheric processes of mountainous regions. In recent years, RCMs have been applied in large-scale, coordinated configurations where a wide range of GCM-RCM combinations are conducted for different regions of the Earth. The advantage of this 'model-chain' or ensemble approach is that the multiple model runs increase the reliability of projections and the mean of all model-chains has been shown to be better than any single-model projection (e.g. Doblas-Reyes et al., 2003; Palmer et al., 2005; Yun et al., 2003), therefore representing the most probable outcome (Tebaldi & Knutti, 2007). Previous coordinated modelling projects include PRUDENCE (Christensen et al., 2002) and ENSEMBLES (Van der Linden & Mitchell 2009), with the most recent project, CORDEX (Coordinated Regional climate Downscaling Experiment; Giorgi et al., 2009), representing the state-of-the-art.

The CORDEX ensemble uses CMIP5 GCMs as boundary conditions. The CORDEX project uses multiple model runs, each utilising different model-chains to increase the reliability of projections. This methodology is aimed to be applied consistently across all regions allowing studies to reliably compare impacts across different regions.

3.1.2.1.1 Types of CORDEX Simulations.

There are several different types of RCM simulations conducted under the CORDEX guidelines. Firstly, *historical simulations*, also known as hind-cast simulations, are GCM-RCM chains that simulate past climate, in order to assess how well the model reproduces externally forced climate changes. In historical simulations, the RCM is forced by the outputs from the driving

GCM as boundary conditions, therefore internal and external variability are prescribed by the GCM with no real-world link. GCMs are capable of accurately simulating the effects of external forcings (Houghton, 2009). However, GCMs cannot be expected to reproduce the timing of internal variability with the same accuracy due to the inherently stochastic nature of internal variability, a reflection of the complex, non-linear relationships between the atmosphere and ocean, for example (Houghton, 2009). As such, historical simulations should accurately simulate long-term changes caused by external forcings, but are not expected to predict the *timing* of internal variability, although they should aim to reproduce the magnitude of internal variability.

The second type of simulation conducted under the CORDEX guidelines are *evaluation simulations*. These differ from historical simulations in that the boundary conditions that force the RCM are reanalysis datasets which are constrained by observations, rather than a GCM as is the case for historical simulations. In the example of the CORDEX framework, the reanalysis data set used to force RCMs is ERA-Interim (Dee et al., 2011), which assimilates meteorological observations, for example temperature and precipitation, into a climate model to produce a global, sub-daily resolution dataset of gridded climate variables. Forcing RCMs with reanalysis data means that they inherently incorporate both internal and external variability in the climate system, simply because they are based on observations. Therefore, the timing and magnitude of internal variability can be expected to be accurate, a key difference to historical simulations.

Finally, *future simulations* are the third type of simulation conducted within the CORDEX framework. Future simulations run from 2010-2100 and use the same model-chain as historical simulations, whereby the boundary conditions of the RCM are forced by the GCM. In order to simulate the effects of external climate forcings, GCMs are forced using the RCPs described in Section 1.3.1 producing a number of scenarios for future climate. Future simulations initiate from the end-point of the historical simulation, rather than the evaluation simulations, which is important for the statistical downscaling process used here. Additionally, the forcing of the RCM with the GCM means that both historical and future simulations inherit both GCM error (e.g. inadequate representation of the Indian monsoon – see Turner and Annamalai, 2012) and RCM error (e.g. inadequate representation of topography, or incorrect lapse rates). In comparison, evaluation simulations contain only RCM and reanalysis data error (Kotlarski et al., 2014).

3.1.2.2 Statistical Downscaling.

Statistical downscaling, as outlined above, is the process of statistically translating GCM or RCM outputs onto fine scale or point scale observations (Maraun et al., 2010). This practice is particularly important in mountainous regions due to the high spatial variability in temperature and precipitation induced by the complex topography. Statistical downscaling is advantageous

in that it is computationally efficient in comparison to dynamical downscaling, i.e. the use of RCMs. However, accurate constraint of the statistical relation requires long-term observational data. Additionally, a key assumption of statistical downscaling is that the statistical relationship from the observational period remains the same in the future (Fowler et al., 2007). The combined use of dynamical downscaling (i.e. CORDEX RCM simulations) and statistical downscaling (i.e. the methods used in this chapter) incorporates the benefits of both these approaches (Yoon et al., 2012; Vrac et al., 2012). For example, Guyennon et al. (2013) found that because dynamical downscaling is physically based, it captures the non-stationarity of local climate, thus compensating for the stationary statistical connection between model and observations in statistical downscaling. Moreover, Guyennon et al. (2013) recommends that statistical downscaling is also essential in addition to dynamical downscaling in order to produce reliable results at the local scale. This suggests that the two approaches complement each other. In this thesis, the combination of these approaches is achieved by using CORDEX model data to provide the dynamical downscaling, and the bias correction approach described in Section 3.1.2.3 to provide the statistical downscaling.

The next section will consider approaches for the statistical downscaling, providing a brief overview of each method before describing the methods used this thesis in detail in the following section.

3.1.2.2.1 Delta-change Approach.

This approach is commonly applied to hydrological and glaciological studies (e.g. hydrological: Andréasson et al., (2004); Graham et al., (2007a, 2007b); Shabalova et al., (2003); e.g. glaciological: Akhtar et al., (2008); Chen et al., (2011); Farinotti et al., (2012); Gabbi et al., (2012); Jouvet et al., (2011); Sorg et al., (2014)) and provides a computationally efficient, simple method to improve simulations. Essentially, differences between simulated and observed variables are used to calculate scaling factors, which are then applied to the rest of the time-series for which observations are not available. However, this method has several issues particularly relevant to precipitation correction. Firstly, change factors only adjust the mean of variables, so changes to the distribution are unaccounted for. Secondly, precipitation corrections do not adjust the number of wet-days, which are typically overestimated in both RCM and GCM simulations (Boberg et al., 2007; Piani et al., 2010). Finally, this method assumes the bias between GCM and observation is constant through time (Fowler et al., 2007). Despite Harrold and Jones (2003) improving the representation of wet day frequency, more complex statistical downscaling methods show superior performance.

3.1.2.2.2 Quantile Mapping approach.

The quantile mapping approach, developed in Piani et al. (2010), is able to consider not only the mean, but also the variability, yet remains computationally efficient and has therefore been widely applied in hydrological studies (e.g. Bennett et al., (2011); Boé et al., (2007); Finger et al., (2012); Guyennon et al., (2013); Themeßl et al., (2011); Salerno et al., (2015)). This approach matches the intensity distributions of simulations to those of the observations. Thus, this methodology provides a time-series that is constrained by the observations in terms of variability and starting temperature/precipitation, but follows the trend of the RCM. Importantly, by adjusting the variability of precipitation as well as the mean, the quantile mapping approach removes the overestimation of low-frequency rainfall, or drizzle, which is commonly overestimated by RCMs. The main disadvantage of this approach is that it removes the physical basis of the RCM and thus assumes that current bias is representative of future bias.

Although there are several alternative techniques that are variations on the aforementioned methodologies, and more advanced techniques such as weather typing (e.g. Fowler et al., 2000, 2005) and weather generators (e.g. Dubrovský et al., 2004), quantile mapping shows similar performance to these other methodologies (Guyennon et al., 2013; Fowler et al., 2007).

3.1.2.3 Downscaling Approach in this Thesis.

This thesis will implement a combined dynamical-statistical downscaling approach, where the CORDEX GCM-RCM simulations represent the dynamical downscaling component, and the quantile mapping methodology represents the statistical downscaling component. CORDEX is chosen as it represents the state-of-the-art in dynamical downscaling, provides a range of model outputs which allow multiple model runs, and applies the same framework in both the Alps and South Asia, allowing comparison of the results. Quantile mapping statistical downscaling is implemented as it retains the computationally efficient nature of the delta-change approach, but crucially adjusts for both the distribution and the mean of temperature and precipitation bias. Therefore, this combined dynamical-statistical approach should improve on the approach taken in many glacio-hydrological studies, and ensure that climatological model inputs are as robust as possible.

3.2 Climate Model and In-Situ Data Availability.

This section will outline the range of CORDEX GCM-RCM combinations available in both the Alps and the Himalaya. It will also outline available observations of temperature and precipitation, required in order to calculate the bias in the RCMs for the quantile mapping statistical downscaling. The quantile mapping approach requires that *evaluation* and *historical* simulations

are both available, as explained in Section 3.1.2.1.1. Since data availability differs between the sites in the Alps and Khumbu, this section will treat these regions separately.

Table 3.1: Meteorological data used for the bias correction of CORDEX data. *full duration of meteorological data could not be used in the Alps since overlap with evaluation simulations from CORDEX is required to constrain the statistical downscaling.

Site	Data Type	Data Source	Duration	Resolution
Griesgletscher	Meteorological	Begert et al., (2005) & Schwarb et al., (2001)	1884-2010*	Daily
Rhonegletscher	Meteorological		1874-2010*	Daily
Khumbu	Meteorological	Salerno et al., (2015)	1994-2013	Daily

3.2.1 Climate Data at Griesgletscher and Rhonegletscher, European Alps.

3.2.1.1 Observations of Temperature and Precipitation.

Although the European Alps contain a relatively dense meteorological monitoring network, meteorological stations close to the study glaciers are limited in terms of long-term records. Thus, for the bias-correction, observed data comprise the temperature and precipitation time-series described fully in Section 4.3.1.2, based on the datasets of Begert et al. (2005) and Schwarb et al. (2001), and provided by Matthias Huss (Table 3.1). These provide daily temperature and precipitation time-series by which the statistical-downscaling can be constrained. Since these data are used for simulations of the past glacier and runoff evolution in Chapter 4, using these as a basis for bias-correction allows consistency with future simulations.

3.2.1.2 Availability of CORDEX-Europe Climate Model Outputs.

The decision to utilise RCM simulations under the CORDEX experiment was justified in that these models represent the state-of-the-art in dynamical downscaling of the most recent CMIP5 GCM simulations. However, the availability of CORDEX outputs during the period of study was hampered by the availability of the Earth System Grid Federation (ESGF), the only data portal through which CORDEX data are available, which was taken offline on 18/06/2015 (P. Dwarakanath, 2015, personal communication). As such, gaining CORDEX simulations proved extremely difficult with accessibility only possible through direct liaison with staff at specific modelling centres. This lack of efficiency combined with high demand for CORDEX simulations limited the number of models implemented in this thesis. Table 3.2 summarises the models that

are used in this thesis in the Alps, representing all the available simulations that included evaluation simulations at the time of analysis.

Table 3.2: Available RCM-GCM combinations that include evaluation simulations in the CORDEX-Europe domain. RMSE is calculated based on annual temperature (°C) or precipitation (mm yr^{-1}).

	Model (RCM)	Driving GCM	RCPs Available		
			2.6	4.5	8.5
A	RCA4	ICHEC-EC-EARTH	✓	✓	✓
B	RCA4	CERFACS-CNRM	×	✓	✓
C	RACMO	MOHC-HadGEM2	×	✓	✓
D	CCLM	ICHEC-EC-EARTH	×	✓	✓
E	HIRHAM	ICHEC-EC-EARTH	✓	✓	✓

3.2.1.3 Initial Bias Between Observations and Simulations in the Alps.

Figure 3.1 clearly shows that, although RCM performance is reasonable, bias-correction of simulated temperature and precipitation is required, with the observations of temperature and precipitation occasionally falling outside the simulations of the RCMs. At Griesgletscher, both temperature and precipitation are relatively well simulated by the multi-model ensemble, but individual RCMs contain clear bias. At Rhonegletscher, precipitation is very poorly simulated by the HIRHAM RCM which strongly over-estimates precipitation. This is potentially due to high levels of parameterisation in processes that influence precipitation in the RCM (e.g. clouds, convection, land surface-atmosphere interactions), that lead to inadequate precipitation simulation (Kotlarski et al. 2014; IPCC Chapter 9, 2013).

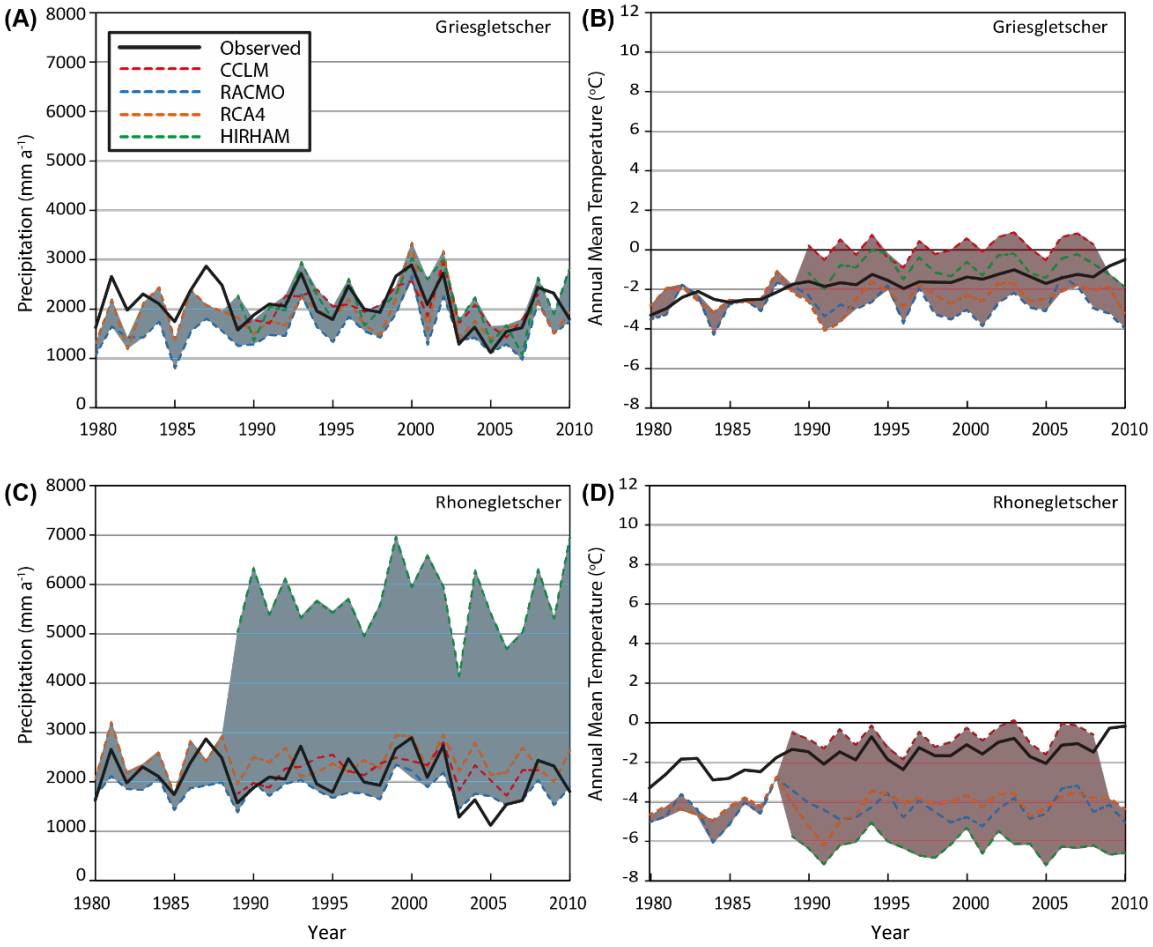

Figure 3.1: Time-series of precipitation and temperature comparing the 4 evaluation simulations of CORDEX to observations. Panels (a) and (b) are at Griesgletscher, panels (c) and (d) are at Rhonegletscher. Coloured bands represent the range of RCM data. The models used are detailed in Table 3.2.

3.2.2 Data at Khumbu Glacier, Nepal.

3.2.2.1 Observations of Temperature and Precipitation.

Himalayan glaciers are situated at such high, remote elevations that widespread monitoring is understandably sparse. Meteorological stations that do exist are difficult to maintain resulting in a lack of observations in High-Mountain Asia (Andermann et al., 2011; Salerno et al., 2015). The combination of limited monitoring and the most extreme topography on Earth results in a limited understanding of climatological processes. For example, how far the reach of the Indian Monsoon extends inland and how this may change in the future (Christensen et al., 2013; Sperber et al., 2013; Lal & Harasawa, 2001). In particular, precipitation is very poorly understood due to the difficulty of accurately observing winter precipitation at high altitude (Immerzeel et al., 2015) owing to significant wind-redistribution which results in gauge undercatch (Yang et al., 1998).

Khumbu Glacier represents one of the most accessible and best observed glaciers in the Himalayan region. Khumbu is located on the South-West slopes of Mount Everest and the most popular 'South Col' route to the summit follows Khumbu closely, as does the popular Everest Base-Camp trek (Figure 6.2, Section 6.2). Because of this, Khumbu Glacier has infrastructure in place enabling access which has resulted in relatively long-term meteorological monitoring, making Khumbu an ideal test-bed for Himalayan glaciology.

The Pyramid Observatory, located just to the West of Khumbu Glacier (Figure 6.2; 5050 m a.s.l.; 27° 57' 32.5" N, 86° 48' 47.6" E), managed jointly by the Ev-K2-CNR-SHARE (Stations at High Altitude for Research on the Environment) and the Nepal Academy of Science and Technology (NAST), provides meteorological observations from 1994-2013. For this thesis, daily temperature and precipitation are used, as well as snow-depth and wind-speed, which are used for the gauge-undercatch correction.

3.2.2.1.1 Processing the Observational Data at Khumbu.

Unlike the sites in the European Alps, the relatively short duration of the dataset from the Pyramid meteorological station (20 years) combined with the limited knowledge of precipitation in High-Mountain Asia, means that further processing was necessary to ensure observational input data are as accurate as possible. The first step in the process is infilling the gaps in the Pyramid dataset. This was done by Salerno et al. (2015) and is described in detail in Section 6.2.1. Although continuous observations are desirable, this approach provides the next-best option.

To further process this data, a correction for precipitation gauge-undercatch is applied, which is fully explained in Section 6.2.2.1, using the methodology of Yang et al. (1998). Although this is the best available observational dataset for the region, and represents an unprecedented continuous time-series considering the remote, high-altitude catchment, there remain considerable uncertainties, particularly in terms of precipitation, which may affect the bias correction.

3.2.2.2 Availability of CORDEX-South Asia Climate Model Outputs.

As explained for the Alps, the lack of access to many CORDEX simulations limited the range of projections available. However, CORDEX-South Asia is at a less advanced stage than CORDEX-Europe, and the modelling centres responsible for CORDEX-South Asia simulations have followed the CORDEX guidelines less stringently. As such, there are very few simulations in South Asia that include the evaluation simulation, essential to the quantile mapping approach applied in this thesis. Specifically, three RCMs included evaluation simulations: RegCM4, REMO, and

RCA4. However, RegCM4 only conducted future simulations to 2050, therefore this was discounted, leaving two model combinations (Table 3.3). Although these provide a range of estimates of future climate, it is encouraged that more models are implemented in the future as more CORDEX-South Asia outputs are made available, to fully constrain uncertainty associated with different models.

Table 3.3: Available RCM-GCM combinations that include evaluation simulations in the CORDEX-South Asia domain.

	Model (RCM)	Driving GCM	RCPs Available			Organisation
			2.6	4.5	8.5	
A	RCA4	ICHEC-EC-EARTH	✓	✓	✓	SMHI
B	REMO	Nor-ESM	✗	✓	✓	GERICS

3.2.2.3 Initial Bias Between Observations and Simulations at Khumbu.

Figure 3.2 shows a comparison between observed and simulated temperature and precipitation at Khumbu, clearly showing a much larger bias than the Alps. In terms of annual precipitation, both REMO and RCA4 overestimate precipitation but RCA4 shows the largest bias, overestimating by a factor of 4 to 10. For temperature, both models perform equally badly, with simulated temperatures much cooler than observed temperatures. To ensure that this bias was not a unique feature of the RCM grid-square over Khumbu, an alternative method of extracting the data from netcdf files was tested where the mean of 9 surrounding grid squares was used, as suggested by Eden et al. (2014). However, the large bias remained, showing that the bias is representative of the RCM as a whole (not shown). Such large biases demonstrate the importance of careful bias correction in mountainous regions and necessitate the use of the quantile mapping methodology outline below (or equivalent).

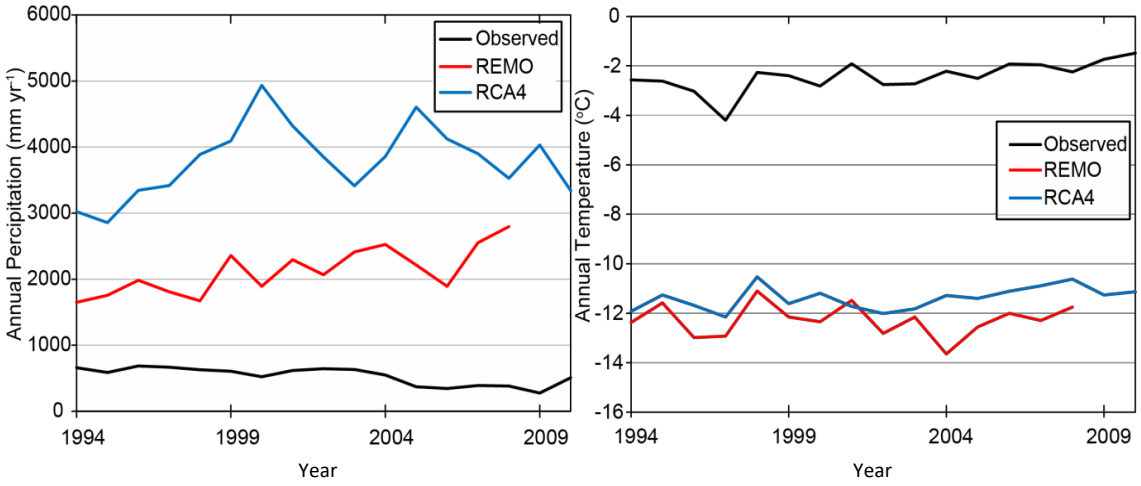

Figure 3.2: Time-series of (a) precipitation and (b) temperature comparing the REMO and RCA4 evaluation simulations of CORDEX to observations at Khumbu, showing large errors for both precipitation and temperature. All time-series are smoothed exponentially with alpha of 0.3.

3.3 Quantile Mapping Methodology.

The quantile mapping technique (a type of statistical downscaling) of Piani et al. (2010) is implemented as it adjusts both the mean and variability of simulated data (Bennett et al., 2011; Ines & Hansen, 2006), and removes 'drizzle' days (e.g. Olsson et al., 2013; Teutschbein and Seibert, 2012), as described earlier. Therefore, this will provide a dataset that is more realistic in comparison to observations compared to the original RCM data, but the future trends will be determined by the modelled scenarios of the GCM.

In this correction, the statistical relationship between observations and simulations is calculated based on the *evaluation* simulation (1980-2010 for the Alps; 1994-2010 for Khumbu). This relationship is then applied to the future simulations, with the results used to drive GERM in subsequent chapters. The use of evaluation simulations is important due to the more accurate representation of the timing and magnitude of internal variability, in comparison to historical simulations. If historical simulations were used to constrain the statistical relationship instead, there is a risk that the relationship would be partially calculated to out-of-phase temporal variability, therefore over- or under-estimating the bias, depending on the timing of internal variability.

The correction for precipitation assumes that both the observed and simulated distributions are described by the gamma distribution, whereas the correction for temperature assumes a normal distribution. For precipitation corrections, the monthly Cumulative Distribution Functions (CDFs) and the number of dry days of the simulated and observed variables are calculated. To calculate the parameters of the CDFs for precipitation, the 'gamfit', 'gamcdf' and 'gaminv' Matlab functions (see details of the Matlab functions at: Mathworks, Inc., 2018a) are used to ensure the approach is systematic. For temperature, the 'normfit', 'normcdf' and 'norminv' Matlab functions are used (Mathworks, Inc., 2018b). These functions are applied to both observed and simulated data. A transfer function, *y=f(x)*, where y is corrected precipitation and x is simulated precipitation, is then calculated as:

$$cdf_{obs}(f(x)) = cdf_{sim}(x) \tag{3.1}$$

This can then be used to apply the difference between the distributions to future precipitation data series, with the shift in the mean and standard deviation, defined by the distribution change, governed by the observations. The annual number of dry days in simulated data is taken as the average annual number of dry days in the observations. For temperature, the same approach is taken except the shape of the distribution used to calculate the CDF is normal. To remove the overestimation of drizzle from simulated precipitation, the number of wet days in the simulations are matched to the number of wet days in the observations. This is done by

obtaining the percentile containing all observed dry days and using the same percentile to define a threshold below which simulated values are reset to zero, therefore ensuring the simulated and observed number of wet days are the same (Olsson et al., 2013).

In summary, the quantile mapping methodology is applied to RCMs, using the evaluation simulation to constrain the bias between simulations and observations in the past, before applying the correction to the future simulations.

3.3.1 Revisions to the Methodology.

Initial testing of the statistical downscaling revealed an issue that required revisions to the quantile mapping methodology proposed in the literature. This issue is described here as well as the alterations to the methodology that are used in the rest of this chapter. The problem only affects correction of temperature, the precipitation time-series are corrected using the original methodology.

3.3.1.1 Issue of 'Offset' in the Bias Correction.

This section will describe the issue identified using the example at Khumbu where RCA4 RCM was corrected using the observations at Pyramid.

After the quantile mapping was applied at Khumbu, it became apparent that there was an offset between the mean of the corrected time-series in the past and the future, as shown in Figure 3.3. Clearly, if the bias-corrected future time-series is to be used to drive GERM in the future, the mean of the bias-correction time-series must initiate from the mean of the observations, forming a continuous time-series from the past (calibration period) to the future. This offset, however, means that if calibrated to BC-evaluation temperatures, the climatic sensitivity of the model will be different (by up to 1.5°C) when future simulations are conducted, for example.

The cause of this offset lies in the fact that evaluation simulations are forced by reanalysis data, whereas future simulations are forced by GCMs. As clearly indicated in Figure 3.3, there is a considerable difference between the temperature simulated by the evaluation compared to historical and future simulations during the overlap period. Therefore, when applying the correction constrained by evaluation data, the corrected future series is not adjusted sufficiently to be in-line with observations.

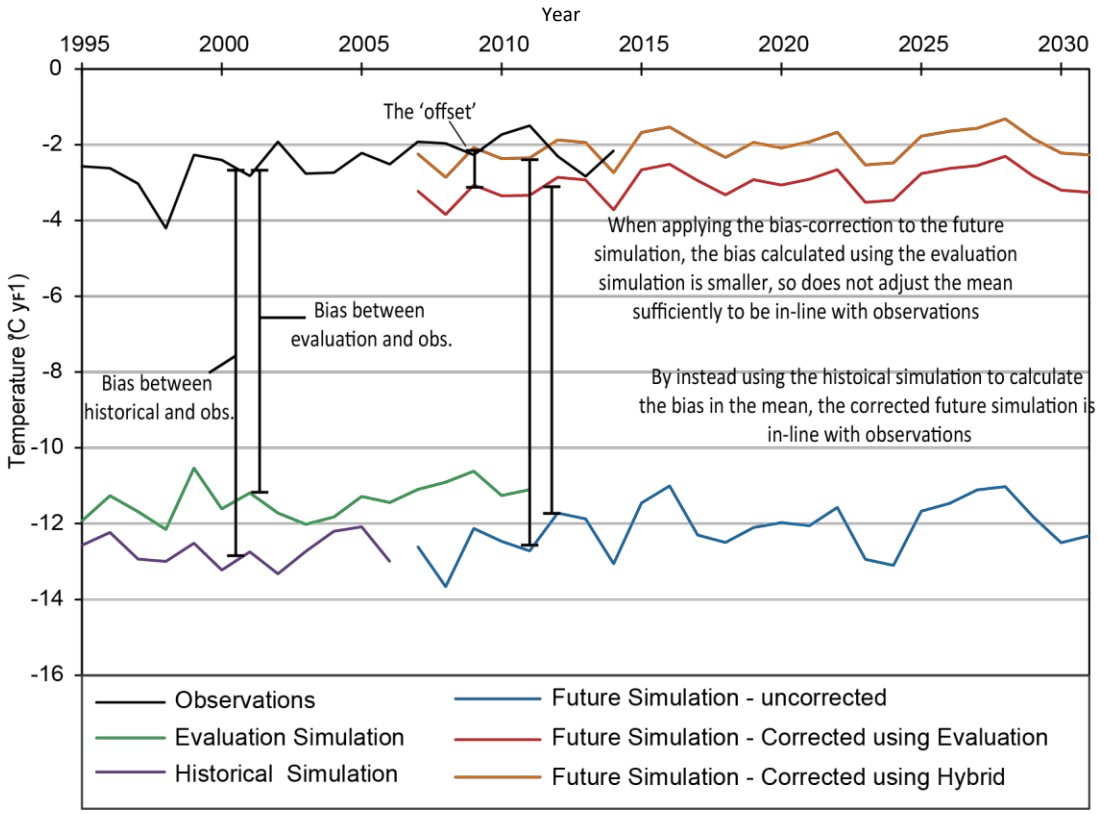

Figure 3.3: Temperature at Khumbu demonstrating the offset between the future time-series corrected using the evaluation simulation to constrain the quantile-mapping, and the observations of temperature. Also included are the historical time-series and the hybrid-correction adopted in this thesis.

3.3.1.2 Revised Quantile Mapping Approach.

Identification and discussion of the issue of offset between evaluation and historical simulations in the literature is very limited, with only Widmann (M. Widmann 2016, personal communication) and Kotlarski (S. Kotlarski 2014, personal communication) having also identified this issue but no full resolution has been offered. Such a lack of discussion in the literature means a pragmatic solution is offered here, whereby a "hybrid-correction" combining use of the historical *and* evaluation bias correction parameters. This thesis proposes that the mean of the historical simulation is used for the mean adjustment, thereby adjusting sufficiently to reproduce mean temperatures similar to the observations at the start of the simulations, but the variability (standard deviation) of the evaluation data set is used, since this most accurately reproduces observed conditions. The results of this modification are shown in Figure 3.3 as the "Future Simulation – Corrected using Hybrid".

To reiterate, precipitation is unaffected by this offset, which suggests that evaluation and historical simulations show good agreement, allowing the original methodology to be utilised. A

full explanation of the issues of "offset" and the implications of this solution is discussed in Section 3.5.4.

3.3.2 Evaluating the Success of the Bias-Correction.

To ensure the bias correction is robust, the corrections were performed using an independent cross-validation approach. The time-series of observations and simulations were divided into two with the first half of the time-series (e.g. 1994-2002 at Khumbu; 1980-1985 in the Alps) treated as 'training' data and the second half (e.g. 2003-2010 at Khumbu; 1986-2010 in the Alps) treated as 'validation'. The training period was used to calculate the parameters of the distribution transfer function (see Section 3.3, page 54, for details) which were applied to the independent validation period. This process was then reversed with the training period becoming the validation period and the results compared to ensure the correction functioned over periods with no observations. The results of this are shown in Section 3.4.2, with the RMSE and absolute error used to quantify performance. Additionally, the start of the melt season in each series was calculated as the first period of consecutive warm days (T>0°) lasting more than five days. This indicates if the correction is accurately reproducing conditions that cause the onset of melt. For precipitation, the number of dry days per year is used to assess the performance of the bias correction to accurately reproduce rainfall frequency and remove the drizzle that impacts RCM simulations.

3.4 Results of Bias Correction.

This section will present the outputs of the bias correction procedure at Griesgletscher, Rhonegletscher, and Khumbu Glacier, employing the original methodology (using evaluation to constrain the correction parameters) for precipitation and the modified methodology (using historical to constrain the *mean* correction parameters) for temperature. First, the bias-correction is applied to the simulations in the past in order to evaluate its success compared to observed data, before applying the bias-correction to future projections.

3.4.1 Bias-Correction of CORDEX RCMs in the Past.

Figure 3.4 shows the Cumulative Distribution Functions (CDFs) of simulated, observed, and corrected daily temperature and precipitation at Griesgletscher and Rhonegletscher, using the five GCM-RCM combinations available, from 1980-2006. For Khumbu, the CDFs are shown in Figure 3.5, using the two GCM-RCM combinations available. These CDFs cover the period over which the statistical relationship between observations and simulations are constrained, which is assessed here before applying the bias-correction to the future projections.

At Griesgletscher, there are small differences between the simulated and observed temperature with RCMs such as CCLM-ICHEC performing well. The corrected CDFs show an improvement in performance for all climate-model combinations. In terms of precipitation, the HIRHAM model requires the most correction with simulated precipitation suggesting a very high probability of low-intensity rainfall events and too few higher-intensity events.

The CDFs at Rhonegletscher (Figure 3.4) show that temperature and precipitation simulated by the CORDEX RCMs contain more bias than at Griesgletscher. For temperature, all models except CCLM underestimate annual temperature, a bias which is successfully corrected by the quantile mapping approach. In terms of precipitation, there is again more of a bias than at Griesgletscher, particularly for HIRHAM, which is also successfully corrected.

At Khumbu (Figure 3.5), the results of the bias correction show the significant changes in the CDFs of both precipitation and temperature, with the corrected CDF showing a much closer match to the observated CDF. The extent of this change, which is a considerably larger correction thatn in the Alps, reflects the very large initial bias at Khumbu (Figure 3.2). Such significant bias underlines the poor performance of models in the Himalaya and the importance of bias-correction to provide estimates of temperature and precipitaiton that are closer to reality than those from raw model outputs.

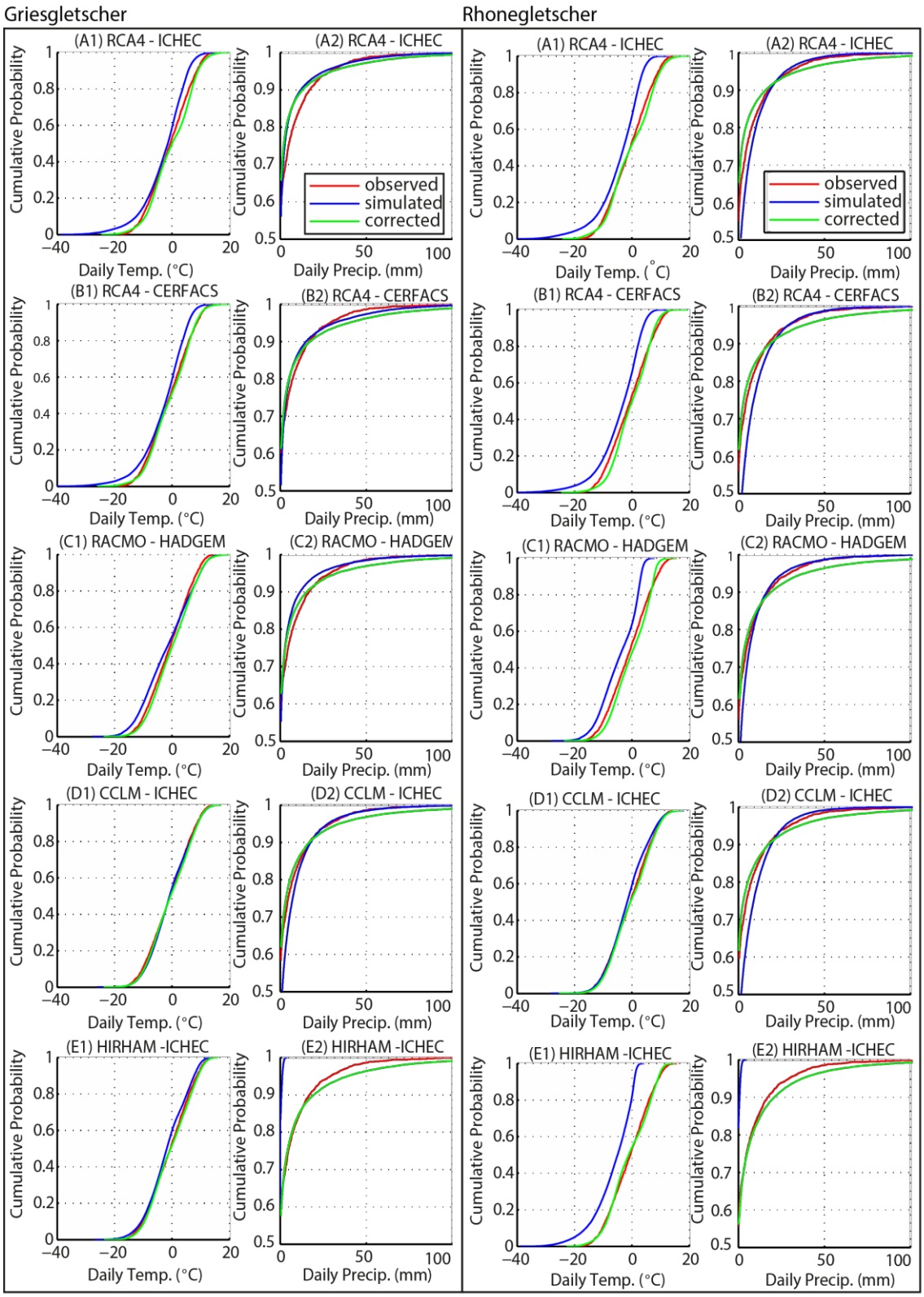

Figure 3.4: CDFs of observed (1980-2010), simulated (1980-2006), and corrected (1980-2006) temperature and precipitation at Griesgletscher (left) and Rhonegletscher (right). Note the axes for precipitation are different.

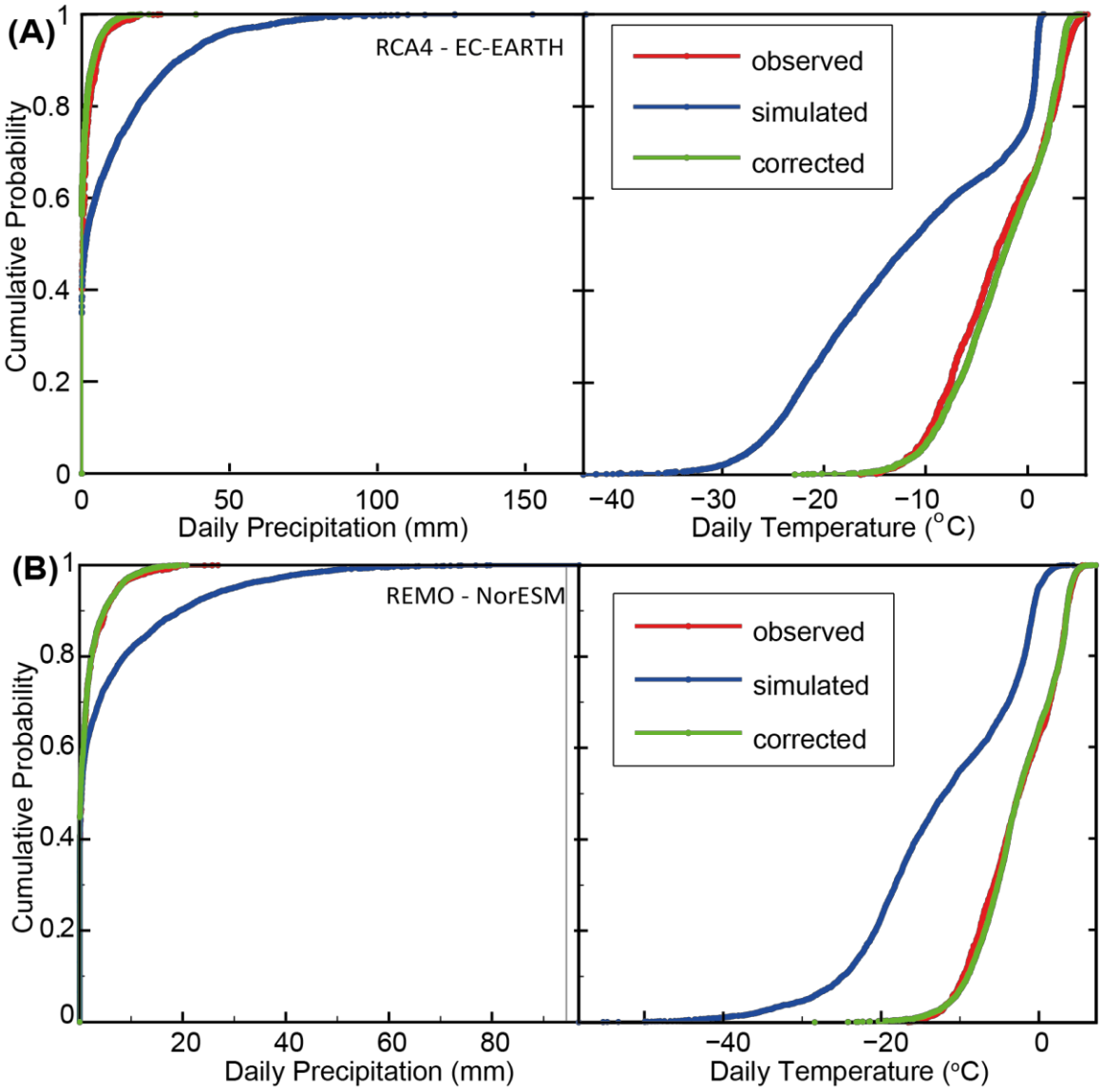

Figure 3.5: CDFs of simulated, observed and corrected precipitation and temperature for the two GCM-RCM combinations available at Khumbu: (A) RCA4-EC-EARTH; (B) REMO-NorESM. Note the x-axes differ between the two models.

3.4.2 Cross-Validation of the Bias-Correction.

Before this correction can be applied to future simulations, the independent cross-validation (described in Section 3.3.2) of bias-corrected time-series is conducted to assess how well the quantile mapping method is correcting the time-series. Tables 3.4, 3.5, and 3.6 show the evaluation metrics for Griesgletscher, Rhonegletscher, and Khumbu Glacier, respectively. All metrics are calculated using independent data (i.e. there is no overlap between the calibration and validation periods), so are deemed representative of the performance when future simulations are corrected.

Clearly, there is a considerable improvement following bias correction at both sites in the Alps, with smaller RMSE and absolute errors in all cases. The corrected time-series also more accurately reproduces the number of dry days per year and the onset of the melt season. At Khumbu (Table 3.6), the bias-correction shows much larger improvements, owing to the larger initial bias.

Finally, it is important to ensure that seasonal changes are adequately corrected to capture the increase in temperatures in summer and any seasonal sifts in precipitation. Figure 3.6 shows the shift in temperature and precipitation that is applied by the bias correction, considerably improving simulated temperature and precipitation at both sites in the Alps, and dramatically improving the seasonal pattern of temperature and precipitation at Khumbu. In particular, precipitation during the Indian Monsoon (July – September) is much closer to observations with the non-corrected simulations suggesting precipitation would be several orders of magnitude too high.

Table 3.4: Evaluation of the performance of the bias correction "BC" in comparison to the original simulation "sim" and observations, for 5 RCMs at Griesgletscher. Metrics were calculated using the independent cross-validation period, and calculated on annual means. Also included are the number of dry days per year and the onset of the melt season, defined as the first period of consecutive warm days (T>0°) lasting more than five days.

			A	B	C	D	E
RMSE	Pr (mm)	Sim	2.1	1.7	2.2	1.9	2.4
		BC	1.1	1.1	1.9	1.2	0.8
	TAS (°C)	Sim	3.2	2.7	2.0	0.8	1.4
		BC	0.9	0.7	0.6	0.7	0.8
Absolute Error	Pr (mm)	Sim	-1.1	-0.3	-1.5	0.6	1.8
		BC	0.3	-0.2	0.1	0.3	-0.1
	TAS (°C)	Sim	-3.0	-2.5	-1.9	-0.1	-1.2
		BC	0.0	0.0	0.1	-0.1	0.0
Number of Dry days per year		Obs			251		
		Sim	126	104	68	77	110
		BC	246	246	251	249	245
Start of melt season (day of year)		Obs			129		
		Sim	161	157	140	144	152
		BC	121	130	128	127	132

Table 3.5: Evaluation metrics for Rhonegletscher. See caption of Table 3.4 for details.

			A	B	C	D	E
RMSE	Pr (mm)	Sim	1.6	1.6	1.5	1.3	10.1
		BC	1.4	1.3	1.9	1.2	1.6
	TAS (°C)	Sim	2.8	2.8	3.0	0.7	4.5
		BC	0.6	0.6	0.6	0.2	0.4
Absolute Error	Pr (mm)	Sim	0.2	1.0	-0.6	0.5	10
		BC	0.4	0.4	0.5	0.3	0.2
	TAS (°C)	Sim	-2.8	-2.7	-3.0	0.7	-4.7
		BC	-0.2	-0.2	-0.2	-0.1	0.1
Number of Dry days per year		Obs			251		
		Sim	128	84	49	92	72
		BC	240	240	241	249	242
Start of melt season (day of year)		Obs			129		
		Sim	163	156	140	145	156
		BC	121	130	127	129	135

Table 3.6: Evaluation metrics for Khumbu. See caption of Table 3.4 for details.

			RCA4	REMO
RMSE	Pr (mm)	Sim	8.9	5.1
		BC	0.8	1.6
	TAS (°C)	Sim	5.1	10.7
		BC	1.0	1.7
Absolute Error	Pr (mm)	Sim	9.3	4.0
		BC	0.4	-0.1
	TAS (°C)	Sim	-9.1	-9.7
		BC	0.0	0.1
Number of Dry days per year		Obs	165	
			165	
		Sim	143	262
		BC	197	201
Start of melt season (day of year)		Obs	138	
			138	
		Sim	166	188
		BC	134	140

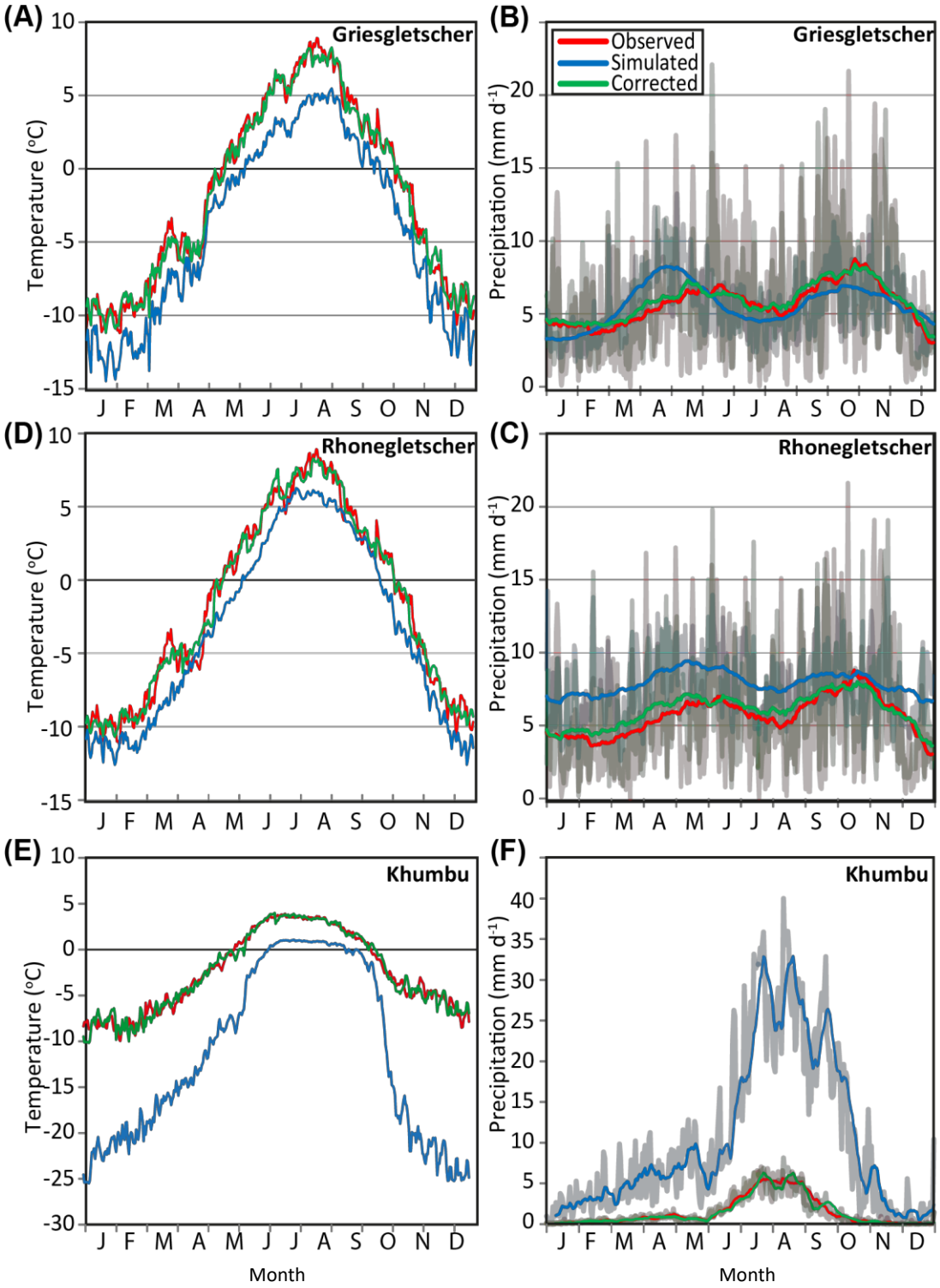

Figure 3.6: Seasonal temperature and precipitation at Griesgletscher (top), Rhonegletscher (middle), and Khumbu (lower) showing the improved representation of the seasonal cycles. Khumbu, in particular, shows dramatic improvement. Temperature data are daily means whereas precipitation is shown as 30-day running mean as well as daily means. Plots calculated using the mean of all simulations (5 for Alps, 2 for Khumbu) from 1980-2006. Note the y-axes on (E) and (F) differ to (A), (B), (C) and (D).

3.4.3 Corrected Future Projections at Griesgletscher.

The trends (calculated over 2010-2100) in the bias-corrected future RCM projections at Griesgletscher are shown in Figure 3.7 and the time-series in Figure 3.8. For temperature, significant positive trends ($p<0.01$) are shown in all but one projection (A-RCP 2.6), with RCP 8.5 projecting a greater increase in temperature than RCP 4.5, and with RCP 2.6 projecting only small temperature increases by 2100. For RCP 8.5, temperature is increasing through the 21st century whereas RCP 4.5 shows a curtailing of temperature increases after 2080 (e.g. D1-CCLIM-ICHEC-EC-EARTH), indicative of the stabilising of radiative forcing prescribed in the RCP 4.5 scenario (see Figure 1.1). The extent of the difference in temperature between the RCPs varies between different model combinations. For example, climate model combination A (RCA4-ICHEC-EC-EARTH) projects a 3.7°C difference between RCP 4.5 and 8.5 in the period 2090-2100, compared to 2.4°C in E (HIRHAM-ICEHEC-EC-EARTH). This is interesting since both these model combinations are forced by the same GCM, ICHEC-EC-EARTH, so this difference must relate to the different RCMs.

In terms of precipitation, the projected changes are much less clear with only one significantly positive trend (B-8.5), and no consistent patterns among the different RCP scenarios. However, there is consensus among climate model combinations that a positive trend is projected, with only model combination C-4.5 suggesting a negative trend. These meagre trends suggest there will be some increase in precipitation associated with warmer air temperatures, but this is not significant ($p<0.01$) in all but one projection. Despite less clear trends, there are notable differences in the mean of different climate model combinations, with A (RCA4-ICHEC-EC-EARTH) showing a lower level of precipitation than E (HIRHAM-ICHEC-EC-EARTH), for example. Additionally, there are differences in the magnitude of decadal-scale variability. For example, C (RACMO-HadGEM) shows considerable variability, particularly from 2060-2080, compared to B (RCA4-CERFACS) which shows smaller variations. Such differences may be caused by the representation of internal climate variability in the driving GCM and RCM.

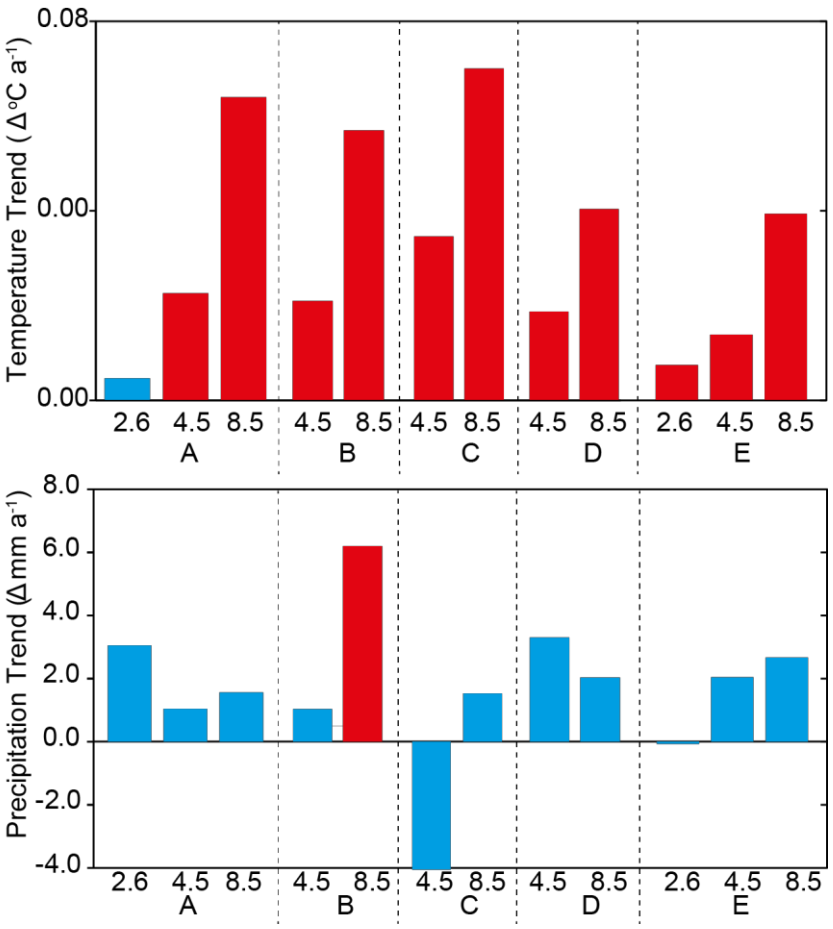

Figure 3.7: Future temperature and precipitation trends at Griesgletscher for 5 GCM/RCM combinations. Trends calculated using Mann-Kendall test from 2010-2100 and significance ($p<0.01$) indicated with red bars. Blue bars are insignificant trends ($p<0.01$). A-E refer to the combinations of GCM-RCM models, as detailed in Table 3.2.

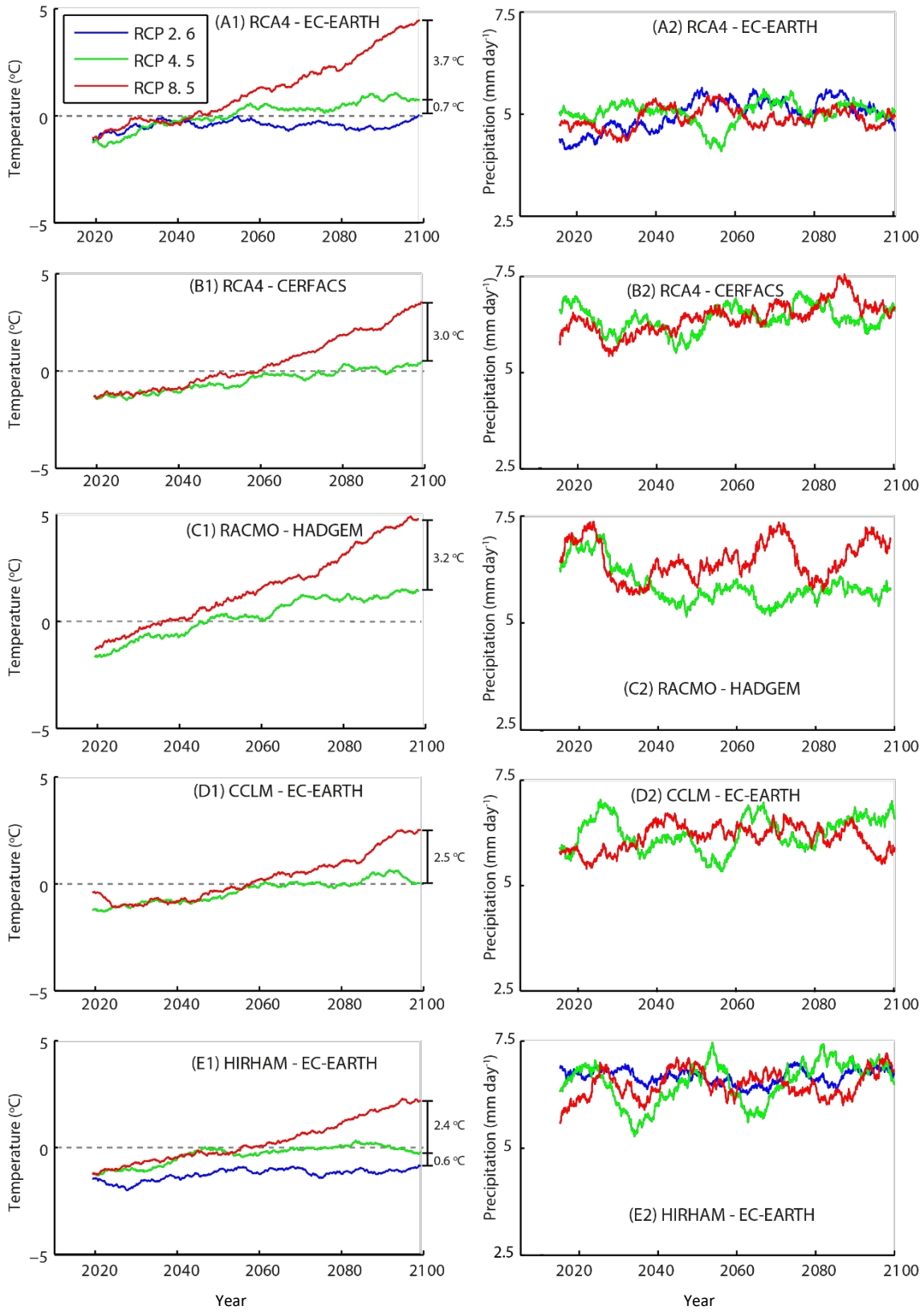

Figure 3.8: Annual mean temperature and precipitation at Griesgletscher for 5 GCM/RCM combinations (10 year moving averages). The numbers between the end-points of temperature time-series represent the difference between the final 10 years of each RCP.

3.4.4 Corrected Future Projections at Rhonegletscher.

The time-series of bias-corrected future RCM projections at Rhonegletscher are shown as trends (2010-2100) in Figure 3.9 and time-series in Figure 3.10. The patterns of change are similar to Griesgletscher, not surprising considering the GCM-RCM combinations are the same, so this section will describe any differences between the projections at the two sites.

In terms of temperature, the projections are similar with consistent positive trends (significant at $p<0.01$), with RCP 8.5 again showing continuous temperature increases whereas RCPs 4.5 and 2.6 show initial positive trends before curtailing later in the 21st century. However, at Rhonegletscher, the differences between the RCPs in each GCM-RCM combination are smaller than at Griesgletscher. For example, climate-model combination A (RCA4-EC-EARTH) projects a difference of 3.4°C between RCP 4.5 and 8.5, compared to 3.7°C at Griesgletscher, a feature that is consistent across all GCM-RCM combinations.

In terms of precipitation, the projections are again similar to Griesgletscher. However, there are some interesting features that are not projected at Griesgletscher. For example, GCM-RCM combination B (RCA4-CERFACS) shows a strong divergence between RCP 4.5 and 8.5 after 2080, resulting in a significantly positive trend ($p<0.01$) for RCP 8.5 and no significant trend for RCP 4.5. Another feature relating to RCP 8.5 is clear in climate model combinations C and E, both of which project an increase in precipitation from 2070-2080, a feature not projected for RCP 4.5, likely caused by external forcing or purely coincidental.

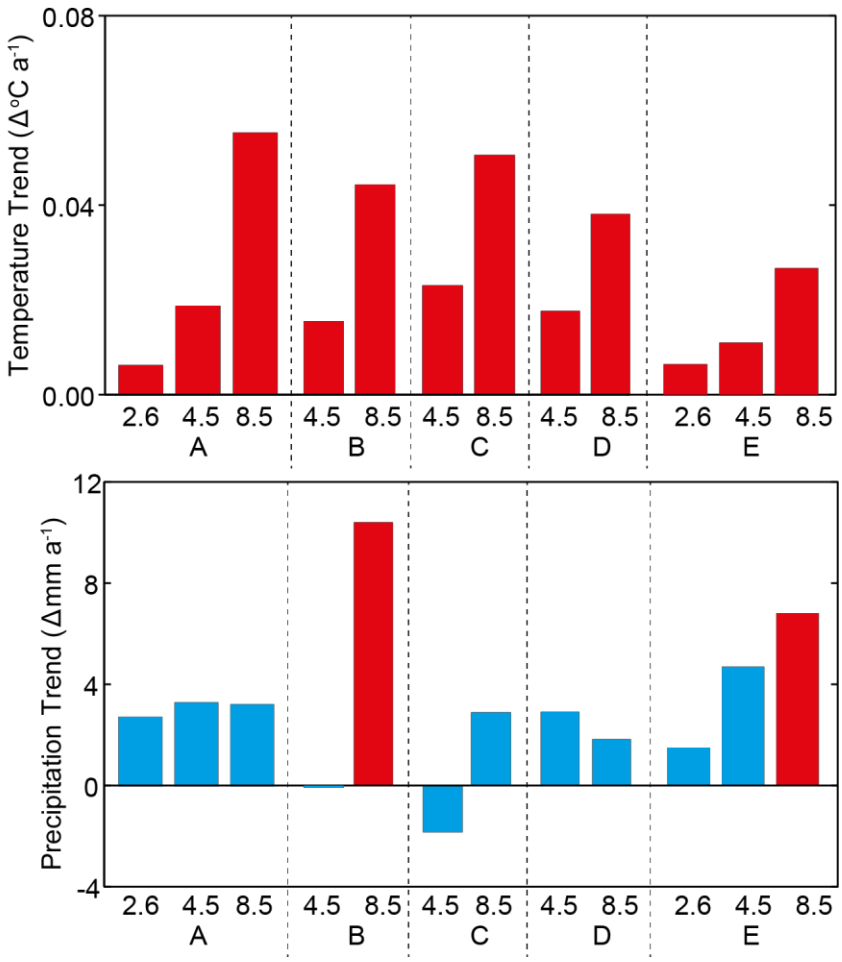

Figure 3.9: Future temperature and precipitation trends at Rhonegletscher for 5 GCM/RCM combinations. Trends calculated over 2010-2100 using Mann-Kendall test and significance indicated with red bars. Blue bars are insignificant trends (p>0.01). A-E refer to the combinations of GCM-RCM models, as detailed in Table 3.3.

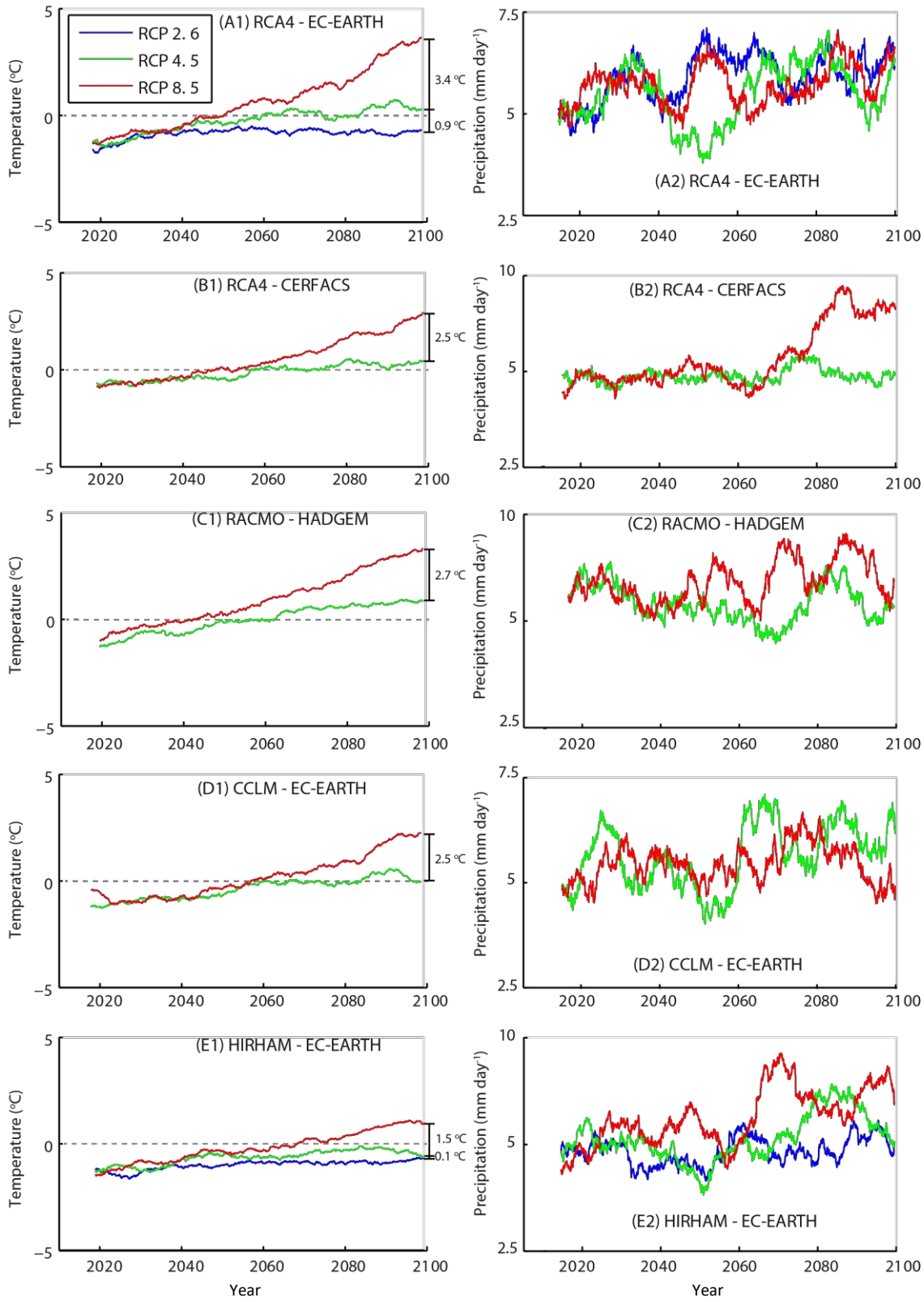

Figure 3.10: Annual mean temperature and precipitation at Rhonegletscher for 5 GCM/RCM combinations (10 year moving averages). The numbers between the end-points of temperature time-series represent the difference between the final 10 years of each RCP. Note, y-axes differs on precipitation plots.

3.4.5 Corrected Future Projections at Khumbu.

The bias-corrected future RCM projections at Khumbu are shown as trends (calculated over 2010-2100) in Figure 3.11 and time-series in Figure 3.12.

Projections of temperature changes at Khumbu are broadly similar to the Alps in terms of consistently positive trends ($p<0.01$), however, the magnitude of temperature increases are smaller at Khumbu. For example, the largest positive trend projected at Khumbu by GCM-RCM B-8.5 (REMO-NorESM) is 0.036°C yr^{-1}, compared to the highest trend of 0.7°C yr^{-1} at Griesgletscher. Similarly to the Alps, RCP 8.5 projections show continual temperature increases throughout the 21st century whereas RCP 4.5 projections curtail around 2075, and RCP 2.6 shows only a small positive temperature trend (insignificant at $p<0.01$). There are also differences in the magnitude of decadal variability between the GCM-RCM combinations with A-4.5 projecting large decadal temperature variations (e.g. 2045-2060), which are not shown by B-4.5.

In terms of precipitation, there are differing projections among the two GCM-RCM combinations, with A (RCA4-EC-EARTH) projecting negative trends in precipitation which increase with the magnitude of warming. However, GCM-RCM combination B (REMO-NorESM) projects a significant positive precipitation trend for RCP 4.5 and an insignificant negative trend for RCP 8.5 ($p<0.01$).

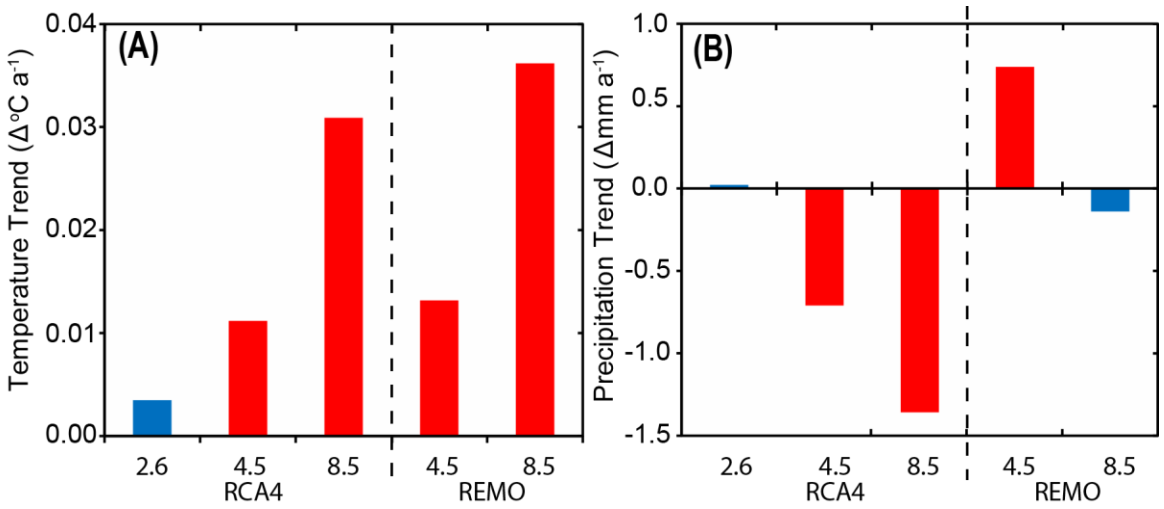

Figure 3.11: (A) Future temperature and (B) precipitation trends at Khumbu for RCA4-EC-EARTH and REMO-NorESM models. Trends calculated from 2010-2100 using Mann-Kendall test and significance indicated with red bars. Blue bars are insignificant trends ($p>0.01$).

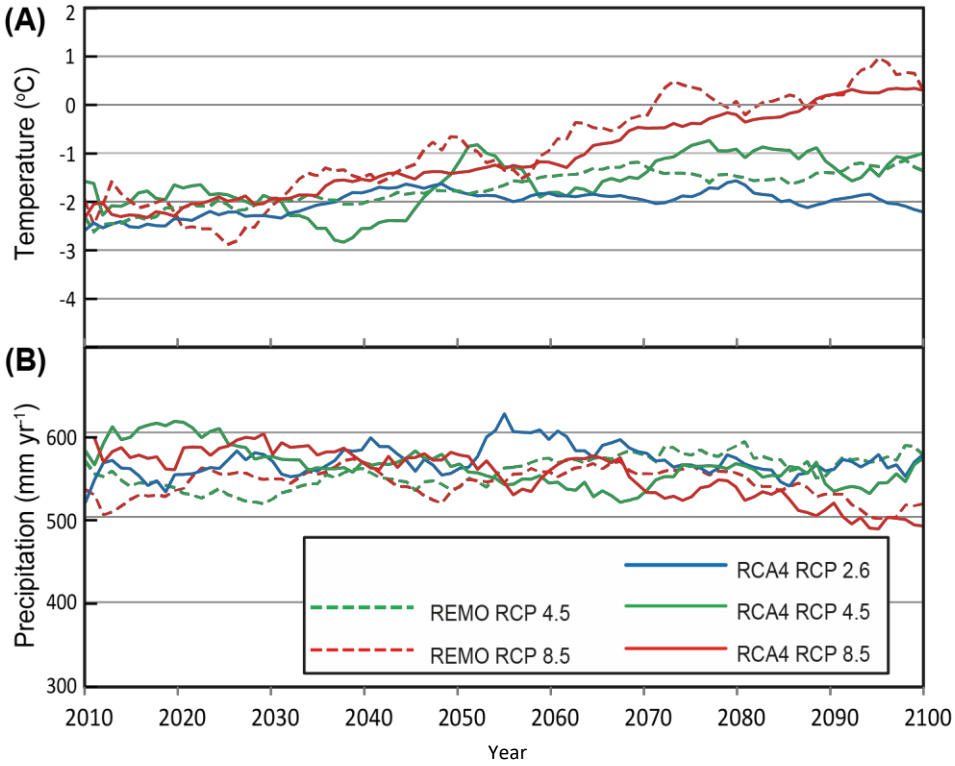

Figure 3.12: Bias corrected future projections of temperature and precipitation at Khumbu using the RCA4-EC-EARTH and REMO-NorESM RCM-GCM combinations.

3.5 Discussion and Implications.

The statistical-dynamical downscaling process described and performed in this chapter provides a range of future climate scenarios which can be used to drive GERM from 2010-2100. These scenarios utilise state-of-the-art dynamical-downscaling by using RCMs (from the CORDEX project) together with an advanced statistical downscaling method to ensure that the time-series are as close to reality as possible. However, there are limitations involved in some parts of this process, including the availability of CORDEX outputs and the offset that was identified preventing widespread use of evaluation simulations when correcting temperature. This section will discuss the issues encountered in this chapter and how the outputs can be used.

3.5.1 Summarising the Projections in the Alps and at Khumbu.

The projections of temperature and precipitation changes are relatively consistent across Griesgletscher and Rhonegletscher, but there are large differences at Khumbu, particularly in terms of the magnitude of temperature increases. At Griesgletscher, the temperature increases range from 0.45°C (A-2.6) to 6.3°C (C-8.5). However, at Khumbu, although warming trends are significant, temperature increases range from 0.25°C (A-2.6) to 3.25°C (B-8.5) over the period 2010-2100. These differences in the projections should be considered when interpreting future

glacio-hydrological changes. In terms of precipitation, at both sites in the Alps and at Khumbu, precipitation changes are typically not consistent across different GCM-RCM combinations and across different RCP scenarios. The lack of consistent precipitation trends has been noted in other studies (e.g. Pellicciotti et al., 2014; Rajczak et al., 2013; Immerzeel et al., 2013; Li et al., 2016) and will be discussed in detail in Section 8.1.1.1.

A key aspect of precipitation in the Himalaya pertains to the Indian Monsoon. The initial performance of the GCM-RCM combinations was very poor at Khumbu Glacier (Figure 3.2), with both the RCA4-EC-EARTH model and the REMO-NorESM model strongly overestimating precipitation. The reasons for such poor representation of precipitation lies in the highly spatially variable orographic rainfall processes (Isotta et al., 2014) that RCMs are not capable of resolving due to their limited spatial resolution (e.g. Immerzeel et al., 2012), and the representation of the Indian monsoon in the driving GCM. For example, Salerno et al. (2015) suggests that the monsoon has lost the majority of its humidity over 3000 m, yet the models used in this thesis show highly overestimated precipitation during the monsoon period (July-September). This suggests that the climate models in this thesis are overestimating the reach of the monsoon. A more thorough discussion of the influence of the monsoon and its representation in climate models will be provided in Section 8.1.1.1.

3.5.2 Understanding of Precipitation in High-Mountain Catchments.

The complex changes in precipitation with altitude in mountain regions are a further factor that RCMs may struggle to reproduce. For example, Salerno et al. (2015) showed that precipitation lapse rates are highly variable below 3500 m, whereas precipitation lapse rates are very small above 3500 m. RCMs are not capable of resolving such complex variability with elevation resulting in overestimation of precipitation, a widespread limitation of RCMs in mountainous regions (Behera & Yamagata, 2015). Another issue relating to precipitation at Khumbu is the recent negative trend observed by Salerno et al. (2015), shown in Figure 3.13, with considerably lower precipitation after 2003. If this trend continues into the future, glacier accumulation will be continually reduced. However, the five GCM-RCM combinations (Figure 3.12) do not agree on a strong negative trend in precipitation until after 2040 (although two combinations show some negative trends before then – see Figure 3.12), and the statistical downscaling process used in this thesis does not capture this trend in the corrected projections. Moreover, it is not known whether this trend is indicative of the long-term trend or is caused by short-term internal-variability in the climate system and the lack of a dense meteorological network makes it difficult to corroborate this trend elsewhere. Therein lies a key issue of precipitation at high-altitude; the difficulty in conducting observations, caused by limited access and the difficulties

in measuring solid precipitation (Yang et al., 1998), means that long-term observations are lacking. Thus, the level of understanding of these very complex, highly variable processes is limited and this limitation is passed onto climate models. Although it is outside the context of this thesis to address these issues, it is important to emphasise that precipitation is poorly understood in high-mountain catchments, particularly the Himalaya.

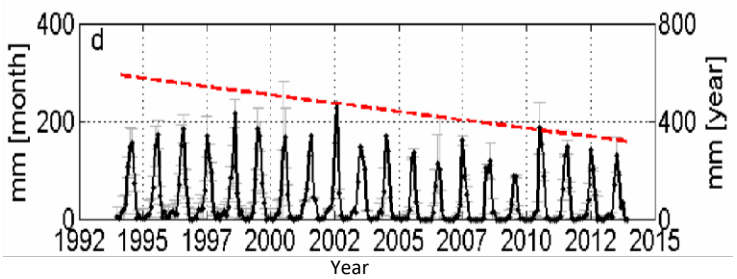

Figure 3.13: Monthly precipitation (black) and linear trend in annual precipitation (red) at the Pyramid station. Figure from Salerno et al. (2015).

3.5.3 Availability of Regional Climate Model Simulations.

The re-organisation of the ESGF servers during the analysis of this study considerably limited the number of GCM-RCM combinations available. Part of the rationale for using CORDEX simulations was the increased awareness of uncertainties allowed by a large range of GCM-RCM model combinations and RCP scenarios. Due to the restricted available data, this uncertainty assessment is more limited. However, the availability of five model combinations for RCPs 4.5 and 8.5 gives a good assessment of RCP scenario uncertainty. Similarly, the RCA4 RCM is forced by two different GCMs, EC-EARTH and CERFACS, giving an indication of the influence that different GCMs have. Finally, EC-EARTH is used to drive three of the GCMs, RCA4, CCLM, and RACMO, providing a reasonable assessment of the uncertainty associated with different RCMs.

However, despite the aforementioned issues, the projections of future climate that will drive GERM from 2010-2100, have been carefully and thoroughly bias-corrected using all available meteorological data, the most recent GCM-RCM combinations, and advanced statistical downscaling methods, allowing the future glacier and hydrological changes to be assessed. The bias correction presented here therefore represents the state-of-the-art in terms of glaciological studies. Although more COREDEX simulations would have enabled greater assessment of uncertainties relating the different GCM-RCM combinations, the projections available still represent a good portion of this uncertainty and the number of projections is comparable to other studies of future glacio-hydrological evolution (Pellicciotti et al., 2014).

3.5.4 Historical vs. Evaluation Simulations when Constraining Bias-Correction Parameters.

The most problematic issue in this chapter relates to the choice of historical or evaluation simulation of the past when constraining the bias-correction to observations. The "best-practice" amongst the downscaling literature is to use the evaluation simulations (Maraun et al., 2010). However, there are clearly issues with the use of evaluation simulations when the study requires continuous, homogeneous time-series from the past (calibration period) to the future (simulation periods), manifested here as the "offset" between BC-evaluation simulations and BC-future simulations. This section will explore this issue in more detail, first looking at the source of this problem in the wider context of climate modelling, before considering the validity of the "hybrid" approach suggested for this thesis.

To understand the source of the offset, we must first consider what climate models are attempting to simulate.

External Forcing. Firstly, the GCM must simulate the effect of **external** climate forcings such as solar irradiance, greenhouse gas concentrations, volcanic forcing etc. This externally forced variability will provide the long-term trends in warming predicted over the 21st century, for example. The RCM will then incorporate the climate response to these external forcings as it is forced by the GCM in the case of historical simulations, or forced by observations in the form of reanalysis in the case of evaluation simulations.

Internal Variability. Secondly, the GCM must simulate **internal** variability in the climate system, caused by interaction between the various components of the Earth system (atmosphere, oceans, cryosphere). For example, the troposphere responds to forcings quickly (days), the stratosphere more slowly (weeks to months) and the ocean even slower (decades to centuries; McGuffie & Henderson-Sellers, 2005). Such varied response times and non-linear relationships dictate that the various components are constantly changing and interacting with each other, thus equilibrium is never reached (McGuffie & Henderson-Sellers, 2005). This is internal variability in the climate system, examples of which include the ENSO and the NAO. In terms of downscaling of climate models, the internal variability is the key difference between evaluation and historical simulations. Specifically, evaluation simulations inherently include internal variability accurately since they are forced by real-world observations. However, historical simulations incorporate internal variability through GCM/RCM reproduction of inherently unpredictable processes. If the GCM and RCM perform well, the magnitude of internal variability may be close to reality; however, the timings of the internal variability cannot reproduce reality because of the highly varied response times of the components. Thus, historical simulations

cannot accurately predict the timings of internal variability in the climate system. This can be demonstrated using the non-corrected data at Griesgletscher in Figure 3.14, clearly demonstrating that although the historical simulations are not always worse in terms of the mean or magnitude of variability, the timing of this variability is incorrect.

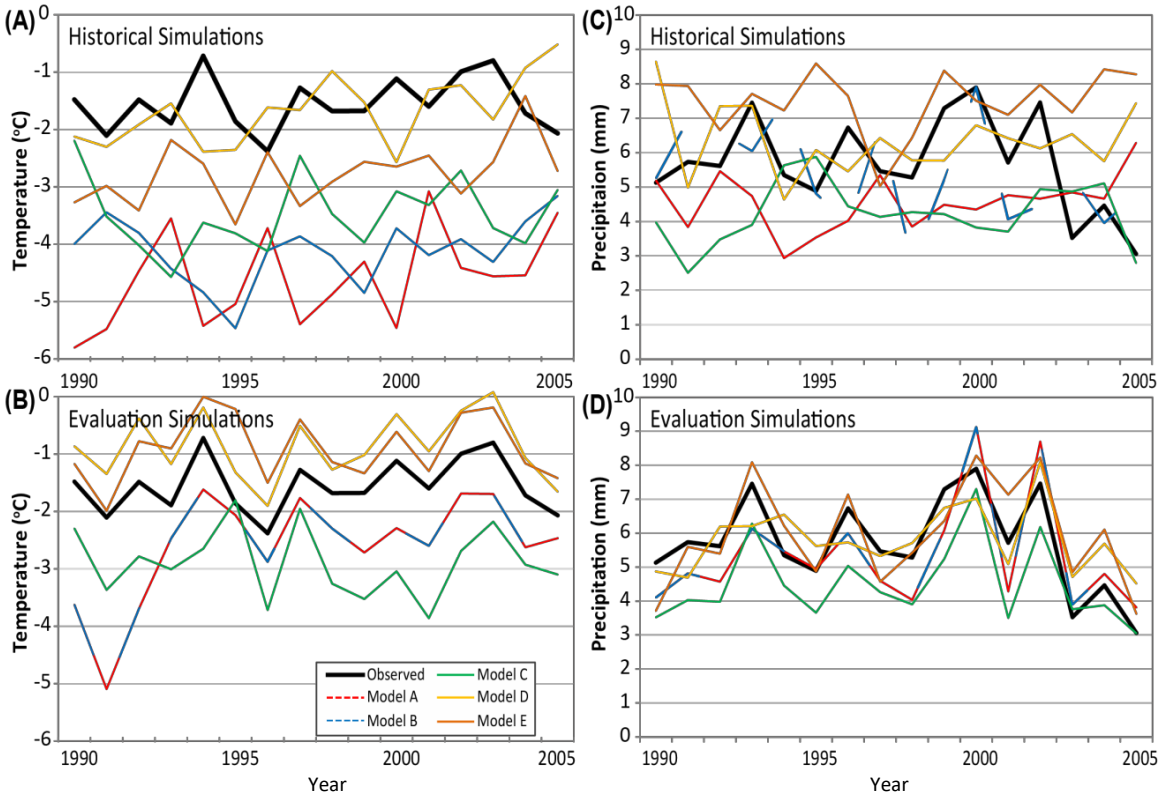

Figure 3.14: Simulated temperature (A and B) and precipitation (C and D) at Griesgletscher. The top row shows historical simulations whereas the bottom row shows evaluation simulations. Note that, although all simulations simulate the magnitude of variability reasonable, only the evaluation simulations (B and D) correctly simulate the timing of this variability in comparison to observations. In evaluation simulations, climate models A and B both use the same RCA4 RCM so the lines overlap.

Offset. The result of these factors is that there is often an offset between temperature and precipitation from the evaluation and the historical simulations. This was evident in this thesis (Figure 3.3) and, since simulations of future climate are initiated from the end point of the historical simulations, this prevents proper calibration of the GERM. For example, if GERM is calibrated to corrected evaluation simulations with a mean temperature of 2°C, but the same correction applied to future simulations produces a mean temperature of 3°C, the climatic sensitivity of GERM will be wrong resulting in overestimation of mass loss. Thus, it is essential for studies of future climate that there is a continuous time-series of temperature and precipitation.

The above leads to two key issues:

1: To correct both the RCM and GCM bias, historical simulations must be used to constrain the correction, since this will remove both the bias in the driving GCM (e.g. inaccurate monsoon simulation) and the bias in the RCM (e.g. poor representation of topography or lapse rates). Using the evaluation simulation would only remove the RCM bias since evaluation simulations are forced with reanalysis data rather than a GCM. Thus, when applied to future GCM simulations, an evaluation-type correction would leave an offset. A historical-type correction, however, would not leave an offset.

2: Using the historical simulations to constrain the correction is conceptually flawed since, as outline above, there is no direct link between the full temporal evolution of the simulations and observations. Specifically, GCM-forced RCMs, or historical simulations, are linked to real climate only through external forcings, so there is no real-world link to internal variability in the climate system. This lack of a direct link means that observed and simulated day-to-day weather is unrelated and internal fluctuations will not occur in time with observed internal fluctuations. Thus, using historical simulations does not provide a sound basis for BC. For example, biases between the historical RCM simulation and the observations may be falsely attributed to model bias, and therefore corrected, where they are actually a result of large-scale internal weather variability in the observations or historical simulations. The only solution to this is to use a simulated time-series that has real, direct links to observed weather, i.e. evaluation simulations, thus allowing statistical relationships that only remove genuine model bias to be established.

Clearly, the solution to (1) is to use historical simulations, since this will remove any offset; however, (2) stipulates that, to ensure only model bias is removed, evaluation simulations must be used.

In this thesis, a solution to this problem was proposed:

- Perform BC using evaluation simulations and analyse the magnitude of the offset between the corrected evaluation simulation and initial means of the corrected future simulations. If there is no offset then it suggests the historical simulations produced similar weather to the evaluation simulations and the future scenarios need no further correction.
- However, if there is an offset, an alternative “hybrid” solution is proposed whereby the correction is repeated using the historical simulation for constraint. By then using the mean adjustment from the historical correction combined with the variability adjustment of the evaluation correction, a hybrid correction is formed. This corrects such that the mean of corrected simulation in the past and future is the same, thus can

be used continually, yet the variability of the corrected series remains constrained by evaluation data, and thus maintains a viable direct link to real weather.

Although the correction proposed here is not suggested as a final solution, it forms a compromise that satisfies both of the problems associated with bias correction. It is important to stress that an alternative solution has not been identified in the literature, and this issue is not widely discussed.

The extent of offset varies somewhat between the Alps and the Himalaya. Interestingly, this thesis found that simulations in the Himalaya showed smaller bias between evaluation and historical simulations, initially thought to represent improved model performance compared to the Alps, counterintuitive with the more extreme topography and less well-understood climatology in the region. However, a more likely reason the evaluation and historical simulations are closer in the Himalaya than the Alps is that the reanalysis data in the Himalaya are very poor due to many fewer meteorological stations and more varied topography. As such, the influence of the less dense reanalysis dataset on evaluation simulations is small so there is only a small offset between evaluation and historical simulations. However, in the Alps, the more dense reanalysis dataset dictates that the evaluation simulations are more strongly influenced by the reanalysis data, which itself is more strongly constrained by the assimilated observations than in the Himalaya, producing a larger offset.

3.5.5 Description of Downscaling Methodologies in Glaciological Studies.

The interdisciplinary nature of combined climatological-hydrological-glaciological studies dictates that a wide-range of expertise is required if all disciplines are to be considered equally stringently. However, much of the glaciological literature neglects to thoroughly disclose and explain the climatological aspect of studies. For example, there are many glaciological studies that conduct downscaling of climate model simulations of future climate change (e.g. Farinotti et al., 2012; Immerzeel et al., 2013) but none, to the best of the author's knowledge, that consider whether to use GCM-forced simulations of the past, or reanalysis-forced simulations of the past, when constraining the statistical downscaling relationship. The lack of open discussion of this potentially important methodological consideration brings into question the robustness of future climate projections used to drive impact studies.

Furthermore, many glaciological impact studies utilise the delta-change approach in their statistical downscaling (e.g. Akhtar et al., 2008; Chen et al., 2011; Farinotti et al., 2012; Gabbi et al., 2012; Jouvet et al., 2011; Sorg et al., 2014). Although this corrects for bias in the mean, it

provides no correction of the distribution of simulated temperature or precipitation which could lead to considerable errors in simulations of glaciers (e.g. Akhtar et al., 2008; Singh and Kumar, 1997) and does not remove overestimation of drizzle days. Inadequate consideration and explanation of the climatic data input to the glacier models threaten the credibility of the conclusions science supplies to policy and decision makers (N. Guyennon 2015, personal communication). A key conclusion of this chapter, therefore, is to encourage that equal weighting is given to glaciological and climatological concepts of future studies, and that inter-disciplinary publications do more to encourage this.

3.5.6 Applying Bias-Corrected Scenarios in GERM.

The results presented in this chapter aim to provide the best possible estimates of future temperature and precipitation at sites in alpine regions, utilising a dynamical-statistical downscaling approach that represents the current state-of-the-art. GERM requires these daily estimates of temperature and precipitation to produce glacio-hydrological changes. However, it is urged that care is taken when applying these future estimates and that they should not be seen as realistic predictions or forecasts, rather possible projections and should be treated as an ensemble to provide an indication of potential future glacier evolution.

Future studies that equally combine climatological and glacio-hydrological interests are encouraged. In particular, glaciological studies should explicitly define their downscaling methodology, so that the reader can follow each step, and ensure that the considerable limitations in the understanding of meteorology in Alpine regions are acknowledged. The performance of non-corrected CORDEX simulations varies strongly between the Alps and Himalaya, but also varies depending on the driving GCM and RCM. Therefore, it is encouraged that more studies utilise the CORDEX simulations and that a comparison between the performance of the various models is conducted in the Himalaya, similar to the study of Kotlarski et al. (2014) who evaluated the performance of CORDEX models over Europe.

3.6 Conclusions.

This chapter has applied a dynamical-statistical downscaling technique to climate mode simulations, using a consistent methodology across all sites in the Alps and the Himalaya. Estimations of future temperature and precipitation for different emissions scenarios can now be applied to GERM to assess future evolution of glacier and runoff changes in different regions. This will be done in Chapters 5 and 7. The benefit of the quantile mapping approach implemented here is that it adjusts for differences between observations and simulations in terms of both the mean and distribution. This improves upon the delta-change method utilised

in many glaciological studies in that known limitations of climate models, for example overestimation of drizzle days, are removed.

Raw climate simulations in the Himalaya are very poor with significant biases between simulations and observations. This raises concerns on the skill of climate models over such extreme terrain with a very limited spatial and temporal observational network. Moreover, the limited availability of CORDEX simulations that include reanalysis-forced evaluation runs means that only a limited number of CORDEX simulations can be used to provide estimates of future temperature and precipitation for GERM. Because of this, the full range of uncertainty associated with different GCM-RCM combinations cannot be assessed, which will need to be considered when estimating future glacio-hydrological changes (Chapters 6 and 7). Future work should repeat the bias-correction applied here when more GCM-RCM model combinations are available to fully constrain the uncertainty.

Raw RCM performance in the Alps is much improved in comparison to the Himalaya, yet still needs further correction through statistical downscaling. The quantile mapping approach presented here is imperfect and a key finding of this thesis was the offset between evaluation simulations of temperature and historical simulations of temperature. This is a highly under-reported aspect of statistical downscaling that could potentially have major implications. Specifically, consistency using historical simulations to constrain bias-correction will produce time-series that potentially constrain the correction incorrectly. In this thesis, quantile mapping is modified to implement an alternative hybrid correction which represents a partial solution to the problem.

In terms of projected changes to temperature and precipitation, all sites show significant positive temperature trends for RCP 8.5, with the extent of warming decreasing for RCP 4.5 and further for RCP 2.6. The magnitude of temperature changes is larger in the Alps than at Khumbu. In terms of precipitation, there is little consensus among models and it appears that increased temperature will not result in increased precipitation, so the projected changes reflect changes the atmospheric circulation, rather than a purely temperature-driven effect. The future scenarios presented in this chapter provide five GCM-RCM combinations to estimate future glacier changes at Griesgletscher and Rhonegletscher, and two GCM-RCM combinations for Khumbu. The following chapters will implement these scenarios into GERM to assess to potential changes in glacier and runoff evolution.

4. LONG-TERM VALIDATION OF MODEL PERFORMANCE.

The aim of this chapter is to rigorously test GERM in the *past,* using validation periods of equivalent length to that of future typical simulations. The data-rich catchments of Griesgletscher and Rhonegletscher in the Swiss Alps are used for this purpose, due to the long-term monitoring of glacier and discharge in these catchments. This will provide a comprehensive assessment of the uncertainties associated with modelling glacio-hydrological evolution. Chapter 5 then applies these uncertainty estimations to simulations of *future* glacio-hydrological evolution, allowing future projections to be made with far greater awareness of uncertainties than previous studies have been able to provide. This chapter addresses Aim 1.

4.1. Introduction.

Estimating the future changes in runoff from glaciated catchments requires the use of models that attempt to represent mathematically the complex natural processes taking place and allow glacier and runoff estimates to be calculated. In alpine glaciated catchments a considerable component of runoff originates from the melt of snow and ice, with the glacier acting as a reservoir, delaying the delivery of precipitation downstream. Therefore, estimating future changes in catchment discharge requires accurate projections of the glacier volume available for melt. In the European Alps, snowmelt contributes most strongly to discharge in the spring months, whereas ice melt contributes mostly in the summer months after the removal of the snow-pack from the ablation zone (Birsan et al., 2005). Therefore, reductions in the size of the ice reservoir will reduce the potential volume of summer discharge. Moreover, the discharge regime may switch from ice-dominated to snow-dominated with continued deglaciation, with earlier onset of the spring snow-melt season (Horton et al., 2006).

In order to interpret predictions of how glaciated catchments will behave in the future and be able to quantify such changes, it is vital that we can understand the reliability of model simulations and incorporate accurate estimates of uncertainty. This can only be done by validating simulations against known glacier and catchment behaviour in the past, over similar time periods of 120 years. Studies often use relatively short calibration and validation periods (e.g. less than ten years; Immerzeel et al., 2013; Finger et al., 2012; Schaefli et al., 2007), thus their appropriateness over 90-100 year time-scales is poorly known considering that mountain glaciers typically respond to climate changes over periods of 15-60 years (Cuffey & Paterson, 2010), with very few exceptions (e.g. the Fox and Franz Josef Glacier in New Zealand (Mackintosh

et al., 2017)). Although short validation periods are often attributed to data limitations, they limit how comprehensive the model uncertainty assessment can be, as well as the robustness of projected glacio-hydrological.

Simulation of glacier changes over 80-100 year periods is complicated by a range of factors. For example, melt models assume a constant relationship between glacier melt and climate (temperature in the case of GERM), as described in Section 1.2.1.2. This relationship has been shown in reality to vary on decadal timescales due to changes in cloudiness and solar irradiance (e.g. Huss et al., 2009). Additionally, the response of glaciers to climate changes is complicated by topographic factors such as retreating through ice falls or overdeepenings. Glacio-hydrological models are not sophisticated enough to explicitly model the dynamics of a glacier retreating over complex terrain (Li et al., 2015), therefore it is important to assess model performance during these periods. In addition, there may be changes in glacier dynamics motivated by internal or external factors, the most notable being changes of bed slope (e.g. ice falls and overdeepenings; see Chapter 1). By using long validation periods, over which time the glaciers considered in this chapter have retreated by approximately 2 km, the uncertainty assessment will incorporate more of the complexities of glacier response to climate that are likely to occur under similar glacier shrinkage in the future, and therefore the uncertainty assessment will be a more realistic evaluation of model performance.

Recently, there has been some progress in assessing uncertainties associated with glacio-hydrological modelling over shorter periods. For example, Huss et al. (2014) conducted an overall uncertainty assessment of glacier-hydrological modelling, comparing the model performance with both short (2005-2010) and long (1982-2007) calibration periods at Findelgletscher, Switzerland. However, these periods are still shorter than the response times of mountain glaciers (Cuffey & Paterson, 2010). They found that simulated ice mass loss was reduced with the short calibration period and runoff in 2100 was 17 % higher than the simulation using the long calibration period. Another recent study, Gabbi et al. (2014), compared the skill of different types of melt models to reproduce glacier and runoff changes from 1929-2012 at Rhonegletscher, Switzerland, when calibrating each model to mass balance from 2006-2012. Gabbi et al. (2014) found that the ETI and SEB models outperformed the TI and HTI (used in GERM) models over long time-scales, but that performance over shorter-timescales was comparable. Moreover, the ETI and SEB models used in their study were also calibrated using hourly observations of cloudiness and incoming radiation, therefore are not directly comparable to HTI models which were calibrated using only temperature.

As stated in Huss et al. (2009), it is therefore essential to ensure that sufficiently long calibration-periods are used to confirm the model parameters are representative of long-term glacier-

climate sensitivity. The study presented in this chapter differs from Gabbi et al. (2014) in that it is designed to assess the uncertainty of the GERM model, which includes all the modules described in Section 2.1, including the Δh retreat parameterisation and hydrological components, rather than compare performance of different methods of calculating mass balance. Moreover, the work presented here forms the basis of future simulations that utilise the uncertainty estimation of this chapter, as well as developing the model for application to a Himalayan catchment. This work also extends the period of model evaluation, considering the period 1884-2003.

In this study, Griesgletscher catchment in Switzerland is modelled from 1884-2003 to review how successfully GERM can reproduce observed changes in both glacier retreat and runoff. Griesgletscher is selected because it represents a challenging catchment in which to test GERM, due to the recession through an over-deepening and a pro-glacial dammed lake into which the glacier calved for several decades, therefore presenting a complex pattern of recession for GERM to reproduce. GERM is then applied to a second catchment, Rhonegletscher, in order to demonstrate model portability and to corroborate findings from Griesgletscher. Rhonegletscher forms an ancillary part of the analysis, which will be presented in the discussion.

4.2. Study site and data.

4.2.1. The Griesgletscher Catchment.

Griesgletscher is situated in the Southern Swiss canton of Valais on the border of Italy (Figure 4.1; coordinates: 8.34 Lat., 46.44 Lon.) and flows into a dammed reservoir used for hydropower energy generation (Hauenstein 2005). Griesgletscher is a small sized valley glacier covering an area of ~5 km^2, has an approximate south-west-north-east orientation, and an altitudinal range of 2240 m to 3350 m. The catchment boundary (Figure 4.1) was derived using the watershed function of ArcMap, using the DEM from 2003.

Griesgletscher is accessible, relatively small and has abundant, available data, and has thus been the subject of many scientific studies. Hambrey (1977), Hambrey & Milnes (1977), and Hambrey et al. (1980) carried out detailed surveys of the dynamics and structure of Griesgletscher during a period when the main means of ice wastage was through calving into the proglacial, artificially dammed lake. These studies noted the area of maximum ice flow (40 m yr^{-1}) was immediately downslope of a small ice-fall just below the ELA (Figure 4.1). More recently, Picasso et al. (2004) applied a numerical flow model to Griesgletscher, before Huss et al., (2008b, 2009) applied mass balance models to the glacier and Farinotti et al. (2012) used GERM to simulate runoff at Griesgletscher, as well as other catchments in the Swiss Alps, from 2010 to 2100. Such

comprehensive study makes Griesgletscher the ideal pilot-study glacier, and the small size of Griesgletscher allows a large number of model simulations to be conducted with limited computational resources. This thesis builds on these previous studies by applying GERM for the longest possible periods in the past, in order to understand and quantify the uncertainty associated with the model, before running the model into the future, using bias-corrected climate inputs (see Chapter 3) that have previously not been applied at this catchment, nor in any other glacier studies.

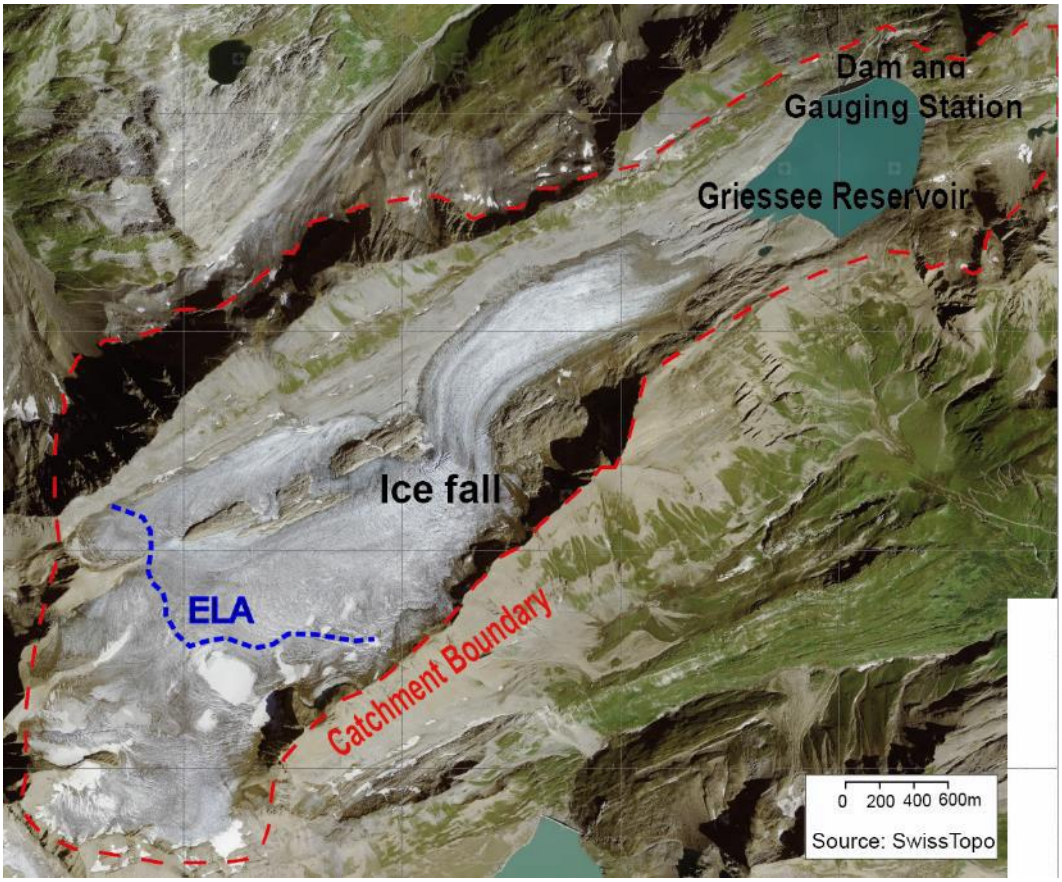

Figure 4.1: Aerial image of Griesgletscher around 2010, with the catchment denoted by the red-dashed line. Note the pro-glacial dammed lake to the North-East of the terminus. The glacier receded through an overdeepening between 1923 and 1961 with the dam constructed in 1965, creating a calving glacier terminus until around 1995. Image provided by SwissImage (Federal Office of Topography SwissTopo).

4.2.2. Data used in this Study.

Griesgletscher has been heavily monitored with long-term glaciological data sets (Table 4.1) readily available courtesy of the World Glacier monitoring Service (WGMS) as well as long-term meteorological from MeteoSwiss stations. Discharge data have been collected by the hydropower company 'Kraftwerke Aegina AG' since 1957. In addition to time-series data, a total

of eight Digital Elevation Models (DEMs) exist from 1884 to 2003. These DEMs have been processed in Bauder et al. (2007) to provide data on volume change. Bauder et al. (2007) collated topographic maps and photogrammetric surveys and converted elevation information onto a regular grid before interpolating this grid to provide a continuous elevation surface for each DEM. Finally, DEM differencing calculated volume changes between successive DEMs thus completing a comprehensive range of datasets available for model calibration and validation.

Table 4.1: Data availability at Griesgletscher.

Data	Years	Resolution	Source
Temperature and Precipitation	1884-2007*	Daily	MeteoSwiss
Glacier Volume Change	1884-2003	DEM dependent	Bauder et al. (2007)
Mass Balance	1993-2009	Annual	WGMS
Discharge	1957-2005	monthly	Alpiq Hydropower
DEMs	1884, 1923, 1961, 1986**, 2003	90 m	ETH Zurich

* Meteorological series based on 12 stations with closest, Ulrichen, 7 km away.

** 1986 DEM contains significant errors so is not used in this study

4.3. Methods.

4.3.1. Application of GERM.

GERM, described in detail in Chapter 2, is used here on a 25 m grid for the drainage basin of Griesgletscher defined using the watershed function of ArcGIS. Hereafter, the model specifications unique to Griesgletscher are described, with more detail on the general methods in Section 2.1.

4.3.1.1. Bed Topography.

The method to calculate ice thickness described in Section 2.2.1 was initially applied to Griesgletscher for each DEM allowing GERM simulations to be initiated from 1884, 1923, 1961, and 2003. This initial calculation is important since it dictates the ice volume that is available for melting in the future. However, the older topographic map derived DEMs showed clear inconsistencies with the more recent satellite derived DEM. Therefore, the most recent DEM (2003) has been used to generate the bed topography used for all simulations (Figure 4.2). For the area beneath the lake, which is flat in the 2003-DEM, the 1961 DEM was masked and interpolated into the 2003 DEM using the lake boundary as a soft breakline. Doing this helps to minimise errors associated with older DEMs.

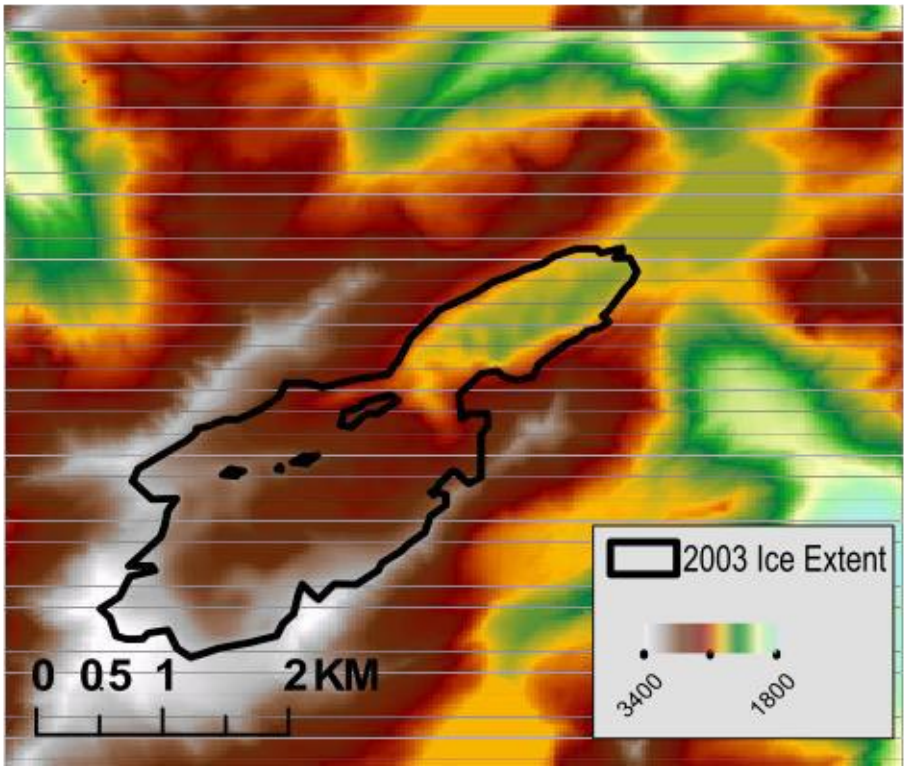

Figure 4.2: Bed topography calculated using the DEM from 2003. The area of the lake is to the North-East of the terminus in this DEM. This bed-DEM is used for all simulations to minimise errors associated with older DEMs.

4.3.1.2. Meteorological Time Series.

The meteorological time-series used in this thesis for sites in the Alps were provided by MeteoSwiss, with the methods used to process the data described here. GERM is driven by temperature and precipitation. These variables are not recorded within close proximity of the glacier for the long time-scales of the intended simulations, as is typical in alpine regions, so measured data must be scaled to the catchment using the methods of Huss et al. (2008a), which have been well proven in Huss et al. (2008b; 2010; 2014) and Farinotti et al. (2012). Extrapolation of air temperature data can be conducted with confidence since Begert et al. (2005) showed relatively good correlations between air temperature and horizontal distance, so temperature is treated separately to precipitation. The study of Begert et al. (2005) produced a homogenised time-series of monthly temperature from 1864-2000 that covers much of Switzerland and is freely available at MeteoSwiss, that uses twelve meteorological stations managed by MeteoSwiss with sufficiently long records. These records were then quality checked and analysed by Begert et al. (2005) before being used to generate a gridded monthly temperature time-series from 1864-2010. The temperature grid over Griesgletscher is then extracted, with daily variability imposed based on the daily fluctuations recorded at the nearest station, Ulrichen, 7 km to the North at an elevation of 1350 m. The temperature time series is

adjusted to the mean glacier elevation using the monthly average lapse rate from six local stations within 30 km of the glacier (Ulrichen, Grimsel Hospiz, Robiei, Binn, Cevio, and Eggishorn).

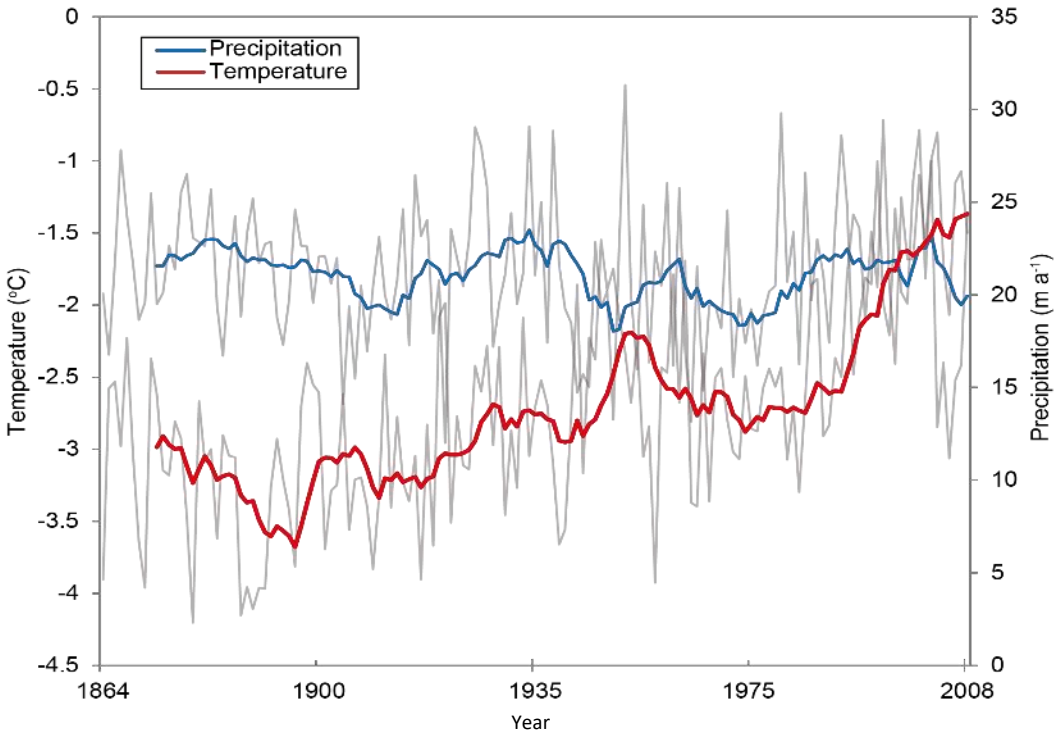

Figure 4.3: Annual temperature and precipitation from 1864-2008, with 10-year running mean in bold.

Precipitation is treated separately to temperature and is more uncertain due to the complex topographic influences and the highly variable distribution in alpine regions (Barry 1992). For example, precipitation lapse rates are spatially and temporally highly variable (Frei & Schar 1998; Schwarb et al., 2001) and precipitation measurements are less reliable than temperature, particularly in winter, due to effects of wind and gauge undercatch of snow (Sevruk 1982; Yang et al., 1998; Huss et al., 2008a). Due to these difficulties in precipitation extrapolation, the PRISM dataset of Schwarb et al. (2001) is used to provide the spatial pattern of precipitation. The PRISM dataset provides a continuous, observation-based, precipitation product for the European Alps at a 2 km resolution from 1970-1990, utilising data from over 6000 precipitation gauges (Frei & Schar 1998). PRISM extrapolates precipitation from stations based on the distance from the stations, elevation, aspect, and slope, using the methods described in Daly et al. (1994).

Time-series of precipitation are obtained by scaling the precipitation of local weather stations to the values given by PRISM for Griesgletscher, such that monthly means of Ulrichen match the monthly means of the PRISM dataset. Daily variability, as for temperature, is superimposed based on the closest station. Thus the PRISM dataset provides the spatial distribution of

precipitation and the local stations provide the temporal variations, producing the time-series in Figure 4.3.

To summarise, for temperature, the gridded dataset of Begert et al. (2005) is used to provide monthly temperatures, with local stations providing lapse rates and daily variability. For precipitation, the gridded PRISM dataset is used to scale the precipitation of local stations to Griesgletscher, with local stations again providing lapse rates and daily variability. Although long term in-situ observations of precipitation may be more accurate, the aforementioned difficulties of precipitation monitoring and the centennial time-scale desired dictate that the use of PRISM data combined with local stations should provide the most comprehensive possible data, and several studies have adopted this approach (e.g. Huss et al., 2008a; 2010; 2014; Farinotti et al., 2012; Paul et al., 2003). Both temperature and precipitation data are centred in the middle of the catchment, with GERM using temperature and precipitation lapse rates to adjust these data for each grid-square in the catchment.

4.3.2. Calibration of GERM.

GERM is an empirical model therefore requires catchment-specific calibration to observed glacier and discharge data to identify the empirical relationship between glacier ablation and temperature (Huss et al., 2008; Farinotti et al., 2012), regardless of the aim of the study (whether validating using past simulations, or projecting using future simulations). The abundance of available data at Griesgletscher makes it possible to perform a multivariate calibration using both glacier volume change and catchment discharge. This is important as the validity of the calibration is dependent on the amount and independence of input data; for example, biases that exist in discharge data will differ from biases in DEM-derived volume change data, therefore minimising potential errors (Huss et al., 2014). Moreover, using multiple data sources prevents the model reproducing observations for the wrong reasons; for example, if GERM was only calibrated to volume change it would reproduce mass balance observations, but would not accurately reproduce discharge as inputs and outputs into the catchment cannot be extracted from volume change alone. The advantage of multiple sources of calibration data has been shown in several studies (Huss et al., 2014; Finger et al., 2015). For example, Grayson et al. (2002) showed that that advantages of multiple, independent calibration data sources can outweigh the advantages of increase model complexity.

Another consideration for calibration is the range of years used for the calibration period. Ideally, this should be long enough to capture long term responses of glacier behaviour but must also be computationally efficient such that the large numbers of model runs required for parameter optimisation are feasible, therefore a compromise is necessary. It was decided that

a period of 10 years captures sufficient annual to decadal scale changes with reasonable computational times, and is a period that is typical of much of the literature (e.g. Horton et al., 2006; Farinotti et al., 2012; Hagg et al., 2006; Kobierska et al., 2013). For Griesgletscher, the period 1998-2007 was used for calibration. At Rhonegletscher 1997-2007 was used (see Section 4.6).

4.3.2.1. Automating the Calibration Procedure.

All previous applications of GERM have utilised a relatively manual approach to calibration, as described in Section 2.2.3. Here, a new approach is developed which systematically explores parameter combinations between set boundaries, adjusts parameters at set intervals, and produces statistical outputs to inform the model user of the goodness-of-fit of each parameter combination. This approach is advantageous for several reasons. First, this new approach explores the full parameter space and allows identification of the optimum parameter combination as well as identifying any secondary areas of the parameter space that produce good results. Second, the calibration procedure can be repeated for different catchments by different model users, with a consistent and systematic approach that will provide repeatable outputs. Thirdly, although the computational demands of this approach are greater than a manual calibration, the time spent by the model user is significantly reduced. The new calibration procedure employs a multi-grid approach (Box & Draper, 2014) which adjusts parameter combinations according to a 'coarse' grid with relatively large set intervals, selects the optimum parameters, and then further adjusts the parameter combinations on a 'fine' grid with much smaller intervals, as shown in Figure 4.4 and described below. This systematic approach is preferred due to the deterministic nature of GERM, rather than a random (e.g. Monte Carlo) approach, which is more appropriate for non-linear, chaotic systems (Hutter et al., 2011). The approach developed for this thesis is outlined below.

- Adjustment of calibration parameters:
    - Ablation parameters (F_m, R_{ice}, R_{snow}): Farinotti et al., (2012) applied GERM to nine catchments (the largest scale study using GERM) and found the optimum ratio between these parameters was 1:1.6:1.2 across all catchments, with the ratio between R_{ice} and R_{snow} based on the albedo of ice compared to snow. Therefore, this ratio is used in this thesis and is kept constant throughout calibration, thus treating this group as one parameter to be systematically adjusted. The advantage of this approach is that it reduces the number of potential parameter combinations from tens of thousands to hundreds, thus maintaining one of the original strengths of GERM in that it is computationally efficient.

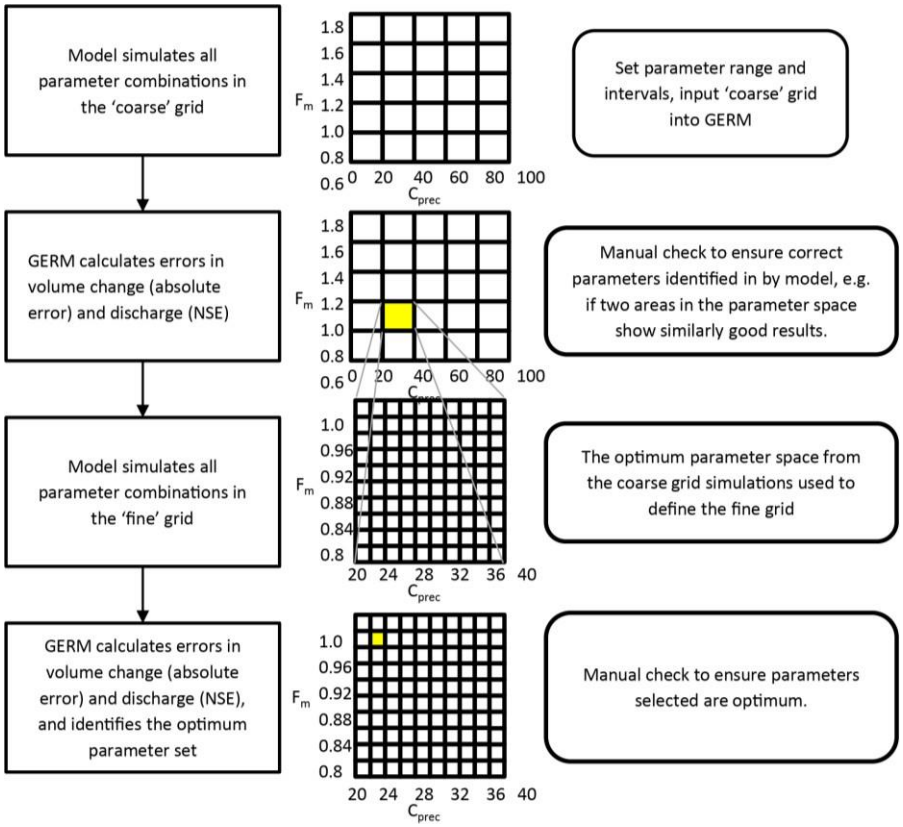

Figure 4.4: Schematic representation of the automated calibration procedure demonstrating how the optimum results of the 'coarse' grid are used to define the limits of the 'fine' grid, where parameters are adjusted over much finer intervals.

- The range within which the parameters are adjusted is constrained by previous applications of GERM plus/minus a buffer to ensure all potential parameters are considered; for example, the lowest value for F_m in literature is 0.84, therefore the lower limit for this calibration procedure is 0.6. The full range of parameter adjustment for F_m is from 0.6 to 1.8 see Table 4.2).

- Accumulation (C_{prec} - correction for under-reading of precipitation gauges): this is adjusted at Griesgletscher and Rhonegletscher since the input data are based on a gridded dataset that originates from rain-gauges. Therefore the precipitation needs to be 'calibrated' to the local precipitation. As for the melt parameters, previous studies show that C_{prec} can range from 0 % to 90 %, so these values are used as lower and upper limits. At Khumbu, the rain-gauge data were provided directly from one rain gauge rather than a gridded dataset, therefore was corrected for undercatch externally, thus it is not necessary to adjust this parameter over such a large range, as described in Section 6.2.2.

Table 4.2: Parameter ranges to be used as constraints for the systematic calibration, with upper and lower values calculated as highest/lowest value in the literature plus/minus 10 %

Parameter	Units	Upper	Lower
f_M	10^{-3} m (d °C)$^{-1}$	1.8	0.6
r_{ice}	10^{-5} m^3 (W d °C)$^{-1}$	2.9	0.9
r_{snow}	10^{-5} m^3 (W d °C)$^{-1}$	2.2	0.7
C_{prec}	%	90	0

- Since temperature and precipitation lapse rates are based on observations from Farinotti et al., (2012), these are not altered during calibration.
- The coarse and fine grids:
    - Within the maximum range of each parameter, the calibration procedure systematically adjusts each parameter by set intervals to identify areas in the parameter space that produce good results, with goodness of fit assessed as described below. This coarse grid is also designed to identify if there are several areas of the parameter space that produce equally good parameter combinations.
    - The best performing area identified from the coarse grid is then used to constrain the limits of the fine grid, where parameters are adjusted with much smaller intervals and the same goodness of fit assessment is calculated, thereby identifying the optimum parameters for the catchment.
- Assessing model performance:
    - Both volume change and catchment runoff need to be reproduced accurately for GERM to be used to assess changes in runoff in the future, since the volume of glacier remaining has a strong influence on seasonal and annual runoff. Therefore, assessing goodness of fit accounts for both of these. Volume change and discharge are assessed using the VE and NSE goodness-of-fit measures described in Section 2.2.4.3, over the full simulation period.
    - Both the NSE and VE equations (Section 2.2.4.3) express error as a fraction of the observed quantity being measured, averaged over the full simulation period. These two measures of model performance are then multiplied to produce one goodness of fit output that is used to select optimum parameter combinations. These are used in each iteration of both the coarse and fine grid.

4.3.3. Validation of GERM Performance.

The validation process is designed to assess how robust GERM is when reproducing observed changes, thus inferring information on the accuracy of future model outputs. By extending the short validation periods used in much of the literature (Table 4.3) to over 100 years, this thesis will more rigorously test how accurately GERM can reproduce long-term glacier changes compared to observed glacier volume changes.

Table 4.3: Various studies modelling runoff from highly glaciated catchments, with their calibration, validation and simulation periods.

Study	Region	Glacier(s)	Calibration Period	Validation Period	Simulation Period
Braun et al. (2000)	E.Alps	various	6	13	1974-1995
Rees & Collins (2006)	Himalaya	various	Various	Various	1990-2100
Hagg et al. (2006)	C.Asia	5	10	8	NA
Horton et al. (2006)	Swiss Alps	11	9	9	2070-2099
Huss et al. (2008b)	Swiss Alps	3: Zinal, Weisshorn, Moming	27	44	2010-2100
Farinotti et al. (2012)	Swiss Alps	9	Various	-	2010-2100
Immerzeel et al. (2013)	Himalaya	2: Langtang and Baltoto	6 (1 year for glacier)	-	2010-2100
Koboltschnig et al. (2008)	Austrian Alps	Salzach	3	3	none
Kobierska et al. (2013)	Swiss Alps	3: Chelen, Rotfirn, Damma	13	13	2010-2100

Here a variety of validation model runs are performed to assess how well GERM performs over increasingly long simulation periods. The parameter set calibrated from 1998-2007 is used for all simulations. The duration of simulations is dictated by available DEMs, thus simulations run from: 1884-2003, 1923-2003, and 1961-2003.

To assess the performance of these simulations in terms of long term glacier evolution, each simulation is separately evaluated by comparing simulated volume change to observed volume change in each DEM-period. Additionally, monthly discharge measurements from 1961-2003 are compared with simulated discharges in order to assess the performance of the model in terms of runoff.

4.4. Results.

4.4.1. Calibration Results.

Coarse Grid. The initial calibration simulations produced the model performance indices shown in Table 4.4. From these results, it is clear that GERM produces smooth outputs with clear areas of the grids showing optimum results, demonstrating that there are no major model instabilities and that the systematic approach taken to calibration is appropriate. From the combined results, the parameter combination highlighted in yellow is optimum. This parameter set was the used to define the 'fine' grid shown in the next stage of calibration.

Table 4.4: Calibration results for the 'coarse' grid, using red to represent worse model performance and blue to represent better model performance. Values highlighted in yellow are the optimum parameter combination to go forward to the fine grid calibration.

F_m	R_{ice}	R_{snow}	Glacier Volume Change Error (VE):																		
1.80	2.88	2.16	-0.69	-0.62	-0.55	-0.48	-0.41	-0.34	-0.27	-0.20	-0.13	-0.05	0.02	0.09	0.16	0.23	0.31	0.38	0.45	0.52	0.60
1.70	2.72	2.04	-0.46	-0.39	-0.31	-0.24	-0.17	-0.10	-0.03	0.05	0.12	0.19	0.26	0.34	0.41	0.48	0.56	0.63	0.70	0.77	0.85
1.60	2.56	1.92	-0.22	-0.15	-0.08	-0.01	0.07	0.14	0.21	0.29	0.36	0.44	0.51	0.58	0.66	0.73	0.80	0.88	0.95	0.98	0.90
1.50	2.40	1.80	0.02	0.09	0.17	0.24	0.32	0.39	0.47	0.54	0.61	0.69	0.76	0.86	0.96	0.99	0.94	0.87	0.80	0.72	0.65
1.40	2.24	1.68	0.26	0.34	0.41	0.49	0.56	0.64	0.72	0.79	0.87	0.94	0.99	0.87	0.75	0.72	0.69	0.62	0.54	0.47	0.40
1.30	2.08	1.56	0.51	0.59	0.67	0.74	0.82	0.90	0.97	0.95	0.88	0.81	0.73	0.63	0.54	0.49	0.44	0.37	0.30	0.23	0.16
1.20	1.92	1.44	0.77	0.85	0.92	1.00	0.92	0.85	0.77	0.70	0.62	0.55	0.48	0.40	0.33	0.26	0.19	0.12	0.05	-0.02	-0.09
1.10	1.76	1.32	0.97	0.89	0.82	0.74	0.67	0.59	0.52	0.44	0.37	0.30	0.23	0.16	0.09	0.02	-0.05	-0.12	-0.19	-0.25	-0.32
1.00	1.60	1.20	0.71	0.63	0.56	0.48	0.41	0.33	0.26	0.19	0.12	0.05	-0.02	-0.09	-0.16	-0.22	-0.29	-0.36	-0.42	-0.49	-0.55
0.90	1.44	1.08	0.45	0.38	0.30	0.23	0.16	0.09	0.02	-0.05	-0.12	-0.19	-0.26	-0.32	-0.39	-0.45	-0.52	-0.58	-0.65	-0.71	-0.77
0.80	1.28	0.96	0.19	0.12	0.05	-0.02	-0.09	-0.16	-0.23	-0.29	-0.36	-0.42	-0.49	-0.55	-0.62	-0.68	-0.75	-0.81	-0.87	-0.93	-1.00
0.70	1.12	0.84	-0.07	-0.14	-0.15	-0.28	-0.35	-0.35	-0.46	-0.55	-0.61	-0.68	-0.74	-0.80	-0.84	-0.92	-1.00	-1.06	-1.12	-1.18	-1.24
0.60	0.96	0.72	-0.33	-0.39	-0.37	-0.53	-0.60	-0.57	-0.71	-0.80	-0.86	-0.92	-0.99	-1.04	-1.07	-1.15	-1.24	-1.30	-1.36	-1.42	-1.47
			0	5	10	15	20	25	30	35	40	45	50	55	60	65	70	75	80	85	90
F_m	R_{ice}	R_{snow}	Discharge Error (NSE):																		
1.80	2.88	2.16	0.54	0.49	0.43	0.38	0.32	0.26	0.19	0.12	0.05	-0.02	-0.10	-0.18	-0.26	-0.34	-0.43	-0.52	-0.61	-0.71	-0.81
1.70	2.72	2.04	0.64	0.60	0.55	0.50	0.45	0.39	0.34	0.28	0.21	0.15	0.08	0.01	-0.07	-0.15	-0.23	-0.31	-0.39	-0.48	-0.57
1.60	2.56	1.92	0.73	0.69	0.65	0.61	0.56	0.52	0.47	0.41	0.36	0.30	0.24	0.17	0.11	0.04	-0.04	-0.11	-0.19	-0.27	-0.35
1.50	2.40	1.80	0.80	0.77	0.74	0.70	0.66	0.62	0.58	0.53	0.48	0.43	0.38	0.32	0.26	0.20	0.14	0.07	0.00	-0.07	-0.15
1.40	2.24	1.68	0.86	0.83	0.81	0.78	0.75	0.71	0.68	0.64	0.59	0.55	0.50	0.45	0.40	0.34	0.29	0.23	0.16	0.10	0.03
1.30	2.08	1.56	0.90	0.88	0.86	0.84	0.82	0.79	0.76	0.73	0.69	0.66	0.61	0.57	0.53	0.48	0.43	0.38	0.32	0.27	0.21
1.20	1.92	1.44	0.93	0.92	0.91	0.89	0.87	0.85	0.83	0.80	0.77	0.74	0.71	0.67	0.63	0.59	0.55	0.51	0.46	0.41	0.36
1.10	1.76	1.32	0.94	0.94	0.93	0.93	0.91	0.90	0.88	0.86	0.84	0.82	0.79	0.76	0.73	0.69	0.66	0.62	0.58	0.54	0.50
1.00	1.60	1.20	0.95	0.95	0.95	0.95	0.94	0.93	0.92	0.91	0.89	0.88	0.86	0.83	0.81	0.78	0.75	0.72	0.69	0.66	0.62
0.90	1.44	1.08	0.93	0.94	0.95	0.95	0.95	0.95	0.94	0.93	0.92	0.91	0.90	0.88	0.86	0.84	0.82	0.80	0.78	0.75	0.72
0.80	1.28	0.96	0.91	0.92	0.93	0.94	0.94	0.95	0.95	0.95	0.94	0.94	0.93	0.92	0.91	0.89	0.88	0.86	0.85	0.83	0.81
0.70	1.12	0.84	0.87	0.89	0.90	0.92	0.93	0.93	0.94	0.95	0.95	0.95	0.95	0.94	0.94	0.93	0.92	0.91	0.90	0.89	0.88
0.60	0.96	0.72	0.81	0.84	0.86	0.88	0.89	0.91	0.92	0.93	0.94	0.94	0.95	0.95	0.95	0.95	0.95	0.95	0.94	0.94	0.94
			0	5	10	15	20	25	30	35	40	45	50	55	60	65	70	75	80	85	90
F_m	R_{ice}	R_{snow}	Combined Error:																		
1.80	2.88	2.16	-0.37	-0.30	-0.24	-0.18	-0.13	-0.09	-0.05	-0.02	-0.01	0.00	0.00	-0.02	-0.04	-0.08	-0.13	-0.20	-0.28	-0.37	-0.49
1.70	2.72	2.04	-0.29	-0.23	-0.17	-0.12	-0.08	-0.04	-0.01	0.01	0.03	0.03	0.02	0.00	-0.03	-0.07	-0.13	-0.19	-0.28	-0.37	-0.48
1.60	2.56	1.92	-0.16	-0.11	-0.05	0.00	0.04	0.07	0.10	0.12	0.13	0.13	0.12	0.10	0.07	0.03	-0.03	-0.10	-0.18	-0.26	-0.32
1.50	2.40	1.80	0.01	0.07	0.12	0.17	0.21	0.24	0.27	0.29	0.30	0.30	0.29	0.28	0.25	0.20	0.13	0.06	0.00	-0.05	-0.10
1.40	2.24	1.68	0.22	0.28	0.33	0.38	0.42	0.46	0.48	0.50	0.51	0.52	0.49	0.39	0.30	0.25	0.20	0.14	0.09	0.05	0.01
1.30	2.08	1.56	0.46	0.52	0.58	0.63	0.67	0.71	0.74	0.69	0.61	0.53	0.45	0.36	0.28	0.23	0.19	0.14	0.10	0.06	0.03
1.20	1.92	1.44	0.71	0.78	0.84	0.89	0.81	0.72	0.64	0.56	0.48	0.41	0.34	0.27	0.21	0.15	0.10	0.06	0.02	-0.01	-0.03
1.10	1.76	1.32	0.92	0.84	0.76	0.69	0.61	0.53	0.46	0.38	0.31	0.24	0.18	0.12	0.06	0.01	-0.03	-0.07	-0.11	-0.14	-0.16
1.00	1.60	1.20	0.67	0.60	0.53	0.46	0.38	0.31	0.24	0.17	0.11	0.04	-0.02	-0.07	-0.13	-0.18	-0.22	-0.26	-0.29	-0.32	-0.34
0.90	1.44	1.08	0.42	0.36	0.29	0.22	0.15	0.08	0.02	-0.05	-0.11	-0.17	-0.23	-0.28	-0.33	-0.38	-0.43	-0.47	-0.50	-0.53	-0.56
0.80	1.28	0.96	0.18	0.11	0.05	-0.02	-0.09	-0.15	-0.21	-0.28	-0.34	-0.40	-0.45	-0.51	-0.56	-0.61	-0.66	-0.70	-0.74	-0.77	-0.81
0.70	1.12	0.84	-0.06	-0.12	-0.13	-0.25	-0.32	-0.32	-0.44	-0.52	-0.58	-0.64	-0.70	-0.75	-0.79	-0.86	-0.92	-0.97	-1.01	-1.05	-1.09
0.60	0.96	0.72	-0.26	-0.33	-0.32	-0.47	-0.54	-0.52	-0.65	-0.74	-0.81	-0.87	-0.93	-0.98	-1.02	-1.10	-1.17	-1.23	-1.28	-1.33	-1.38
			0	5	10	15	20	25	30	35	40	45	50	55	60	65	70	75	80	85	90
			C_{prec} (%)																		

Fine Grid. The fine grid simulations produced the model performance indices shown in Table 4.5, which explores the parameter space around the optimum results from the coarse grid. From these results, GERM clearly identifies the optimum parameter calibration to be used for the long-term model validation, summarised in Table 4.6.

Table 4.5: Calibration results for the 'fine' grid, using red to represent worse model performance and blue to represent better model performance.

F_m	R_{ice}	R_{snow}	Glacier Volume Change Error (VE):					
1.15	1.84	1.38	0.90	0.91	0.93	0.94	0.96	0.98
1.14	1.82	1.37	0.92	0.94	0.96	0.97	0.99	1.00
1.13	1.81	1.36	0.95	0.97	0.98	1.00	0.99	0.97
1.12	1.79	1.34	0.98	0.99	0.99	0.98	0.96	0.95
1.11	1.78	1.33	1.00	0.98	0.97	0.95	0.94	0.92
1.10	1.76	1.32	0.97	0.96	0.94	0.93	0.91	0.89
1.09	1.74	1.31	0.94	0.93	0.91	0.90	0.88	0.87
1.08	1.73	1.30	0.92	0.90	0.89	0.87	0.86	0.84
1.07	1.71	1.28	0.89	0.88	0.86	0.85	0.83	0.82
1.06	1.70	1.27	0.87	0.85	0.84	0.82	0.81	0.79
1.05	1.68	1.26	0.84	0.83	0.81	0.79	0.78	0.76
1.04	1.66	1.25	0.81	0.80	0.78	0.77	0.75	0.74
1.03	1.65	1.24	0.79	0.77	0.76	0.74	0.73	0.71
1.02	1.63	1.22	0.76	0.75	0.73	0.72	0.70	0.69
1.01	1.62	1.21	0.74	0.72	0.71	0.69	0.68	0.66
1.00	1.60	1.20	0.71	0.69	0.68	0.66	0.65	0.63
			0	1	2	3	4	5

F_m	R_{ice}	R_{snow}	Discharge Error (NSE):					
1.15	1.84	1.38	0.94	0.94	0.94	0.93	0.93	0.93
1.14	1.82	1.37	0.94	0.94	0.94	0.94	0.93	0.93
1.13	1.81	1.36	0.94	0.94	0.94	0.94	0.94	0.94
1.12	1.79	1.34	0.94	0.94	0.94	0.94	0.94	0.94
1.11	1.78	1.33	0.94	0.94	0.94	0.94	0.94	0.94
1.10	1.76	1.32	0.94	0.94	0.94	0.94	0.94	0.94
1.09	1.74	1.31	0.95	0.95	0.94	0.94	0.94	0.94
1.08	1.73	1.30	0.95	0.95	0.95	0.94	0.94	0.94
1.07	1.71	1.28	0.95	0.95	0.95	0.95	0.94	0.94
1.06	1.70	1.27	0.95	0.95	0.95	0.95	0.95	0.95
1.05	1.68	1.26	0.95	0.95	0.95	0.95	0.95	0.95
1.04	1.66	1.25	0.95	0.95	0.95	0.95	0.95	0.95
1.03	1.65	1.24	0.95	0.95	0.95	0.95	0.95	0.95
1.02	1.63	1.22	0.95	0.95	0.95	0.95	0.95	0.95
1.01	1.62	1.21	0.95	0.95	0.95	0.95	0.95	0.95
1.00	1.60	1.20	0.95	0.95	0.95	0.95	0.95	0.95
			0	1	2	3	4	5
			C_{prec} (%)					

F_m	R_{ice}	R_{snow}	Combined Error:					
1.15	1.84	1.38	0.84	0.86	0.87	0.88	0.90	0.91
1.14	1.82	1.37	0.87	0.88	0.90	0.91	0.92	0.93
1.13	1.81	1.36	0.90	0.91	0.92	0.93	0.93	0.91
1.12	1.79	1.34	0.92	0.93	0.93	0.92	0.90	0.89
1.11	1.78	1.33	0.94	0.93	0.91	0.89	0.88	0.86
1.10	1.76	1.32	0.92	0.90	0.89	0.87	0.86	0.84
1.09	1.74	1.31	0.89	0.88	0.86	0.85	0.83	0.82
1.08	1.73	1.30	0.87	0.85	0.84	0.82	0.81	0.79
1.07	1.71	1.28	0.85	0.83	0.82	0.80	0.79	0.77
1.06	1.70	1.27	0.82	0.81	0.79	0.78	0.76	0.75
1.05	1.68	1.26	0.80	0.78	0.77	0.75	0.74	0.72
1.04	1.66	1.25	0.77	0.76	0.74	0.73	0.71	0.70
1.03	1.65	1.24	0.75	0.73	0.72	0.70	0.69	0.67
1.02	1.63	1.22	0.72	0.71	0.69	0.68	0.66	0.65
1.01	1.62	1.21	0.70	0.68	0.67	0.65	0.64	0.63
1.00	1.60	1.20	0.67	0.66	0.64	0.63	0.62	0.60
			0	1	2	3	4	5
			C_{prec} (%)					

Table 4.6: Calibrated parameter sets for Griesgletscher. * refers to parameters that are constrained by observations so were not adjusted as part of the calibration.

	Units	Calibrated Values
f_M	10^{-3} m (d °C)$^{-1}$	1.11
r_{ice}	10^{-5} m^3 (W d °C)$^{-1}$	1.78
r_{snow}	10^{-5} m^3 (W d °C)$^{-1}$	1.33
***dP/dz** **	10^{-2} % m^{-1}	1
***dT/dz** **	10^{-3} °C m^{-1}	-5.47
C_{prec}	%	0

GERM performance during calibration. Figures 4.5 and 4.6 show the performance of GERM using the optimum parameter set, in terms of discharge and mass balance, compared to observations. This parameter set shows a good simulation of observed monthly discharge (Figure 4.6; $R^2 = 0.97$ at $p<0.01$; NSE = 0.98), with the exception of 2001 where simulated discharge was considerably lower, an overprediction also observed in mass balance. The reasons for this anomaly appear to

be a very cold August that coincided with a high-intensity precipitation event. In GERM, this appears to have caused considerable summer snow-fall resulting in reduced glacier ice melt, hence positive mass balance, and high discharge when the accumulated snow melted.

With the exception of 2001, these results show that GERM reproduces observed discharge and mass balance well during the calibration period, giving confidence that the new calibration procedure applied here correctly produces optimum parameter combinations.

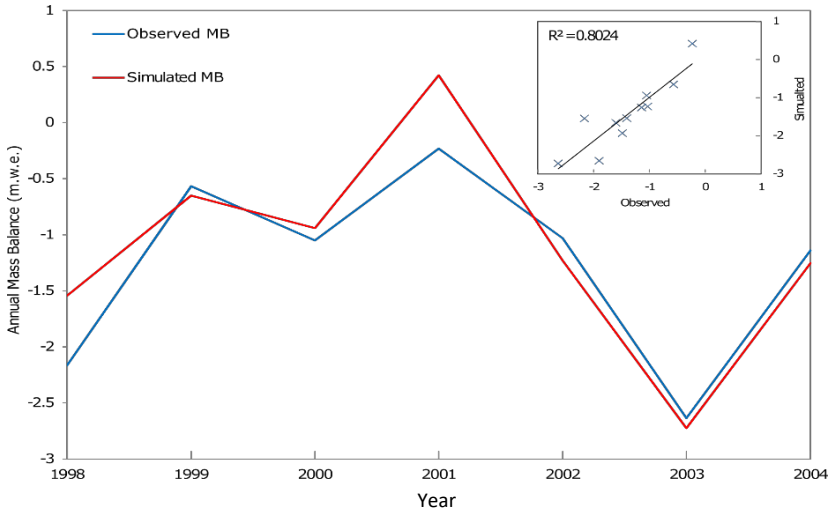

Figure 4.5: Comparison of simulated and observed annual mass balance at Griesgletscher during the calibration period. With the exception of 2001, mass balance are simulated accurately.

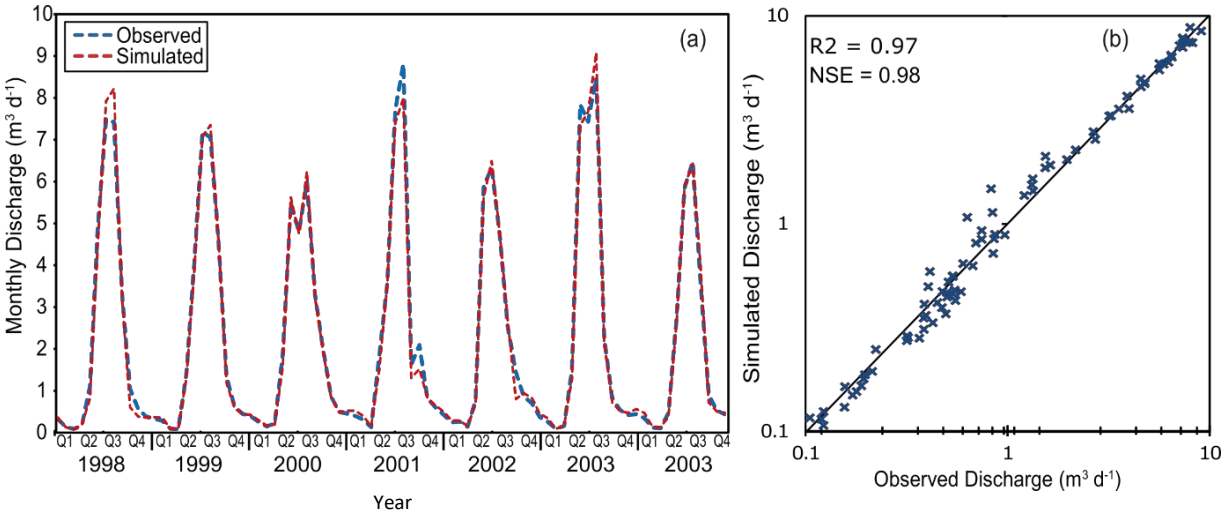

Figure 4.6: Performance of simulations of monthly discharge at Griesgletscher compared to observations, during the calibration period.

4.4.2. Long-term Validation Results.

Volume Change. The skill of GERM to reproduce observed volume changes over various long time-scales is tested here. The rationale behind these simulations is to understand how well GERM is able to reproduce changes in catchment runoff and glaciers over long time periods, such that the calculated uncertainties can be used to better constrain future simulations. Without long-term validation periods, future simulations may have a false level of confidence. The objective here is not to accurately reconstruct observed changes, but to quantify the uncertainty associated with GERM, considering the calibration period used (1998-2004) is much shorter than the simulation period, but is a calibration length period typical of similar studies.

GERM is initiated in 1884, 1923, and 1961. These years were chosen as DEMs are available in these years, allowing the simulations to initiate with the correct glacier outline and volume. For all simulations, the most recent, accurate DEM is used for all periods of the validation simulations, to reduce errors associated with older DEMs and help to isolate the source of any errors in model outputs.

1884-2003. Table 4.7 shows modelled and observed volume changes for each model period. Clearly, Figure 4.7 shows that, with the model initiated in 1884, modelled volume losses underestimate observed losses, particularly between 1884-1923 where simulated ice volume slow declines during a period when observations suggests ice loss was rapid. Spatially (Figure 4.7), simulated ice area change does not accurately reproduce observed spatial changes over this long time-scale. Potential reasons for the performance of GERM will be discussed in Section 4.5.1.

1923-2003. Although the final error is lower (9.1 %) than the 1884-2003 simulations, ice loss is underestimated, particularly in terms of area (Figure 4.7d). This period is also significant due to the emergence of an over-deepening that produced a pro-glacial lake. The lake was dammed in 1965 for hydropower generation producing water levels that turned Griesgletscher into a calving glacier which will be discussed in Section 4.5.4.

1961-2003. Modelled ice loss from 1961-1986 is relatively accurate with a volume change error in 2003 of 2.6 %. Spatially, the pattern of ice loss does not show sufficient frontal recession (Figure 4.7f), but performance is improved over the longer simulations.

Table 4.7: Performance of three simulations in terms of volume change at Griesgletscher with varying initiation and duration. Observations are based on Bauder et al. (2007)

Model Run	Initial Volume (modelled-km³)	Obs. Vol. change in km³ (% of initial volume)	Sim. Vol. change in km³ (% of initial volume)	Error in 2003 (km³)	Error (% of initial volume)
1884-2003	0.921	-0.621 (-67.5 %)	-0.440 (-47.7 %)	0.181	19.7 %
1923-2003	0.764	-0.374 (-49.0 %)	-0.340 (-44.4 %)	0.035	4.6 %
1961-2003	0.620	-0.155 (-25.0 %)	-0.139 (-22.4 %)	0.016	2.6 %

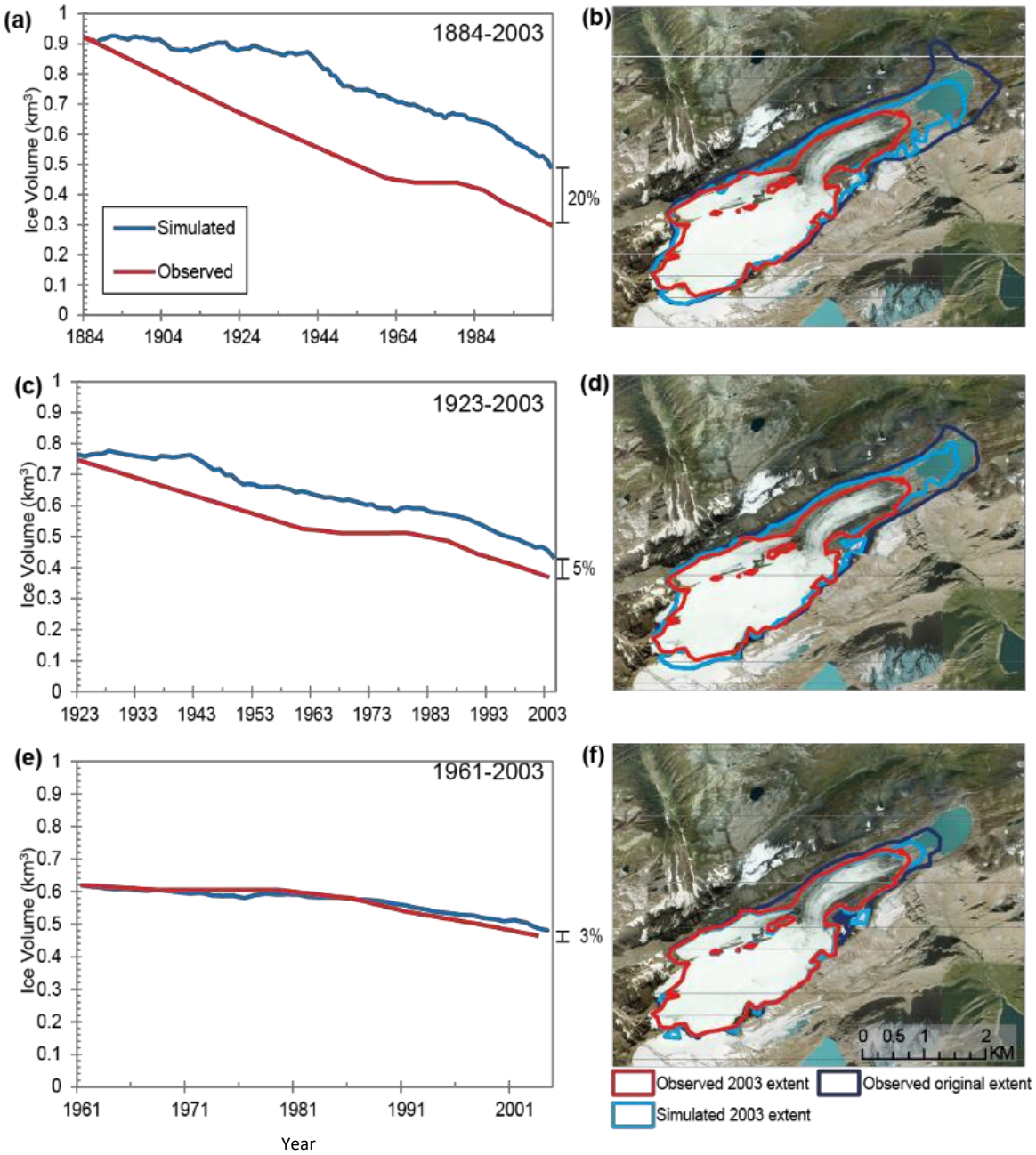

Figure 4.7: Left panel: modelled volume change compared to observed volume change, as well as spatial patterns of ice loss (right panel).

Discharge. Modelled annual discharge is reasonable with R^2 values around 0.65 ($p<0.01$; Figure 4.8) suggesting that the temporal variability is significantly correlated. However, despite significant correlations, the performance is not as high as for the calibration period ($R^2=0.8$ at $p<0.01$) and shows no improvement for more recent, shorter simulations (e.g. 1961-2003). Additionally, there appears to be a consistent overestimation of simulated discharge after 1965 for all simulations with the 1961 simulation showing the smallest errors in this regard. In terms of decadal scale variability, the running means (Figure 4.8a) show that decadal variability is well reproduced after around 1970; however the observed decrease in discharge from 1957 to 1970 is not captured in any of the simulations. However, some decrease in performance is to be expected outside the calibration period, so these results provide a measure of the uncertainty associated with modelling catchment hydrology and incorporate the error produced by the underestimation of glacier volume losses.

Monthly discharge (Figure 4.8b) shows improved performance with good simulation of the seasonal cycle. The overestimation of discharge in July in the 1884 and 1923 simulations is not apparent in the 1961 simulation. Additionally, in all simulations there is an over-estimation of runoff in October, suggesting summer melt is stored for longer than in reality. In general, the simulations of monthly discharge reflect the overestimation of annual discharge; however, the 1961-2003 simulation shows the smallest overestimation in this regard.

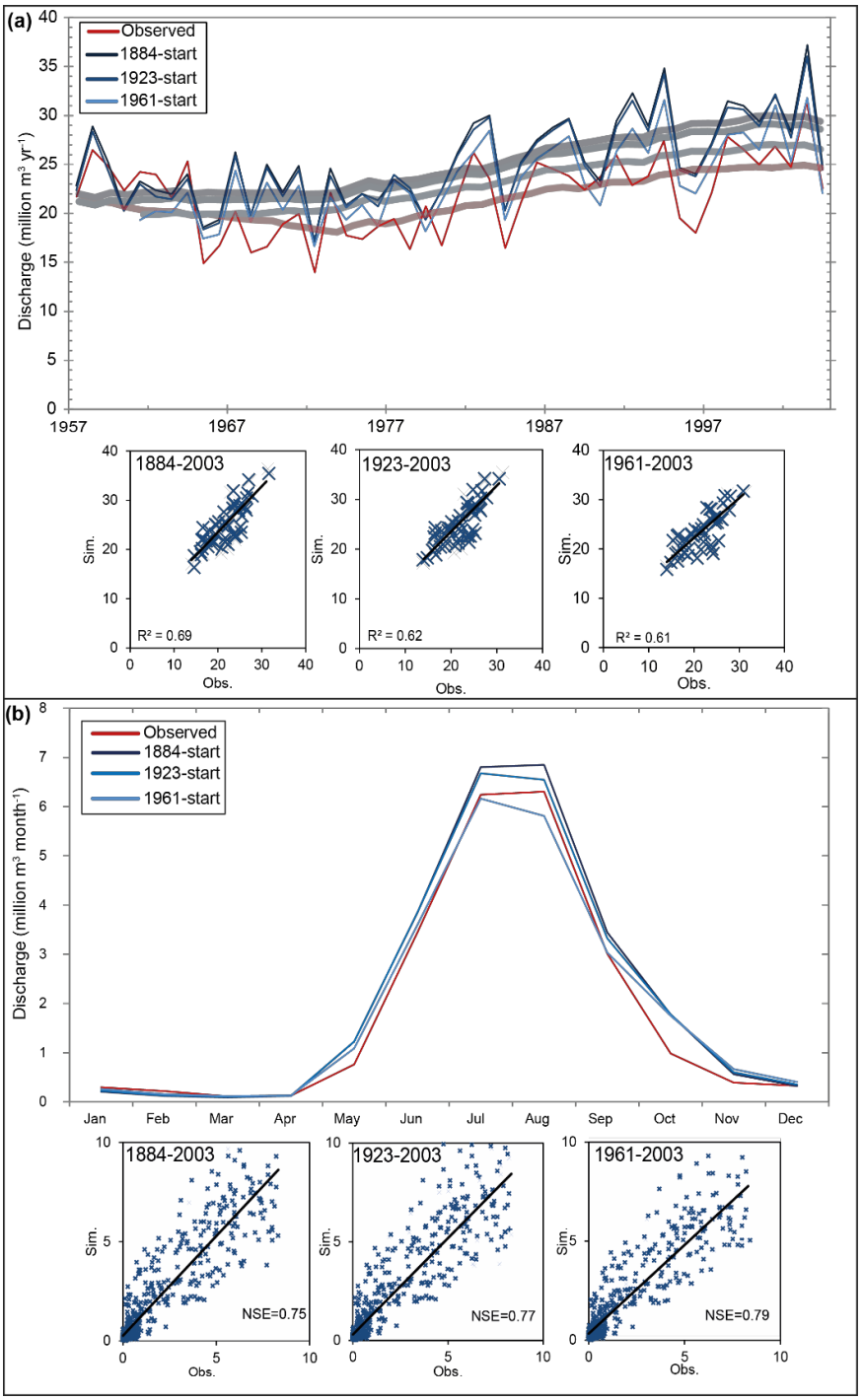

Figure 4.8: Annual (a) and monthly (b) discharge of the three long-term validation simulations, compared to observations. Subplots in (a) show performance for each separate simulation period. In (b), monthly discharge is averaged over full simulation period in main plot, and subplots include all monthly discharge estimates. Thick lines in (a) refer to 8-year moving averages. All correlations (R^2) are significant at $p<0.01$.

4.5. Discussion of Results at Griesgletscher.

4.5.1. Volume loss.

The long-term simulation shows a consistent underestimation of ice volume loss, despite the model being calibrated to volume changes between 1998 and 2007. Potential reasons for this are discussed here.

Stationarity of Model Parameters. The sensitivity of the model to climate, i.e. how ice and snow react to changes in temperature, is assumed to be stable over time in all types of glacier melt models. This is a known limitation (e.g. Braithwaite, 1995; Hock, 2005; Huss et al., 2009) but using time-varying parameters is not possible for future simulations. The changes in the climatic-sensitivity of the glacier are likely caused by fluctuations in the relationship between temperature and melt. For example, GERM relies on the typically strong correlation between temperature and several components of the glacier surface energy balance, as described in Section 1.2.1, with the radiation component of GERM remaining linked to temperature. However, Huss et al. (2009) showed how enhanced solar radiation during summer in the 1940s considerably altered the relationship between temperature and glacier melt, which would require re-calibration of the model parameters. Any changes in this relationship will introduce errors in the model and, since the relationship is known to have changed in the past 100 years, it has potential to change in the next 100 years. This change in climatic-sensitivity can only be assessed using the long-term validation in this thesis.

Similarly, the periods where Griesgletscher retreated through an overdeepening or lost mass through calving will have altered the rate of mass loss. Since GERM is not capable of explicitly modelling these processes, assessing uncertainty over long periods that include a range of different glacial processes to test how well the model can perform is essential. This is important because future glacier responses are likely to also go through periods where mass loss is altered by a change in dynamics, thus the models performance in the past can be used to constrain future uncertainties.

Variations in the sensitivity of the glacier to climate are demonstrated in the study of Huss et al. (2008b), who reconstructed mass balance at several glaciers including Griesgletscher from 1865-2005. It is important to note that the aim of their study was mass balance reconstruction, rather than model evaluation as in this thesis. Their study used a similar model to GERM, but differed considerably from this thesis because, to obtain the best reconstruction, they recalibrated the model repeatedly for each period with new DEMs. Their study used the model to infill gaps in the mass balance record, with the aim of providing a continuous time series of mass balance.

Although the aim of this chapter is to investigate model performance with relevance to future simulations, i.e. re-calibrating regularly is not an appropriate option, the approach of Huss et al. (2008b) forms an interesting comparison, since it uses the same DEM differencing data (Bauder et al., 2007) but uses repeat calibrations, so therefore helps to isolate the source of error in the simulations of this thesis. Specifically, the short-term periods highlighted in Figure 4.9 (taken from Huss et al. (2008b) which show positive balances (~1920 and ~1975) are also clear in the results presented in this chapter (Figure 4.7), as are the periods of particularly rapid mass loss (~1945 and ~2000). The reasons for these short periods of mass gain become clear when considering the meteorological data (Figure 4.3). Specifically, the mass gain in 1920 and 1975 coincided with cool temperatures and increased precipitation. Conversely, the rapid mass loss in the 1940s appears to be caused by strongly increased temperatures with anomalously low precipitation, combined with the aforementioned enhanced solar radiation (Huss et al., 2008b). However, the reconstruction of Huss et al. (2008b) does not show the relatively stable period simulated in this thesis from 1884-1940, instead showing continuous mass loss in agreement with the volume change observations. Since the models used in both these studies are similar and the key difference is that their model was repeatedly recalibrated, the different results are most likely to be a consequence of melt parameters that are not consistent in time, which contributes to the underestimation of mass loss at Griesgletscher here.

A potential solution to the non-stationarity of glacier sensitivity to temperature is to calibrate to the longest-available period, i.e. 1884-2007, however, this introduces computational stresses, uses potentially inaccurate DEMs, and the more recent time-period (1998-2007) could be deemed more representative of future sensitivity of glaciers to climate change. Finally, it is important to note that Griesgletscher, compared to the other glaciers in the study of Huss et al. (2008b), demonstrates considerably higher rates of mass loss up to a factor of 2 greater than Silvretta or Rhonegletscher. The reasons for this are unknown particularly when considering the close proximity of Rhonegletscher and Griesgletscher.

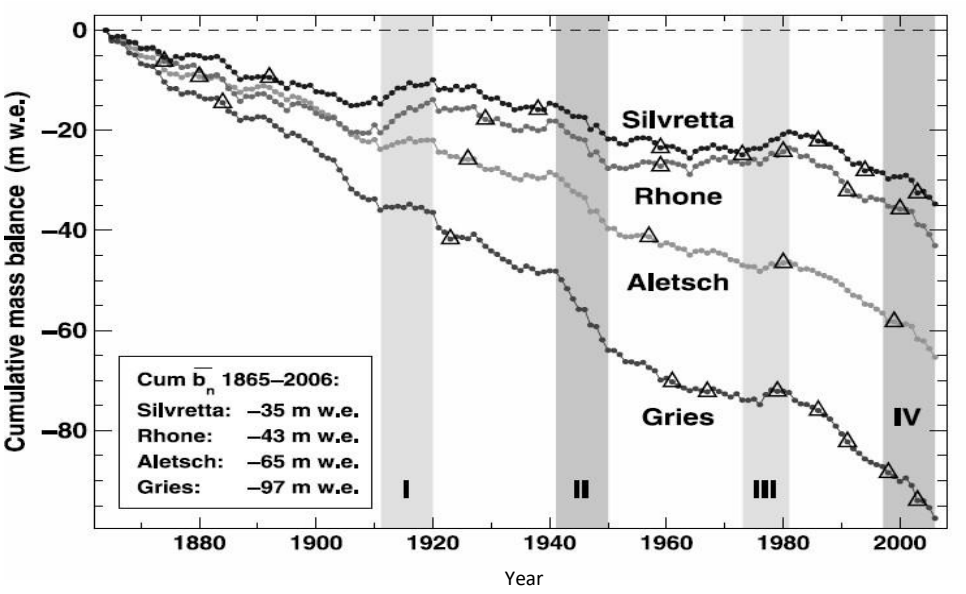

Figure 4.9: Cumulative net balance from Huss et al. (2008b) for several glaciers in the Swiss Alps. These simulations use separate calibrations for each DEM sub-period, to reconstruct mass balance time-series. Here, two decadal periods of positive mass balance (I, III) and negative mass balance (II, IV) are highlighted. Triangles show when DEMs were available.

Accuracy of DEM-derived Volume Change Observations. To mitigate errors associated with older DEMs, the bed topography used in GERM is based on the 2003 DEM for all simulations, as explained in Section 4.3.1.1. This means that the remaining errors associated with DEMs are limited to the surface DEMs and the volume estimates of Bauder et al. (2007), used as observations in this study. The study of Bauder et al. (2007) uses photogrammetry and contour lines to define elevation points which are interpolated onto a grid. Volume changes are then calculated based on glacier outlines and changes in elevation inside of the ice boundary between consecutive DEMs. Bauder et al. (2007) estimate uncertainty of their method at 5 %, with errors introduced by: 1) the quality of the original map in terms of vertical and horizontal precision, 2) accuracy of contour line evaluation or photogrammetry, and 3) error due to interpolation of elevation points. Although 2 and 3 produce small errors of 0.3-2.5 m and 0.05 m respectively, the vertical error introduced by map quality is difficult to quantify with estimates ranging from metres to tens of metres, with the oldest maps, for example 1884, showing the largest errors. Bauder et al. (2007) does conduct quality control on topographic maps and estimates a total volume change error of ±5 % in most cases.

Although these data have limitations, they remain extremely useful for comparisons of volume change. An error of ±5 % is insufficient to fully explain the differences between simulated and observed volume change in the long-term validation simulations here. Therefore, these errors can most likely be attributed to GERM.

4.5.2. Quantifying the Uncertainty of Long-Term Simulations.

Quantifying the overall uncertainty associated with long-term simulations is important so that simulations running into the future can be interpreted with awareness of uncertainties. The lack of stationarity of model parameters over the long validation period demonstrated how using a short calibration period leads to errors associated with glacier-climate sensitivity.

Quantifying the overall uncertainty can be achieved through comparison of the simulated and observed volume change from 1884-2003. This is longer than most future simulations which typically cease in 2100 due to climate model limitations, so is sufficiently long to capture the uncertainty associated with changes in glacier climatic-sensitivity. To quantify the uncertainty associated with modelling glacier volume change, the simulation error (the difference between simulated and observed volume change) was calculated as a percentage of initial volume and divided by the number of years. This provides an estimation of volume change error per year that can be translated to future simulations at Griesgletscher. Figure 4.10 shows the simulated volume change from 1884-2003 with an error of 0.18 km^3 (19.7 % of initial volume) resulting in an uncertainty of ±0.165 % yr^{-1}. This uncertainty estimation assumes that this represents the upper bound of uncertainty, since it is calculated on the longest simulation and assumes that the error is in the same direction (i.e. consistently overestimates, or consistently underestimates) each year.

Figure 4.10b shows a future simulation with this uncertainty imposed, which is calculated by adding and subtracting the error calculated (0.165 % yr^{-1}) to modelled volume change for each year of the simulation. When the glacier volume loss is 100 %, around 2073 in Figure 4.10b, the uncertainty bands can be used to demonstrate that 100 % volume loss may occur as early as 2050 or after 2100. This simulation is based on extrapolation of 1980-2000 climate data so should not be considered an accurate forecast; simulations of future glacier evolution driven with downscaled climate model data are performed in Chapter 6. It is important to emphasise that this range is the maximum uncertainty using the longest possible simulation, with shorter simulations showing lower uncertainties, e.g. 1923-2003 indicates ±0.058 % yr^{-1} and 1961-2003 ±0.006 % yr^{-1}. These lower uncertainties reflect the improved performance of GERM for shorter simulations, as described previously (Figure 4.7).

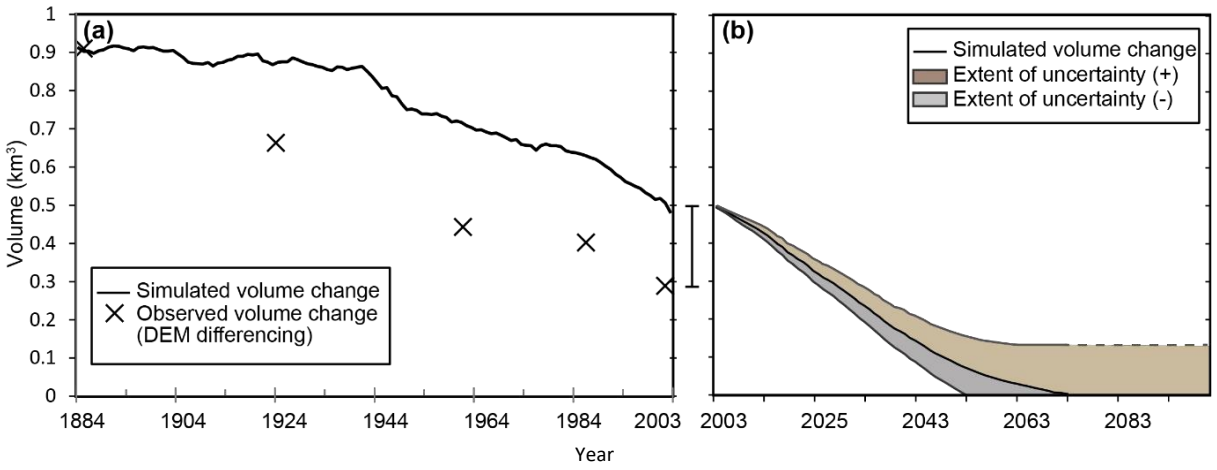

Figure 4.10: (a) simulated volume change of Griesgletscher from 1884-2003 as well as (b) future simulated volume change using linear extrapolation of temperature from 1980-2000 (used only as a demonstration of future uncertainty, the following Chapter will apply this to future projections driven by climate model outputs), showing the maximum range of uncertainty calculated using the error in (a). The dashed line in (b) represents the period when modelled ice volume is zero, therefore the upper bound for uncertainty is unknown.

4.5.3. Impact of Uncertainty on Runoff Simulation.

Interestingly, the performance of the simulations in terms of discharge does not show improvement with more accurate volume change estimates. For example, the simulated discharge of the 1884-2003 simulation produces a similar R^2 and NSE value (Figure 4.8) to the 1961-2003 simulation of discharge. Monthly discharge does demonstrate some improvement with better volume change simulation. It is also interesting that GERM appears to reproduce discharge more accurately when discharge is above average, with the lowest NSE values in low flow years for all simulations. This is consistent with a systematic overestimation of discharge.

The reasonable reproduction of discharge for all simulations suggests that the calibration to current conditions is appropriate for the duration of the discharge record (1958-2007). However, this does not mean that accurate volume change simulation is not important, since the 1961-2003 simulation shows the best reproduction of discharge, likely because the errors associated with glacier evolution are the smallest.

To calculate the uncertainty associated with simulation of discharge, the mean error between simulated and observed discharge per year during the 1884-2003 simulation is used. As such, the uncertainty in discharge should be considered a maximum bound for discharge uncertainty. At Griesgletscher, the error associated with the discharge simulation is $\pm 0.039\ 10^6\ m^3\ yr^{-1}$, which can be applied to future simulations.

4.5.4. Retreat through the Overdeepening.

The unique setting of Griesgletscher may partially explain some part of the underestimation of volume change in GERM simulations; the DEMs of Griesgletscher show that the glacier receded through an overdeepening between c.1926 and c.1990. Topographic maps provided by SwissTopo (Figure 4.11) show how a small lake formed between 1947 and 1961, before the construction of the dam created a much larger area of water after 1965, creating a lake terminating glacier (Figure 4.12). It is estimated that 150 000 m^3 of ice detached from the tongue shortly after the construction of the dam (Vischer, 1979) and that the dynamics of the glacier ablation changed with mass loss through calving. In selecting Griesgletscher as a test-catchment, it was anticipated that modelled volume changes may struggle to match observations during this period because overdeepenings can cause very rapid loss of ice mass for relatively small changes in climate (e.g. Oerlemans, 1997). The results show that, although model performance during this period is better than during earlier periods (e.g. 1884-1923, when different topographic factors may have been influencing mass loss), the model does not accurately reproduce mass loss during this period.

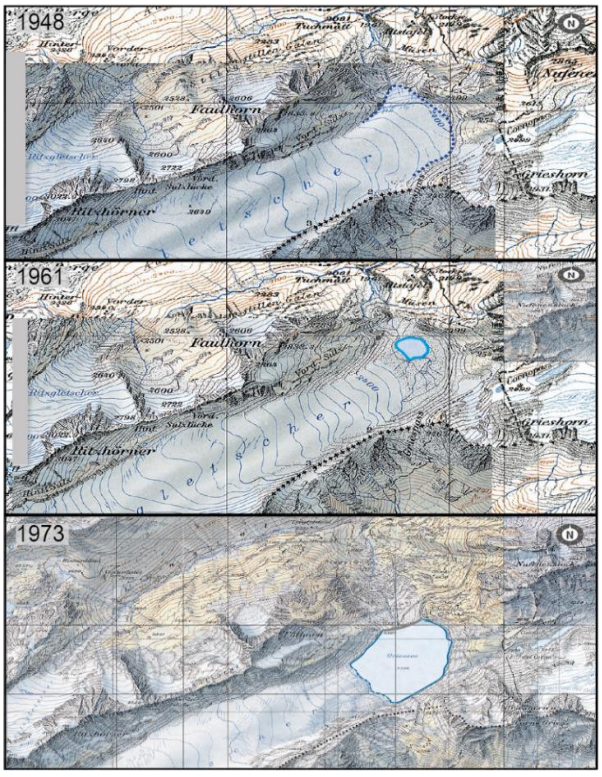

Figure 4.11: Topographic maps of Griesgletscher showing (a) the glacier shortly before retreating through the overdeepening; (b) the overdeepening has been exposed leaving a small pro-glacial lake; (c) the dam has been constructed resulting in a much larger lake and a calving front at the terminus of Griesgletscher. Maps provided by SwissTopo.

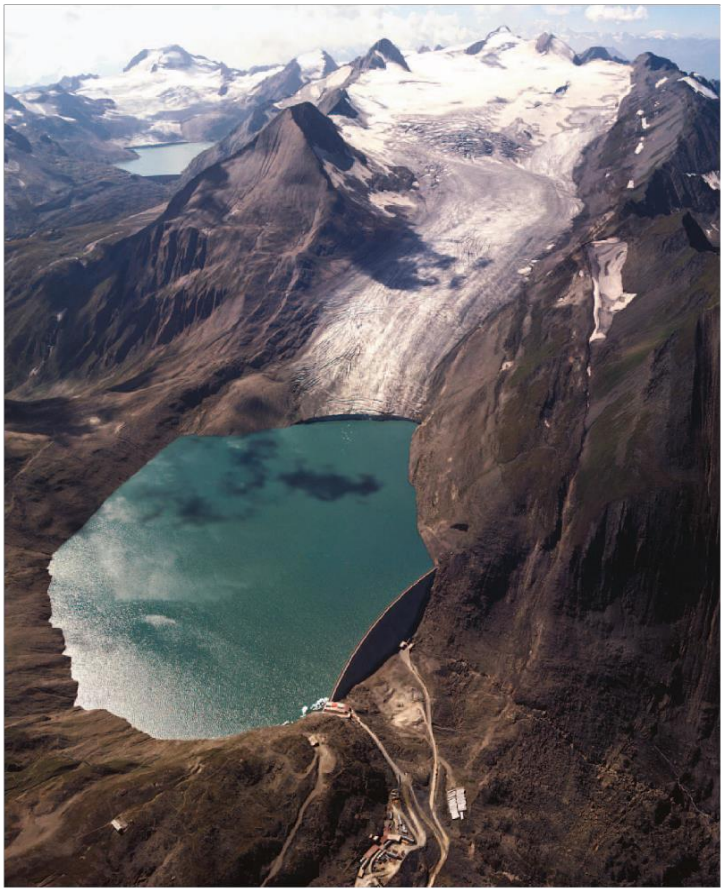

Figure 4.12: Oblique aerial photograph of Griesgletscher in 1973 showing the calving front. Since 1973, the glacier has retreated significantly, becoming a land-terminating glacier again in the 1990's. Note that the depth of the overdeepening was exaggerated by the artificial dam. Source: Hauenstein (2005); ©Luftbild Schweiz.

4.6. Applying GERM to Rhonegletscher.

4.6.1. Study Site, Data, and Calibration.

The longest simulation at Griesgletscher was also conducted at Rhonegletscher to test the portability of GERM at long time scales. Additionally, Rhonegletscher retreated through an ice-fall (see Figure 4.13) from 1900 to 2000, providing an interesting morphological feature that will test GERM in a contrasting way to the overdeepening at Griesgletscher.

Rhonegletscher is located just 14.5 km from Griesgletscher, and the closest meteorological station, Ulrichen, is located equidistant between both sites, so no further processing of meteorological data was necessary. Rhonegletscher is around 7.5 km in length and has an area of 16.4 km^2, facing south and meltwater flows into the Rhone River which is the primary inflow into Lake Geneva. The retreat of Rhonegletscher is perhaps the best-documented of all glaciers

in the Alps, with numerous paintings, topographic maps and satellite images showing significant terminus retreat (Figure 4.13).

Table 4.8: Data availability and duration of calibration and validation simulations at Rhonegletscher.

	Period
Calibration	1997-2007
Validation	1874-2005
Discharge Data	1975-2005
Volume Change Data	1874-2005

Rhonegletscher has similarly excellent glaciological data available to Griesgletscher (see Table 4.8), with volume change available since 1874 and runoff from 1975 courtesy of Bauder et al. (2007). Since the uncertainty estimation at Griesgletscher represents the maximum bound, using the longest available simulation, only a single long-term simulation, from 1874-2005, is conducted at Rhonegletscher at 25 m resolution. The same methodology applied at Griesgletscher is implemented here, so this is not repeated, but diagrams of bed topography are included in Appendix Figure A.1.

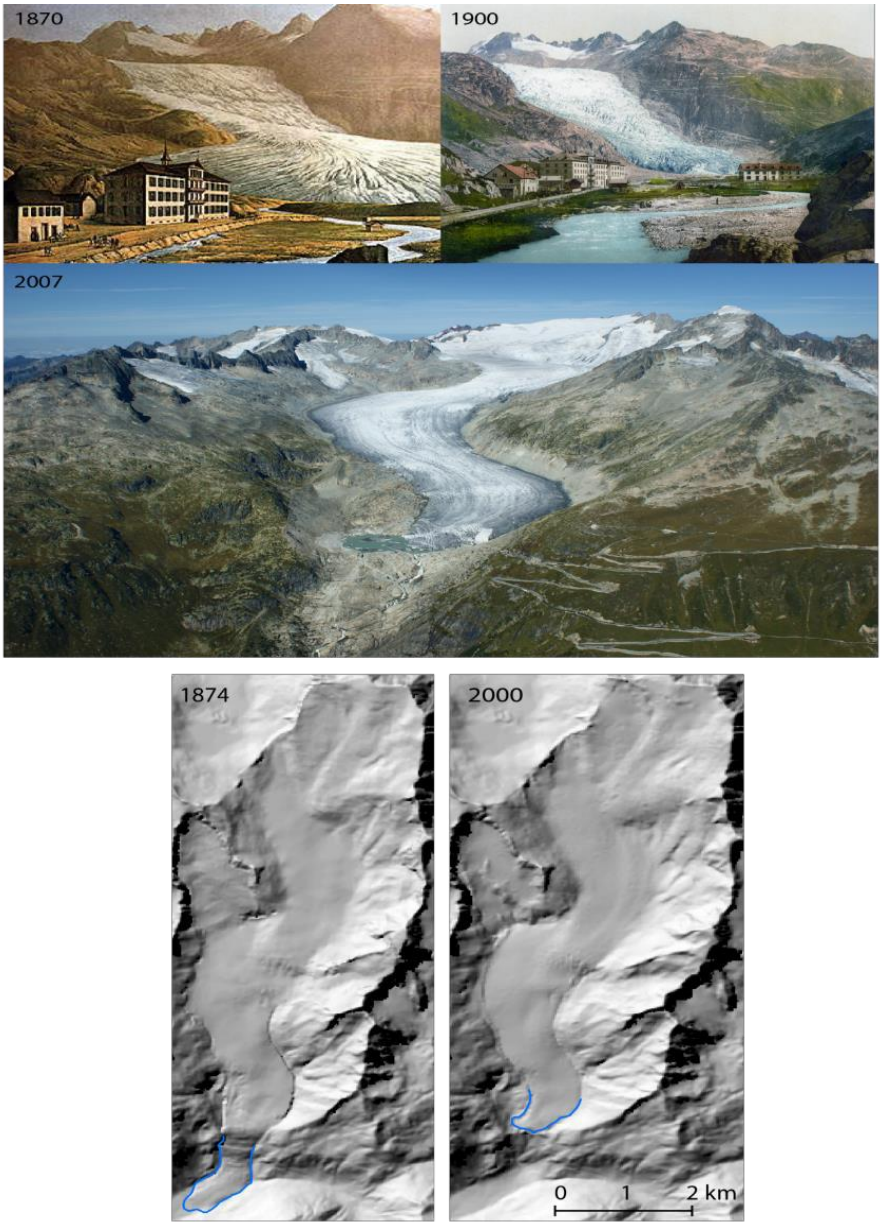

Figure 4.13: Documenting the retreat of Rhonegletscher since 1870. Upper panel shows a series of art (1870), photochrom print (1900) and photograph (2007) showing significant terminus retreat. Lower panel shows DEMs (provided by ETH-Zurich) with the terminus traced in blue for emphasis. Images in public domain.

Calibration results. Using the automated, systematic calibration procedure that was devised in this thesis, and explained in detail in Section 4.3.2 for Griesgletscher, Rhonegletscher was calibrated to glacier volume change and monthly discharge using both a coarse grid and a fine grid (Table 4.9). The results of the individual volume change and discharge calibration showed similarly smooth outputs to those of Griesgletscher. The combined results produce the parameter set shown in Table 4.10. During the calibration period (1999-2007), monthly discharge simulation produced a NSE of 0.79 and R^2 of 0.80 ($p<0.01$). These statistics and Figure 4.14 suggest that discharge is simulated well in terms of the temporal variability.

Table 4.9: Calibration results for the 'fine' grid at Rhonegletscher, using red to represent worse model performance and blue to represent better model performance. The parameters highlighted in yellow are the optimum parameters according to the calibration procedure.

F_m	R_{ice}	R_{snow}	Combined Error:										
0.95	1.52	1.14	0.682	0.702	0.721	0.739	0.756	0.771	0.784	0.797	0.808	0.818	0.827
0.94	1.50	1.13	0.712	0.732	0.751	0.769	0.786	0.801	0.815	0.828	0.839	0.849	0.859
0.93	1.49	1.12	0.742	0.762	0.781	0.799	0.816	0.832	0.846	0.859	0.871	0.881	0.892
0.92	1.47	1.10	0.772	0.792	0.811	0.829	0.846	0.862	0.876	0.890	0.902	0.914	0.924
0.91	1.46	1.09	0.802	0.822	0.841	0.859	0.876	0.892	0.907	0.921	0.934	0.919	0.903
0.90	1.44	1.08	0.825	0.845	0.864	0.882	0.899	0.915	0.930	0.929	0.912	0.896	0.880
0.89	1.42	1.07	0.861	0.881	0.900	0.919	0.936	0.927	0.909	0.891	0.874	0.857	0.839
0.88	1.41	1.06	0.891	0.911	0.930	0.936	0.917	0.897	0.879	0.861	0.843	0.825	0.808
0.87	1.39	1.04	0.920	0.940	0.926	0.906	0.886	0.867	0.849	0.830	0.812	0.794	0.776
0.86	1.38	1.03	0.935	0.915	0.895	0.876	0.856	0.837	0.818	0.800	0.781	0.763	0.744
0.85	1.36	1.02	0.904	0.885	0.865	0.846	0.826	0.806	0.788	0.769	0.750	0.732	0.713
			10	11	12	13	14	15	16	17	18	19	20
			C_{prec} (%)										

Table 4.10: Calibrated parameter sets for Rhonegletscher. *refers to parameters that are constrained by observations so were not adjusted as part of the calibration.

Parameters	Units	Calibrated Values
f_M	10^{-3} m (d °C)$^{-1}$	0.87
r_{ice}	10^{-5} m^3 (W d °C)$^{-1}$	1.39
r_{snow}	10^{-5} m^3 (W d °C)$^{-1}$	1.04
***dP/dz** **	10^{-2} % m^{-1}	7
***dT/dz** **	10^{-3} °C m^{-1}	-5.55
C_{prec}	%	11

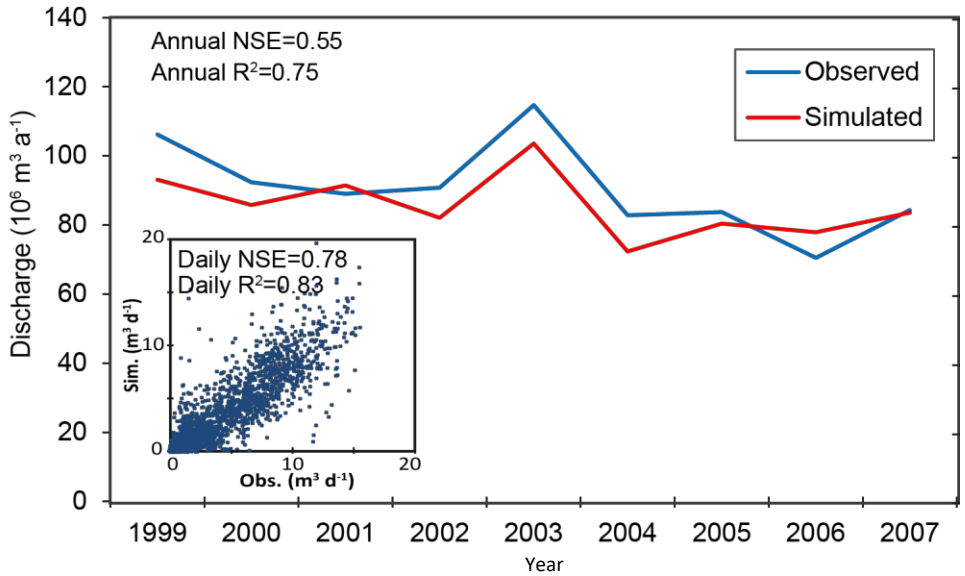

Figure 4.14: Simulated annual discharge at Rhonegletscher during the calibration period compared to observed discharge, with the inset showing daily discharge. NSE refers to Nash Sutcliffe Efficiency.

4.6.2. Validation and Discussion: Rhonegletscher.

Using the same methodology as for Griesgletscher, GERM was run from 1874-2005 to test the ability of GERM to reproduce observed volume changes. As for Griesgletscher, the discharge simulation will also be compared.

Volume Change Reproduction. Simulated volume changes (Figure 4.15) show an underestimation of volume loss from Rhonegletscher, similar to Griesgletscher, when compared to the volume losses calculated in Bauder et al. (2007). Moreover, GERM simulates a period of glacier growth from 1880 to 1940, which the observations of Bauder et al. (2007) suggest did not occur, although rates of mass loss were lower than in recent decades and Huss et al. (2008b) reconstructed a period of positive mass balance at Rhonegletscher from 1910-1920. After 1940, simulated mass balance more closely matches observations including correctly capturing a brief period of positive mass balances in the 1970s (Bauder et al., 2007; Huss et al., 2008b).

In comparison to Gabbi et al. (2014), who conducted a similar study at Rhonegletscher on a shorter time-scale, the results here confirm that the HTI model (used to calculate melt in GERM) underestimates volume losses. However, the magnitude of the underestimation is considerably less in this thesis. For example, Gabbi et al. (2014) simulated continued glacier growth until 1990 with final glacier volume representing an overall mass gain. The results here, however, show continued mass loss since around 1940, and perform better in comparison to the observations. The reasons for the different approaches are likely the longer calibration period in this thesis (1999-2007 vs. 2007-2012 in Gabbi et al., 2014), and the calibration to volume change and discharge in this thesis, compared to only mass balance in Gabbi et al. (2014). These results further demonstrate the impact differing calibration strategies may have on glacier and runoff simulation.

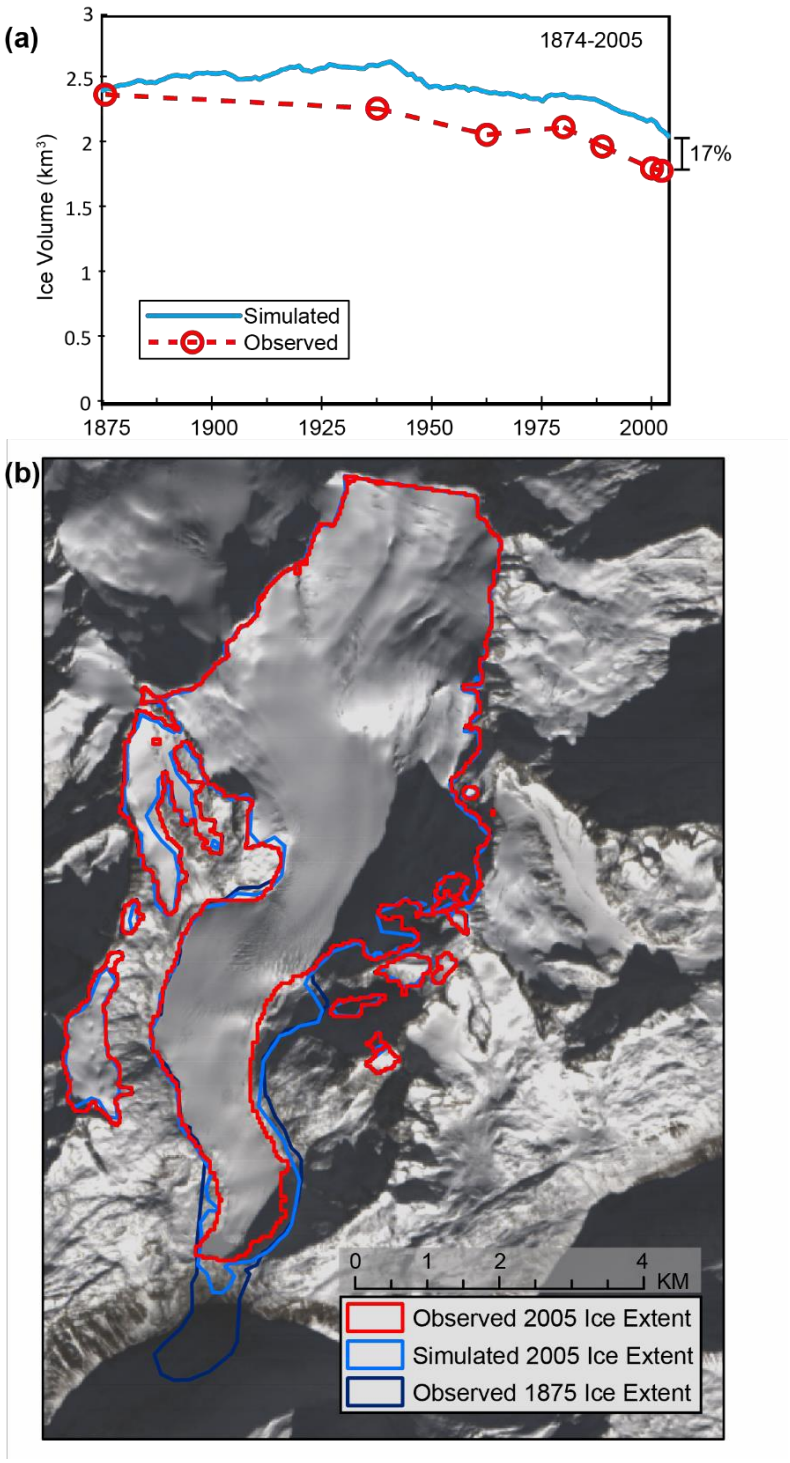

Figure 4.15: (a) Simulated and observed ice volume change at Rhonegletscher from 1874-2005. (b) Simulated and observed glacier outlines from start of simulation (1875) to end of simulation (2005), showing relatively good simulation of the glacier outline.

Spatial Glacier Changes. Simulated glacier extent in 2005 is close to the observed extent (Figure 4.15b). The paradox of accurately simulated ice extent and underestimation of ice volume suggests that ice thickness is not accurately simulated, likely due to the glacier growth until 1940, which is not accurately redistributed in GERM. Specifically, when a positive mass balance is calculated, the consequential increase in ice volume can only be expressed as thickening, since

GERM cannot reproduce ice advances (Huss et al., 2008a). Ice advances are poorly reproduced in terms of spatial ice extent because there is no model component to redistribute ice mass to grid-squares where no ice exists. For example, because the ice mass redistribution uses the Δh-parameterisation rather than an actual flow model, the ice does not know where to go - it can only retreat through thinning or remain and thicken. The impact of poor representation of glacier advances is minimal for most future modelling studies since glacier recession is so widespread and is likely to continue or accelerate with future warming. However, for long-term modelling in the *past*, the lack of accurate glacier advances are problematic due to the creation of a positive feedback with increased ice elevation (during thickening) demoting melt, so should be considered a model limitation and the model should not be applied where considerable glacier growth is expected.

Rhonegletscher retreating over an Ice Fall. The recent retreat of Rhonegletscher has passed through an area where there was previously an ice fall, from approximately 1900-2000. The influence of the ice fall could potentially reduce the sensitivity of the glacier to warming. For example, as the elevation of the ELA moves upwards through the icefall, the steep nature of the glacier in this area results in a relatively small loss of ice mass. Although GERM does underestimate mass losses at Rhonegletscher, it is not possible to distinctly attribute this to the ice fall, however it is likely that the change in the rate of mass loss over this period contributes to the overall underestimation of mass loss.

Discharge Reproduction. The simulation of annual discharge in GERM shows a consistent, significant (t-test; $p<0.05$) underestimation of discharge (Figure 4.16), with the negative NSE value reflecting a difference in the means between simulated and observed discharge. Similarly for seasonal discharge (Figure 4.16b), there is a significant (t-test; $p<0.05$) underestimation during July and August. However, other months show improved representation of discharge with smaller gross and relative errors, suggesting that the main contribution to the underestimation in annual discharge is a result of underestimation of peak summer discharge. Since most seasonal snow melt has occurred before July and August, the simulated underestimation during these months is likely caused by the underestimation of ice melt. Moreover, it appears that GERM is not sufficiently reproducing the mass turnover of Rhonegletscher, with too little melt compensated for by too little precipitation, resulting in the correct volume changes (during calibration) but incorrect discharge reproduction. Such underestimation of mass turnover was not clear during calibration (1999-2007) where annual discharge is correctly reproduced, again demonstrating the issues of short-term calibration.

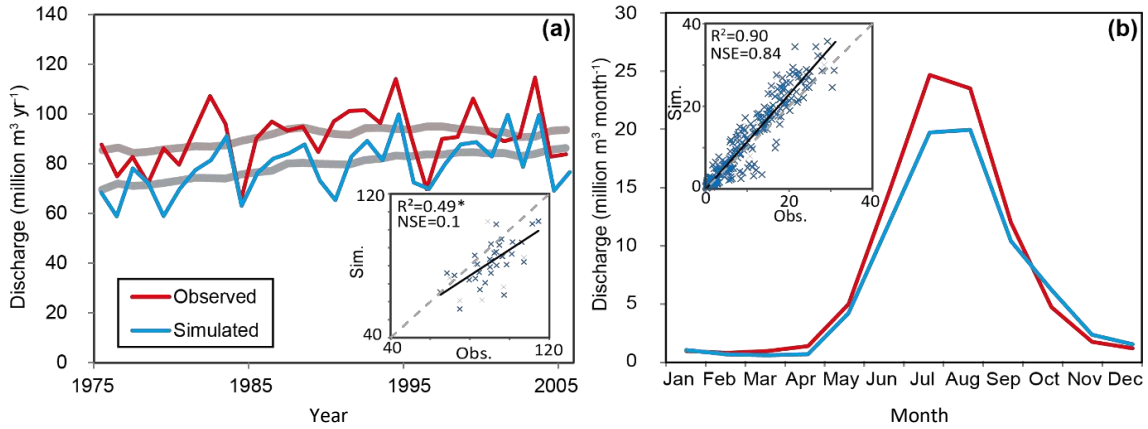

Figure 4.16: Annual (a) and seasonal (b) discharge simulations at Rhonegletscher, compared to observed discharge from 1975-2005. Note the consistent underestimation in simulated annual discharge in (a) that is likely caused by underestimation of peak summer discharge in (b). Thicker paler lines in (a) refer to 8-year moving averages. * signifies the R^2 is insignificant at $p<0.05$.

Quantifying Uncertainties. The uncertainty associated with the 1874-2005 simulation at Rhonegletscher is ±0.132 % yr^{-1}, compared to ±0.165 % yr^{-1} at Griesgletscher. Although both simulations show underestimation of ice volume lost, Rhonegletscher exhibits less uncertainty than Griesgletscher. Although it is not possible to identify the cause of the differing performances, it is likely that there are contributing factors that are not accounted for in GERM. For example, Huss et al. (2008b) shows that, when re-calibrating for each DEM period, Griesgletscher loses ice mass unexpectedly rapidly compared to Silvretta and Rhonegletscher, with mass loss up to a factor of two greater. Such rapid recession may be influenced by the changing albedlo of the glacier surface (e.g. see Rabatel et al., 2017) which is not incorporated in GERM, and the results here show that GERM is not reproducing this recession accurately.

In terms of discharge, the observations from 1975-2005 allow uncertainty to be calculated as the mean bias divided by the number of years, resulting in an error of ±0.16 10^6 m^3 yr^{-1}.

4.7. Conclusion.

The results of this chapter represent the first uncertainty analysis of any glacio-hydrological model over a period of over 100 years and will be used to constrain the future modelling uncertainty at Griesgletscher and Rhonegletscher in Chapter 5. This chapter also developed a new systematic calibration procedure for GERM that improves the transparency and robustness of previous methods.

The uncertainty analysis assessed the ability of the model to reproduce long-term glaciological and hydrological changes using a relatively short calibration period, with results showing that there are considerable uncertainties. Considering many glacio-runoff studies use similarly short

calibration periods before running long-term future simulations, it is reasonable to suggest that uncertainties of future model projections may be underestimated in many of these studies. In this thesis, using the longest possible simulation, uncertainty in modelling volume change at Griesgletscher is estimated to be ±0.165 % yr^{-1}, and ±0.132 % yr^{-1} at Rhonegletscher.

The considerable uncertainty that exists over simulations ranging from 42 to 119 years suggests that the climatic sensitivity of Griesgletscher and Rhonegletscher is not stationary due to a changing relationship between melt and temperature, caused by increased cloudiness or enhanced solar irradiance, for example. Additionally, Both Griesgletscher and Rhonegletscher have retreated through or over complex topographic features in the past 100 years, in the form of an overdeepening at Griesgletscher and an ice fall at Rhonegletscher. These cannot be explicitly modelled in GERM, so testing the model in such demanding catchments over long periods provides a more realistic assessment of uncertainty on scales of glacier change associated with 90 year future model runs than short-term validation where the glacier may not be retreat over complex topography.

Considerations such as these emphasise how complex simulation of glacial catchments can be, and how necessary it is to incorporate uncertainties into future simulations. The lack of time-varying melt parameters is a key limitation of many glacio-runoff models and should be acknowledged when performing future simulations. However, the attribution of all of this uncertainty to model skill is problematic, since there are known issues with DEM differencing data used as observations (estimated to be 5 %).

Discharge reproduction in GERM is generally good, however, the results clearly show that, where glacier volume loss is underpredicted, annual runoff is overpredicted due to a greater ice reservoir available for melt, emphasising why it is important to correctly predict glacier volume in order to accurately predict annual catchment runoff. Performance at Griesgletscher was better that that at Rhonegletscher with an annual mean error of ±0.039 10^6 m^3 yr^{-1} compared to 0.16 10^6 m^3 yr^{-1} at Rhonegletscher.

Finally, the simulations and observations at both these sites clearly indicate that glacier mass loss has been considerable since the 1880s and that the rate of mass loss appears to be accelerating in the most recent decades. At Griesgletscher, it appears that the accumulation zone is not at a high-enough elevation to sustain glaciation at current temperatures. In Chapter 5, simulations in the future are performed to assess how long the glacier will remain when climate change scenarios are used to drive GERM. At Rhonegletscher, there is a larger mass of high-elevation ice suggesting that the glacier may be more sustainable. Again, this will be assessed in Chapter 5.

5. FUTURE GERM SIMULATIONS: THE EUROPEAN ALPS.

This chapter uses the bias correction and validation outlined in Chapters 3 and 4 respectively to conduct simulations of future glacier volume change and runoff at Griesgletscher and Rhonegletscher, which can be used in mitigation and adaptation studies. Chapter 4, in which long term records were used to validate the performance of GERM over 120 year time periods, will be used to provide calibration parameters and to constrain the uncertainty of future projections. Chapter 3, in which CORDEX RCM outputs were bias-corrected using in-situ meteorological data, will be used to provide estimates of future temperature and precipitation that are needed to drive GERM from 2010-2100. This chapter addresses Aim 2C.

5.1. Introduction.

Previous studies have applied glacio-hydrological models to project future runoff evolution at both Griesgletscher and Rhonegletscher on 100 year timescales (e.g. Farinotti et al., 2012; Huss et al., 2010; Jouvet et al., 2011; Sugiyama et al., 2007). However, the work reported in this thesis is novel because (1) it more robustly assesses uncertainties from the long-term validation are applied to the future projections, and (2) the most up-to-date RCM data (CORDEX) are used to drive GERM, which includes application of a novel advanced bias correction method for the climatic input data.

The first key difference between this thesis and previous attempts to project changes in glaciers and runoff in the European Alps is the long-term validation of GERM performance in Chapter 4, which provides the best possible assessment of uncertainty given the available data, particularly in relation to glacier mass losses, necessary when future glacier changes are expected to be significant. The second key difference is the driving climate data. As described in Chapter 5, CORDEX RCM simulations represent the state-of-the-art of dynamical downscaling of CMIP5 GCMs. Thus, the combined dynamical-statistical downscaling approach outlined in Section 5.3 improves upon previous studies in the European Alps (e.g. Farinotti et al., 2012; Finger et al., 2012; Gabbi et al., 2012; Horton et al., 2006; Huss et al., 2008a; Machguth et al., 2009). It is the combination of better awareness of glacier-hydrological modelling uncertainties and the best possible climate model outputs that ensures that both the uncertainties associated with GERM and the uncertainties associated with the driving climate model are more accurately accounted for than in previous studies. Therefore, this section provides a thorough assessment of future glacier and runoff changes at Griesgletscher and Rhonegletscher, and fully quantifies the uncertainty associated with GERM, as well as providing an indication of the uncertainty associated with climate inputs.

5.2. Methods.

The majority of the GERM methodology and calibration has been described in Chapters 2 and 4, respectively, so this section will only briefly recap these. The main focus of this section will instead be to outline the simulations of future glacier change.

5.2.1. Calibration Parameters.

The calibrated parameter sets from Chapter 4 are used here for every simulation (Table 5.1). These parameters were calibrated to glacier volume change and catchment discharge from 1998-2007 and from 1999-2007 for Griesgletscher and Rhonegletscher, respectively.

Table 5.1: Calibrated parameter sets for Griesgletscher and Rhonegletscher.

	Units	Griesgletscher	Rhonegletscher
f_M	10^{-3} m (d °C)$^{-1}$	1.11	0.87
r_{ice}	10^{-5} m^3 (W d °C)$^{-1}$	1.78	1.39
r_{snow}	10^{-5} m^3 (W d °C)$^{-1}$	1.33	1.04
***dP/dz** **	10^{-2} % m^{-1}	1	7
***dT/dz** **	10^{-3} °C m^{-1}	-5.47	-5.55
c_{prec}	%	0	11

5.2.2. Climate Input Data.

Table 5.2: Available RCM-GCM combinations that include evaluation simulations in the CORDEX-Europe domain. The RCPs column includes the names by which simulations are referred to in this chapter.

	RCM	Driving-GCM	RCPs		
			2.6	4.5	8.5
A	RCA4	ICHEC-EC-EARTH	A-2.6	A-4.5	A-8.5
B	RCA4	CERFACS-CNRM	✗	B-4.5	B-8.5
C	RACMO	MOHC-HadGEM2	✗	C-4.5	C-8.5
D	CCLM	ICHEC-EC-EARTH	✗	D-4.5	D-8.5
E	HIRHAM	ICHEC-EC-EARTH	E-2.6	E-4.5	E-8.5

Chapter 5 described the bias-correction of daily temperature and precipitation time-series from the grid squares of the CORDEX RCMs over the relevant catchment. Here, these corrected series are used to drive GERM into the future. The range of five climate model combinations, utilising three GCMs and four RCMs, each with two or three RCPs (summarised in Table 5.2) allows partial assessment of the uncertainty introduced by different climate inputs. For example, three of the RCMs are driven by the ICHEC-EC-EARTH GCM, allowing the influence of RCM uncertainty to be assessed. Similarly, the RCA4 RCM is driven by both ICHEC-EC-EARTH and CERFAC-CNRM, revealing some of the uncertainty associated with driving GCMs. Although it would be preferable to utilise more GCMs and RCMs, the lack of available CORDEX-RCM outputs at the time of analysis limited this. Additionally, RCP 2.6 is only available for two of the GCM-RCM combinations. Therefore, these simulations represent only part of the uncertainty associated with climate inputs.

Table 5.3 and 5.4 summarise the mean temperature and precipitation as well as the trends associated with each climate input (also see Section 3.4 – Figures 3.7-3.10, for plots of trends and time-series), for both catchments.

Table 5.3: Trends, calculated from 2010-2100, from the various bias-corrected climate data used to drive GERM to 2100 at Griesgletscher. Trends calculated using Mann-Kendall test with * indicating significance (p<0.01). Time-series can be found in Section 5.4.

		TEMPERATURE		PRECIPITATION	
MODEL combination	RCP	MEAN °C	TREND Δ °C/10 year	MEAN mm/year	TREND Δ mm/10 year
A	2.6	-0.45	0.05	1837.3	30.43
	4.5	0.03	0.22*	1899.5	10.35
	8.5	1.30	0.64*	1834.3	15.56
B	4.5	-0.45	0.21*	2495.6	10.28
	8.5	0.51	0.57*	2490.2	61.77*
C	4.5	0.20	0.35*	2302.3	-40.44
	8.5	1.58	0.70*	2600.3	15.47
D	4.5	-0.38	0.19*	2455.8	32.91
	8.5	0.36	0.40*	2400.2	20.22
E	2.6	-1.25	0.07*	2699.3	-0.74
	4.5	-0.39	0.14*	2593.4	20.35
	8.5	0.32	0.39*	2577.3	26.63

Table 5.4: Trends, calculated from 2010-2100, from the various bias-corrected climate data used to drive GERM to 2100 at Rhonegletscher. Trends calculated using Mann-Kendall test with * indicating significance (p<0.01). Time-series can be found in Section 5.4.

		TEMPERATURE		PRECIPITATION	
MODEL combination	RCP	MEAN °C	TREND Δ °C/10 year	MEAN mm/year	TREND Δ mm/10 year
A	2.6	-0.85	0.06*	2247.9	27.5
	4.5	-0.27	0.19*	2178.8	33.1
	8.5	0.76	0.55*	2218.9	32.4
B	4.5	-0.07	0.16*	2492.3	-0.2
	8.5	0.70	0.44*	2706.5	104.1*
C	4.5	-0.01	0.23*	2685.4	-18.6
	8.5	1.00	0.51*	2894.5	28.9
D	4.5	-0.44	0.18*	2327.2	29.1
	8.5	0.26	0.38*	2268.5	18.3
E	2.6	-1.11	0.06*	2499.1	15.0
	4.5	-0.80	0.11*	2600.0	46.9
	8.5	-0.31	0.27*	2785.9	68.1*

5.3. Results of Future Simulations in the European Alps.

The following sections will describe the results from all simulations at Griesgletscher and Rhonegletscher. GERM model runs are referred to as described in Table 5.2, with climate-model combinations defined from A to E and RCPs defined as RCP 2.6, 4.5 or 8.5. Firstly, all results will be analysed before identifying specific projections that demonstrate the most extreme changes, least extreme changes, and median changes, which will then be analysed in greater detail.

5.3.1. Results of Future Simulations at Griesgletscher.

5.3.1.1. Glacier and Runoff Evolution at Griesgletscher.

The evolution of Griesgletscher from 2010 to 2100 is shown in Figure 5.1. The general pattern across all model simulations is of significant ice volume loss with only one projection (E–2.6) simulating more than 5 % remaining ice in 2100. 5 % remaining ice is used as an indication of effective glacier disappearance since 0 % is misleading as very small areas of high-altitude ice can survive long after the vast majority of the glacier has melted, due to topographic shading or high levels of avalanche-derived accumulation, for example. Accordingly, mass balances are also strongly negative and shows negative trends for all simulations. However, some model runs do show a partial mass balance recovery towards the end of the century (e.g. A-2.6 and E-8.5), likely due to a small proportion of high-elevation ice remaining. This is further investigated in Section 5.5.1. In terms of discharge, there is considerable variability between the simulations with A and C showing significant negative trends ($p<0.01$), whereas climate model combination B shows no significant trends, and D and E only significantly negative for RCP 8.5 and RCP 4.5 respectively. However, it can be concluded that discharge is not simulated to increase significantly in any of the projections. Select model outputs will now be described and interpreted in turn.

Climate model combination *A* promotes relatively rapid ice retreat in all three RCP scenarios, with over 95 % of ice lost by 2063 in all three RCPs (Figure 5.1-A2). The similar ice loss under these RCPs and the more rapid ice loss under RCP 2.6 in the early part of the century is counterintuitive; one may expect the glacier to lose ice mass more slowly under RCP 2.6 than RCP 4.5. However, the climate trend inputs summarised in Table 5.2, and shown in detail in Section 3.4 (Figures 3.7-3.10.), show that the RCP 2.6 temperature initially increases at a similar rate to RCP 8.5, while initially simulating less precipitation. After 2040, the temperature trend of RCP 2.6 stabilises and precipitation increases, which is reflected in the recovery in mass balance and survival of a small proportion (2 %) of ice until 2100. In terms of discharge (Figure 5.1-A1), model combination A simulates a significant downward trend (see Figure 5.2) for all RCPs, with peak discharge occurring between 2020 and 2030. This decrease in discharge suggests that the current level or discharge (c. 30 10^6 m^3 yr^{-1}) is a result of melting ice and that a lower level of discharge (c. 20 10^6 m^3 yr^{-1}) is reached once the ice has been removed.

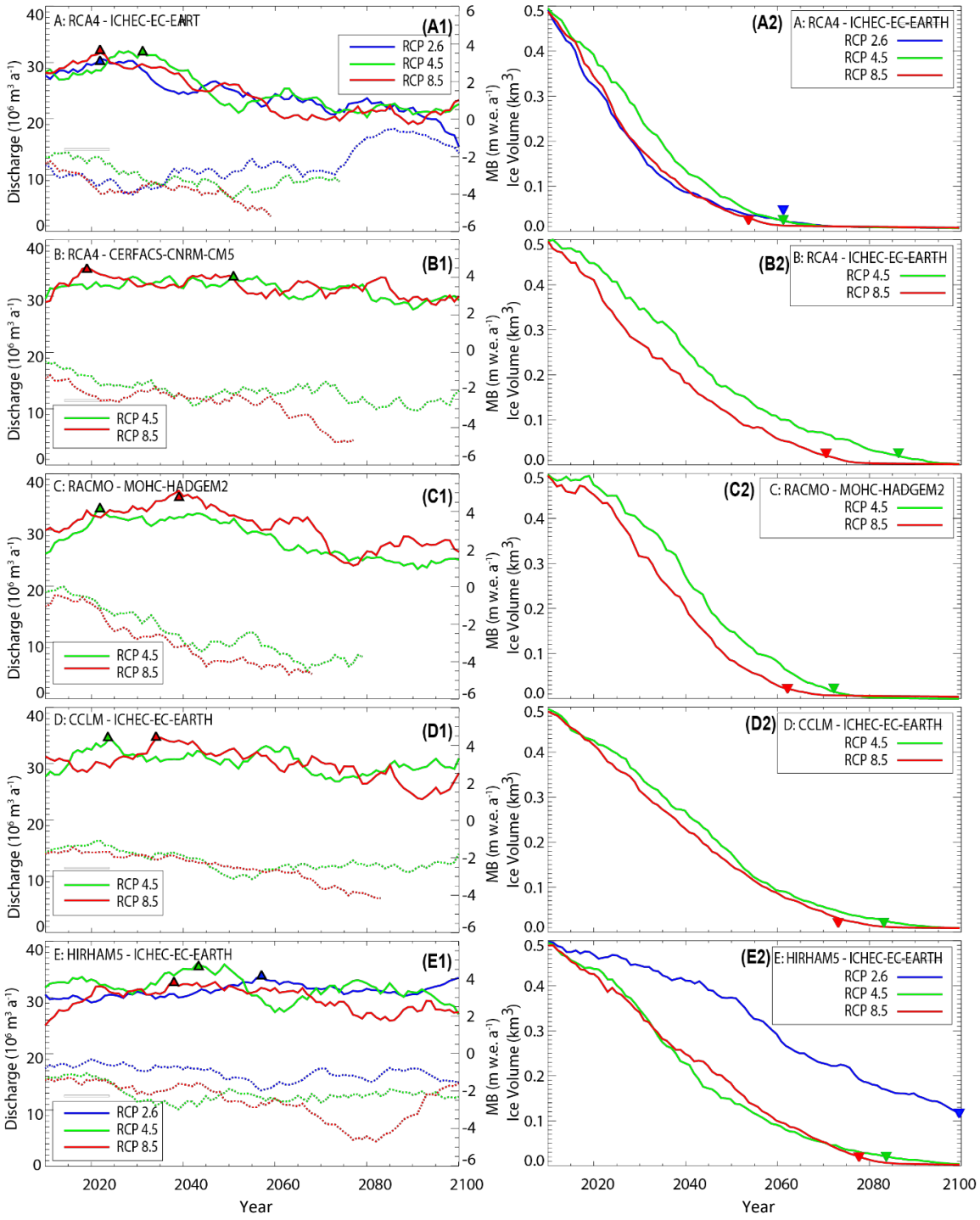

Figure 5.1: Simulations of future annual discharge (solid lines in left panel), mass balance (dashed lines in left panel) and ice volume change (right panel), for Griesgletscher when forced by 5 climate model combinations, each with two or three RCP scenarios. Triangles in the left panel show when peak discharge is reached (calculated based on 10-year running mean). Down-turned triangle in the right panel indicates where 95 % ice volume has been lost. Mass balance and discharge are shown as 10-year running means.

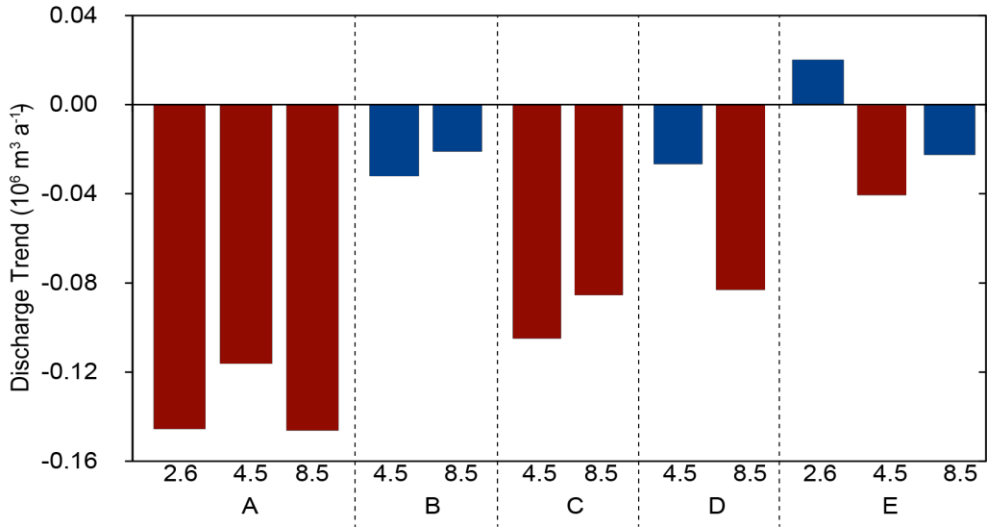

Figure 5.2: Trend analysis for discharge at Griesgletscher calculated using the Mann-Kendall test with significance indicated with red bars (p<0.01). A-E refer to the driving climate model combinations (see Table 5.2) and numbers (e.g. 4.5) refer to the RCP. Trends are calculated over the period 2010-2100, therefore assess the overall trend and do not account for decadal trends.

Conversely, climate model combination E (Figure 5.1-E2) retains 95 % ice volume until 2077 for RCP 8.5, 2082 for RCP 4.5 and 0.11 km^3 ice remains for RCP 2.6 even in 2100, the only scenarios to simulate over 5 % ice remaining at the end of the century. Indeed, RCP 2.6 shows a significantly slower rate of ice decline than all other simulations. This occurs because the E-2.6 climate scenario for this model combination projects the coolest temperatures and the highest precipitation of all model combinations (Table 5.3). Therefore, the mass balance is only slightly negative for much of the 21st century. For this model combination, similar precipitation levels are projected under RCPs 4.5 and 8.5, but with warmer temperatures, resulting in a considerably larger proportion of precipitation falling as rain rather than snow, compared to RCP 2.6. Therefore, RCPs 4.5 and 8.5 exhibit a more negative mass balance and more rapid ice loss. The unusual recovery of mass balance simulated at the end of the century under RCP 8.5 is the result of a small part of high-altitude ice surviving when ice at lower altitudes is removed, thus mass balance of the high-elevation ice is closer to zero. In terms of runoff (Figure 5.1-E1), model combination E simulates no significant trends over the century, in contrast to model combination A, due to the higher precipitation rates. However, there is some evidence that, for RCP 4.5 and RCP 8.5, the discharge is decreasing at the very end of the century with over 95 % of ice removed.

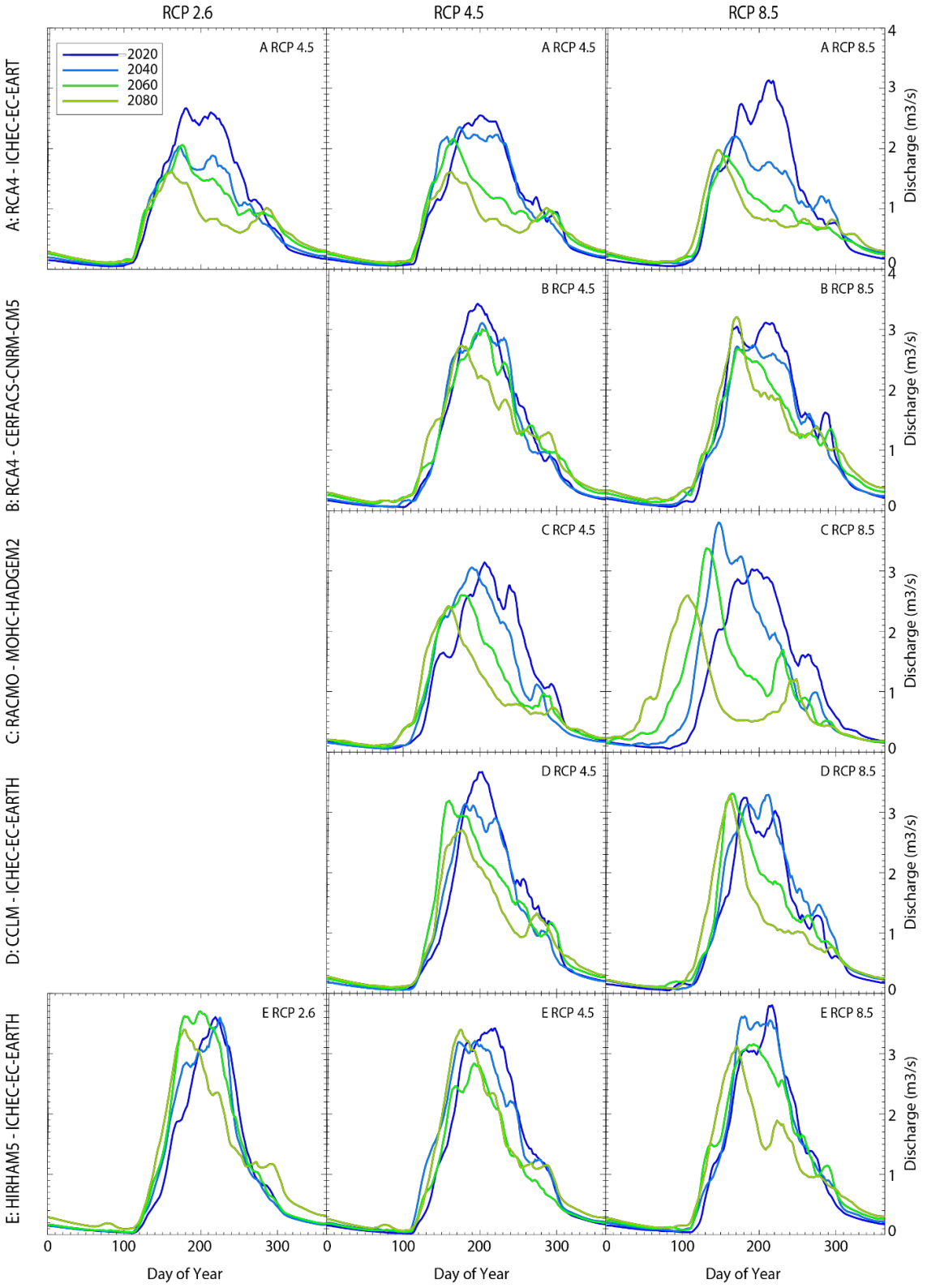

Figure 5.3: Changes in seasonality of discharge at Griesgletscher for all climate simulations. Each line represents the mean of discharge for 10 years, e.g. "2020" is mean discharge from 2015-2025.

5.3.1.2. Seasonal Changes at Griesgletscher.

The seasonal changes in discharge shown in Figure 5.3 suggest that, generally, the discharge curve will become less peaked and that peak discharge will occur earlier in the year, representing earlier onset of snow and ice melt. For example, simulation C-8.5 (Figure 5.3; also see Figure 5.5) shows peak melt changing from c. DOY 200 (mid-July) in 2020 to c. DOY 110 (mid-May) by 2080. However, other simulations show less dramatic changes to the start of the melt season with, for example, E-2.6 showing a change of from c. 220 (8 August) to c. 180 (29 June).

There are considerable differences between the seasonal discharge pattern produced by forcing GERM with different model combinations. For example, both A and B use the same RCM (RCA4), but the RCM is driven by differing GCMs, resulting in A exhibiting shallower peaks in summer discharge and a reduced overall discharge. Similarly, model combinations A, D, and E are all driven by the same GCM (ICHEC-EC-EARTH) but use different RCMs. The seasonal discharge modelled in D and E is similar, however, A is much shallower, showing that RCA4 is behaving differently to CCLM (D) and HIRHAM (E). These results confirm that both the driving GCM and RCM are influential, with the influence of neither dominating over the other.

5.3.1.3. Spatial Pattern of Ice Loss at Griesgletscher.

The following sections will focus on a selection of three model outputs which represent the end-members of all simulations: A-8.5 shows the fastest mass loss; B-4.5 represents the typical mass loss, and E-2.6 represents the least mass loss.

Spatial plots of glacier recession are shown for selected model outputs in Figure 5.4, with plots for all other model runs included in Appendix Figure A.3. The general pattern of ice loss in all simulations is terminus recession with a detachment between the upper and lower glacier, demonstrated in (B) at 2060. Such a detachment prevents the redistribution of ice from the accumulation area causing the ablation area to quickly decline. The remaining accumulation area then gradually declines with the last ice to melt occurring in the thickest part of the glacier, visible as the only remaining ice in (A). In some projections, for example E-8.5 (Figure 5.1-E), this high-altitude ice causes a slight recovery in the mass-balance. However, there are clearly large differences between the spatial patterns of mass loss in the simulations. For example, model A-8.5 shows near-complete ice loss by 2060, comparable to the ice lost by 2100 in model B-4.5, whereas model E-2.6 shows a much lower area of ice lost by 2100.

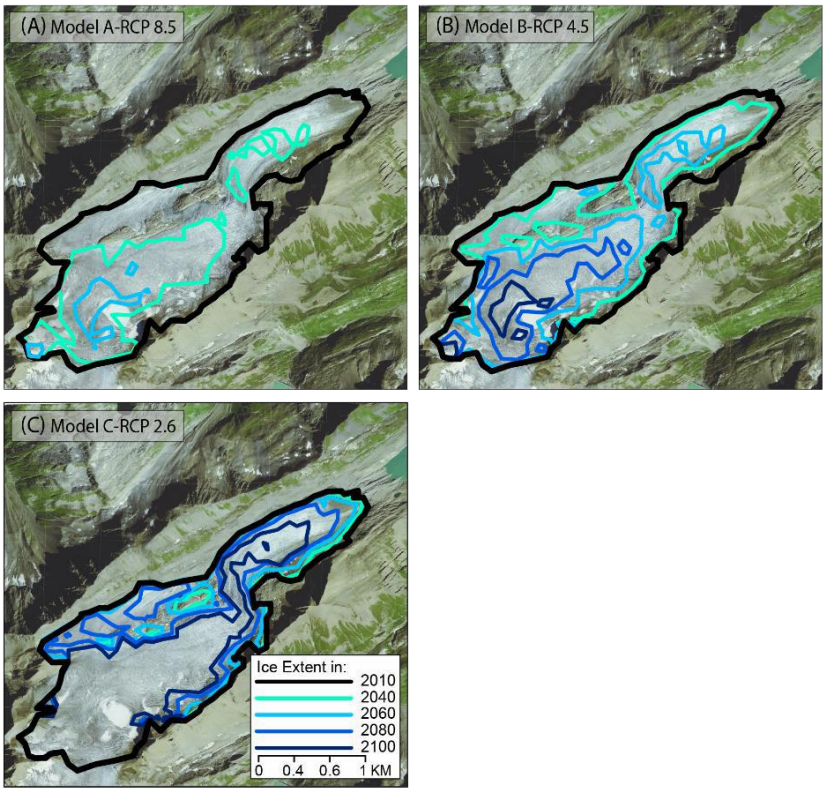

Figure 5.4: The spatial pattern of mass loss for a selection of GERM simulations. (A) model combination A-8.5, the fastest receding glacier. (B) model combination B-4.5, deemed a 'typical' simulation indicative of the median rate of mass loss of all projections. (C) model combination E-2.6, with the slowest mass loss. 2080 and 2100 ice extents are not included in (A) as no ice remains.

5.3.1.4. Glacier Contribution to Discharge at Griesgletscher.

The contribution of ice melt to overall discharge at Griesgletscher is shown alongside snow melt contribution (Figure 5.5). Clearly, the decline in ice volume in all simulations causes a lessening contribution of ice melt to overall runoff between 2020 and 2080, with the exception of E-2.6 which actually shows an increase from 10 % to 17 %. This increase reflects the fact that E-2.6 exhibits the lowest ice volume loss of all simulations with a large body of ice still remaining in 2080 and thus contributing to melt, leading to a positive (not significant) trend in annual discharge. Figure 5.5 also shows a shift in the timing of the snow and ice melt peaks, both of which occur earlier in the year in 2080 than 2020, due to the increased temperatures promoting snow and ice melt earlier in the season.

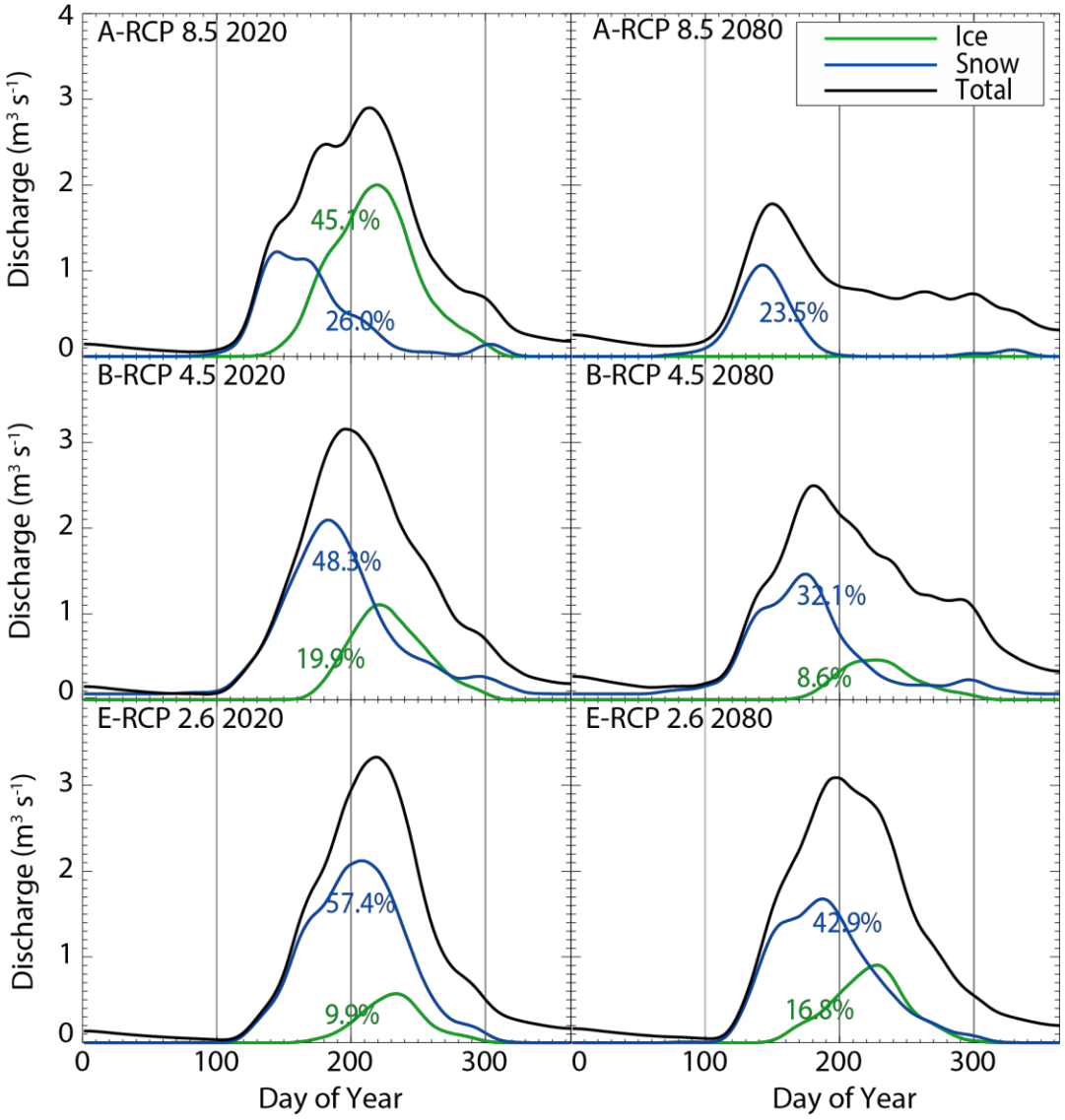

Figure 5.5: the contribution of snow and ice melt to overall discharge in 2020 and 2080, calculated as mean of +/- 5 years, for three select simulations. Percentages quantify the contribution of ice and snow to overall discharge.

5.3.2. Results of Future Simulations at Rhonegletscher.

5.3.2.1. Glacier and Runoff Evolution at Rhonegletscher.

Figure 5.6 shows the evolution of the Rhonegletscher catchment from 2010-2100. In general, there is a continued pattern of mass loss throughout the century (Figure 5.6; panel 2) with negative mass balances (Figure 5.6; panel 1 - dashed line) in all simulations except one (C-4.5) throughout the century. In several simulations, however, the mass balance shows recovery to less negative values towards the end of the century (e.g. A-2.6 and 4.5; C-4.5 and 8.5; D-4.5 and 8.5), which will be explored more closely when looking at the spatial patterns of ice loss. In

contrast to the substantially smaller Griesgletscher, only one simulation suggests that no ice will remain by 2100, with all except A-8.5 projecting more than 5 % ice remaining in 2100.

In terms of discharge, the pattern is more complex than Griesgletscher, with Figure 5.6 showing contrasting trends between the different climate model combinations. Specifically, model combination A shows significant ($p<0.01$) negative trends whereas all other models simulate positive trends, not all of which are significant. The contrast between model combination A and the other model combinations is in line with the glacier volume loss simulations, and suggests that, for B-E, discharge may indeed decrease in the other simulations once ice volume decreases further, but this is not projected to occur before 2100. This is reflected in the timing of peak discharge which, with the exception of A and E-2.6, occurs after 2050. Specific projections will now be discussed in more detail.

Interestingly, of the simulations that use the GCM, ICHEC-EC-EARTH, HIRHAM5 (E) behaves quite differently to RCA4 (A) and CCLM (D). This contrasts the pattern at Griesgletscher, where RCA4 exhibited different behaviour. Such a difference suggests that the RCMs can differ considerably, even over the relatively short distance between Griesgletscher and Rhonegletscher (c. 15 km). Additionally, there are strong differences in glacier and discharge evolution between the two model-combinations that both use RCA4 (A and B), but are forced with different GCMs.

There is clearly considerable variability in the glacier evolution projected under different climate model combinations. For example, model combination A suggests ice loss will be near complete for both RCPs 4.5 and 8.5, with RCP 2.6 simulating just 11 % ice remaining in 2100. This is in contrast to other outputs driven by climate model combinations B-E, which suggest considerably less ice loss, with only B-8.5 and D-8.5 projecting near complete ice loss by 2100. The runoff response of A also contrasts the other simulations with peak discharge reached between 2020-2030, followed by a continual significant decline (Figure 5.7), suggesting that the removal of ice mass will cause lower discharges than at present. As for Griesgletscher, the climate inputs (Table 5.2 and Section 3.4.4) need to be considered when interpreting these changes, with model combination A showing the lowest precipitation levels of all climate model combinations. Such low precipitation limits the accumulation of snow in the accumulation area resulting in the highly negative mass balance. The mass balance of A-4.5 and A-2.6 does begin to recover after 2060 after removal of low elevation ice, suggesting that a new equilibrium could be reached, particularly for A-2.6.

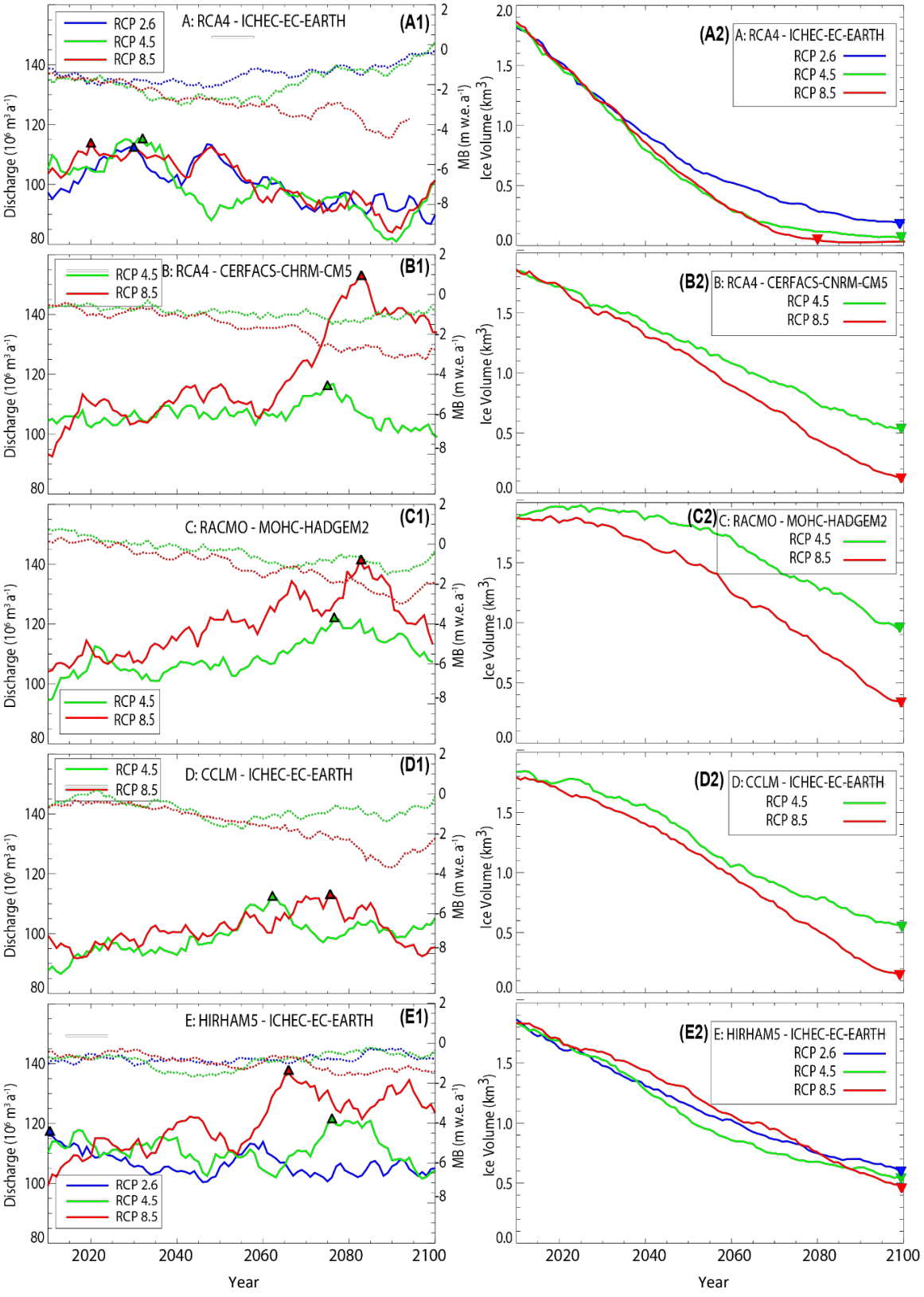

Figure 5.6: Simulations of future discharge (solid lines in left panel), mass balance (dashed lines in left panel) and ice volume change (right panel), for Rhonegletscher when forced by 12 different climate scenarios. Crosses in left panel show when no ice is left in the catchment. Triangles in left panel show when peak discharge is reached (calculated based on 10-year running mean). Down-turned triangle in right panel indicates where 95 % ice volume was lost. Mass balance and discharge shown as 10-year running means.

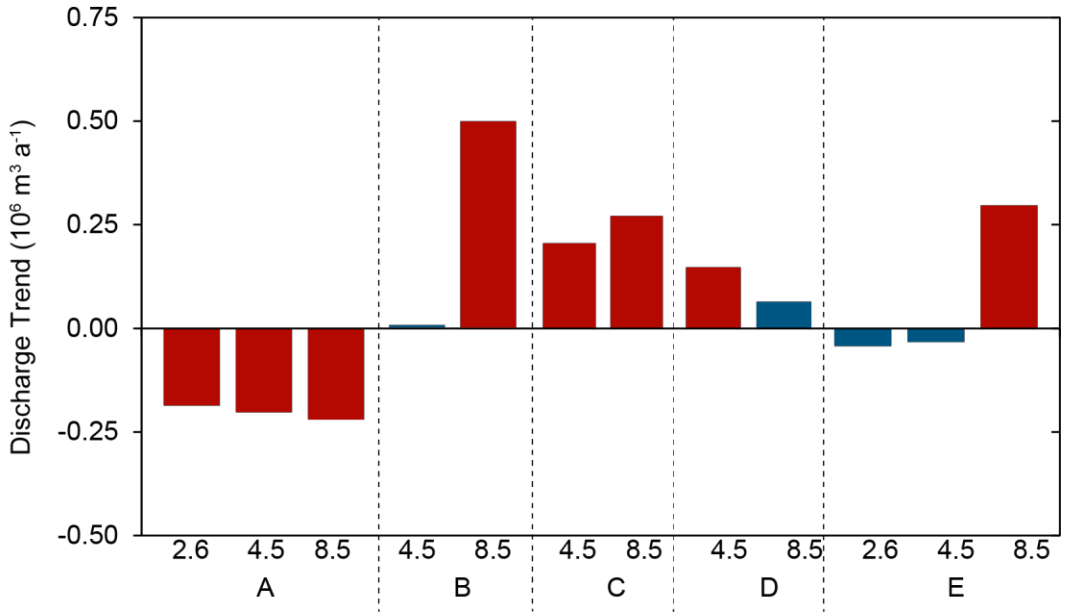

Figure 5.7: Trend analysis for discharge at Rhonegletscher, calculated using the Mann-Kendall test with significance indicated with red bars (p<0.01; period 2010-2100). Note y-axis intervals differ to Griesgletscher (Figure 5.2). A-E refer to the driving model (see Table 5.2) and numbers (e.g. 4.5.) refer to the RCP.

In stark contrast to A, the simulated runoff evolution in C (Figure 5.7) shows a significant positive trend (p<0.01) throughout the century, likely due to the high precipitation in the RACMO-HADGEM2 model combination. A consequence of this high precipitation in the early part of the century, from 2010-2020, is positive mass balances and slight ice mass gains (Figure 5.7 – C2), due to high accumulation rates. However, after c.2040, when average temperatures increase sufficiently to become positive, the increased precipitation is more likely to fall as rain, thus causing the mass balance to become increasingly negative and ice mass to decrease. Because of the high precipitation rates and initially positive mass balance, peak discharge occurs around 2080, later than all other simulations, after which there is a decrease in discharge.

5.3.2.2. Seasonal Changes at Rhonegletscher.

The seasonal changes in discharge at Rhonegletscher (Figure 5.8) present a similar pattern to Griesgletscher with the onset of the melt season occurring earlier in 2080 compared to 2020. For example, C-8.5 shows this clearly. However, the pattern is less uniform than Griesgletscher, likely due to the less complete ice loss. For example, the outputs of model combinations B and E show no clear pattern. Additionally, the reduced peakedness of the discharge curve, visibly in the majority of model runs at Griesgletscher, is only seen with model combination A at Rhonegletscher, a reflection of the positive discharge trends for several simulations.

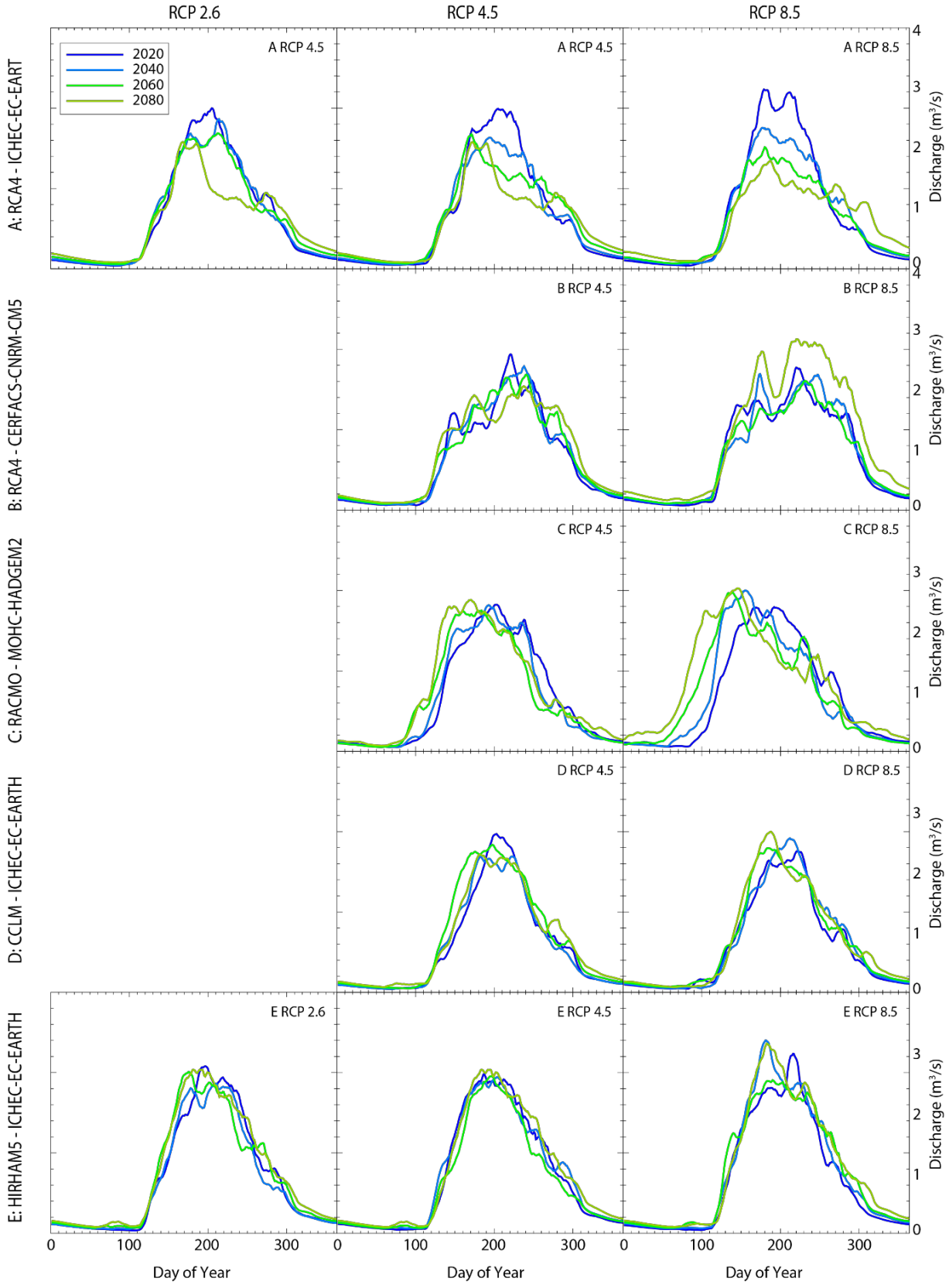

Figure 5.8: Changes in seasonality of discharge at Rhonegletscher for all climate simulations. Each line represents the mean of discharge for 10 years, e.g. "2020" is mean discharge from 2015-2025.

5.3.2.3. Spatial Pattern of Ice Loss at Rhonegletscher.

As for Griesgletscher, the following section will focus the analysis on a selection of three model outputs which represent the end-members of all simulations: A-8.5 shows the fastest mass loss; B-4.5 represents the typical mass loss, and C-4.5 represents the least mass loss. The full range of spatial plots is included in Appendix Figure A.4.

Rhonegletscher exhibits mass losses through frontal recession, thinning and narrowing of the main trunk of the glacier (Figure 5.9). As explained above, there are sizeable differences between the simulations with Figure 5.9 demonstrating a selection of notable results. Firstly, Figure 5.9A shows A-8.5 with complete ice loss by 2100 and near complete ice loss by 2080, with only a small section of the accumulation area remaining. Conversely, Figure 5.9C shows much more limited ice loss with 2040 showing almost no change, before gradually receding by 2060-2080 with around 2 km of terminus recession by 2100. Figure 5.9B shows what is considered typical of simulations at Rhonegletscher; gradual terminus recession until much of the tongue is removed by 2100, leaving only the current accumulation area.

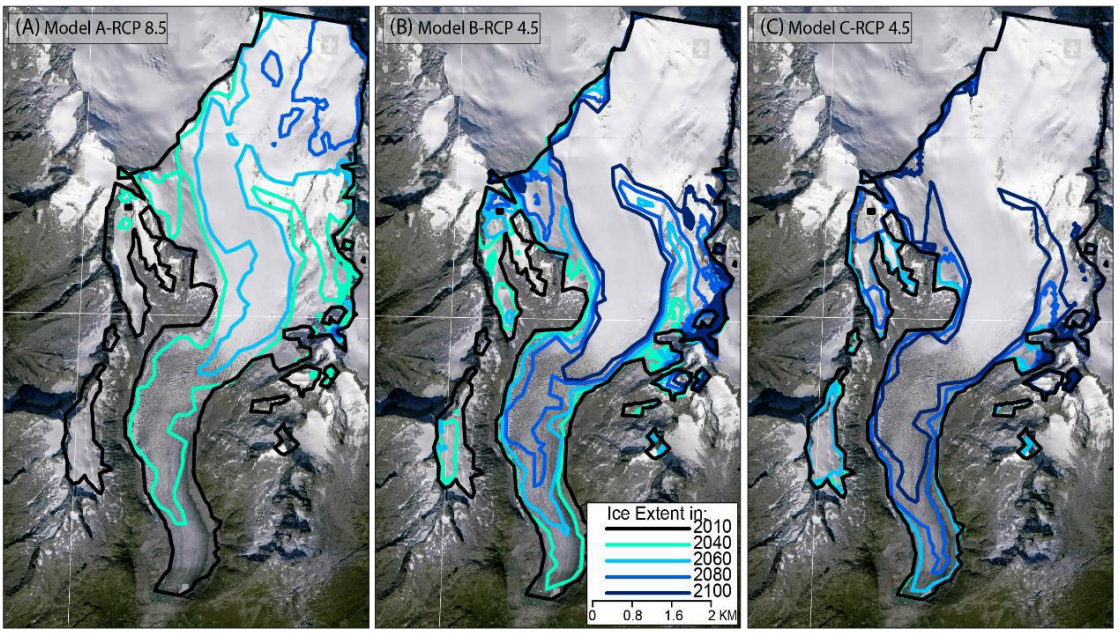

Figure 5.9: the spatial pattern of mass loss for select model simulations at Rhonegletscher. (A) model A-8.5, the fastest receding glacier. (B) model B-4.5, deemed a 'typical' projection indicative of the rate of mass loss of the median outputs of the simulations. (C) model C-4.5, with the slowest mass loss and some mass gain in the early 21st century. 2100 ice extent is not included in (A) as no ice remains.

5.3.2.4. Glacier Contribution to Discharge at Rhonegletscher.

The contribution of ice and snow melt to overall discharge at Rhonegletscher is shown in Figure 5.10. In A-8.5, there is a clear reduction in the contribution of ice from 30 % in 2020 to 7 % in 2080. However, B-4.5 shows that ice melt contributes equally in 2020 and 2080, and B-4.5 suggests that ice melt becomes a more significant contributor in 2080. Such contrasts reflect the lack of a consistent trend in overall discharge at Rhonegletscher (e.g. Figure 5.10) and the large variation in remaining ice volume between the model outputs. As for Griesgletscher, the peak discharge and peak-snow melt occur earlier in the year in 2080 than 2020, with the ice melt peak doing the same for climate model combinations A and B.

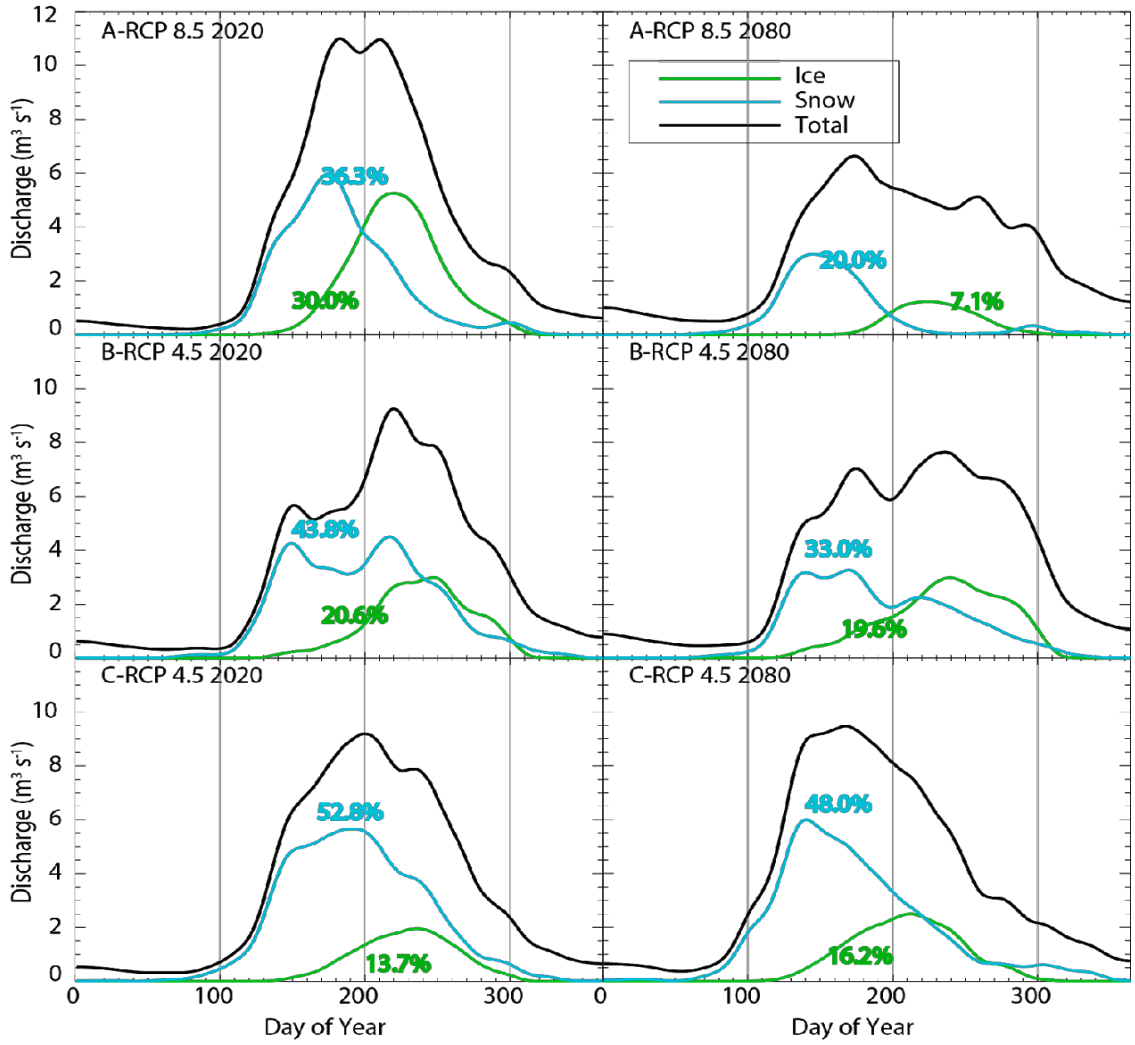

Figure 5.10: the contribution of snow and ice melt to overall discharge in 2020 and 2080, calculated as mean of +/- 5 years, for three select simulations. Percentages quantify the contribution of ice and snow to total discharge.

5.4. Incorporation of Uncertainty in Future Projections.

This section will assess the uncertainty associated with emissions scenarios (RCPs), climate model combinations (GCM-RCM), and with GERM itself. Figure 5.11 represents the main sources of uncertainty influencing the projections of GERM. In this section, the uncertainties associated with 'climate' have been addressed using the very wide range of climate-model combinations (GCM and RCM uncertainty) and scenarios (RCPs), as well as the more advanced downscaling methodology (Chapter 3) than previous studies. The bias-correction uncertainty is not considered. In terms of the uncertainties associated with GERM, the uncertainties are assessed based on the results of the long-term validation (Chapter 3).

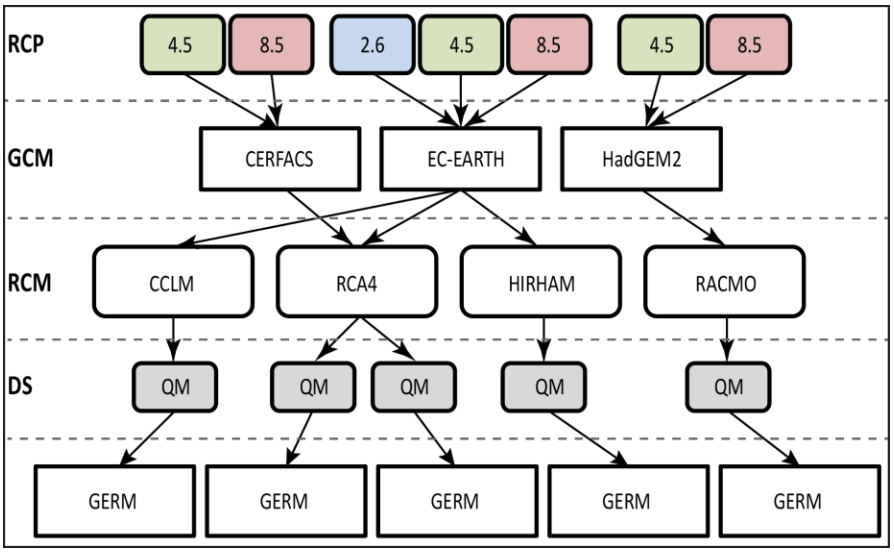

Figure 5.11: Schematic showing the main sources of uncertainty impacting GERM due to the climate inputs. In this section, the RCP uncertainty, GCM-RCM uncertainty, and GERM uncertainty are included. 2.5, 4.5, and 8.5 refer to the RCP scenario driving the GCM. DS is Downscaling and QM is Quantile Mapping.

5.4.1. Climate Scenario Uncertainty.

The purpose of forcing GERM with a range of bias-corrected RCM outputs was to provide an indication of the uncertainty introduced by different GCM-RCM combinations. Due to the lack of available RCM simulations, the results here do not demonstrate the full range of uncertainty, nor is the uncertainty introduced by the statistical downscaling assessed as it is likely to be minor in magnitude compared to the magnitude associated with climate models and scenarios (e.g. San-Martin et al., 2017).

Figures 5.12 and 5.13 show the climatic uncertainty (RCP uncertainty, and GCM-RCM uncertainty) at Griesgletscher and Rhonegletscher, respectively. These plots are calculated using the mean volume change (a) and discharge (b) for each RCP scenario across all models, shown

as the dashed coloured lines. These lines therefore represent the most likely projections for each RCP scenario, based on the available GCM-RCM combinations in this thesis. Additionally, the grey shaded areas are the minimum and maximum volume change (a) and discharge (b) across all simulations, thus represent the upper and lower bounds of uncertainty based on all the GCM-RCM combinations employed in this thesis. Since RCP 2.6 was only available for model combinations A and E, the means calculated for this scenario are only based on only two simulations.

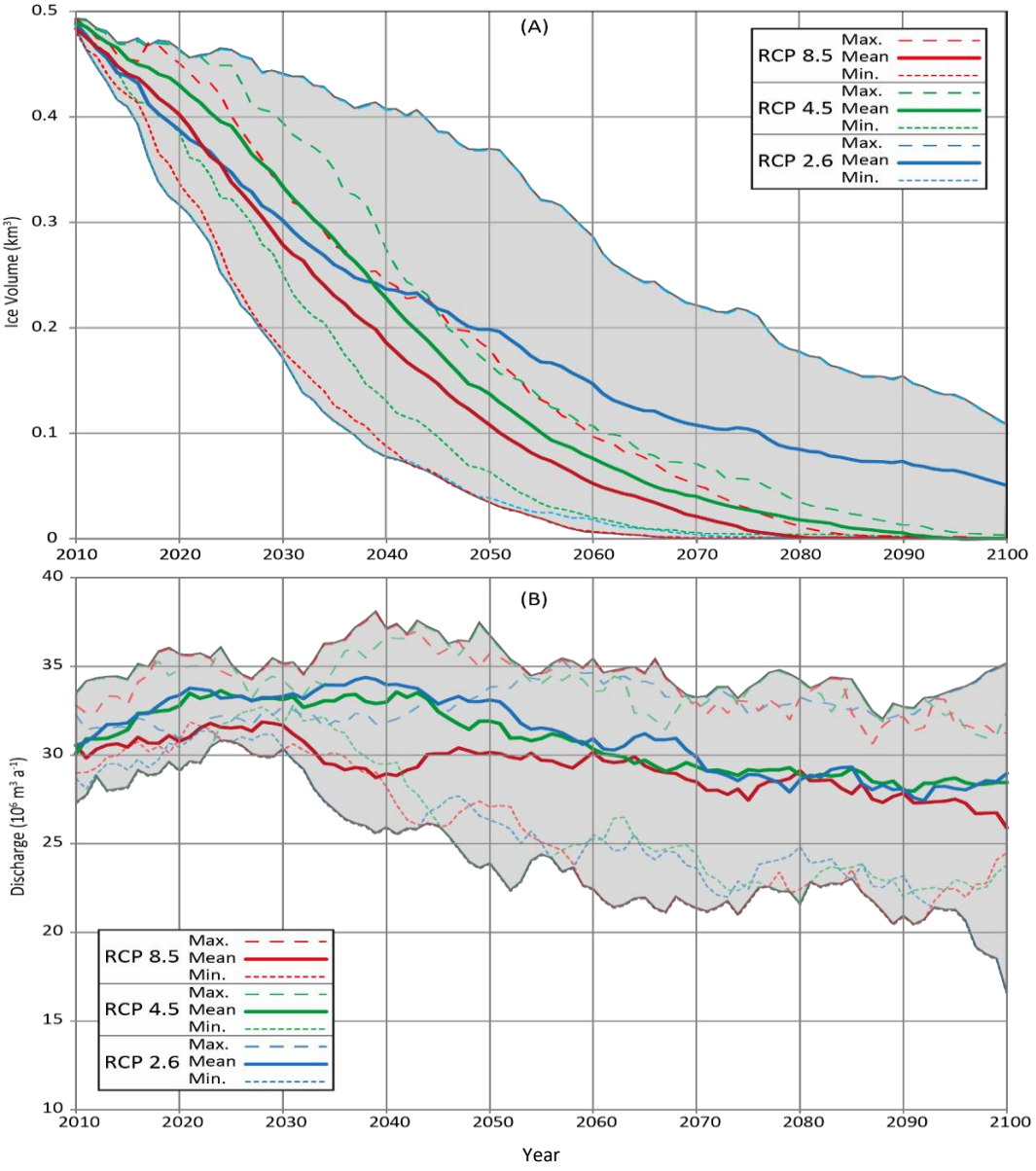

Figure 5.12: Future glacier evolution (A) and discharge (B) at Griesgletscher. RCPs represent the mean of all model combinations including that RCP (e.g. RCP 4.5 represents the mean volume change from models A-E from RCP 4.5). The 'range' represents the minimum and maximum volume change from all simulations.

The modelled volume changes vary moderately depending on the climate scenario used to force GERM at both catchments (Figures 5.12A and 5.12A), particularly RCP 2.6 which shows very rapid initial volume loss at Rhonegletscher which curtails towards the end of the 21st century. However, RCPs 4.5 and 8.5 show less considerable deviations. When considering the minimum and maximum range of uncertainty, the range of volume change varies more considerably with glacier disappearance occurring at Griesgletscher in 2065 at one extreme, and a remaining ice volume of 0.11 km^3 (21 %) at the other extreme. At Rhonegletscher, the range of volume projections is even greater, with glacier disappearance by 2086 at one extreme, versus a remaining volume of 0.9 km^3 (48 %) at the other extreme. Interestingly, at Griesgletscher, RCP 4.5 and 8.5 diverge early in the simulation before nearly converging later in the model run, whereas, at Rhonegletscher, RCPs 4.5 and 8.5 remain on a similar trajectory until after 2060, ending the century with a considerable difference in remaining ice volume.

A similar pattern occurs for discharge with Griesgletscher diverging in the 2030s before converging again after 2060, while discharge at Rhonegletscher diverges in the 2060s and does not re-converge. These differences are related to the remaining ice mass at each site. For example, at Griesgletscher, near total ice loss is projected for the majority of simulations, leaving less uncertainty regarding the remaining ice available for melt, which means that discharge is largely governed by liquid precipitation and snowmelt in 2100 (as shown by Figure 5.5). However, at Rhonegletscher, the projections of remaining glacier volume in 2100 vary considerably meaning some model runs have a large ice mass available for melting, whereas other model runs have less remaining ice resulting in a decrease in discharge. This large range of discharge projections at Rhonegletscher is reinforced by the trends show in Figure 5.7.

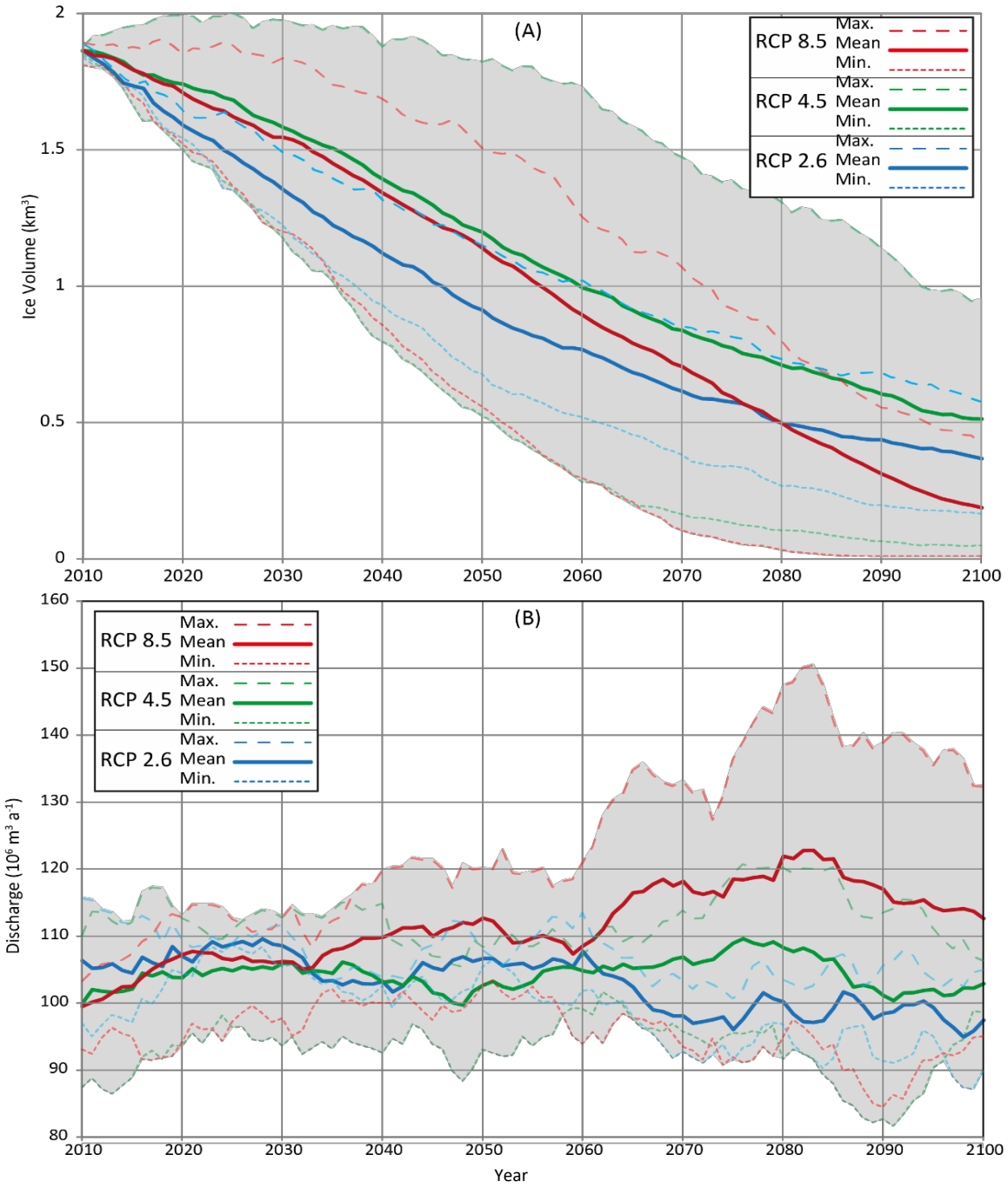

Figure 5.13: Future glacier evolution (A) and discharge (B) at Rhonegletscher. RCPs represent the mean of all simulations for that RCP (e.g. RCP 4.5 represents the mean volume change from models A-E from RCP 4.5). The 'range' represents the minimum and maximum volume change from all simulations.

5.4.1.1. Assessing the Uncertainty of Individual RCMs and GCMs.

The previous section explored the overall range of glacio-hydrological projections when GERM is forced by the full range of GCM-RCM combinations and scenarios available. However, in this section, the GCM and RCM uncertainty will be analysed allowing the uncertainty introduced by the GCM and RCM to be compared. Such assessment of uncertainty is well-established in climate science (e.g. Hawkins and Sutton, 2011), but, to the best of the author's knowledge, has been

little addressed in estimates of future glacier changes. It is only by understanding the sources of uncertainty that efforts can be best guided to reduce these uncertainties. This uncertainty can only be partially assessed due to the limited number of GCM-RCM combinations available, which does not allow each GMC to be assessed with different RCMs, and vice versa. The following results all utilise the outputs at Griesgletscher under RCP 4.5, for comparison.

Firstly, the uncertainty associated with differing RCMs is assessed by comparing the GERM projections forced by climate model combinations A, D and E, all of which use the ICHEC-EC-EARTH GCM but use different RCMs (A: RCA4; D: CCLM; E: HIRHAM). Since only three RCMs were available, this does not fully represent the uncertainty associated with the use of different RCMs. The model outputs assessing RCM uncertainty are shown in Figure 5.14 (a) and (c). Clearly, there are considerable differences, particularly with A showing a stronger negative discharge trend and more rapid ice volume loss, with Griesgletscher disappearing more than 15 years prior to D and E. These results show that the magnitude of RCM uncertainty is sizable considering that the same GCM is used to force each of these RCMs, suggesting that RCMs do vary considerably in their representation of temperature and precipitation in mountain environments.

Secondly, the uncertainty associated with differing GCMs is assessed by comparing the GERM projections forced by climate model combinations A and B, both of which use the same RCA4 RCM, but are forced by different GCMs (A: ICHEC-EC-EARTH; B: CNRM-CERFACS). It should be emphasised that, due to limited available data, this is only a sample of two GCMs, thus only provides an indication of the uncertainty associated with different GCMs. The model outputs assessing GCM uncertainty are shown in Figure 5.14 (b) and (c). Again, there is a sizable deviation in modelled discharge (6 $10^6 m^3 yr^{-1}$) and glacier evolution (25 year difference in timing of a glacier free catchment), with A (ICHEC-EC-EARTH) projecting more rapid mass loss and a negative discharge trend, than B (CERFACS-CNRM-CM5) which projects relatively constant discharge. These results show that the differences resulting from an RCM forced by different GCMs can be considerable and are similar in magnitude to the RCM uncertainty.

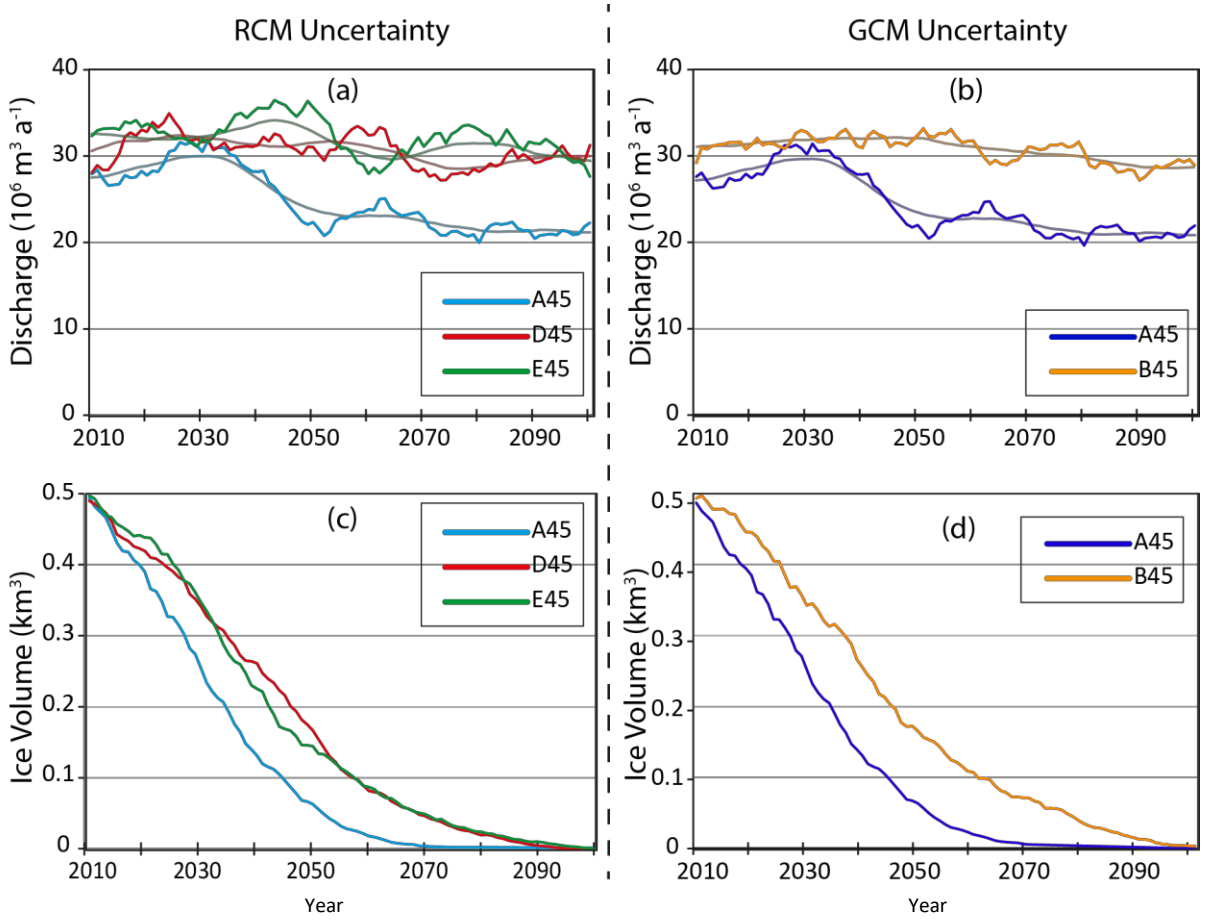

Figure 5.14: Comparison between RCM (left panel) and GCM (right panel) uncertainty, when driving GERM with differing bias-corrected climate model outputs. (a) and (c) are three RCMs (A: RCA4; D: CCLM; E: HIRHAM) all forced by the ICHEC-EC-EARTH GCM. (b) and (d) use the same RCM (RCA4) forced by two different GCMs (A: ICHEC-EC-EARTH; B: CNRM-CERFACS). Discharge plots include 10-year moving averages.

5.4.2. GERM Uncertainty.

The uncertainty related to GERM includes errors during calibration, errors in input data, and assumptions of the model itself, for example, the assumed stationarity of melt factors with temperature. These were assessed in Chapter 4 using the long-term validation and are applied to volume change and discharge projections here.

For Griesgletscher, the uncertainty of ±0.165 % of initial volume per year is applied to the mean of each RCP as well as the minimum and maximum volume change projections (i.e. all the simulations shown in Figure 5.1). At Rhonegletscher, the uncertainty is ±0.132 % of initial volume per year.

The results of these calculations are shown in Figures 5.15 and 5.16 for Griesgletscher and Rhonegletscher, respectively. The coloured bands represent the uncertainty introduced by GERM for the mean of each RCP scenario, with the grey band representing the combination of

climate and GERM uncertainty. Clearly, the range of uncertainty is extensive for both catchments when both ice volume and all three RCPs are included. However, the range of uncertainty associated with each individual RCP is more encouraging in terms of the ability of GERM. Griesgletscher exhibits more uncertainty than Rhonegletscher, with rapid glacier decline in the past not fully reproduced in GERM leading to relatively high glacier volume errors. Rhonegletscher simulations in the past also underestimate volume loss but to a lesser extent, resulting in smaller uncertainties for future projections.

In terms of discharge, uncertainty is shown in Figure 5.15B and 5.16B. The uncertainty is calculated based on the validation against observed annual discharge (1957-2003 at Griesgletscher; 1975-2005 at Rhonegletscher), and is applied to the mean discharge simulated by each RCP scenario. The upper and lower bounds are calculated by applying the error to the maximum and minimum of all climate model combinations, thus providing the maximal range of discharge. Clearly, the uncertainty associated with modelling discharge is considerable by 2100, with Rhonegletscher less certain than Griesgletscher. However, it is important to emphasise that the coloured bands represent the maximum range of error for each RCP scenario, and the grey bands the maximum range of error for all uncertainty associated with climate inputs and GERM uncertainty. At Griesgletscher, the relative agreement among RCP scenarios is clear after 2050, whereas, at Rhonegletscher, the RCPs diverge much more, a reflection of the lack of consistent volume change projections.

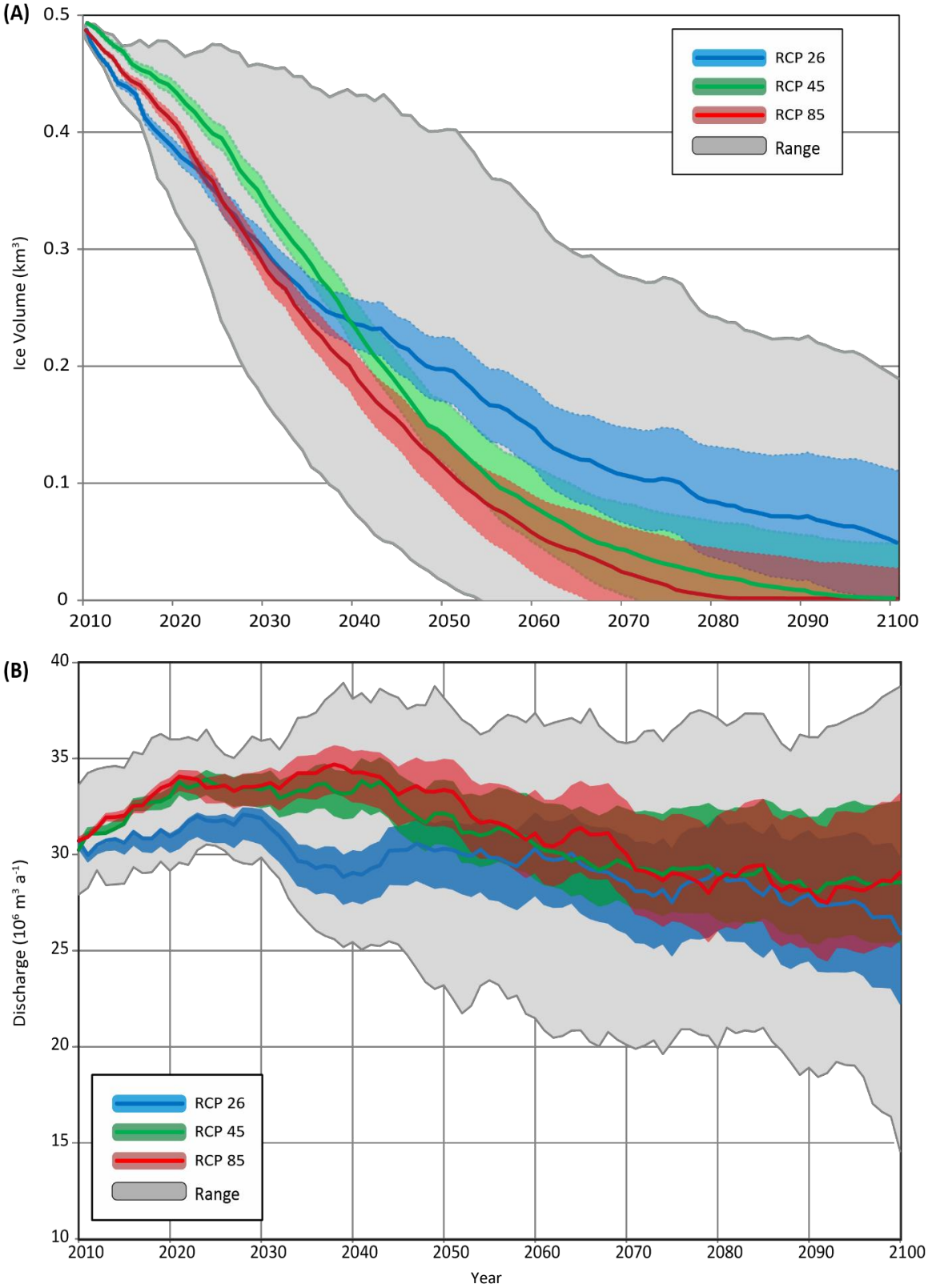

Figure 5.15: Simulated (a) ice volume change, and (b) discharge, with combined climate and glacier modelling uncertainty at Griesgletscher. The coloured bands refer to the uncertainty associated with GERM for the mean of each RCP scenario, and the grey bands reflect the maximum uncertainty associated with both the climate inputs and GERM. The uncertainty ranges are calculated by taking the errors based on long-term validation, and applying these to the mean projections of RCPs 2.6, 4.5 and 8.5 (coloured bands), as well as the individual projections that simulate the maximum and minimum volume changes (grey shaded area).

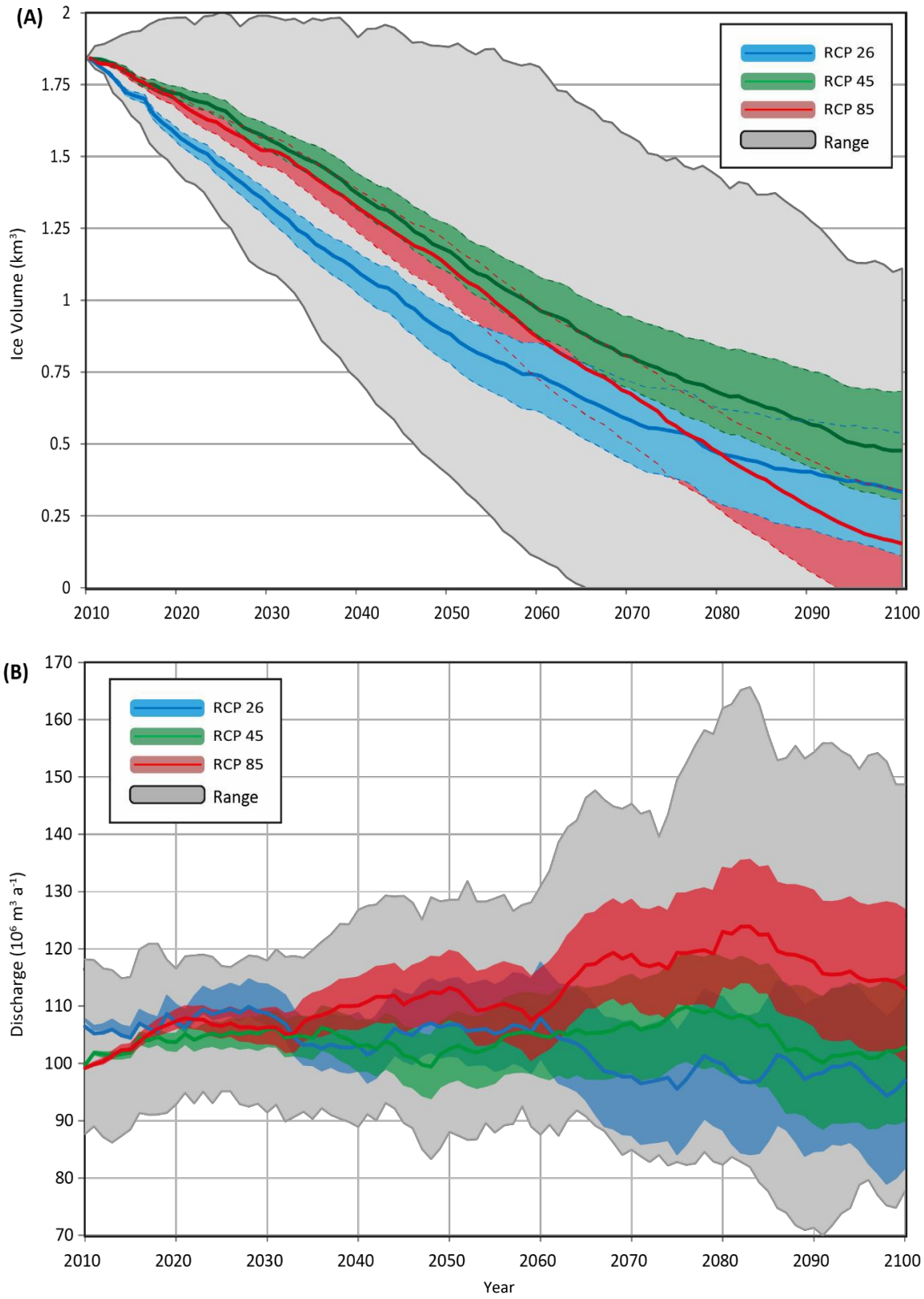

Figure 5.16: Simulated (a) ice volume change, and (b) discharge, with combined climate and glacier modelling uncertainty at Rhonegletscher. The coloured bands refer to the uncertainty associated with GERM for the mean of each RCP scenario, and the grey bands reflect the maximum uncertainty associated with both the climate inputs and GERM.

5.5. Discussion.

This section will identify and summarise the key findings from future simulations in the Alps and assess the uncertainty associated with these future projections. The key findings will be compared to other studies at these sites from the literature, before suggesting where future research efforts should focus in this active research discipline.

5.5.1. Future Glacier and Runoff Evolution of Griesgletscher and Rhonegletscher.

At Griesgletscher, it is clear that the considerable reduction in ice volume (mean RCP 4.5: 98 % loss in 2100) corresponds to a reduction in annual runoff. With only one exception, the simulations suggest that this decline will lead to a glacier-free catchment before 2100, with some projections (e.g. A-8.5) suggesting this could occur as early as 2054. The reasons for this become clear when considering the future projections of temperature (Section 3.4 – Figure 3.8) and the hypsometry of Griesgletscher (Figure 5.17): considering that the size of the accumulation area above the ELA is very small, even a small increase in temperature will lift the ELA to elevations above the glacier. The influence of glacier hypsometry on glacier changes will be further discussed in further in Chapter 8.

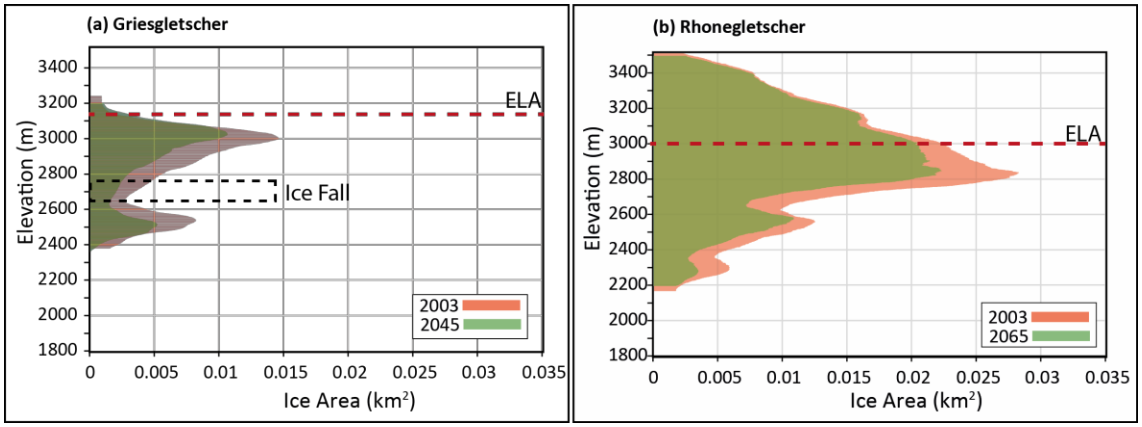

Figure 5.17: Glacier hypsometry at Griesgletscher and Rhonegletscher, showing the relationship between ice area and elevation in 2003 compared to the hypsometry when 50 % of ice volume is lost (2045 at Griesgletscher; 2064 at Rhonegletscher). Red line denotes ELA averaged over 2010-2012.

At Rhonegletscher, the reduction in ice volume remains considerable (mean RCP 4.5: 72.6 % loss in 2100) but the larger ice mass ensures that some ice will remain in 2100. Unlike at Griesgletscher, the glacier hypsometry (Figure 5.17) shows a relatively large area of ice above the ELA in 2010. Therefore, moderate temperature increases will not cause complete ice loss. The consequences for discharge are less clear than at Griesgletscher with considerable deviation

between the different model runs, due to the fact that the ice mass is still melting at the end of the century, and thus contributing to discharge. If the pattern from Griesgletscher is followed at Rhonegletscher, as it is for A (Figure 5.6), it is likely that discharge will decrease when ice loss is more complete. For both sites, mass balances are negative for almost the entire duration of the 21st century, with mass balances of -2 m w.e. yr^{-1} or lower simulated consistently. Such negative balances are in line with those observed in 2003 (Zemp et al., 2009; Farinotti et al., 2012), an extremely hot year over the Alps (Rebetez 2004) that had substantial impacts on the hydrology of glacial catchments (e.g. Koboltschnig et al., 2008).

An interesting phenomenon revealed by several simulations is the recovery of mass balance in the latter part of the century, from highly negative balances to less negative balances. For example, simulations A-2.6 and E-8.5 at Griesgletscher (Figure 5.1), and A-2.6, A-4.5, C, and D at Rhonegletscher (Figure 5.6), all exhibit this pattern. The cause of this mass balance recovery is the removal of low-elevation ice: as low elevation ice with a highly negative mass balance is removed, the overall glacier mass balance becomes more and more influenced by the high elevation ice, which experiences a less negative mass balance. If the mass balance recovers sufficiently to become neutral or positive, it suggests the glacier has reached a new equilibrium with the climatic conditions.

5.5.2. Comparison with other studies at Griesgletscher and Rhonegletscher.

Several studies have applied models to Griesgletscher and Rhonegletscher, providing a valuable source of comparison for the results obtained here.

Farinotti et al. (2012) applied GERM to both sites using the ENSEMBLES RCM outputs (Van der Linden & Mitchell 2009), the predecessor to CORDEX, as climate inputs. The results of this thesis agree well with Farinotti et al. (2012) at Griesgletscher where both studies suggest an initial increase in discharge followed by an overall reduction by 2100, concurrent with the loss of much of the glacier before 2100. For Rhonegletscher, Farinotti et al. (2012) simulated a similar reduction in ice volume and an initial increase in discharge, but found a clearer negative trend in discharge by 2100, than this thesis, which found no consistent trends. Since projected volume changes are similar in the two studies, the difference between these results in terms of discharge is likely to stem from the precipitation inputs, as liquid precipitation will become a more sizable contributor to discharge in catchments with continued glacier recession (Huss, 2011). For example, Farinotti et al. (2012), only used one scenario of future climate (A1B- approximately in between RCP 4.5 and 8.5) whereas this thesis uses three scenarios (RCP 2.6, 4.5, 8.5) resulting in a wider range of precipitation trends. Moreover, Farinotti et al. (2012) implemented the delta-

change statistical downscaling approach, which does not account for the distribution of the precipitation when calculating the statistical relationship between simulated and observed precipitation. Their approach also neglected to consider the overestimation of 'drizzle' in many climate models. Therefore, it is likely that the trend in discharge at Rhonegletscher in Farinotti et al. (2012) resulted from differing climatic inputs, because of both different downscaling methods, but also a smaller range of scenarios considered.

Sugiyama et al. (2007) applied a dynamical flow-line model to Rhonegletscher and conducted future simulations using constant mass balance forcings to assess glacier volume changes. They found that Rhonegletscher is expected to lose 18 % of ice mass by 2050 which, for comparison with this thesis, equates to a remaining volume in 2050 of 1.52 km^3. In comparison, this thesis finds ice volume in 2050 to be 1.22±0.9 km^3; however, the mass balance reported in this thesis is climate-driven and is therefore not comparable to a constant mass balance forcing. Jouvet et al. (2011) use a coupled dynamical ice-flow model with a mass-balance and runoff model at Rhonegletscher, using three climate change scenarios to drive future projections. Their "current" scenario simulates 36 % ice loss by 2100, with their "hot" and "cold" scenarios projecting 89 % ice loss by 2100 and a doubling of ice mass, respectively. Since these model runs are not driven by climate model outputs, direct comparison is difficult; however, it is clear that these studies agree that considerable mass loss is likely in the 21st century.

Finally, Huss et al. (2010) developed the Δh retreat parameterisation used in this thesis at Rhonegletscher and Silvretta by comparing results with those of a dynamical ice-flow model (Jouvet et al., 2011a; 2011b). Again, climate model outputs were not used to drive the glacier model; however, results agree well with those in this thesis, with discharge trends ranging from negative to positive depending on the scenario, as well as considerable ice volume loss.

5.6. Conclusions.

This chapter has taken the results of the long-term model validation (Chapter 4) and the bias-correction of climate data (Chapter 3) to apply GERM to two catchments in the Swiss Alps: Griesgletscher and Rhonegletscher. The main conclusions of the projections are a continued loss of glacier mass with negative mass balances throughout the 21st century, at both sites. In terms of discharge, Griesgletscher shows a negative trend for most projections, whereas Rhonegletscher shows no discernible trend. This lack of trend is likely due to the current size of the glacier meaning that ice melt is still strongly contributing to discharge by 2100.

- An ice-free catchment is projected at Griesgletscher before 2100 in all but one model run. Such considerable ice loss reflects the lack of a large area of high-elevation ice in the

accumulation area. However, Rhonegletscher is likely to remain glacierised after 2100, due to the larger ice mass and higher elevation accumulation area.

- At Rhonegletscher, a recovery of mass balance is projected in some model runs, suggesting the glacier may be approaching equilibrium with the climate in 2100, albeit as a much smaller, high-elevation glacier.
- The decreased contribution of ice-melt, together with earlier onset of the melt season, will have a considerable influence on seasonal runoff at both catchments, but most strongly at Griesgletscher due to higher ice loss. This will have implications for hydropower generation at Griesgletscher, discussed in more details in Section 8.4.
- The results of this thesis agree well with the literature in terms of the initial increase in discharge followed by a long-term decrease at Griesgletscher. At Rhonegletscher, the initial increase in discharge is clear in the results of this thesis; however, overall negative trends are only modelled by climate model combination A. For climate model combinations B-E, peak discharge is reached later in the 21st century so discharge has not become strongly negative by 2100.

This chapter also undertook an assessment of the relative magnitude of errors due to scenario, GCM, RCM and GERM:

- The range of climate scenarios used to force GERM produces a considerable range of glacier and runoff projections, with Griesgletscher ice free by 2060 in one projection, compared to a remaining ice volume of 20 % in another projection. In terms of discharge, uncertainty from climate models/scenarios alone causes discharge in 2100 to differ by ±9 10^6 m^3 yr^{-1} at Griesgletscher and ±22 10^6 m^3 yr^{-1} at Rhonegletscher.
- In terms of the relative contribution of GCM and RCM error, this study shows that these sources of error are comparable in magnitude. For example, the same GCM forcing two different RCMs causes complete loss between 2060 and 2095, and produces a runoff uncertainty in 2100 of ±5 10^6 m^3 yr^1. Similarly, two different GCMs forcing the same RCM causes complete loss between 2060 and 2095, and projects a runoff uncertainty in 2100 of ±3 10^6 m^3 yr^{-1}.
- The uncertainty associated with GERM produces a large range of glacier and runoff projections, but remains smaller than uncertainties associated with climate models and scenarios. For example, discharge uncertainty from GERM causes discharge in 2100 to differ by ±3.5 10^6 m^3 yr^{-1} at Griesgletscher and ±14 10^6 m^3 yr^{-1} at Rhonegletscher.
- Therefore, it is clear that both climate uncertainty and GERM uncertainty are considerable and should be assessed in future studies, by using a wide range of climate models and scenarios, and by validating glacio-hydrological models by comparing simulated changes to

observed changes. If it is not possible to validate the model and quantify uncertainty (e.g. if no long-term data are available), it is essential that this is acknowledged as a limitation such that projections can be interpreted correctly.

6. APPLICATION TO A HIMALAYAN CATCHMENT: KHUMBU, NEPAL.

This chapter will modify GERM to incorporate debris-covered ice and glacier downwasting, such that it can be applied to debris-covered glaciers in the Himalaya and elsewhere. The modified form of GERM is applied to the Khumbu Glacier in Nepal, which has been chosen as it is one of the few Himalayan glaciers with some field data available and is typical of glaciers in the Everest region in terms of debris cover and pattern of mass loss. In Chapter 7, the modified form of GERM is used to perform simulations of future glacio-hydrological changes at Khumbu Glacier. This chapter addresses Aim 3a.

6.1 Introduction.

Runoff models including GERM have been applied to many catchments in the European Alps, as discussed in Section 1.3. However, their implementation in other regions is far less comprehensive. The Himalayan region in particular presents challenges because of spatially and temporally limited meteorological, glaciological and hydrological data; different climatological regimes (e.g. Indian Monsoon - Salerno et al., 2015); and very different glacier response to climate changes, particularly the style of retreat, which is characterised by downwasting rather than length change (e.g. Benn et al., 2012).

This chapter will attempt to overcome some of these challenges and develop GERM such that it is more applicable to Himalayan and other debris-covered glaciers. Two novel modifications are made: (1) the Δh-retreat parameterisation is altered to simulate glacier downwasting; and (2) the reduced melt beneath debris is accounted for by incorporating a fully distributed debris layer. These adaptations allow the final aim of this thesis to be achieved, which is to use these modifications to simulate the future glacier and runoff changes at the Khumbu catchment, which will be presented in Chapter 7.

6.1.1 The importance of Runoff in the Himalaya.

Several studies have emphasised the importance of freshwater resources in Asia to the huge populations that depend on an agricultural sector based around precipitation and river runoff (Miller et al., 2012; Xu et al., 2009; Barnett et al., 2005; Akhtar et al., 2008). Notably, Lal (2011) showed that future demand on water is highly likely to increase due to population growth, agricultural growth and industrial development. Glacier and snow melt in the Hindu Kush-Himalaya (HKH) provide the source of many of the major river systems in Asia, which are shown in Figure 6.1. Immerzeel et al. (2010) showed that climate change

does affect these high elevation catchments, but catchment response is not spatially uniform due to the highly varied climate systems in the region. Moreover, the impact of glacier and snow melt on runoff is more difficult to assess than in the European Alps because the peak melt season coincides with the peak summer monsoon rainfall (Immerzeel et al., 2013).

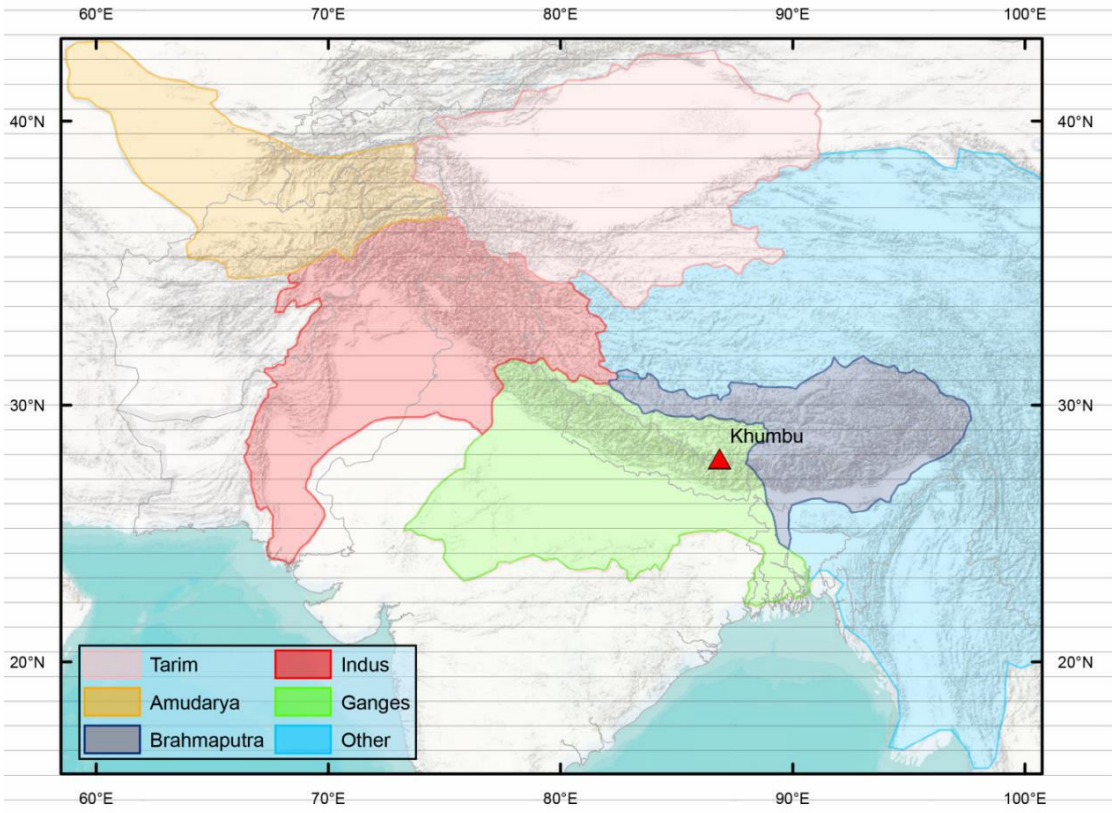

Figure 6.1: Map showing the location of the Khumbu Glacier and the various drainage basins of the Himalaya. "Other" Rivers include the Yellow, Yangtze, Mekong, Irrawaddy, and Salween.

The contribution of glacier and snow melt to runoff is highly scale and location dependent. For example, Thayyen et al. (2007) showed a strong glacier contribution to runoff during dry periods in the upper Bhagirathi River basin (Indian Himalaya), where the Dokriani Glacier contributes 87 % of runoff (Singh et al., 2006). However, on a larger scale, Jain (2008) showed that the mass loss of the Gangotri Glacier (Indian Himalaya) will have a negligible impact on flows of the River Ganges due to the dominance of monsoon rainfall during the melt season. Similarly, Miller et al. (2012) concluded that the effect of glacier decline on the Ganges and Brahmaputra would be minor and that the monsoon rainfall would mask much of the impact. Miller et al. (2012) also state that, with the reducing influence of the monsoon further to the west of the HKH, glacier contribution to discharge in the River Indus becomes more important and can supply up to half of total discharge (Laghari, 2013). This is due to the dryer climate, suggesting a spatial control on glacier contribution dependent upon the strength of the monsoon in each basin.

At the Khumbu catchment, the contribution of glacier and snow melt to annual discharge has been estimated as 55 % (Soncini et al., 2016) but with considerable variation throughout the year with peak glacier and snow melt contribution during the warm summer months and very low contribution during winter (e.g. <5 %). This pattern is typical of glaciers in this region (Chen et al., 2017). As explained in Section 2.2.2, GERM has a range of sophisticated modules that allow for accurate modelling of snow redistribution, snow melt, and runoff routing both inside and outside of the glacier boundary, therefore precipitation or snow falling outside of the glacier boundary are explicitly included and modelled in GERM.

As described in the literature review, there have been several recent studies investigating the future glacier and runoff evolution of specific catchments (e.g. Immerzeel et al., 2012; Immerzeel et al., 2013; Soncini et al., 2016; Ragettli et al., 2015; Shrestha & Aryal, 2011) and over large regions (e.g. Lutz et al., 2014; Immerzeel et al., 2010). For example, Immerzeel et al. (2012) applied a coupled glacier-runoff model to the Langtang catchment in central Nepal, driving their model with the statistically downscaled outputs of five GCMs, all forced by the SRES A1B scenario (Van der Linden & Mitchell, 2009). They found that temperature and precipitation increases will result in gradual glacier decline from 2010-2100, leading to increases in river flow while glacier mass is lost. Immerzeel et al. (2013) repeated this study as well as expanding it to the Baltoro catchment (Karakomam Range) and applying updated climate data from four GCMs forced by RCP 4.5 and 8.5. Their findings corroborated the initial study. Studies that have attempted to simulate the future evolution of the Khumbu catchment specifically, are reviewed further in Chapter 7.

6.1.2 Differences between Glaciers in the Alps and Himalaya.

Supra-glacial debris is prominent on Himalayan glaciers due to the high, steep surrounding slopes which are prone to rock avalanching onto the ice surface. Additionally, mass loss in the HKH is manifested through downwasting, rather than frontal recession (Hambrey et al., 2009; Bolch et al., 2008). This downwasting further promotes thickening of debris on the ice surface since englacial debris is revealed as the ice melts. Moreover, the observations of ice stagnation in the lower sections of many glaciers prevent debris transport to proglacial moraines, resulting in further thickening of debris (Benn et al., 2012). With 14-18 % of the total glacierised area in the Everest region debris-covered (Kääb et al., 2012), it is important to understand how these glaciers react to climate changes.

Debris cover affects the melt rate of ice according to the Østrem Curve (Østrem 1959; see Figure 6.8 for the shape of Østrem curve applied in this thesis) whereby a thin layer of debris (<3 cm)

reduces the albedo of the surface and therefore transmits incoming energy to the ice surface, enhancing melt. However, a sufficiently thick (>3 cm) debris layer acts to insulate the ice surface from incoming radiation by absorbing incoming radiation during the day before releasing this energy to the atmosphere during the night, thus minimising transmission of energy to the ice surface (Nicholson & Benn, 2013). Therefore, debris-covered glaciers exhibit a reversal of mass balance gradients with higher ablation rates on the upper, debris-free glacier and lower ablation rates near the debris-covered terminus, leading to reduced ice flow rates (see Figure 6.2 for example; Quincey et al., 2009). The final feature of Himalayan glaciers is the abundance of ice-cliffs and supraglacial ponds which form amongst the debris. Ice-cliffs form as a result of differential ablation rates on the highly spatially heterogeneous debris surface (Reid & Brock, 2014; Sakai et al., 2000) and cause locally enhanced melt rates due to exposed low-albedo ice and aspect (Sakai et al., 1998). Furthermore, such locally enhanced melt rates can lead to the development of supraglacial ponds which have been shown to transfer atmospheric energy into the glacier interior through melt-pond drainage (Miles et al., 2016; Steiner et al., 2015).

6.1.3 Inclusion of Debris in Models.

Although several studies have investigated the impacts of debris upon melt rates (e.g. Ragettli et al., 2015; Rounce et al., 2015; Fyffe et al., 2014; Nicholson & Benn, 2013), many energy-balance approaches are point-scale studies that require significant in-situ data which limit their application to many Himalayan catchments. Furthermore, extrapolating debris thickness and melt rates from point-scale to distributed scale is difficult due to the highly heterogeneous nature of debris (Nicholson & Benn, 2013; Fujita & Sakai, 2014). As described earlier, the study of Shea et al. (2015) simulated glacier change in the Everest region from 2010-2100 using a coupled mass balance-ice distribution model, finding sustained loss in the 21st century; however, the incorporation of debris cover in this simulation was crude. Specifically, constant melt reduction rates, irrespective of debris thickness, were employed for each glacier and ice-cliffs were not incorporated. Another study, Rowan et al. (2015) modelled the long-term (since the Little Ice Age to 2200) evolution of the Khumbu Glacier using a coupled ice-flow mass-balance model to determine the relationship between glacier evolution, climate and debris cover but, unlike this thesis, did not consider runoff. They found that debris cover promotes downwasting and prolongs the glacier's response to climate change, with debris-covered ice persisting at much lower altitudes than clean ice. Despite several process-based studies on specific aspects of Himalayan glaciers, for example, stagnation (Quincey et al., 2009), debris-surface energy balance (Collier et al., 2015; Rounce et al., 2015; Fujita & Sakai, 2014), and ice-cliffs and supraglacial ponds (Miles et

al., 2016; Steiner et al., 2015; Sakai et al., 2000), there is only a limited understanding of how important these factors are for future impact studies, particularly in terms of runoff.

Ice stagnation, downwasting, and debris cover all mean that GERM, in its original specification, is not suited to simulating catchments in the Himalaya; GERM was originally developed to simulate glacier evolution and runoff for small, highly glacierised catchments in the European Alps, a setting with distinct climatological regimes and relatively 'typical' glacier behaviour. For example, most glaciers in the European Alps are valley-type, relatively debris-free and non-surging (Benn & Evans, 2010), although there are exceptions (e.g. Miage Glacier – Reid & Brock, 2010). Additionally, glaciers in the Alps typically respond to climatic changes through terminus recession, rather than downwasting (e.g. WGMS, 2015). For these reasons, GERM cannot be applied to Himalayan catchments without consideration of the different behaviour of glaciers in the region. Furthermore, the Δh-retreat parameterisation is designed for glacier retreat rather than downwasting.

6.2 Application to the Khumbu Catchment, Nepal.

6.2.1 Background and Data.

GERM will be applied in the Khumbu catchment (136 km^2; close to Pheriche: 27.88° N, 86.82° E; Figure 6.2). This catchment is selected primarily because of its relatively good data availability in comparison with other Himalayan catchments, despite still being data-poor compared to the Alps, particularly in terms of *long term* data. The relatively high volume of data available at Khumbu is associated with tourism which his attracted by the proximity of Mount Everest, leading to investment in infrastructure that has enabled relatively easy access to the glacier and the establishment of detailed monitoring, epitomised by the Pyramid observatory (Figure 6.2). This scientific observatory is situated on the lateral moraine of the main trunk of Khumbu (27.959° N, 86.813° E, 5035 m a.s.l.) and provides unprecedented data at such extreme elevations and topography. A further reason for choosing the Khumbu catchment is its similarity to other glaciers in the Everest region in terms of its hypsometry and highly debris-covered ice surface (Rowan et al., 2015). However, in comparison to the Alps, meteorological, glaciological, and hydrological data remain poor with only short-term records available. In particular, glaciological data at the Khumbu Glacier is very limited, not surprising considering the accumulation elevation is situated at over 6000 m a.s.l.

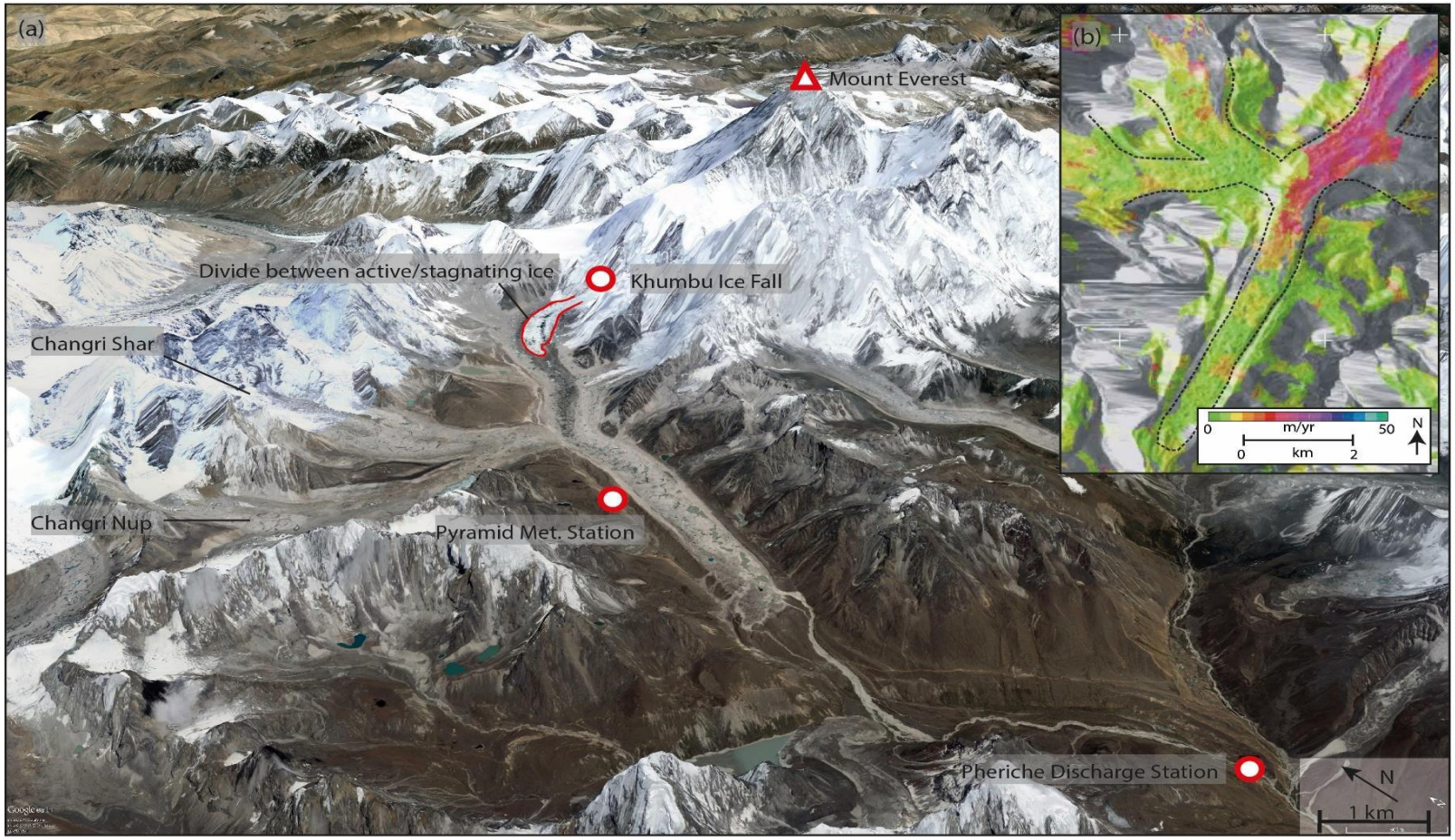

Figure 6.2: The Khumbu Glacier in Nepal, showing the locations of the Pheriche discharge station, the Pyramid meteorological station, and the Khumbu ice fall. Inset shows ice flow rates from Quincey et al. (2009), showing very low flow rates over much of the lower glacier. Red line shows divide between the active and stagnating ice. Map data: Google, DigitalGlobe. Inset Figure from Quincey et al. (2009).

Meteorological Data. Temperature and precipitation time-series from the Pyramid observatory have been extended by Salerno et al. (2015), providing continuous daily time-series from 1994-2012. Specifically, Salerno et al. (2015) used seven neighbouring stations to fill gaps (constituting 10 % of daily data for temperature and 16 % for precipitation) in the original time-series, and to calculate lapse-rates. Their approach used the Pyramid station as the principle dataset, and used the correlations between data at Pyramid and the seven surrounding stations to select appropriate stations that were used to fill the gaps in the Pyramid record. Although the location of the meteorological station on the lateral moraine may cause higher temperatures to be observed than on bare ice, the location of the observatory is adjacent to the debris-covered parts of the glacier, thus should be representative of the lower glacier area. Additionally, the Pyramid observatory is the only meteorological data set available. By analysing the data of Salerno et al. (2015; Figure 6.3), it is clear that summer monsoons dominate the climatic regime (Ichiyanagi et al., 2007) with 90 % of annual precipitation concentrated in the summer months of June-September, out of a total annual precipitation of 446 mm yr^{-1} (1994-2013 mean). The mean annual temperature at Pyramid is -2.45°C with a mean winter temperature of -7.54°C and a mean summer temperature of 3.14°C.

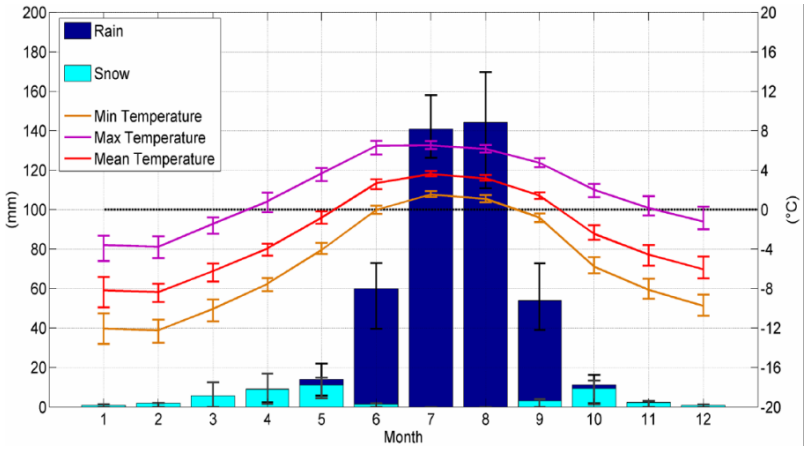

Figure 6.3: Mean monthly precipitation separated into snow and rain (left axis), and mean, minimum and maximum temperature (right axis) at the Pyramid station (5050 m a.s.l.). Bars represent the standard deviation of precipitation. Figure from Salerno et al. (2015).

Discharge Data. Discharge measurements, as is typical for Himalayan catchments, are very limited. However, through collaboration with the Italian Research Institute, ISRA-CNR, discharge data from the Pheriche discharge station is available from 2012-2014. Discharges are calculated using a stage-discharge curve developed using flow tracking and salt tracers (developed by Personnel of Politecnico di Milano). Such a short-term dataset means it cannot be used for calibration where long-term simulations are the goal; however, it is nonetheless extremely

useful for evaluation of model performance over these years and calibration of the runoff routing module.

Glaciological Setting. The Khumbu catchment includes two glaciers, Khumbu and Changri, which occupy 32 % of the catchment, and are mostly fed by summer accumulation from the South Asian monsoon system (Ageta & Fujita, 1996). Both glaciers exhibit significant supra-glacial debris cover (Khumbu: 37 % and Changri: 24 % of total glacier surface), particularly where ice flow rates are low (less than 10 m yr^{-1}; Quincey et al., 2009). Figure 6.2b shows the debris distribution in the Khumbu catchment as well as ice flow rates, demonstrating the widespread stagnation on the lower sections of Khumbu Glacier. Figure 6.4 shows the hypsometry of the Khumbu catchment.

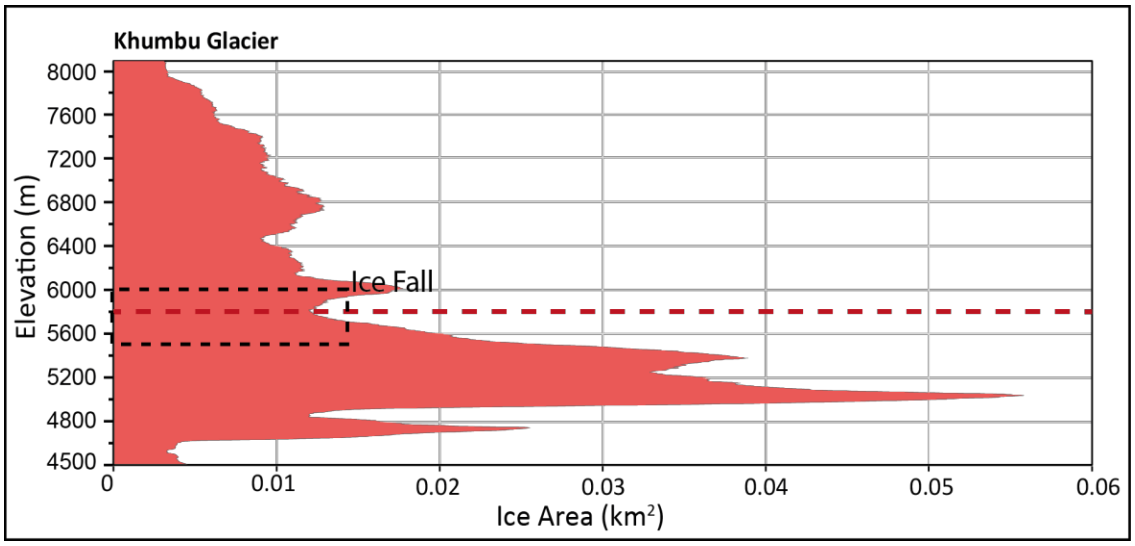

Figure 6.4: The hypsometry of the Khumbu Glacier, also showing the location of the current ELA (red dashed line) and the location of the Khumbu ice-fall.

Glaciological Data on Khumbu Glacier is limited and, in line with much of Himalayan glaciology, remote-sensing-based approaches provide the vast-majority of glaciological observations (e.g. Bolch et al., 2012; Scherler et al., 2011; Kääb et al., 2012; Berthier et al., 2007). At Khumbu, Thakuri et al. (2014) traced the change in surface area and snow line altitude of glaciers in the wider Everest region since the early 1960s, showing that the snow line shifted approximately +327 m and +232 m for Khumbu and Changri Glaciers, respectively, suggesting consistently negative mass balances since the 1960s. Other glaciological studies include short mass balance surveys (Inoue 1977) and ice thickness estimates (Gades et al., 2000; Moribayashi 1978). Additionally, the study of Soncini et al. (2016) conducted a mass balance survey using seven stakes (four in debris-covered ice, three in clean ice) in spring 2014; however these measurements were not available at the time of analysis. Furthermore,

the short-term nature of these studies dictates that remote-sensing-based geodetic surveys of glacier mass balance are the only suitable basis for calibrating GERM. Available geodetic surveys are presented in Table 6.1, showing broad agreement that Khumbu Glacier has been losing mass since the 1970's, a trend that appears to be accelerating with the most recent studies estimating higher rates of mass loss, however there are considerable uncertainties associated with these geodetic mass balance surveys.

Table 6.1: Data availability at Khumbu.

Data type	Years	Site/Details	Source	Mass balance (m w.e. yr^{-1})
Meteorological	1994-2013	Pyramid	Salerno et al. 2015	-
Geodetic MB	1999-2010	Khumbu Glacier	Gardelle et al. 2013	-0.51 ±0.19
	2002-2007	Khumbu Glacier	Bolch et al. 2011	-0.45 ±0.52
	2000-2008	Khumbu Glacier	Nuimura et al. 2012	-0.76 ±0.52
	2003-2008	Everest region	Kaab et al. 2012	-0.39 ±0.11
	1970-2007	Khumbu Glacier	Bolch et al. 2011	-0.27 ±0.08
Discharge	2012-2014	Pheriche	Franco Salerno (pers.com.)	-
Debris Thickness	2002-2008	Remote-sensing	Rounce & McKinney, 2014	-
	2000	Modelled debris	Rowan et al., 2015	-

6.2.2 Method.

In this section, the modifications made to GERM will be described and the model will be calibrated to the Khumbu catchment at 50 m resolution.

6.2.2.1 Preparing Meteorological Data.

The considerable influence of wind-blown snow and light rain on precipitation gauges in high-mountain regions necessitates correction. Here, a correction for precipitation gauge-undercatch is applied using the methodology, based on gauge height and wind speed, of Yang et al. (1998) where:

If solid precipitation (T<0°C): $$R = P_r\,(\exp(4.606 - 0.157\,Ws)) \quad (6.1)$$

If mixed precipitation (T=0-1.5°C): $$R = P_r\,(100.77 - 8.34\,Ws) \quad (6.2)$$

If liquid precipitation (T>1.5°C): $$R = P_r\,(\exp(4.605 - 0.062\,Ws)) \quad (6.3)$$

where R is the corrected precipitation, P_r is the raw precipitation at the gauge and Ws is the wind speed at the height of the gauge. At Pyramid, this was reduced from the anemometer height of 5 m to the gauge height of 1.5 m according to:

$$U(h) = U(H)\left[\frac{In\left(\frac{h}{z_0}\right)}{In\left(\frac{H}{z_0}\right)}\right] \quad (6.4)$$

where *U(h)* is the corrected wind speed at the gauge height (m/s), *U(H)* is the observed wind speed at the anemometer height, *h* and *H* are the heights of the gauge and anemometer respectively, and Z_0 is the roughness parameter (m) defined as Z_0 =0.2 according the Sevruk, (1982) and Golubev et al. (1992) based on a roughness between bare snow and short grass. The classification into solid, mixed and liquid precipitation is based on temperature and is necessary due to the larger gauge-undercatch for snow compared to rain (Yang et al., 1998). Where snow-depth data are available, the change in snow-depth was also used to correct precipitation according to equation 6.5 where P_c is corrected precipitation, ρ is the density of snow, *S* is the snow-depth and *t* represents the time-step:

$$P_c = \rho(S_t - S_{t-1}) \tag{6.5}$$

Figure 6.5 shows the comparison between original and corrected precipitation with the largest corrections occurring in winter where precipitation falls as snow. This correction was applied to the 1994-2013 meteorological record, for which wind speed and snow depth were not always available, using daily correction factors applied according to the number of wet days in each month. Although winter precipitation remains uncertain, this method makes use of available data to reduce uncertainties and produce a time-series on which the bias correction can be applied. Hereafter, the gauge-corrected time-series of precipitation (Figure 6.5) is referred to as observed precipitation.

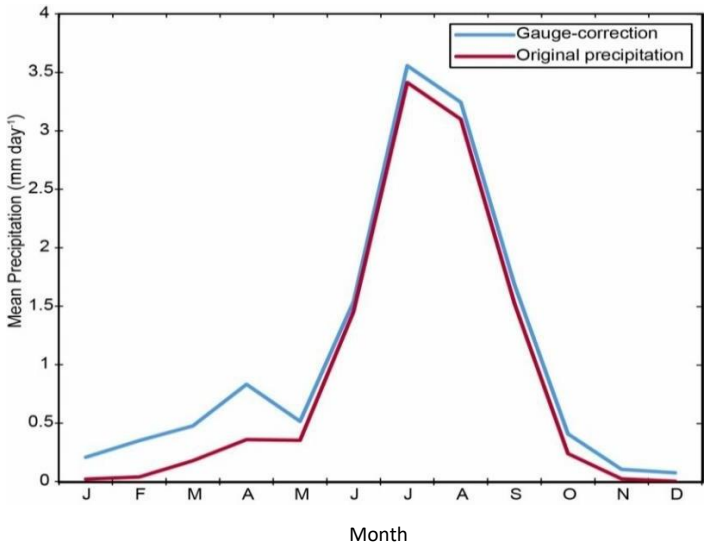

Figure 6.5: Comparison of the original precipitation series from Salerno et al. (2015) and the series used in this thesis which includes a correction for precipitation gauge-undercatch.

6.2.2.2 Configuring GERM for the Khumbu Catchment.

The only aspects of GERM described here are those unique to this catchment. For details on the main components of GERM please refer to Chapter 2. Outputs of the snow-redistribution module for the Khumbu catchment are shown in Appendix Figure A.2.

Ice Thickness. As described in Section 2.2.1, the ice thickness estimation employed in this thesis requires only a DEM and a glacier outline, thus no glacier-specific features of glacier dynamics are accounted for. At the Khumbu Glacier, this is problematic due to the aforementioned stagnation of much of the ice and the significant debris coverage. Since Gades et al. (2000) measured ice thickness across several transects using GPR, it is possible to compare estimated ice thickness with observed ice thickness, making Khumbu Glacier an ideal test of the glacier thickness model at a downwasting glacier.

The initial application of the ice thickness model was compared to the observations of Gades et al. (2000), revealing an underestimation of ice thickness below the icefall and an overestimation in the glacier tongue, owing to over-steepening of the bed under the lower section of Khumbu. This produced a volume estimate for Khumbu of 3.402 km^2. To remedy this, the approach of Huss and Farinotti (2012) was combined with GIS-based interpolation of the ice thickness data from Gades et al. (2000). Specifically, the observed transects from Gades et al. (2000) were combined with estimations of central flow line bed elevations which were then interpolated using Empirical Bayesian Kriging with known glacier boundary elevations used as hard break-lines to ensure accurate glacier boundaries. This was merged with the original modelled bed topography to produce a full bed DEM beneath Khumbu (Figure 6.6A), which produced an ice volume of 2.99 km^2, a 12.2 % reduction on the original method. The ice thickness estimation produced similar results to that of Rowan et al. (2015; Figure 6.6B), who estimated ice volume by assuming that thickness is determined by surface slope and basal shear stress, and tuning their thickness estimate to Khumbu using against observations.

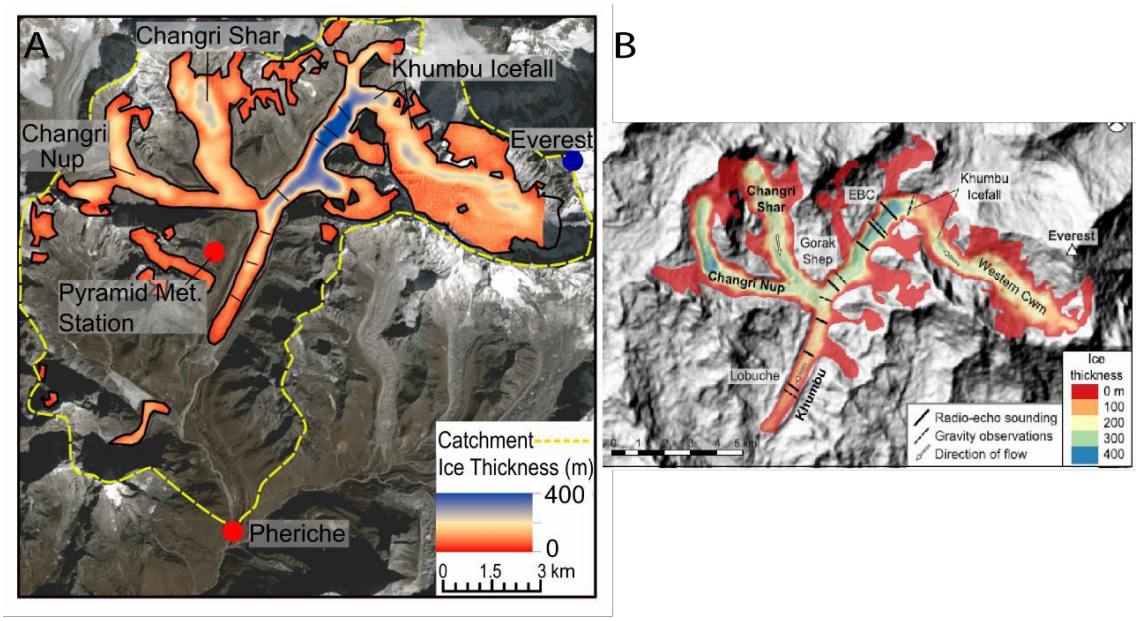

Figure 6.6: (A) Map of the catchment with simulated ice thickness included. Ice thickness estimations uses a combination of the methodology outlined in Section 2.2.1 and an interpolation of available ice thickness observations from Gades et al. (2000). (B) The ice thickness estimation from Rowan et al. (2015), who calculated similar thicknesses.

6.2.2.3 GERM Modifications.

6.2.2.3.1 Δh Parameterisation.

It is clear from the geodetic surveys described previously that the manifestation of mass loss at Khumbu Glacier and indeed the wider HKH region is surface lowering. Therefore, the Δh parameterisation of GERM, based on glaciers in the Alps, is altered for debris-covered glaciers in order to prevent simulations of mass loss resulting in terminus recession. To do this, the detailed surface elevation changes observed by Nuimura et al. (2012) for the period 1992-2008 are used to assess where mass changes are exhibited on Khumbu, in respect to elevation. Specifically, Figure 6.7A, from Nuimura et al. (2012), was used to calculate average elevation changes at different points over the glacier surface. Clearly, thickness changes are relatively homogeneous over much of the glacier beneath the ice-fall, with the exception of the mid-elevation parts (between "Area 3" and "4" in Figure 6.7A) where thinning is greatest. These points were then assigned elevation values from the SRTM DEM and smoothed to create a plot of elevation change vs elevation. Compared to the 'generic' redistribution curves used in GERM, the effect of this Khumbu-specific curve is relatively homogeneous redistribution of mass changes over the glacier area beneath the ice fall, rather than focussing mass-changes on the terminus, mimicking the geodetic surveys (e.g. Gardelle et al., 2013; Nuimura et al., 2012; Bolch et al., 2011). Additionally, this curve could be applied to other glaciers that show similar behaviour, for example, Lhotse and Imja Glaciers in Figure 6.7A show similar mid-elevation

thinning, or alternative curves could be calibrated for individual glaciers where geodetic-surveys have been carried out (all of Himalaya; Bolch et al., 2008; Nuimura et al., 2012; Kääb et al., 2012; Gardelle et al., 2013).

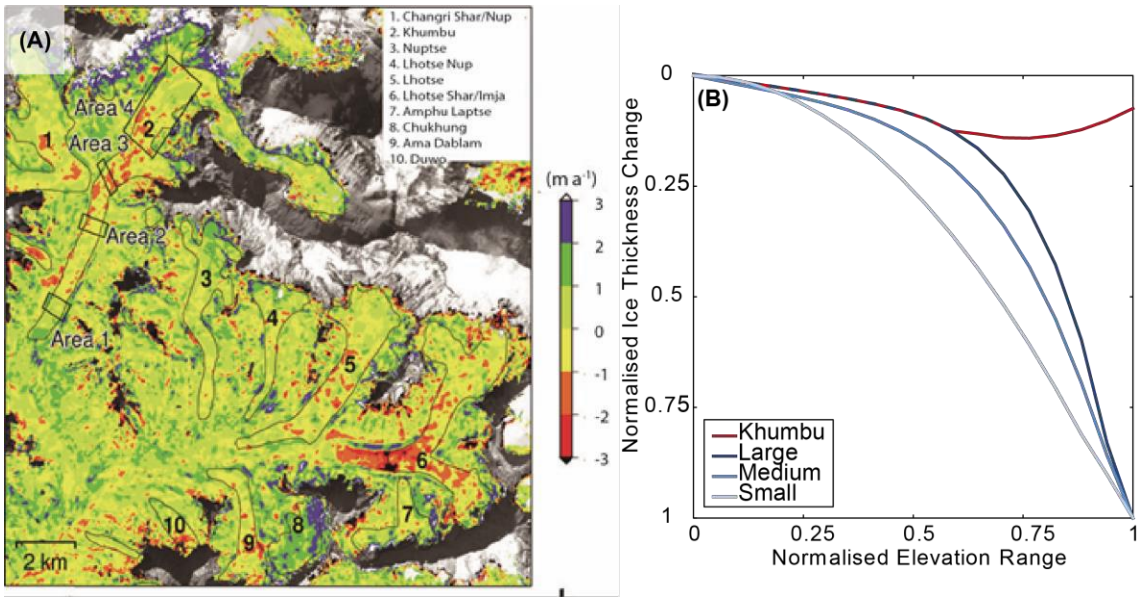

Figure 6.7: (A) the thinning rates at Khumbu (2) and surrounding glaciers, from Nuimura et al. (2012), and (B) the modified Δh curve developed using the thickness changes observed in (A).

6.2.2.3.2 Melt Beneath Debris.

Distributed melt reduction factor. The influence of thick debris cover on ice ablation rates dictates that it is essential to incorporate debris cover in GERM where it covers a significant proportion of the ice surface. At Khumbu Glacier, 37 % of the ice surface is debris-covered. Previous runoff modelling of debris-covered glaciers have utilised a constant melt reduction factor, regardless of debris depth, where melt is reduced homogeneously for any parts of the glacier defined as debris-covered (e.g. (Braun et al., 1993; Parajuli et al., 2015; Konz et al., 2006; Immerzeel et al., 2012; Konz et al., 2007; Bauder et al., 2007; Huss et al., 2008a). The main issue with this simplistic approach is that the debris layer is extremely heterogeneous in thickness (Rowan et al., 2015), therefore, the spatial distribution of melt will not be captured with a constant reduction factor.

The ablation module of GERM is therefore modified to include a melt reduction factor which reduces melt individually for each grid-square, depending on the depth of debris in individual grid-squares (50 m resolution; see following section for details of debris thickness), according to:

If T > 0°C and debris-covered: $$M = ((f_M + r_{ice} . I_{pot,i}). T_i) . f_{\text{debris}} \quad (6.6)$$

$$f_{\text{debris}} = e(c. D_t) \quad (6.7)$$

where f_{debris} is the correction factor for debris-covered ice, e is the exponential constant, and c is the coefficient that describes the shape of the melt reduction curve depending on debris thickness, D_t. The melt reduction curve (Figure 6.8) is calculated using an exponential curve that is based on observations of melt beneath debris at several glaciers (Nicholson and Benn, 2006) which are similar to those at Ngozumpa Glacier (Nicholson & Benn, 2013) and Khumbu Glacier (A. Rowan 2016, personal communication). A similar approach has been used in several modelling studies (e.g. Hagg et al., 2008; Konrad and Humphrey, 2000; Rowan et al., 2015). The decision was taken to exclude the part of the Østrem curve that increases ablation rates for thin debris since the overwhelming signal at Khumbu, and indeed most Himalayan glaciers, has been shown to be one of melt reduction as the majority of the debris is sufficiently thick (Pratap et al., 2015; Inoue & Yoshida 1980). This curve is therefore not specific to Khumbu Glacier and is transferable to other glaciers. The applicability of this melt-reduction curve will be discussed in Section 8.1.3.1.

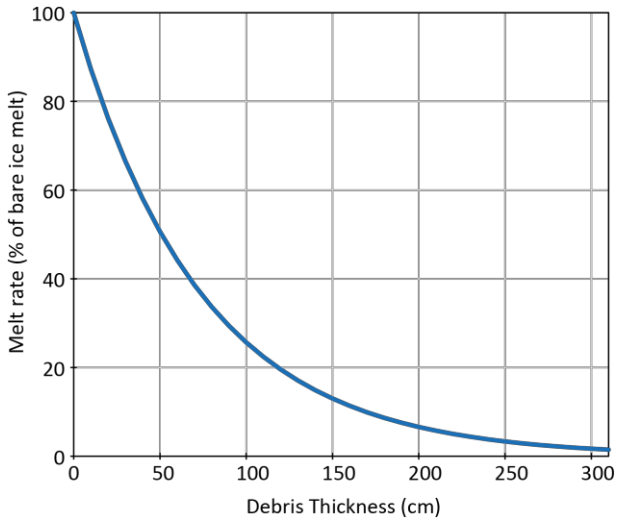

Figure 6.8: The exponential melt reduction curve developed for Khumbu Glacier.

Debris Thickness. In order to incorporate debris cover into GERM, it is essential to know the debris distribution and thickness over the ice surface. However, estimating debris thicknesses over large areas is problematic for several reasons. Firstly, the debris cover is extremely variable in thickness, making it difficult to extrapolate thickness samples to a larger area (Ragettli et al., 2015). Secondly, conducting field studies at Khumbu Glacier is limited by difficult and dangerous terrain, confounded by the high elevation and harsh weather conditions. As such, the true depth of debris at Khumbu Glacier remains largely unknown. Therefore, two different sources of data

on debris thickness are implemented in this thesis providing a conservative estimate of thicknesses ('thin debris') and maximum estimate of thicknesses ('thick debris') to capture variability in debris thickness distribution. Both of these layers are variable in thickness. GERM will be calibrated separately for each debris surface and the results compared.

Firstly, the remote-sensing based debris surface from Rounce and McKinney (2014) is used. Their study uses the thermal infra-red band of Landsat remote sensing imagery, combined with an energy balance model to estimate debris thickness on the Imja-Lhotse Shar Glacier (12 km from Khumbu). Their study then applied their methodology to Khumbu Glacier to provide a spatial map of debris thickness at 60 m resolution. This surface, shown in Figure 6.9a, estimates a highly heterogeneous debris surface that is likely a conservative estimation of true debris thickness, due to the limited resolution of the DEM (Rounce, personal communication; Rowan, personal communication; Rounce & McKinney 2014; 60 m). Therefore, this surface is used as a lower-bound for debris thickness in this thesis.

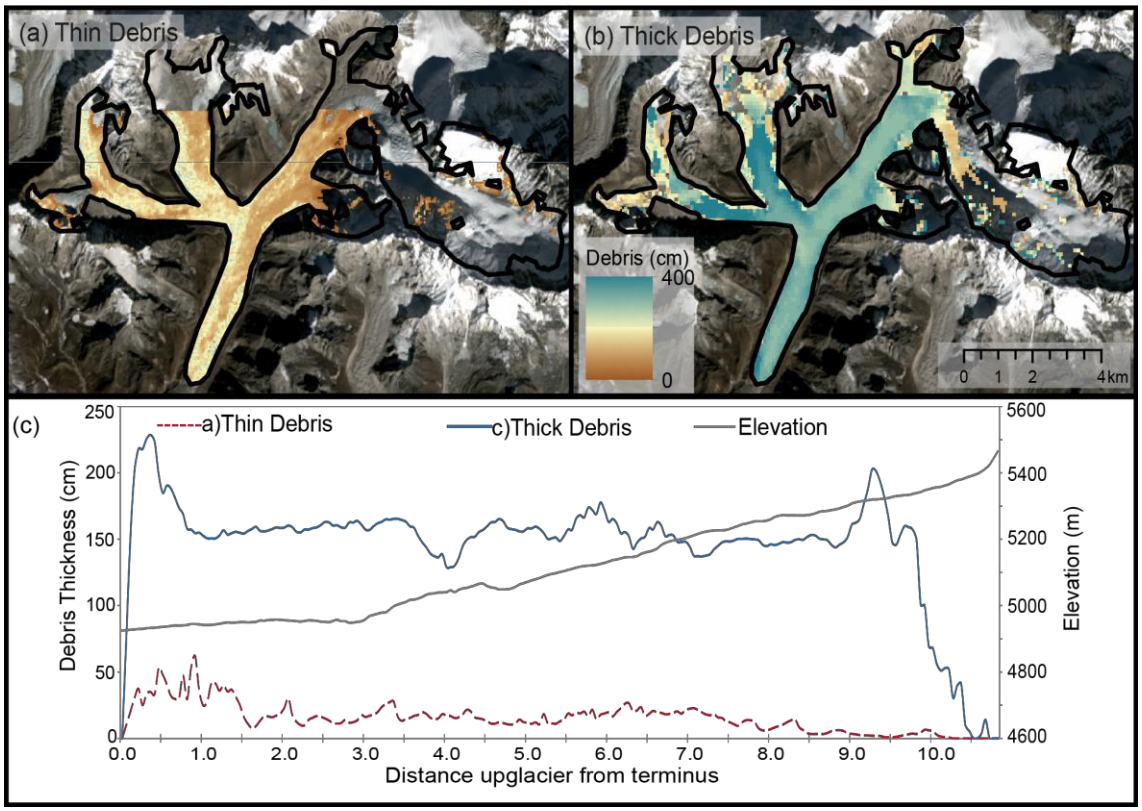

Figure 6.9: Comparison between (a) 'thin debris' layer estimated in Rounce & McKinney (2014); and (b) 'thick debris' layer modelled in Rowan et al. (2015). (c) Central 100 m swath of debris thickness. Debris thickness is spatially variable in both layers, but 'thin' is a generally conservative estimate and 'thick' is a maximum estimate of thickness.

Secondly, the modelled debris surface of Rowan et al. (2015) is used, who use long-term numerical modelling of ice flow and debris transport to reconstruct the development of the debris surface, therefore providing the depth of debris in each grid square. Since this surface is more homogeneous in thickness than reality, it is used as a maximum bound for debris thickness in this thesis, and is compared to the 'thin debris' surface of Rounce and McKinney (2014) in Figure 6.9.

Summary of modifications. The results of the aforementioned modifications are two GERM configurations providing lower and upper bounds for the thickness of the debris layer: 'thin debris', and 'thick debris'. Each of these configurations is calibrated separately to the same geodetic mass balance using the same meteorological data, using the new calibration approach, fully described in Section 4.3.2. Thus, the performance of these configurations can be evaluated by comparing observed and simulated discharge.

6.3 GERM Performance at Khumbu.

6.3.1 Calibration.

Due to the lack of long-term discharge data, only geodetic mass balance is used for calibration from 1999-2010. Specifically, Gardelle et al. (2013) surveyed a mass balance of -0.51 m w.e. yr^{-1} from 1999-2010, which is used since their mass balance estimation sits between those of Bolch et al. (2011) and Nuimura et al. (2012). Additionally, the time-period of the meteorological data (1994-2013) best fits with the timing of the geodetic survey performed over the period 2000-2011 in Gardelle et al. (2013). The available discharge data from Pheriche (2012-2014) do not coincide temporally with the meteorological data, therefore is not used during calibration but instead used to validate the model outputs (see following section). To drive GERM during the calibration period, bias-corrected RCM outputs are used (see Chapter 3 for full description of models implemented as well as the bias-correction process) to ensure continuity with future simulations; the ultimate aim of this work is to make projections of future glacier and runoff evolution.

Table 6.2: Calibrated parameter sets for two separate calibrations of GERM with a thin debris layer and a thick debris layer. ****dP/dz* **and *dT/dz* **were calculated in Salerno et al. (2016).**

Parameter	Units	'Thin Debris'	'Thick Debris'
f_M	10^{-3} m (d °C)$^{-1}$	1.31	1.71
r_{ice}	10^{-5} m^3 (W d °C)$^{-1}$	2.10	2.74
r_{snow}	10^{-5} m^3 (W d °C)$^{-1}$	1.57	2.05
C_{prec}	%	0	0
*dP/dz**	10^{-2} % m^{-1}	0	0
*dT/dz**	10^{-3} °C m^{-1}	-6	-6
Modifications		*-Khumbu-specific Δh parameterisation.* *-Thin Debris (Rounce et al., 2013)*	*-Khumbu-specific Δh parameterisation.* *-Thick Debris (Rowan et al. 2015)*

Tables 6.2 and 6.3 show the results of the calibration at Khumbu. These parameter sets differ due to the insulating influence of debris cover. For example, in the case of 'thick debris', relative melt factors are high, so there is increased melt with warming, yet the insulating effect of the debris balances this to produce very similar overall glacier response with strongly reduced mass loss in the lower ablation area, but higher mass loss above the debris-covered tongue. Conversely, 'thin debris' has lower melt factors because the insulating effect of the thin debris is lower.

Table 6.3: Calibration results for the thin and thick debris configurations at Khumbu, showing the coarse grid (left) and fine grid (right) calibration results, based on comparison between observed and simulated glacier volume change from 1999-2010.

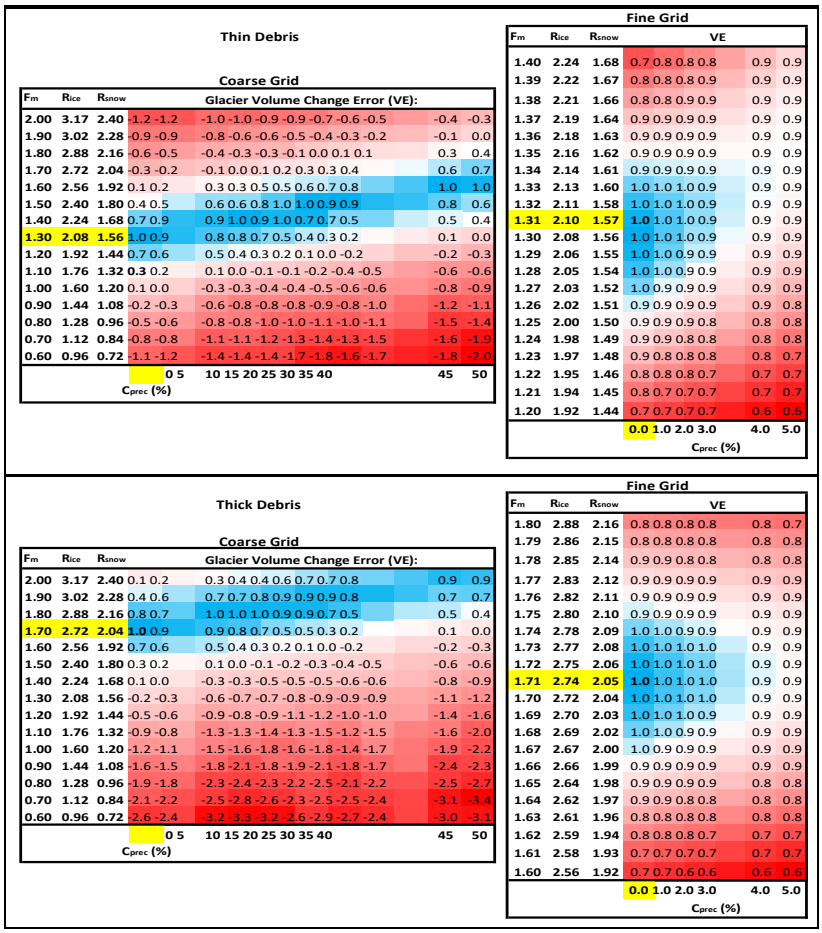

6.3.2 Glacier and Runoff.

Glacier Changes. The two configurations produce near-identical volume change from 1999-2010 (Figure 6.10). However, the spatial mass balances show considerable differences with the 'thin debris' layer causing localised variability, and the 'thick debris' layer strongly insulating the ice surface in the debris-covered area, resulting in more positive local mass balance. This reversal

of the mass balance gradient is a typical characteristic of debris-covered glaciers (Rowan et al., 2015; Quincey et al., 2009; Jouvet et al., 2011).

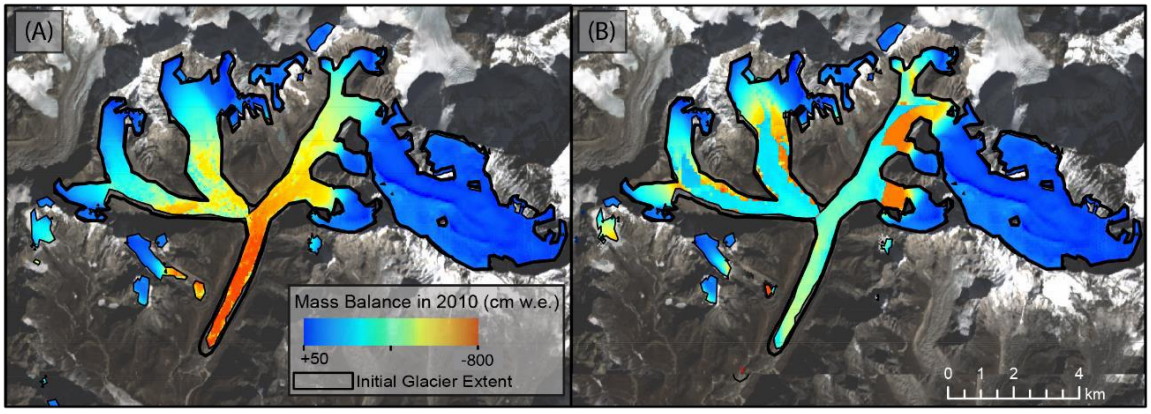

Figure 6.10: Distributed mass balance in 2010, comparing (A) the thin debris layer to (B) the thick debris layer.

Discharge. Evaluating the performance of these configurations by comparing mean simulated discharge during the calibration period to observed discharge from 2012-2014 shows that the thick debris configuration better simulates discharge, despite simulating identical glacier change. Specifically, the thin-debris configuration produces a NSE of 0.76 (Figure 6.11) which is improved in the thick debris configuration (NSE=0.85). Similarly, mean annual runoff simulated using the thin debris configuration underestimates 2012-2014 annual runoff by 21 %, compared to a 2 % underestimation for thick debris. The difference in runoff is discussed in Section 6.4.

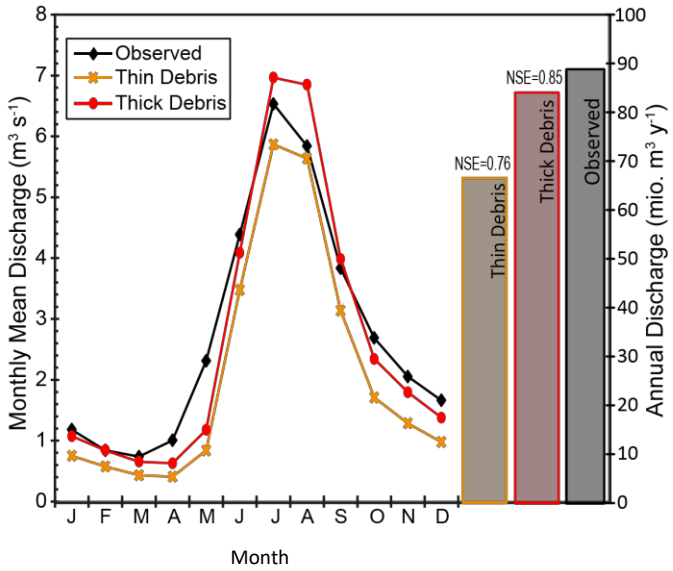

Figure 6.11: Mean monthly discharge comparing the two model configurations to observations of discharge at Pheriche. Bars on the right of the plot show total annual discharge and NSE refers to the Nash-Sutcliffe model efficiency. Data for the model configurations are the mean from the 1999-2010 calibration period. Observed discharge data is based on monthly means from 2012-2014.

The modifications presented here are promising but are uncertain for several reasons. Firstly, the lack of long-term discharge data brings into question how representative the discharge from 2012-2014 is of typical catchment behaviour. Moreover, because the meteorological data are only available until mid-2012, when the discharge measurements commence, direct comparison is flawed so the comparison presented only gives an indication of the accuracy of discharge simulation. Another factor to consider is the seasonal discharge simulation. The 'thick debris' configuration, which reproduces discharge most accurately, appears to overestimate discharge in summer and underestimate discharge in April and May. This suggests that the onset of the melt season is too late in the simulations, resulting in the build-up of snow and ice that is then melted in summer, resulting in overestimation of discharge in these months. This may be a result of deficiencies in the meteorological data, whereby precipitation is not accurately captured.

6.4 Discussion.

The purpose of this chapter was to modify GERM so that it could be applied to regions and catchments where glacier behaviour is atypical and data are limited, and where GERM has previously not been applied. Therefore, the application of GERM to a heavily debris-covered, stagnating glacier demonstrates the changes that need to be made in order to more realistically simulate runoff in the Himalaya. Incorporating downwasting through modification of the Δh parameterisation prevents overestimation of terminus recession. Additionally, by specifically reducing ice melt depending on the depth of overlying debris in a fully distributed manner captures the spatial distribution of melt over the ice surface, as well as the reversal of the mass balance gradient observed on debris-covered glacier (Rowan et al., 2015; Quincey et al., 2009; Jouvet et al., 2011).

The portable nature of GERM, in that it can be applied to different catchments with minimal input data requirements, is maintained even with the modifications presented here: the only essential input requirements are daily temperature and precipitation data. For example, to include ice-stagnation, the curve developed for Khumbu Glacier could be applied to other glaciers with low flow rates, which can be discerned from remote-sensing studies (e.g. Quincey et al., 2009) or from geodetic surveys which cover most of the Himalaya (e.g. Gardelle et al., 2013). Similarly, debris thickness can be estimated using the remote-sensing approach of Rounce and McKinney (2014), or a constant reduction factors can be used where no thickness data are available. Thus, despite the changes, GERM can be applied to other catchments in the Himalaya, and this is a recommendation for future research (see Section 8.5).

The differences in simulated discharge between the thin and thick debris configurations (Figure 6.11), despite both producing near-identical volume change, merits further discussion. Because

the mass balance is the same in both configurations, the difference in discharge is not related to glacier melt, thus is most likely due to be the result of differences in snow melt outside of the glacier mask whereby the 'thin debris' configuration allows non-plausible accumulation of snow and ice, resulting in the storage of water and under-prediction of runoff. Conversely, for 'thick debris', the higher melt parameters cause this snow and ice to melt therefore generating runoff which, when compared to observed runoff, suggests that the model is more accurately reproducing the catchment with the thick debris layer. Similar underestimation of discharge, due to low melt parameters allowing snow accumulation, has been seen in other studies (e.g. Frey & Holzmann, 2015; Bernhardt & Schulz, 2010) but is generally an underreported deficiency and suggests that, with the thin debris layer, accumulation is occurring in areas where there is none in reality. However, it is important to note that a full validation of the discharge simulation is not possible due to the short duration of discharge monitoring.

Issues and Uncertainties. The modifications presented here allow GERM to be applied to debris-covered glaciers. However, several uncertainties remain.

Firstly, *estimation of debris thickness* is difficult. Here, two independent sources on debris depth are implemented. Despite recent advances in debris thickness estimation using remote sensing imagery (e.g. Rounce & McKinney, 2014; Mihalcea et al., 2008a; Mihalcea et al., 2008b; Casey et al., 2012), it is not currently possible to confidently estimate debris thickness using remote-sensing. Therefore, it is suggested that future studies without accurate debris data should consider a range of sources that constrain the uncertainty associated with debris thickness. Additionally, the *melt reduction curve* that varies with depth is a subject of debate. For example, Reid and Brock (2010) suggested that melt under 0.5 m of debris is closer to 20 % of the clean-ice melt rate (compared to 50 % in this thesis), whereas Kayastha et al. (2000) suggest 12 %. The impact of changing the melt reduction curve is assessed and disused in detail in Section 8.1.2.

Validation of the model performance is difficult due to limited glaciological and hydrological data. Although geodetic mass balance (Gardelle et al., 2012; see Section 6.2.1) is used for calibration from 1999-2010, there is potential to use a longer-term mass balance study; for example, Bolch et al. (2011) from 1970-2007, to validate the calibrated parameters. However, there are two issues that prevent this shown in Figure 6.12. Firstly, there is overlap between the calibration and validation periods (1999-2007) meaning that the validation data would not be independent of the calibration data. Secondly, and more importantly, the various geodetic mass balance studies do not agree despite covering the same time-periods, and are each subject to significant uncertainties. This variability between the various geodetic surveys makes validation problematic.

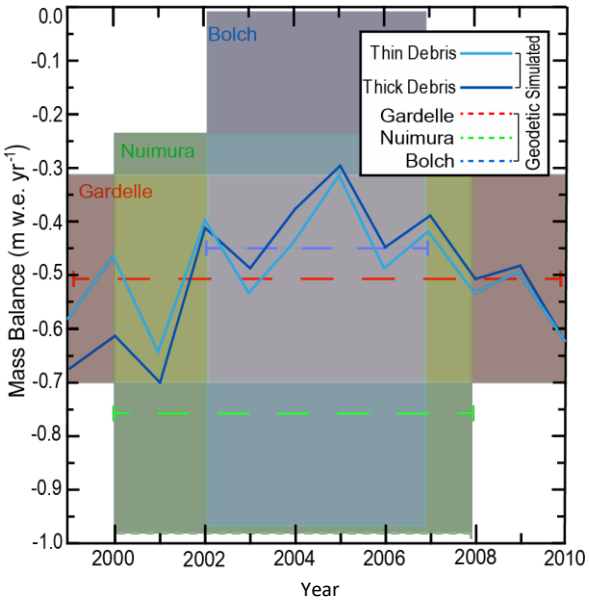

Figure 6.12: A comparison of the geodetic survey conducted at Khumbu, showing considerable uncertainties in each study and sizable differences between studies. The mass balance simulated in the two model configurations is included.

Changes to the debris surface. The changes made to GERM here make an important assumption about the nature of the debris surface: that it remains constant in terms of extent and thickness. However, several studies (e.g. Jouvet et al., 2011; Thakuri et al., 2014; Anderson, 2000; Bolch et al., 2008; Rowan et al., 2015; Kirkbride & Deline, 2013) have shown that debris surfaces are highly dynamic with continued ice stagnation promoting thickening and expansion of the debris surface. Moreover, it is likely that ice-cliffs and proglacial lakes will continue to evolve and expand as the debris cover changes (Watson et al., 2016; Sakai, 2012). Therefore, the important feedback between debris cover and mass-balance is not fully captured here, which will be significant for long-term future simulations. Currently, the understanding of how debris surfaces may evolve over time is too limited to realistically be captured in glacio-hydrological models; however, future simulations should consider the impact of a changing debris surface on glacier evolution and runoff when discussing results.

6.5 Conclusions and Future Outlook.

The modifications made to GERM allow fully distributed debris cover and ice stagnation to be accounted for in GERM without significantly increasing the data requirements, thus maintaining model portability. This represents one of the first attempts to include these modifications in a glacio-hydrological model, and the first study to include fully distributed debris cover where melt is reduces depending on debris thickness, without requiring a network of stake measurements.

The short-term data available at Khumbu allowed some testing of the model, with discharge reasonably well reproduced by GERM. However, it is not possible to fully assess model performance due to the lack of long-term validation data, therefore the analysis of uncertainty associated with GERM, conducted for sites in the Alps, is not possible at Khumbu.

Chapter 7 will conduct long-term future simulations of Khumbu Glacier with the aim of providing a first-order assessment of future glacio-hydrological changes. By using several climate models and scenarios, the uncertainty associated with future climate projections is partially accounted for. However, it is recommended that future research should test GERM at other Himalayan catchments and should seek to improve data monitoring in this region, such that the uncertainty associated with model outputs can be assessed (see Section 8.5 for detailed future recommendations).

7. FUTURE VOLUME AND RUNOFF EVOLUTION OF A DEBRIS-COVERED GLACIER: KHUMBU, NEPAL.

This chapter uses the modified version of GERM (Chapter 6) to project changes in glacier volume and runoff at the Khumbu catchment to 2100. This catchment contains the debris-covered Khumbu Glacier. A range of projections are explored that incorporate debris layers derived from different sources (therefore with different estimations of distributed debris thickness) and are driven by a range of climate scenarios for which model inputs have been downscaled using a novel methodology (Chapter 3). This range of future projections provides improved constraints on the uncertainty of future projections using GERM for catchments with debris-covered glaciers. This chapter addresses Aim 3B.

7.1 Introduction.

The novel method of statistical-dynamical downscaling of GCM simulations developed in Chapter 3 will be used in this chapter, taking the temperature and precipitation in the CORDEX-South Asia RCM grid-box over the Khumbu glacier and using the meteorological data from the Pyramid station to conduct the bias correction. The future simulations will be driven by all available climate simulations at Khumbu (two RCMs driven by two GCMs), giving partial indication of the uncertainty of projected volume and runoff changes associated with the different available GCMs, RCMs, and RCP scenarios. However, as described in Chapter 3, it is noted that at present there are still a limited range of GCM and RCM outputs for the Himalayan region.

Previous work has simulated the future evolution of the Khumbu Glacier but these have either employed more data-intensive approaches, requiring site-specific data that are available for Khumbu but not for other glaciers in the region, or have neglected the impact of debris cover on glacier melt and runoff.

An example of a data intensive appraoche is Soncini et al. (2016), who employed a ETI model (Pellicciotti et al., 2005; see Section 1.2 for details) coupled to a dynamical ice-flow model at Khumbu Glacier. Each component of their model was calibrated locally to seven stake measurements that were used to calculate ablation of debris-covered ice and extrapolated to the glacier scale. Although their approach has merit and represents the correct approach to short-term, catchment specific simulations, the extrapolation of very few short-term observations of debris thickness, ice ablation, and melt beneath debris to the glacier scale introduces significant uncertainties (Fujita & Sakai, 2014) and extrapolation of too few stake

measurements can lead to incorrect melt rates (Nicholson & Benn, 2013) as discussed in detail in Section 8.1.3.1. Moreover, Soncini et al. (2016) used a weather-generator to downscale precipitation and the delta change statistical downscaling approach for simulations of temperature, which only adjusts for mean temperatures therefore not correcting for the variability in simulated temperature. Additionally, the downscaling was applied to GCM output, thus not including the dynamical downscaling applied in this thesis, which can lead to errors in the corrected data (Guyennon et al., 2013)

More simplistic approaches do not incorporate the influence of debris cover on ice ablation or runoff. For exampe, Shea et al. (2015) conducted a study into the future evolution of all glaciers in the Everest region, projecting that remaining ice volume in 2100 will be between 4-27 % of ice volume in 2010, but runoff changes were not assessed. They apply a constant reduction in melt for debris-covered ice which, although an approach taken in many studies (e.g. Immerzeel et al., 2013; Jouvet et al., 2011), does not account for variable debris thickness. In addition, their initial ice thickness estimation, which dictates ice volume at the start of their simulations, strongly underestimates ice volume for the three glaciers shown in their validation study, and is not constrained by observations at Khumbu, unlike this thesis which used Gades et al. (2000) to provide ice thickness estimates (see Section 6.2.2.2). The authors agree that their approach produces an overestimation of ice thickness near to the terminus.

Additionally, Rowan et al. (2015) conducted a study into the evolution of the debris-covered Khumbu Glacier and how the glacier responds over very long time-scales (Little Ice Age to 2200). Therefore, although Rowan et al. (2015) do make simulations of the future, their aim is quite different to this thesis, with no consideration of runoff and a simplified future climate forcing using ELA changes rather than projections based on climate models.

In summary, previous work is characterised by data-intensive approaches that are not suitable to the vast majority of data-limited Himalayan glaciated catchments, methods that do not account for debris thickness when calculating melt beneath debris, or only modelled volume change and neglected runoff. Hence, this part of the thesis differs from those studies above because it applies a more portable model (GERM) with modifications that are suitable for data-poor catchments (i.e. those for which only remote-sensing-derived glacier mass balance and debris coverage are available) and enables assessment of climate uncertainty in future runoff projections.

7.2 Application of GERM to the Khumbu Catchment.

This section implements GERM using both the thin and thick debris layers and conducts future projections of glacier volume and runoff change using a range of downscaled climate inputs.

Two debris layer thicknesses are used in order to constrain the uncertainty associated with the true debris thickness at Khumbu, which likely lies between these two estimates (Rowan, personal communication). Due to the limited availability of long-term volume change or discharge data, the rigorous uncertainty analysis conducted for sites in the Alps, where simulated glacier and hydrological changes were compared to observed changes, cannot be included here. Therefore, only the uncertainty associated with climate data is assessed.

7.2.1 Climate Inputs Used.

Table 7.1: Available RCM-GCM combinations that include evaluation simulations in the CORDEX-South Asia domain.

	Model (RCM)	Driving GCM	RCPs Available			
			2.6	4.5	8.5	Organisation
A	RCA4	ICHEC-EC-EARTH	✓	✓	✓	SMHI
B	REMO	Nor-ESM	×	✓	✓	GERICS

The bias-correction of the CORDEX-South Asia climate models is detailed in Chapter 3. Table 7.1 shows the available climate models at Khumbu Glacier for this thesis. Due to the lack of a large range of climate model outputs, this section cannot fully constrain climate model uncertainty. Scenario uncertainty is somewhat accounted for since RCPs 2.6, 4.5 and 8.5 are available for the model combination RCA4-ICHEC-EC-EARTH, hereafter referred to as climate input A. RCPs 4.5 and 8.5 are available for model combination REMO-Nor-ESM, hereafter referred to as climate input B. Additionally, the uncertainty introduced by the statistical downscaling process is not accounted for here. To consider downscaling uncertainty, one would need to use different downscaling methods, which is outside of the scope of this thesis. Therefore, these simulations provide an indication of the uncertainty associated with climate model inputs; however, it is encouraged that a larger range of climate model outputs are included in any future studies to fully constrain climate model uncertainty.

7.2.2 Volume and Runoff Change Results.

7.2.2.1 General Observations.

The results of the future projections are shown in Figure 7.1. Clearly, considerable ice volume loss is projected in all simulations. There is considerable variability between climate inputs, with climate input A generally simulating less volume loss than climate input B, likely due to the negative precipitation trends projected in A-4.5 and A-8.5, as well as similar warming trends (see Figure 3.12, Section 3.4.5 for temperature and precipitation projections). In terms of RCPs, it is clear that RCP 2.6 simulated the least volume loss and RCP 8.5 the most. Specifically, remaining ice volume in 2100 ranges from 1 % to 41 % of volume in 2010, with a mean of all simulations of 22 %.

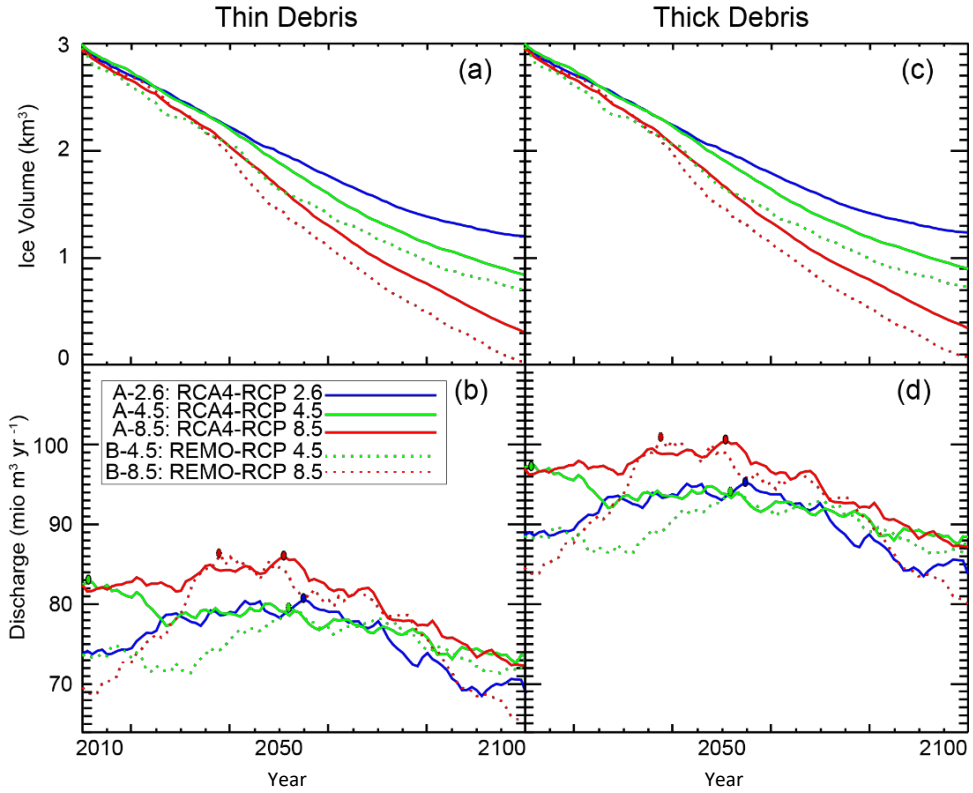

Figure 7.1: Time-series of future glacier and discharge evolution at Khumbu under 5 different climate inputs, for both thin (A and B) and thick (C and D) debris layers. Coloured circles in (B) and (D) represent when peak discharge is reached, with discharge shown as 10-year running means.

The projected trends of discharge evolution are less pronounced, with the majority of simulations suggesting an initial increase in annual discharge, with a peak between 2035 and 2055, followed by a decline. The overall pattern is one of negative discharge trends over the simulation period (2010-2100), as shown in Figure 7.2. The only exception to the negative trends is climate input B-4.6 which maintains relatively constant discharge, due to a positive precipitation trend compensating for a reduction in glacier contribution to discharge. Additionally, climate input A-4.5 simulates peak discharge very close to the start of the simulation.

The difference in ice volume change between the thin and thick debris surfaces is very small, however, there are considerable differences in annual discharge with the thin debris layer projections consistently projecting annual discharges around 15 million m^3yr^{-1} lower than for the thick debris layer. These represent lower and upper bounds for the effect of uncertain debris thickness on discharge using the modified form of GERM.

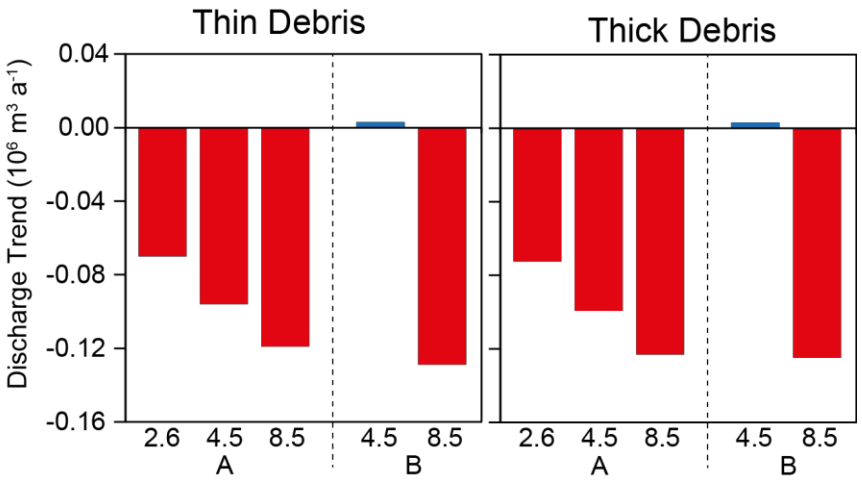

Figure 7.2: Trend analysis for discharge at Khumbu, using Sen's slope for trends based on 2010-2100 and significance indicated with red bars (p<0.05) calculated using Mann-Kendall test. "A" and "B" refer to the driving model-combination (see Table 7.1) and numbers (e.g. 4.5) refer to the RCP. The thin debris layer trends are on the left with the thick debris layer on the right, showing near-identical trends.

7.2.2.2 Seasonal Changes in Runoff.

The seasonal discharge changes (Figure 7.3) at Khumbu show a lowering of peak summer discharges in all simulations, as well as increased baseflow outside of the monsoon and melt season (days 0-130 and 300-365). All simulations suggest a lengthening of the melt/monsoon season. These changes reflect the decrease in discharge (Figure 7.1) as well as the higher temperatures extending the melt season. For climate input A, there is little change to the monthly discharge from 2020-2040, before a gradual reduction, with peak discharge in 2080 reduced by around 2 m^3 s^{-1}, with the greatest change in RCP 8.5. Such reduction in peak discharge echoes the significant negative discharge trends from Figure 7.2.

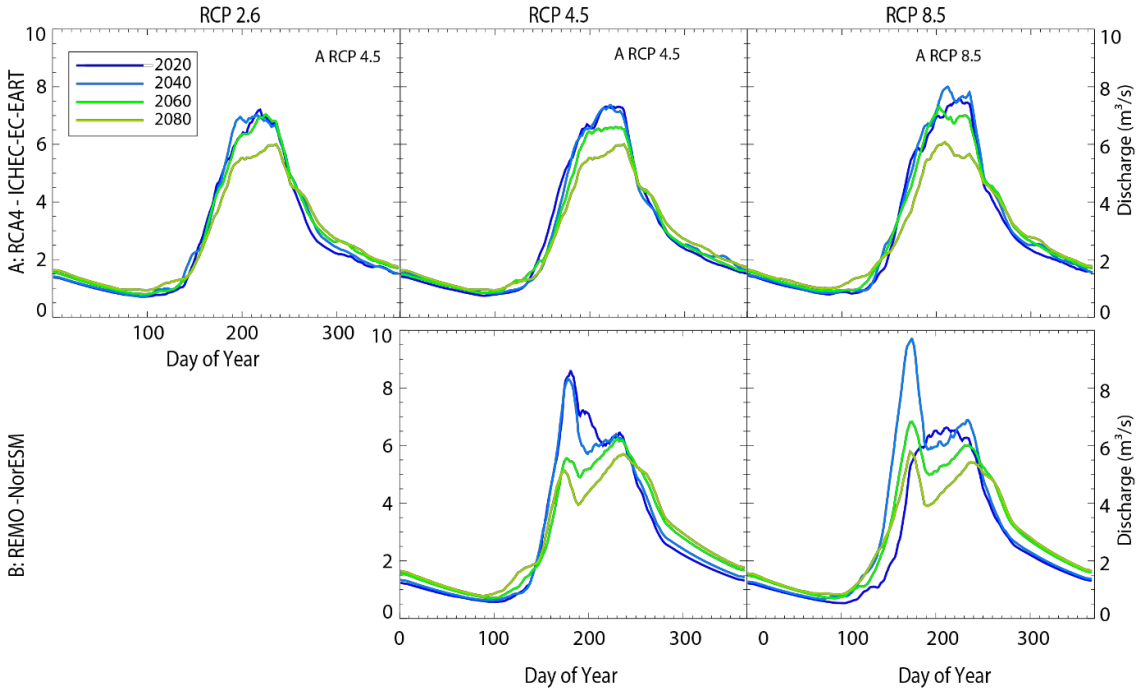

Figure 7.3: Seasonal evolution of discharge at Khumbu. Each line represents mean of ±5 years, e.g. '2020' represents the mean discharge from 2015 to 2025. The results of the thin and thick debris layer simulations have been averaged.

For climate input B, two discharge peaks appear after 2020, with the first peak occurring around day 170 and the second peak in day 230. The timing of these peaks also changes, with the initial peak occurring around 10 days earlier in 2080 compared to 2020, and the second peak occurring progressively later as the century progresses. To explore the reason for this double-peak in discharge, Figure 7.4 shows the seasonal differences between the simulated temperature and precipitation of climate inputs A and B. Clearly, simulated precipitation (averaged over 2010-2100) for climate input B peaks in August (days 214-244) whereas peak temperatures are in June (day 153-182). The peak in temperatures in June is responsible for the initial peak in discharge due to melt of snow and ice, with the peak precipitation in August causing the second peak through liquid precipitation. This pattern is not simulated for climate model A due to the coincidence of peak temperature and precipitation in July and August, a continuation of the present day conditions.

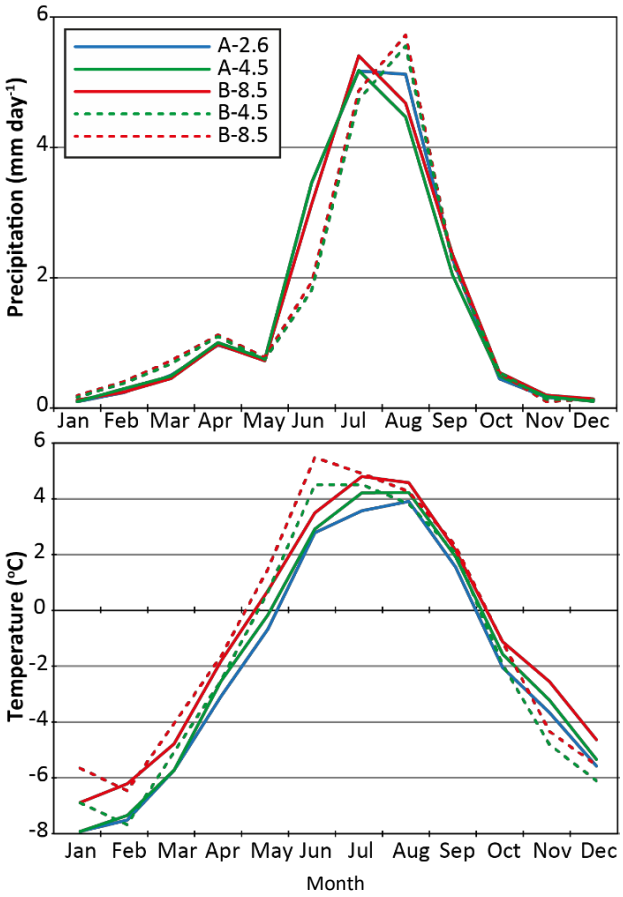

Figure 7.4: Monthly means of bias-corrected future simulations of precipitation and temperature at Khumbu, averaged over 2010-2100. Note the different timings of the peak temperature and precipitation for climate input B, which explains the double-peak in discharge in Figure 7.3.

7.2.2.3 Changes in the Glacier Contribution to Discharge.

The design of GERM prevents separation of the snow-melt contribution to discharge at Khumbu. A limitation of the model is that the individual components of the runoff reservoir; for example, the snow reservoir and the slow reservoir, interact and the outputs only document the runoff exiting the reservoirs rather than the source of the runoff. As a result of this storage, much of the snow-melt runoff is held in the 'rock' reservoir before reaching Pheriche, and cannot be included in the separate discharge plots (Figure 7.5). In the Alps, this was less problematic since the catchments were smaller resulting in less runoff storage within the catchment. To overcome this, a spatial mask was used to isolate runoff originating from within the glacier outline, which includes both snow and ice melt, but excludes snow melt and wet precipitation outside of the glacier mask, shown as the 'glacier' contribution in Figure 7.5. This figure shows the results of the thick debris layer only as the results of the thin debris layer showed a very similar pattern.

Figure 7.5 clearly shows that glacier melt makes up a significant portion of overall discharge during the summer, and that this contribution reduces with time, particularly evident in 2080

for RCP 8.5 for both climate inputs A and B. The seasonal changes observed in Figure 7.3 are also evident here, for example, the double-peak in discharge for climate input B is visible in total discharge for climate input B but not in the glacier contribution, reaffirming that the second peak is likely precipitation rather than melt. Finally, the duration of the melt season appears to increase with time. These results agree well with those of Soncini et al. (2016).

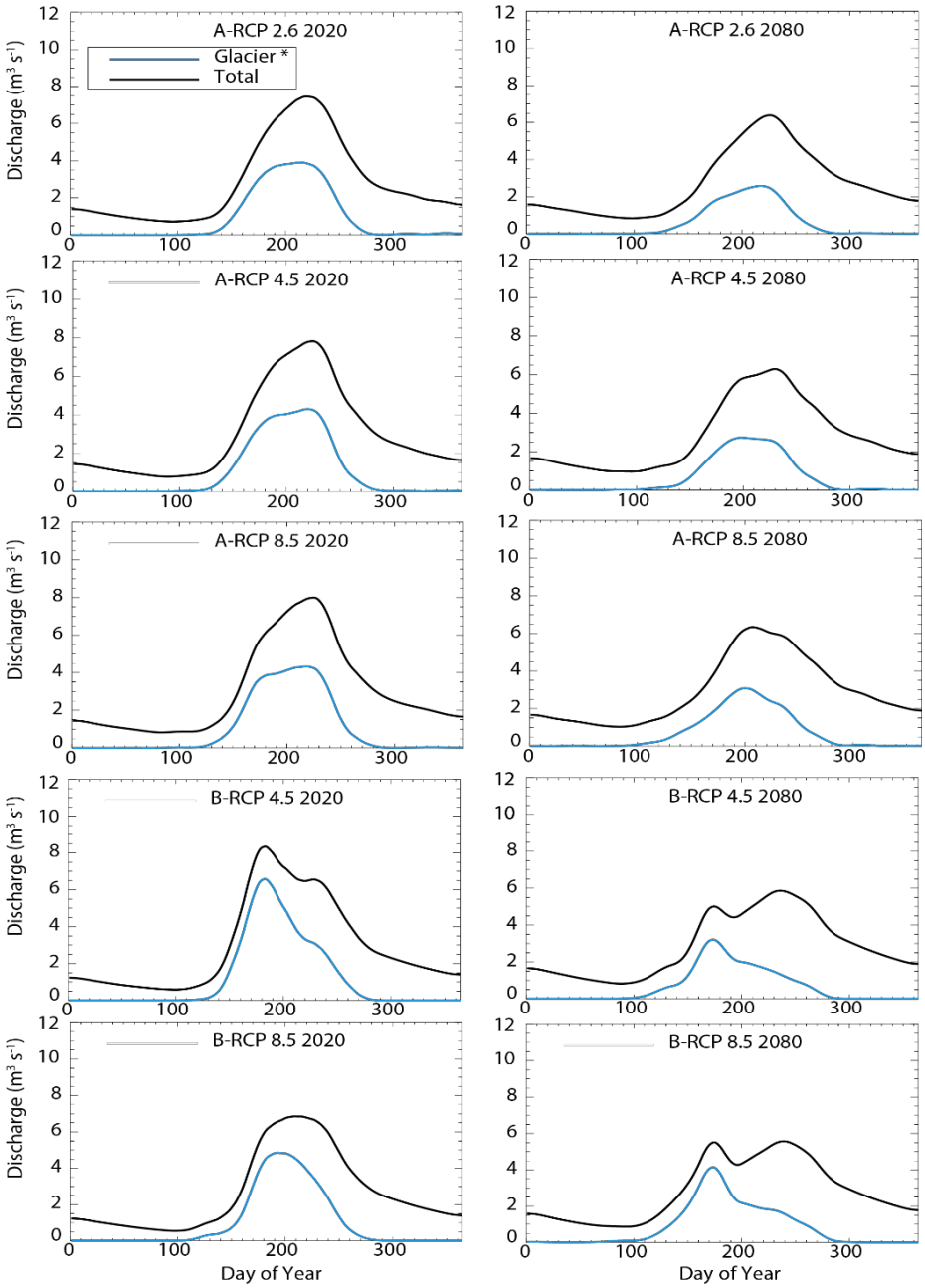

Figure 7.5: The contribution of runoff from the glacier area to total discharge. Note that the glacier melt includes snow melt on the glacier surface.

7.2.2.4 Spatial Patterns of Glacier Volume Loss.

Figures 7.6 and 7.7 show how Khumbu Glacier recedes and loses mass under different climate inputs and with the differing debris layers. These results show that, in terms of the differences

between the spatial patterns of ice loss when using the thin and thick debris layers, it is clear that the thin debris layer provides less insulation to the lower ablation area resulting in faster recession. The thick layer, conversely, provides greater insulation and reduces recession, more accurately reproducing the observed pattern of mass loss for debris-covered glaciers.

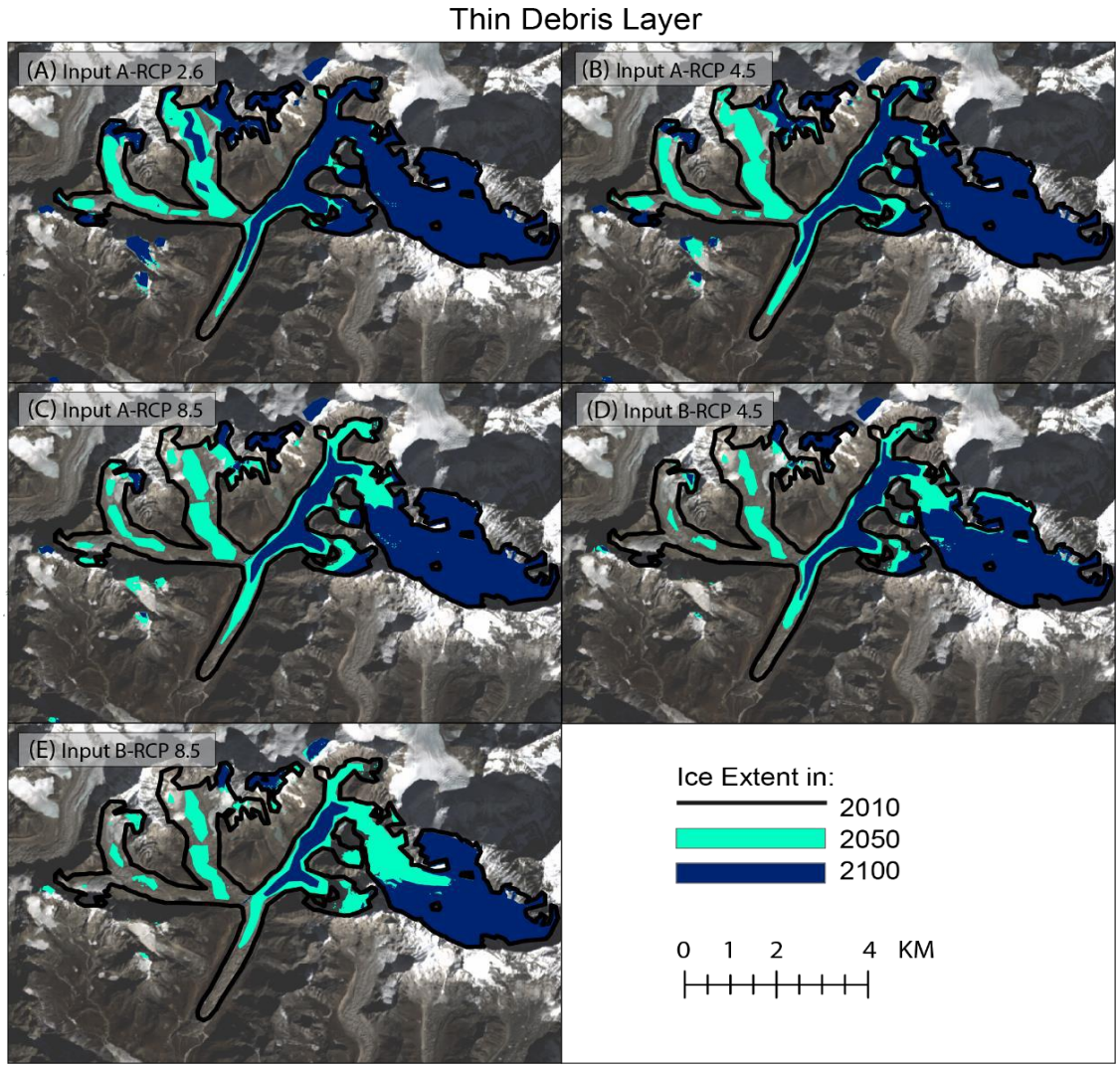

Figure 7.6: Simulated area changes of Khumbu Glacier throughout the 21st century under different climate inputs, using the thin debris layer.

The different climate inputs show considerably differing spatial patterns of volume loss. Climate input A-2.6 shows frontal recession of around 1 km by 2080, compared to 2 km for A-8.5. Climate input B-8.5, which simulates the largest volume loss (Figure 7.1) shows frontal recession of over 3 km by 2080. Considering the significant volume loss in all simulations, spatial ice loss is less substantial than in the Alps, reflecting the observations of thinning dominating over recession on many Himalayan glaciers (e.g. Bolch et al., 2008), suggesting that the changes to the Δh-parameterisation are effective. The performance of the Δh–parameterisation will be discussed in Section 7.3.3.7. Interestingly, Changri Nup and Shar show more considerable recession than the main branch of Khumbu Glacier due to the lower-elevation, smaller accumulation areas

which are unable to replenish lost ice mass. In the case of Khumbu, the large, high-elevation accumulation area is able to redistribute mass to lower elevation parts of the glacier. However, in simulations A-8.5, B-4.5 and B-8.5, the accumulation area and ablation area become disconnected around the ice-fall, preventing the redistribution of mass to lower parts of the glacier.

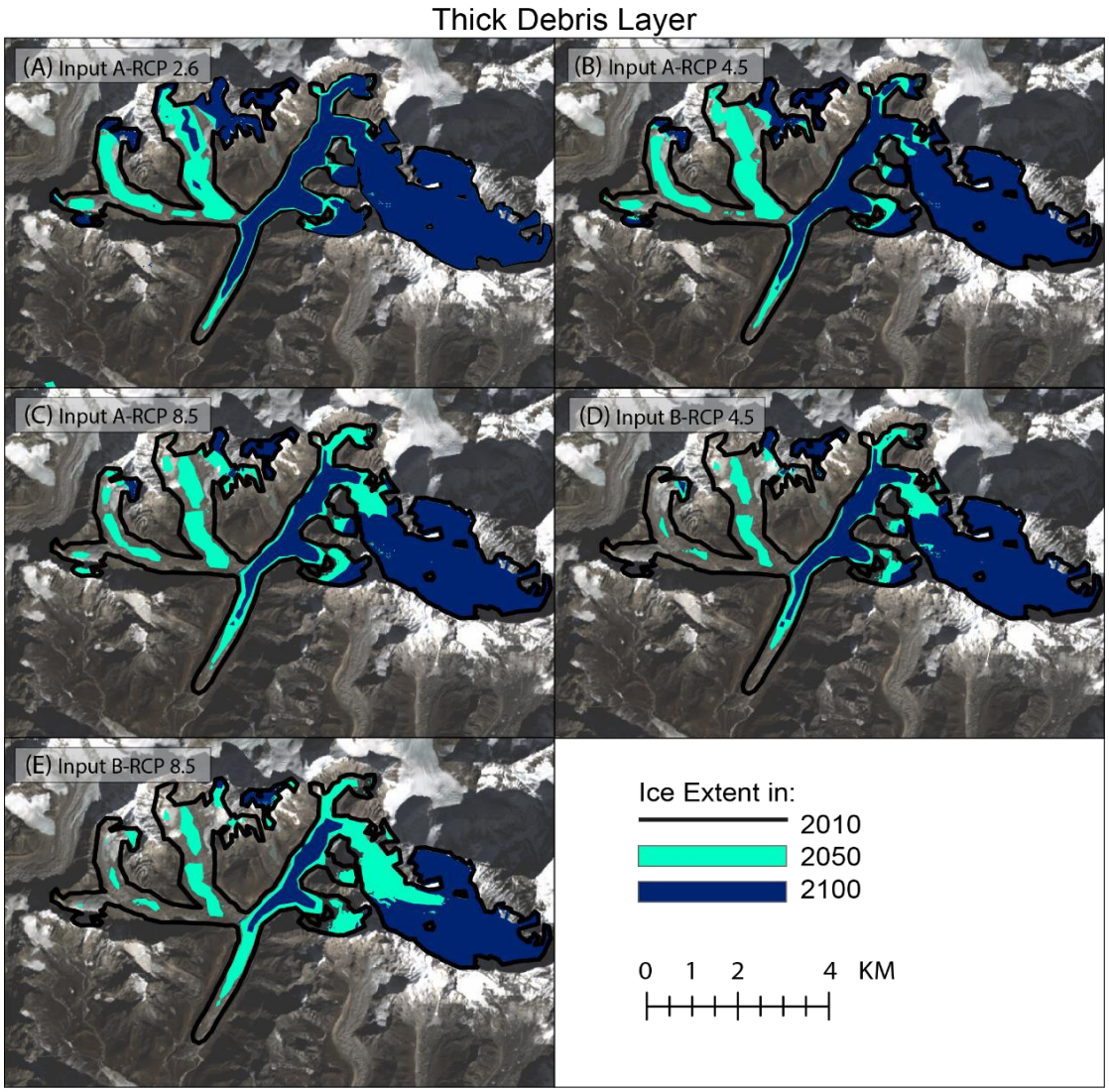

Figure 7.7: Simulated area changes of Khumbu Glacier throughout the 21st century under different climate inputs, using the thick debris layer.

7.3 Discussion.

This chapter has applied the modified version of GERM (Chapter 6) to project future changes at Khumbu. Two key aspects of the results are discussed. First, the future evolution of glacier volume and catchment discharge under the range of climate model outputs will be discussed in relation to the projections of previous studies. Second, the modifications made to GERM

(Chapter 6) will be discussed, and modifications that should be implemented in future studies are suggested.

7.3.1 The Future Evolution of the Khumbu Catchment.

The results of the simulations in this Chapter project significant ice volume loss throughout the 21st century for all climate inputs, but there are considerable differences between simulations. However, what is clear from previous studies and from the results presented in this thesis, is that glacier volume will substantially decrease and discharge in 2100 is projected to be lower than present discharge.

In 2100, projected ice volume ranges from 2 % of 2010 volume (climate input B-8.5, thin debris) to 41 % of 2010 volume (climate input A-2.6, thick debris), broadly agreeing with other studies. For example, the study of Shea et al. (2015) implemented a dynamical-flow model coupled to a mass balance model, driven by climate end-members from CMIP5 RCP 4.5 and RCP 8.5 simulations, to the Everest region. Specifically, rather than using downscaled CMIP5 simulations, Shea et al. (2015) calculated the trends from select CMIP5 simulations, for example, those that produce wet/cool conditions and warm/dry conditions, to represent the maximum range of uncertainty associated with future climate simulations. Shea et al. (2015) estimated that between 4-27 % of current ice volume will remain in 2100 when modelling all glaciers in the Everest region, comparable to the projections of this study (2.6 – 40 % of 2010 ice volume).

Another study, Immerzeel et al. (2012), simulated a continued reduction of ice volume for the Langtang Glacier, when applying a combined mass balance-ice flow model. Four CMIP4 GCM outputs were statistically downscaled using a similar quantile-mapping technique to this thesis; however, dynamical downscaling was not employed which has been shown to reduce the effectiveness of downscaling (e.g. Guyennon et al., 2013) when compared to the dynamical-statistical method used in this thesis. The studies of Immerzeel et al. (2012) and Immerzeel et al. (2013) found an increase in both temperature and precipitation over the 21st century, which resulted in increasing discharge trends. In terms of glacier volume change, Immerzeel et al. (2012) finds that remaining glacier volume is around 12 % of volume in 2000. A second study by Immerzeel et al. (2013) found that remaining ice volume in the Langtang catchment is 40 % of 2010 volume, demonstrating a lack of consensus regarding the precise glacier evolution within the literature.

Finally, Soncini et al. (2016) projected the future evolution of the Khumbu catchment as described in Section 7.1. They estimated an initial ice volume of over 6 km^3, compared to 3 km^3 in this thesis, limiting direct comparison. However, simulated ice volume loss as a percentage of

initial volume is broadly comparable to this thesis, with projected remaining volume in 2100 of between 32 and 56 %, compared to a mean of 22 % in this thesis. In terms of discharge, both studies agree that there is a long-term negative trend following an initial increase for most projection.

The spatial pattern of mass loss (Figure 7.5) shows that volume is lost through a combination of terminus recession and thinning, with areas of ice beneath the ice fall strongly affected whereas high-elevation ice remains largely unaffected (see Figure 6.4 for hypsometry). This high-elevation accumulation zone represents a considerable uncertainty in terms of the modelled ice thickness, since no observations of ice thickness are available and geodetic surveys are known to be uncertain in areas of considerable snow accumulation due to the lack of contrast (Nuimura et al., 2012; Bolch et al., 2011). As such, the ice volume in this accumulation zone may be considerably smaller or larger than simulated in this thesis. Additionally, the loss of much low elevation ice is perhaps more than would be expected considering that other studies, for example, the simulations of Rowan et al. (2015), projected a thin layer of ice in this region even in 2200. However, GERM is not capable of producing 'dead ice' which is likely to remain beneath thick debris (Benn et al., 2012; Humlum 1998). Not including dead ice in GERM could partially explain the higher rate of ice loss in this thesis when compared to Rowan et al. (2015). Moreover, the considerably different climate forcings employed in their study, through simple ELA adjustment, prevents direct comparison between the studies. However, in terms of the pattern of ice loss, the detachment of the debris-covered tongue from the accumulation zone as the active ice area retreats up-glacier, is simulated in both studies

7.3.2 Sources of Uncertainty in Future Projections.

7.3.2.1 Climatic Uncertainty.

The various components making up climatic uncertainty are shown in Figure 7.8. The limited global and regional climate model simulations available at the time of analysis prevent simulations from a large number of GCMs and RCMs to be used. Therefore, the range of climate model inputs only provides an indication of the uncertainty (Figure 7.9) associated with different climate inputs, using two GCMs which force two different RCMs, hence no systematic analysis of GCM or RCM uncertainty can be undertaken. To improve on this assessment of climate model uncertainty, it is recommended that future studies employ a larger range of climate model outputs, which requires additional climate modelling centres to release projections for CORDEX-South Asia. Finally, the uncertainty associated with the statistical downscaling process is not assessed here as it is outside the scope of this thesis, so it is encouraged that future studies include this by using several different downscaling methods.

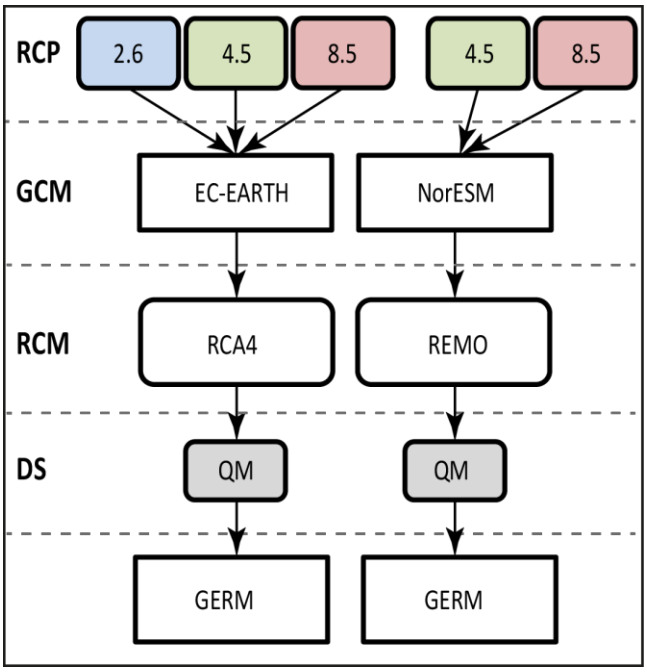

Figure 7.8: Sources of uncertainty at Khumbu due to the climatic inputs. Downscaling uncertainty and Germ uncertainty are not considered in this chapter.

Aside from the climate model outputs, it should be emphasised that the level of understanding of meteorology, particularly precipitation, in high-elevation Himalayan catchments is extremely limited which will impact upon the accuracy of future projections.

7.3.2.2 GERM Uncertainty and Limitations.

Extensive validation of GERM against long-term observations of glacier and runoff changes is not possible at Khumbu Glacier due to the lack of long-term observational data, preventing assessment of glacier modelling uncertainty.

7.3.2.2.1 Debris Thickness Uncertainty.

The only aspect of the uncertainty associated with GERM that is assessed here relates to the thickness of the debris layer and its impact on runoff. Both the debris layers applied in GERM are non-uniform in thickness, with the 'thin' layer representing a conservative estimate of average debris thickness, and the 'thick' layer representing a maximum estimation of average debris thickness. The results show that using the thick debris layer produced higher annual runoff than the thin debris layer. Since the true thickness of the debris layer is likely to be between these two layers, the differing runoff projections capture some of this uncertainty.

Considering GERM is only calibrated to geodetic mass balance, the performance of simulated discharge compared to observed discharge during the short period of observations is encouraging (Section 6.3.2; Figure 6.1.1), but the future simulations remain highly uncertain.

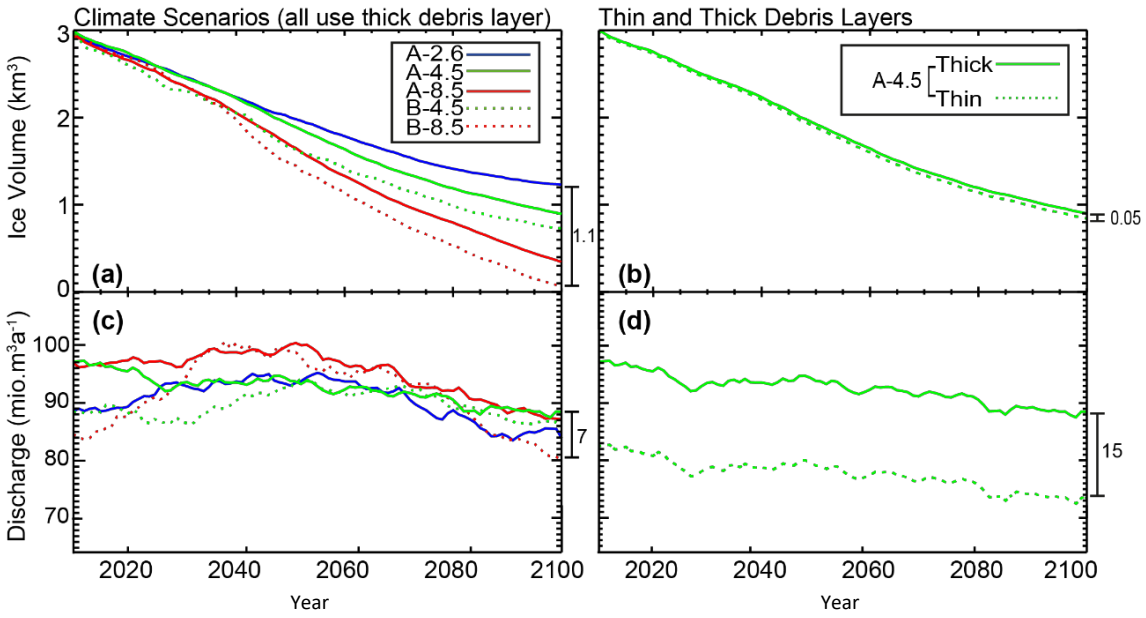

Figure 7.9: Comparison of the range of volume and discharge simulations under different climate inputs ([a] and [c]) and different debris layers ([b] and [d]). (a) and (c) simulations all use the thick debris layer to isolate the variability introduced by the climate models and scenarios. Simulations (b) and (d) both use the A-4.5 climate input to isolate the variability introduced by the differing debris layer. All discharge simulations shown as 10-year moving averages.

7.3.2.2.2 Calibration Uncertainty.

A further source of uncertainty is the calibration of the model to geodetic mass balance. In this thesis the results of Gardelle et al. (2013; see Section 6.3.1 for details) are used, who estimate a geodetic mass balance of -0.51 ±0.19 m w.e. yr^{-1}. Other geodetic studies estimate a large range of values, exemplified in Figure 7.10 which shows the variability of geodetic surveys at Khumbu and the uncertainty ranges of each. Such uncertainties stem from limitations in stereographically deriving DEMs in steep terrain and the lack of contrast in high-elevation accumulation areas (Nuimura et al., 2012; Bolch et al., 2011). As a result, longer-term geodetic mass balance surveys (e.g. Bolch et al., 2011) cannot be used for validation due to the lack of agreement between surveys and the consistent overlap with the calibration period. However, the widespread trend in the Himalaya and the broad agreement between geodetic surveys suggests that recent trends are representative of the long-term glacier response to climate.

7.3.2.2.3 Other Sources of Uncertainty.

Other sources of uncertainty are the stationarity of glacier model melt parameters and the lack of multiple calibration datasets. Firstly, the parameters of the model are assumed to be constant

throughout the simulation period, as is the case at Griesgletscher and Rhonegletscher, and indeed in all glacier-runoff modelling simulating future changes. This will be discussed further in the general discussion chapter (8). Secondly, a secondary calibration dataset in addition to geodetic balance, for example, point mass balance, would ensure that both the accumulation and ablation modules of GERM were correctly calibrated. In this thesis, discharge could have been used for calibration, but the short term dataset (2 years) may not have been representative of long-term catchment behaviour. Using discharge would also have diminished the portability of the model since discharge is scarcely available for Himalayan catchments.

Finally, the glacier mask, delineated by the RGI (Pfeffer et al., 2014), contributes potential uncertainties due to the difficulties discerning between snow, ice, debris-covered ice and rock (Gardner et al., 2013). For example, the study of Vincent et al. (2016) calculated ice flow on Changri Nup Glacier using differential GPS (Global Positioning System) measurements, finding the active ice extent to be substantially smaller than the RGI. However, the RGI inventory was used to ensure the model could be applied to other catchments with minimal data inputs and ensure a standardised method is used at all catchments. Therefore, it is encouraged that glacier masks provided by the RGI are checked for errors at each catchment.

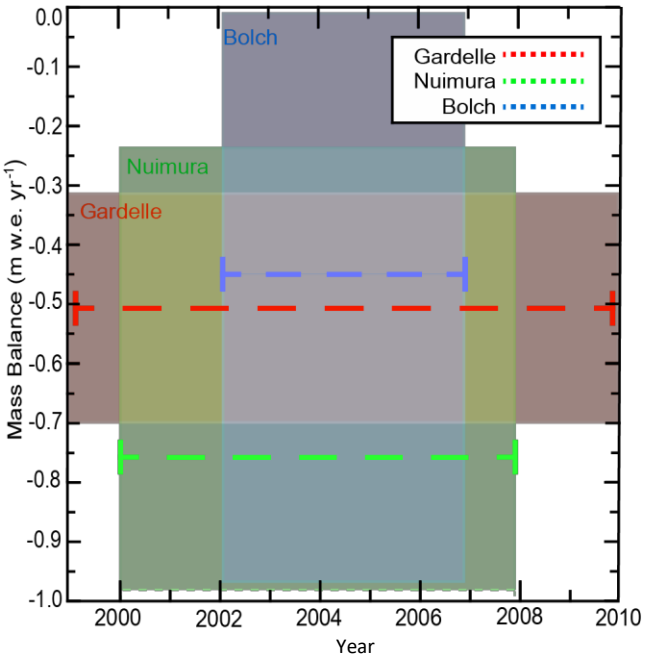

Figure 7.10: Geodetic mass balance surveys at Khumbu Glacier, showing the variability and considerable uncertainties associated with each survey.

7.3.3 Discussion of the Modifications Made to GERM.

The two key modifications made to GERM, the revised Δh parameterisation and the reduction of melt beneath debris of varying thickness, will be discussed here, before discussing additional potential modifications that are recommended for future research.

7.3.3.1 The Δh Parameterisation of Mass Redistribution.

One of the key modifications made to GERM for the Khumbu Glacier was the formation of the Khumbu-specific Δh mass redistribution curve, based on the geodetic survey of Nuimura et al. (2012), as described in Section 6.2.2.3.

Here, a simulation is performed with the original un-modified 'large' Δh curve designed in Huss et al. (2010a) for typical, large glaciers without debris cover, assuming mass loss is manifested in frontal recession rather than downwasting. This experiment allows investigation of how applicable the 'typical' retreat curves of Huss et al. (2010a) are to debris-covered glaciers, and allows the impact of the Khumbu-specific curve to be quantified. Figure 7.11 shows the result of this experiment, clearly displaying increased terminus recession more typical of clean-ice glaciers, compared to the Khumbu-specific curve, which reduces terminus recession but incorporates mass loss through downwasting. By incorporating the unique pattern of mass loss at debris-covered glacier, GERM now reproduces spatial patterns of mass loss more realistically.

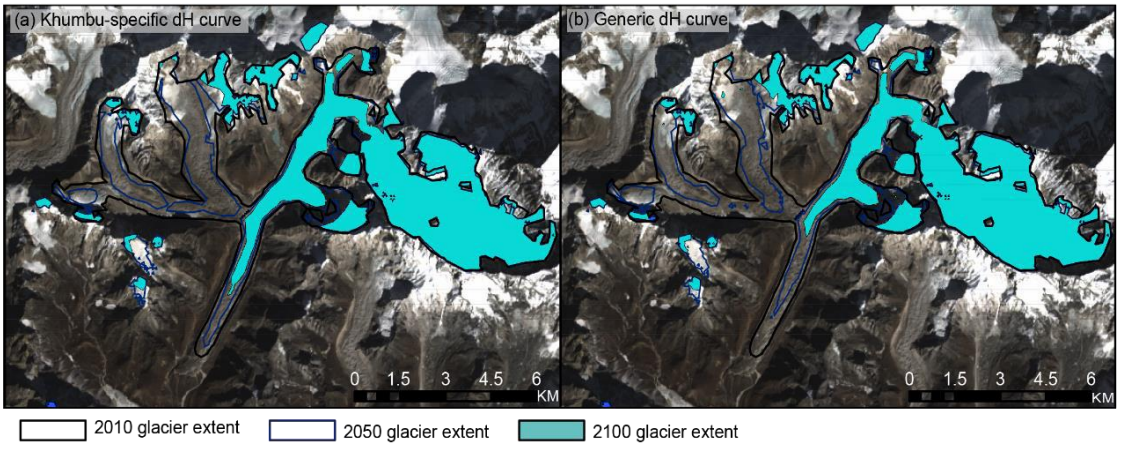

Figure 7.11: Comparison between (a) spatial pattern of glacier retreat using Khumbu-specific Δh curve; and (b) using generic curve not designed for downwasting, debris-covered glaciers.

7.3.3.2 Melt Rates Beneath Debris Cover.

A second key modification made to GERM was the reduction of melt beneath debris of non-uniform thickness, as described in Section 6.2.2.3.

This thesis used a simple approach to calculating the melt rates beneath debris cover, whereby melt exponentially decreases as debris depth decreases, such that melt at 50 cm depth is 50 % of surface melt, and melt beneath 100 cm of debris is negligible. The extent to which melt rates were reduced beneath debris was calculated using an exponential curve that has been used in several modelling studies (e.g. Hagg et al., 2008; Konrad and Humphrey, 2000; Rowan et al., 2015). This curve is based on observations of melt rates beneath debris at several glaciers (Nicholson & Benn, 2006), which are similar to those at Ngozumpa Glacier (Nicholson & Benn, 2013) and Khumbu Glacier (A. Rowan, personal communication. 2016). An important and novel feature of this curve is that it can be applied without additional in-situ data. This chapter will not discuss the methodological advances relating to this debris-reduction curve. However, the following chapter (Section 8.1.3) will provide a comprehensive discussion. Additionally, the uncertainties and methods used to estimate the thickness of debris cover are also discussed in Section 8.1.3.

7.3.3.3 Recommended Modifications for Future Research.

The modifications in the previous section allow GERM to incorporate two of key features of debris-covered glaciers in downwasting and reduced melt beneath debris. However, additional factors that are likely to have a lesser but still significant influence on glacier and runoff projections are debris expansion and thickening, and ice-cliffs. These are discussed here and it is recommended that future research should aim to develop glacio-hydrological models to incorporate these elements.

7.3.3.3.1 Debris Expansion and Thickening.

Methods to implement spatially expanding debris exist, for example, Jouvet et al. (2011). However, at Khumbu Glacier, the current extent of the debris coverage is unlikely to extend significantly in the future since the current ELA is mid-way up the Khumbu ice fall at around 5600 m (Bolch et al., 2011; Benn & Lehmkuhl, 2000). The Khumbu ice fall extends to an elevation of over 6000 m, above which ablation is very limited by the cold temperatures, even in 2100, and accumulation of solid precipitation occurs all year round. These factors mean that debris cover is unlikely to expand to higher elevations and is confirmed by Rowan et al. (2015), who use a dynamic model of glacier and debris and find very little debris above the ice-fall, even in 2200. However, this setting is unique to Khumbu Glacier, so debris-expansion should be considered when applying models to other catchments.

The debris layer is expected to thicken if the glacier continues to downwaste and stagnate; downwasting promotes melt-out of englacial debris and stagnation prevents advection of debris

to the glacier margin (Hambrey et al., 2009). Thicker debris would be expected to increase the insulation of the buried ice due to reduced heat-conduction from the debris surface to the ice. Therefore, the impact of debris thickening at Khumbu Glacier is tested by implementing a debris-thickening scheme where debris is assumed to thicken at a constant rate until 2100. Specifically, the melt reduction factor under debris is continually decreased at a rate that produces a thickening of 50 cm by 2100, based on thickening estimates in Rowan et al. (2015). This debris thickening scheme is applied to the thin debris model configuration because this thin debris is more likely to be influenced by thickening and climate input A-4.5 was used to force GERM.

In this experiment, the simulated volume loss displayed only a 1 % change when debris thickening was implemented. This suggests that the 90-year time-scale of the simulation is insufficient to cause sufficient thickening to have a large impact on melt rates and that debris thickening is more influential over very long simulations or if the initial debris is very thin.

7.3.3.3.2 Incorporating Ice Cliffs into GERM.

Ice-cliffs are known to exhibit significantly more melt than debris-covered ice (Sakai et al., 2002; Reid & Brock, 2014; Sakai et al., 2000), thus it is possible that they partially mitigate the insulating influence of the debris cover (Rowan et al., 2015). However, the understanding of how ice-cliffs form and evolve is largely unknown and certainly not comprehended sufficiently to be incorporated into models on the catchment scale. Therefore, this thesis tests the incorporation of ice-cliffs into GERM in a simple approach that should be further developed in future research.

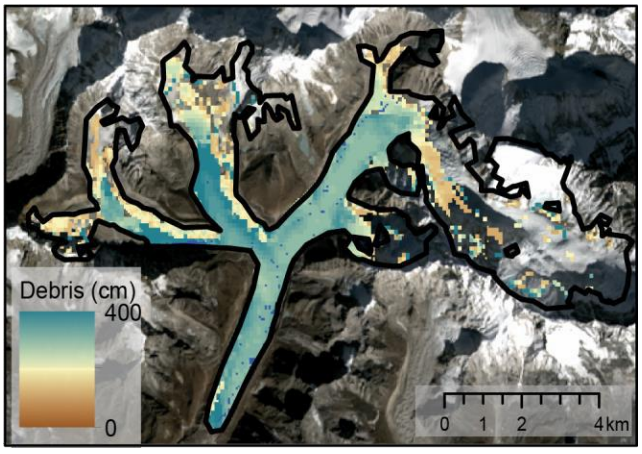

Figure 7.12: The thick debris layer, modified using ice cliff locations from Watson et al. (2016).

The first step of this experiment is to locate ice-cliff features. This thesis uses ice-pond features as a proxy for ice-cliffs since melt-ponds are much easier to map using remote-sensing imagery and have been shown to correspond closely to ice cliffs (Ragettli et al., 2015; Zhang et al., 2011). The problem with mapping of ice-cliff features directly is two-fold. Firstly, a very high-resolution

DEM is required and secondly, most raster DEMs do not adequately represent steep slopes well which prevents the area of the ice cliff being measured (Watson, personal communication). In this thesis, mapping of melt-ponds utilises the study of Watson et al. (2016), who use high-resolution (0.5-2 m) satellite imagery to map changes to supraglacial ponds. Here, the locations of melt-ponds are used to modify the thick debris layer from Rowan et al. (2015), with the melt-pond areas assigned a thickness of zero, dictating that their melt rates are the same as clean ice (Figure 7.12).

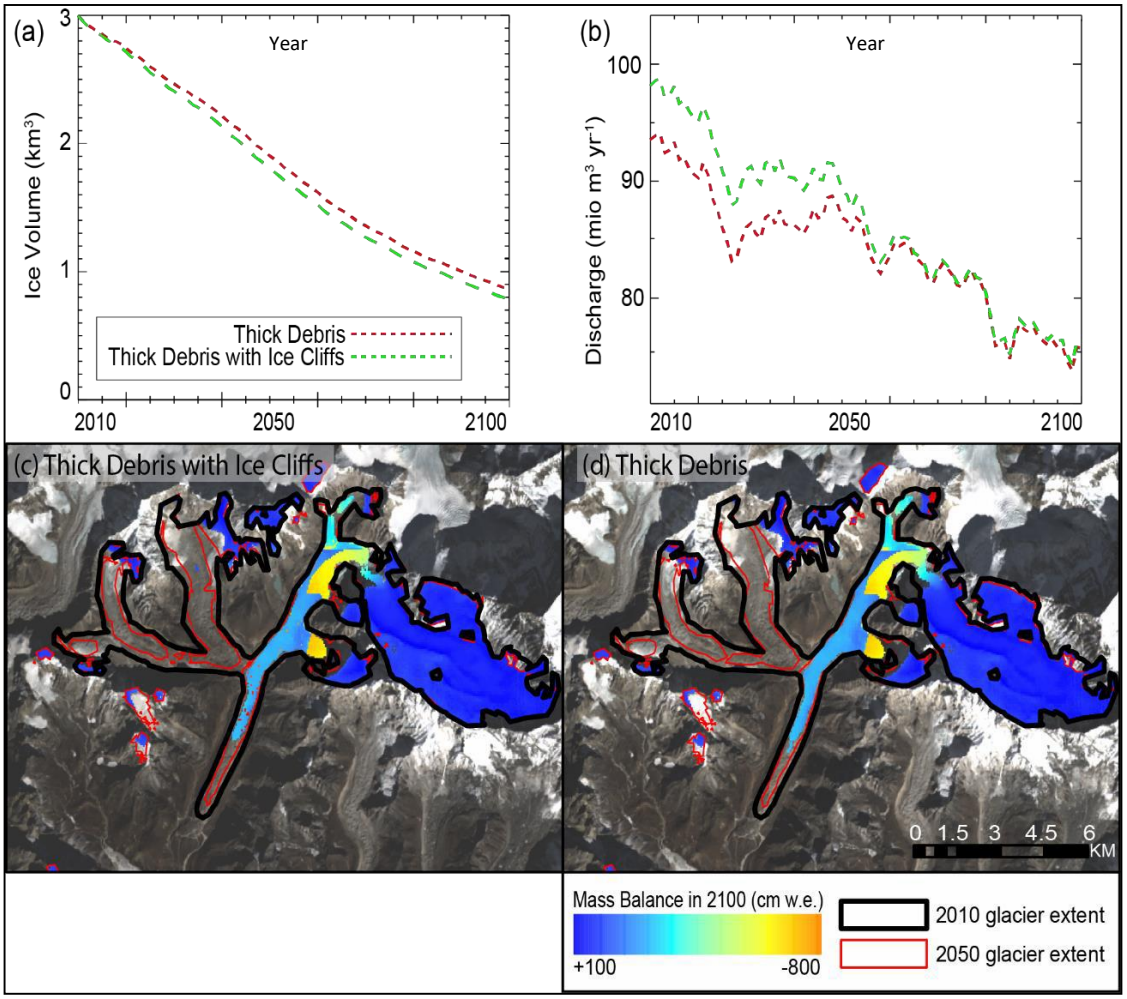

Figure 7.13: (a) and (b) show the future evolution of ice volume and discharge comparing the thick debris layer with the ice cliff layer. (c) and (d) show the differing spatial patterns of mass loss. Both these simulations are driven by the same RCA4-ICHEC-EC-EARTH model with the RCP 4.5 scenario.

Figure 7.13 shows the impact of ice cliffs on ice melt in GERM, with ice cliffs promoting volume losses and increasing annual discharge. The spatial plots also demonstrate that there is increased terminus recession in the simulation that includes ice cliffs. At present, however, the understanding of ice-cliff processes and their future evolution is limited, despite being a very active research area (e.g. Miles et al., 2016; Sakai et al., 2000; Steiner et al., 2015). In particular,

future changes in ice cliff number, distribution and size will alter melt suppression of debris on the glacier scale, but are poorly understood and largely ignored in modelling studies (e.g. Shea et al., 2015; Immerzeel et al., 2013; Soncini et al., 2016). The experiment described above demonstrates how ice cliffs could be included in glacio-hydrological models. Thus, a priority for future research of debris-covered glaciers should focus on the evolution of ice cliffs, perhaps utilising remote sensing imagery to analyse historic changes in ice cliff evolution in order to represent these important features in future modelling studies.

7.4 Conclusions.

The modifications to GERM made in Chapter 6 have been applied to simulate future glacier volume and runoff change, forced by a range of climate projections, for the first time at the Khumbu catchment. By modifying GERM to include spatially distributed debris thickness and ice stagnation, the model has a more physical basis for the processes at Khumbu Glacier, yet retains the portable nature requiring only remote-sensing based estimates of debris thickness.

Although additional Himalayan catchments have not been modelled in this thesis, GERM requires only geodetic mass balance and an estimate of debris thickness to incorporate debris cover, therefore applying GERM to additional catchments is suggested for future work.

Future Projections. The range of the most recently available CMIP5 GCM outputs, bias-corrected using RCM simulations (from CORDEX-South Asia) and statistically downscaled here using quantile mapping, are used to drive GERM, projecting ice volume in 2100 of between 2-42 % of 2010 ice volume. Much of the lower elevation ice is lost in all simulations, whereas high-elevation ice remains mostly unchanged. Annual discharge simulations show an overall decreasing trend for all but one of the simulations, with an average reduction of 14 % following a peak in discharge around the middle of the century. According to these results, the future water resources downstream of the Khumbu catchment will decrease considerably by 2100, with a greater proportion of future water originating from wet precipitation and snow melt. However, these projections have considerable uncertainty that cannot be entirely constrained due to the lack of long-term glaciological data on which to validate GERM.

GERM Modifications. Due to the lack of knowledge on debris thickness, GERM was configured and ran separately using two independent debris, in an attempt to assess the impact of debris thickness on runoff simulation, with results showing a considerable difference, despite identical glacier volume change. An interesting outcome was that discharge is produced more accurately when thick debris cover is included, suggesting that applying models without any consideration for the influence of debris, cannot accurately simulate runoff at the Khumbu catchment. The

alterations made to the Δh parameterisation resulted in a much more realistic pattern of mass loss, with the characteristic downwasting widely observed at debris-covered glaciers reproduce by GERM. Additionally, the influence of ice-cliffs was investigated, showing that they do not override the insulating influence of debris.

8. RESEARCH DISCUSSION AND IMPLICATIONS.

This chapter discusses the key findings of this thesis in terms of how they relate to the stated aims (Section 1.5) and the wider field of runoff projection from glacierised catchments. Because individual chapters have contained detailed discussion of specific findings at each site, this discussion will focus on bringing the findings from all three catchments together and discussing the wider implications of this work. Methodological advances are summarised and discussed in relation to alternative methods in the literature in Section 8.1. Section 8.2 and 8.3 will then discuss the results of these methodological advances and compare the results to other key studies. Finally, Section 8.4 will discuss the wider implications of this thesis, before making suggestions for the direction of future research (Section 8.5).

8.1 Review and Discussion of Methodology.

In this thesis, the Glacier Evolution and Runoff Model was applied to Griesgletscher and Rhonegletscher in the European Alps, and Khumbu Glacier in the Himalaya, in order to project future glacier and runoff change. GERM was applied over long time-scales in both past "validation" runs and future "projection" runs, and a number of methodological advances were implemented. The key advances have been the introduction of:

- a novel bias-correction methodology, which improves upon what has typically been applied in the glacier literature, discussed in Chapter 3 [Aim 2A and 2B];
- a rigorous assessment of the projection uncertainties relating to both GERM and climate models and climate scenarios, discussed in Chapters 4 and 5 [Aim 1 and 2C];
- modifications to GERM to make it applicable to debris-covered glaciers (notably, adjustment of the melt rate beneath debris of spatially variable depths, and adjustment of mass redistribution to simulate downwasting), discussed in Chapters 6 and 7 [Aim 3].

The following section will discuss the methodological advances made in regard to bias correction, assessment of uncertainty, and incorporation of debris cover in GERM.

8.1.1 Bias Correction of Climate Model Data.

An important improvement upon previous applications of GERM (and similar glacio-hydrological models) has been the improved downscaling of climate model data used to drive future projections using GERM. This is important because inadequate downscaling can lead to large uncertainties in the climate input data, which have been minimised in this thesis. This study has

also explored a range of different climate model combinations (GCMs/RCMs) and scenarios (RCPs) that will impact future projections.

The novel method applied can be summarised as the combination of dynamical downscaling, through the use of CORDEX RCMs, and statistical downscaling, through the use of quantile-mapping correction. This represents the current state-of-the-art in dynamical-statistical downscaling (Guyennon et al., 2013) and was applied to the most recent available GCMs, from CMIP5. To the best of the author's knowledge, only one previous study (Li et al., 2016) has utilised CORDEX RCMs for application to glacio-hydrological studies, but their study did not include statistical downscaling.

This thesis has clearly shown the limitations of GCMs and RCMs in the comparison of observed temperature and precipitation to uncorrected climate model outputs in Section 3.2 (Figures 3.1 & 3.2). In particular, the performance of precipitation simulation in RCMs at Khumbu was poor. As detailed in Section 3.1, previous glacio-hydrological studies have typically applied the delta-change downscaling approach (e.g. Akhtar et al., 2008; Chen et al., 2011; Farinotti et al., 2012; Gabbi et al., 2012; Jouvet et al., 2011; Sorg et al., 2014) which can lead to errors in the simulated time-series: for example, previous studies have produced overestimation of high-intensity rainfall events and overestimation of drizzle, which are not corrected using the delta-change approach (Guyennon et al., 2013), but are corrected using the quantile mapping approach in this thesis.

The temperature and precipitation projections after bias correction are fully described in Chapter 3. To briefly summarise, the results show increases in temperature at all sites from 2010-2100, whereas precipitation projections generally show no consistent trend and there are inconsistencies between different GCM-RCM combinations.

8.1.1.1 Precipitation Projections.

The lack of consistency among precipitation projections in comparison to temperature projections warrants further discussion. At Khumbu, in particular, the strongest warming trends appear to correspond with significantly negative precipitation trends in climate model combination A (see Section 3.4.5, Figure 3.12). On a global scale, the expected pattern of precipitation changes are that warmer temperatures will result in increases in precipitation due to acceleration of the hydrological cycle and the greater moisture-holding capacity of warm air (Trenberth & Josey 2007; IPCC, 2014). However, the lack of consistent precipitation projections in this thesis is typical of future projections found in other studies of mountain regions. For example, Pellicciotti et al. (2014) found no clear pattern in projected changes in precipitation for four glaciers in the Swiss Alps, when using the RegCM3 RCM forced by the ECHAM5 GCM.

Additionally, Rajczak et al. (2013) found that precipitation changes simulated by ENSEMBLES RCMs are highly variable in terms of their spatial patterns but also in terms of seasonality, with reduced summer precipitation countered by enhanced autumn precipitation. Similarly in the Himalaya, Immerzeel et al. (2013) found a large spread of precipitation projections among CMIP5 GCMs using RCPs 4.5 and 8.5, when modelling future glacier change in two Himalayan catchments. The aforementioned study of Li et al. (2016) found similar precipitation changes to the results of this thesis, again simulating a lack of consensus among the two GCM-RCM combinations. The lack of positive precipitation trends in the projections suggests that acceleration of the hydrological cycle at higher temperatures is not anticipated in mountain catchments in the climate models employed in this thesis, demonstrating that precipitation changes are more complex than temperature changes (Isotta et al., 2014) and that climate models are better able to reproduce temperature than precipitation (Chaturvedi et al., 2012). This will be further demonstrated with discussion of Indian Monsoon representation in the following section.

Several studies have assessed the skill of climate models to reproduce the Indian Monsoon, showing model ability is limited (Turner & Annamalai, 2012), despite improvements (Sperber et al., 2013), due to the highly complex interactions between the ocean and atmosphere. Figure 8.1 demonstrates the difficulty models have when simulating changes in the strength of the monsoon, showing considerable variability between models in the past and a lack of consensus in the future. Moreover, the recent negative precipitation trend in Figure 8.1 is somewhat counterintuitive considering the observed increase in the Indo-Pacific ocean temperatures (Knutson et al., 2006) and the increasing land-sea temperature contrast experienced with rising temperatures (Sutton et al., 2007), both of which potentially provide increased energy for monsoon intensification (Turner & Annamalai, 2012). The study of Ghimire et al. (2015) assessed the monsoon representation of CORDEX-South Asia RCMs, by comparing modelled precipitation to observations. Their study showed a wide range of precipitation estimates depending upon both the driving GCM and RCM, with a dry-bias over low-elevations and a wet-bias over high-elevations, corroborating the findings of this chapter. Encouragingly, Ghimire et al. (2015) show that the ICHEC-EC-EARTH RCA4 model combination, used in this thesis at Khumbu (model A), best reproduces the monsoon precipitation. The other GCM-RCM combination used in this thesis, NorESM-REMO was not included in their analysis. To summarise, the limited ability of climate models to simulate monsoon behaviour in the past indicates that there may be considerable uncertainties in estimates of the future evolution of the monsoon.

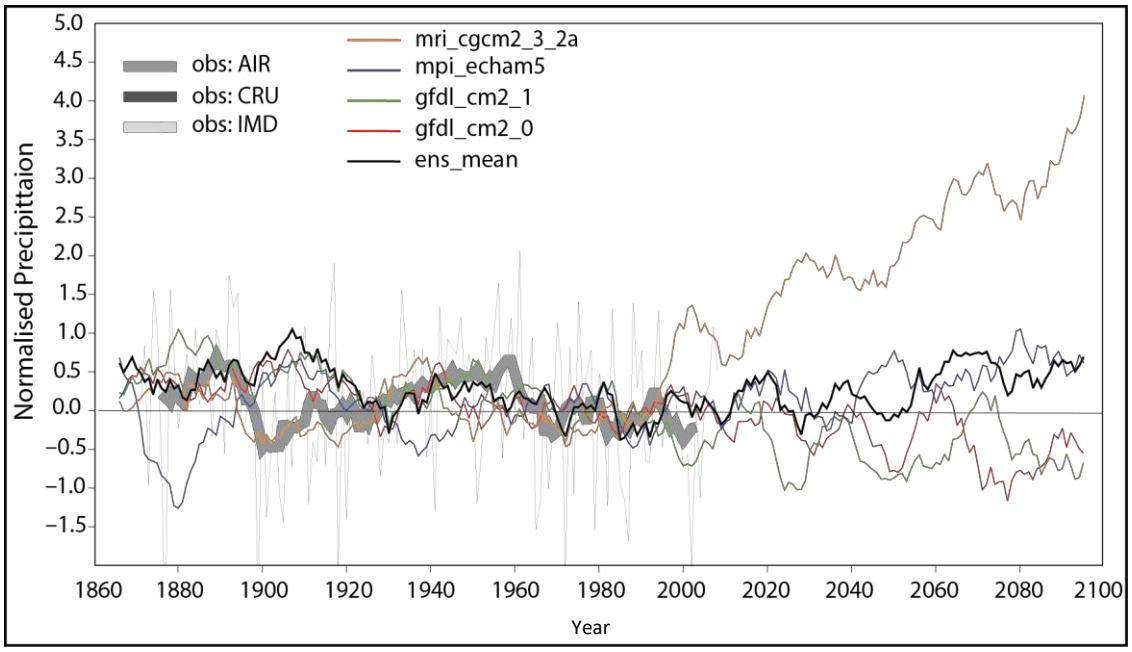

Figure 8.1: Representation of the Indian Monsoon precipitation (June to September) in the past and future by 5 CMIP3 models under the A1B scenario, compared to observations. Figure from Turner and Annamalai (2012).

8.1.1.2 Temperature Projections.

The magnitude of warming in the Alps is projected to be greater than at Khumbu. Specifically, at Griesgletscher, the projected change in average annual temperature ranges from +0.45°C (A-2.6) to +6.3°C (C-8.5) between 2010-2100. However, at Khumbu, although warming trends are significant, the projected change in average annual temperature ranges from 0.25°C (A-2.6) to 3.25°C (B-8.5) over the period 2010-2100. This lower magnitude and rate of change at Khumbu suggests that warming under the RCP 8.5 represents a continuation of recent warming, found to be 0.037°C yr^{-1} (3.3°C when extrapolated over 90 year period) by Salerno et al. (2015). A recent study by Li et al. (2016) applied a similar distribution-based downscaling technique to CORDEX-South Asia climate models, RCA4-EC-EARTH and REMO-MPI-ESM, at two sites in the Himalaya: Chamkhar Chhu and Beas in Central Bhutan and Northern India, respectively. Their study found similar temperature projections to this thesis but a moderately larger magnitude of change (e.g. Li et al., 2016: annual average temperature: RCP 8.5=0.05°C yr^{-1}, compared to 0.036°C yr^{-1} in this thesis). A possible limitation of the methodology applied at Khumbu regarding temperature lies in the source of the observations on which the quantile mapping method is constrained. Specifically, the Pyramid meteorological station is situated upon debris, which may not be representative of the temperature above clean glacier ice due to the cooling influence of the ice on the air immediately above the surface (e.g. Gabbi et al., 2014; Ragettli et al., 2013). This means that projected temperature may be too warm. However, due to the very limited

knowledge of the meteorology in the glacier boundary layer (Pellicciotti et al., 2014), particularly when the ice has spatially variable debris cover, it would be difficult to derive a correction that would be physically correct without extensive fieldwork, hence this thesis does not account for this issue at Khumbu, and the issue is not relevant to the Alps due to the use of a gridded temperature data-set.

An important finding of this thesis was the identification and discussion of an offset between RCM simulations forced by reanalysis data (evaluation) and forced by GCMs (historical). To the best of the author's knowledge, this thesis represents the first impact study to describe this issue and propose an alternative solution. However, a comprehensive discussion of this issue was included in Section 3.5.4 so is not discussed further here.

8.1.1.3 Limitations of Climate Input Data.

Although the bias correction in this thesis was as thorough as possible, there are several shortcomings. Firstly, the lack of available CORDEX simulations at the time of analysis limited the range of GCM-RCM combinations to provide climate inputs for GERM, particularly at Khumbu Glacier. The impact of limited climate models is that this thesis does not account for the full range of uncertainty associated with GCMs and RCMs, although a portion of this uncertainty is accounted for, as discussed in Section 3.5.3. Hence, the future projections presented here for Khumbu must be treated as a subset of potential future glacio-hydrological evolution. Another problem pertinent to Khumbu is the difficulties in measuring precipitation at high-altitudes due to gauge undercatch (e.g. Immerzeel et al., 2015). Although this thesis applied a correction for gauge-undercatch (Yang et al., 1998), something not implemented in a recent study of Khumbu Glacier (e.g. Soncini et al., 2016), the precipitation data used to fit this correction may contain errors. Since the statistical downscaling used the observed precipitation to calibrate the correction, errors in the observational data may therefore be passed onto the corrected future time series. Thus, the climate inputs used to drive GERM at Khumbu are considered to be possible pathways of future changes, rather than accurate projections. In the Alps, although more GCM-RCM combinations would be beneficial, the future projections provide a good assessment of the range of potential future changes. In summary, the bias-correction applied in this thesis improves upon the delta-change approach used in many glacio-hydrological studies and represents the current state-of-the-art in dynamical-statistical downscaling.

8.1.2 Quantifying the Uncertainties in Glacier and Runoff Evolution in Long-Term Simulations.

A novel aspect of this thesis is the thorough assessment of both GERM uncertainty and climate data uncertainty, which have not been as comprehensively assessed in previous glacio-hydrological studies.

There are several different sources of uncertainty in glacio-hydrological modelling, summarised in Figure 8.2, much of which has been assessed in this thesis. However, the uncertainty relating to the downscaling methodology is not considered. This section will discuss how other studies assess uncertainty and the methods used in this thesis. The results of the uncertainty analysis will be discussed in Section 8.2.2.

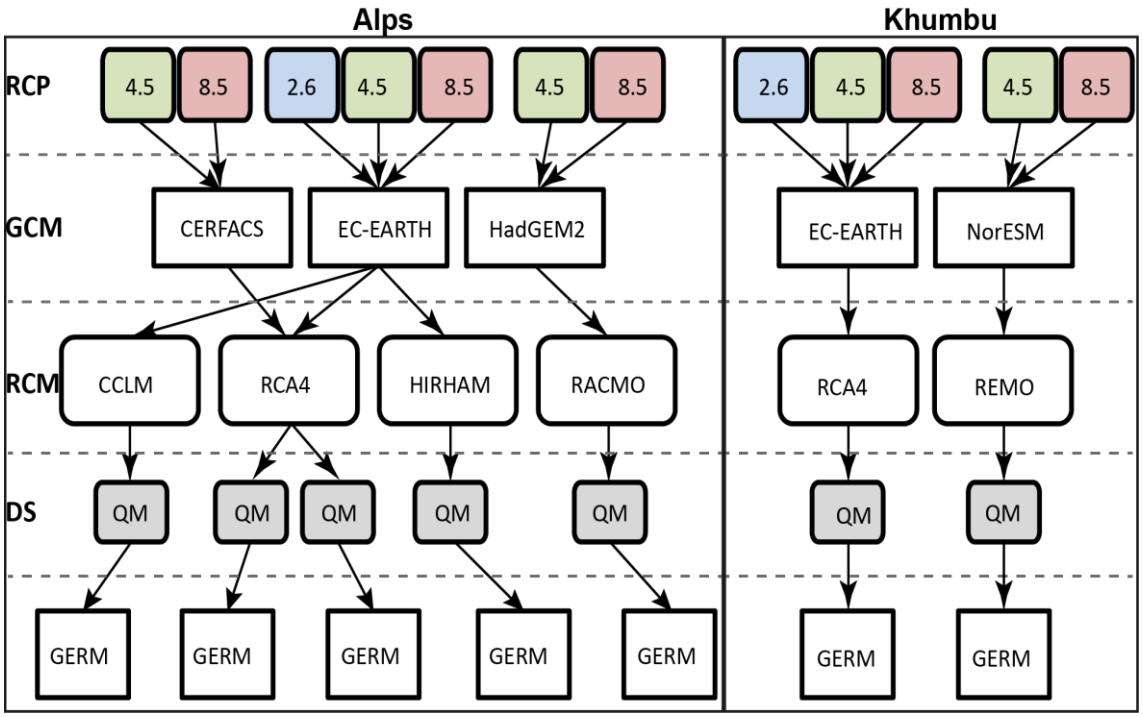

Figure 8.2: Diagram demonstrating the steps, and therefore various sources of uncertainty involved in future glacio-hydrological modelling.

8.1.2.1 Glacio-Hydrological Modelling Uncertainty.

The uncertainty associated with glacio-hydrological modelling has been assessed in this work by means of long-term (120 year) validation runs at GERM at Griesgletscher and Rhonegletscher. The rationale behind such an extensive validation is to comprehensively quantify how well GERM can simulate glacier and runoff changes over long time-scales in catchments with contrasting topographic features. The results of this uncertainty assessment will be discussed in Section 8.2.2.

Other glacio-hydrological modelling studies rarely consider glacier modelling uncertainty on such long-term, multi-decadal timescales. As such, crucial limitations of glacio-hydrological models may not be fully accounted for in uncertainty assessments, limiting the usefulness of future projections in terms of water resources management and adaptation. To date, one of the few studies to assess modelling uncertainty was Huss et al. (2014). However, their study used sensitivity analyses to investigate how sensitive runoff is to specific modelling components, rather than assessing modelling uncertainty as a whole. Similarly, several studies have assessed uncertainties associated with calculating ice or snow ablation (e.g. Hock, 2005; Kobierska et al., 2013; Pellicciotti et al., 2005), but have not assessed this in an integrative way that includes all model components. The typical approach to assessing uncertainties in glacio-hydrological simulations is to only account for the uncertainty introduced by different climate inputs (e.g. GCM, RCM and RCP uncertainty), with no quantification of glacio-hydrological modelling uncertainty (e.g. Farinotti et al., 2012; Lutz et al., 2013; Ragettli et al., 2013; Stahl et al., 2008).

Although this thesis has quantified uncertainty at Griesgletscher and Rhonegletscher, the lack of long-term glaciological or hydrological data at the Khumbu catchment means the uncertainty associated with GERM cannot be assessed. Although applying the uncertainty calculated at Griesgletscher and Rhonegletscher is an option, the different glacier dynamics (e.g. stagnation and downwasting) and impact of debris cover on melt at Khumbu Glacier mean that transferring the uncertainty is not appropriate. This is considered to be a limitation of the Khumbu projections.

8.1.2.2 Emissions Scenario Uncertainty.

The uncertainty associated with different scenarios (RCPs) is well accounted for in the future simulations of the Alps. In climate modelling, scenarios are used to force GCMs, as described in Section 1.3.1, to account for the uncertain choices of humanity in the 21st century. For example, changes in energy and climate policy, technological advances, population changes, and the level of industrial development will have considerable impacts on future climate, which will have an effect on future glacio-hydrological changes (van Vuuren et al., 2011b). In this thesis, future simulations in the Alps are forced by RCPs 2.6 (two GCM-RCM combinations), 4.5 (five GCM-RCM combinations), and 8.5 (five GCM-RCM combinations). However, additional GCM-RCM combinations that include RCP 2.6 would be beneficial. Due to data availability, simulations of future glacio-hydrological evolution at Khumbu are more limited with RCP 2.6 (one GCM-RCM combination), 4.5 (two GCM-RCM combinations) and 8.5 (two GCM-RCM combinations). Thus, the uncertainty pertinent to emissions scenarios at Khumbu is not fully assessed.

Recent studies of future glacio-hydrological changes typically use similar methods to this thesis, in order to assess the influence of emissions scenarios. For example, Immerzeel et al. (2013) used RCP 4.5 and 8.5, and Sorg et al. (2014) used RCPs 2.6 and 8.5. However, several studies only use one emissions scenario therefore only projecting changes for one specific course of human activity. For example, Farinotti et al. (2012) used 10 GCM-RCM combinations all of which assumed the SRES A1B scenario (Van der Linden & Mitchell 2009).

The results of the differing projections under different RCPs will be discussed in Section 8.2.

8.1.2.3 GCM-RCM Uncertainty.

The final source of uncertainty pertinent in future glacio-hydrological modelling relates to the combinations of GCMs and RCMs that are used to force GERM. For example, Griesgletscher and Rhonegletscher have five GCM-RCM combinations whereas Khumbu has two GCM-RCM combinations. In the Alps, these represent a good portion of the uncertainty relating to GCM-RCM combinations. However, to account for all the uncertainty, the full range of CMIP5 GCMs would need to be combined with full range of CORDEX RCMs. For example, to assess GCM uncertainty, a range of GCMs forcing the same RCM are needed; to assess RCM uncertainty, one GCM forcing a large range of RCMs is needed. Although Section 5.4 makes an attempt to separate the uncertainties associated with GCMs and RCMs, indicating that the uncertainties are approximately equal, the lack of available GCM-RCMs at the time of analysis restricts this aspect of the study. However, the range of GCM-RCM combinations used in this thesis is greater than many similar glacio-hydrological studies. For example, Immerzeel et al. (2013) used four GCMs at two Himalayan catchments (no RCMs because dynamical downscaling was not applied); Soncini et al. (2016) applied three GCMs at the Khumbu catchment; Li et al. (2016) used two GCM-RCM combinations in two Himalayan catchments; Farinotti et al. (2012) used ten GCMs in the Swiss Alps; and Finger et al. (2012) used seven GCM-RCM combinations in the Swiss Alps.

The results of GCM-RCM uncertainty will be discussed in Section 8.2.2.

8.1.3 Debris Cover.

A novel methodological advancement made in this thesis was the development of GERM to account for the unique features of debris-covered Himalayan glaciers (i.e. the reduced melt rates beneath debris and to the pattern of glacier downwasting that has been widely observed), such that it can now be applied to glaciers with considerable supraglacial debris cover, with testing conducted at Khumbu Glacier, Nepal. Although further testing is required, the modifications made to GERM account for the unique features of debris-covered Himalayan glaciers.

Importantly, these modifications only marginally increase the data-requirements, and thus maintain the portability of GERM.

8.1.3.1 Melt Reduction Under Debris.

The methodology used in this thesis has fewer data requirements than existing approaches, therefore represents a middle-ground between typical glacio-hydrological models (either no adjustment for debris or the use of a constant reduction factor) and physically based glacio-hydrological models that require abundant field data.

The ablation module of GERM was modified so that calculated melt was reduced according to an exponential curve (see Figure 8.3A – curve '50') which reduces melt depending on the depth of debris cover in that specific grid-square, with thin debris only slightly reducing ice melt rates and thick debris strongly reducing ice melt rates, with bare-ice melt rates not affected by the reduction factor. The justification for the curve used was discussed in Section 6.2.2.3.2, so it is not repeated here. However, a key novelty of this curve is that it can be applied without ablation stake measurements of the density and coverage required to avoid errors in melt rate estimation when extrapolated to the entire debris-covered area. The value of methods that do not use stakes has been emphasised by Nicholson & Benn (2013), who observe that, because ablation is highly spatially variable on debris-covered ice, observations at stakes are not representative of large areas, whilst the high ablation rates and rates of surface change make repeat measurements very difficult.

In much of the literature, the typical approach to simulate melt beneath debris is to use an energy balance model that calculates the conduction of energy through the debris later at the point scale (e.g. Nicholson and Benn, 2006; Reid and Brock, 2010). However, such approaches cannot be applied on the catchment scale due to their intensive data requirements and because thermal conductivity and debris thickness are highly spatially variable (Fujita & Sakai, 2014). Thus, many glacio-hydrological models in Himalayan catchments parameterise the reduced ice melt beneath debris, using constant reduction factors or re-calibrated degree day factors (e.g. Immerzeel et al., 2013).

Another group of glacio-hydrological models implement data-intensive approaches to calculating melt beneath debris and achieve reasonable results, but cannot be applied elsewhere without meteorological observations at several sites on the glacier surface. For example, Fujita and Sakai (2014), developed a method to calculate melt rates beneath debris using remote sensing data for a glacier in Nepal. Specifically, they use ASTER (Advanced Spaceborne Thermal Emission and Reflection Radiometer) data to estimate the surface temperature of debris and, from this, infer the thermal resistance of conduction through debris,

assuming the temperature at the debris-ice interface is zero and a linear-temperature within the debris. Using these methods they were able to estimate melt rates beneath the debris using the energy balance approach. However, despite the good performance of their model to simulate discharge, their approach requires direct measurements of solar radiation, relative humidity, and wind speed at several sites on the glacier surfaces, limiting its application elsewhere.

In the methodology presented in this thesis, the main additional data requirement is debris thickness estimates over the whole glacier. Although debris thickness is highly spatially variable and very difficult to measure directly over a wide area, debris-thickness estimates from satellite sensors have advanced rapidly in recent years (e.g. Foster et al., 2012; Mihalcea et al., 2008a, 2008b; Rounce and McKinney, 2014), using remote-sensing derived surface temperatures to infer debris depth. Therefore, debris-thickness estimates can be generated for any glacier on Earth using freely available Landsat data, for example (e.g. Rounce and McKinney, 2014). However, estimating debris thickness using remote sensing methods remains uncertain (Ragettli et al., 2015), limited in resolution (Landsat is 60 m in thermal band), and the limited availability of ground truth data to constrain the relationship between debris depth and surface temperature prevents comprehensive validation of remote-sensing data. Because of such uncertainties, this thesis tested GERM with both satellite-based debris thickness estimates (Rounce & McKinney, 2014) and modelled debris thickness estimates (Rowan et al., 2015) to provide a lower and upper bound for debris thickness.

The study of Carenzo et al. (2016) developed a model based on the ETI method of simulating ablation (Pellicciotti et al., 2005) that also accounts for variable melt beneath debris of heterogeneous depth. Their model was applied at the point-scale and compared to a full energy balance model, producing similar estimations of melt beneath debris. The approach used was to introduce a lag term to the ETI model to account for the delay in energy transfer through the debris, therefore simulating non-linear conduction of energy through debris, and has been applied for the first time to catchments in the Himalaya and Andes (Ragettli et al., 2016) in a fully distributed manner. Their approach therefore represents one of the most advanced attempts to simulate melt beneath debris, and although in-situ data are recommended to calibrate the melt beneath debris, the method requires considerably less in-situ data than energy balance approaches. Thus, a suggestion for future work is to compare the two approaches at Khumbu Glacier, as detailed in Section 8.5.

Since the true melt rate beneath debris is uncertain, and the effects of this uncertainty on future runoff projections are very poorly known, a brief experiment to investigate the potential significance of differing melt reduction curves for glacier and runoff changes is carried out below. Although it is outside the scope of this thesis to implement and compare all of the methods for

estimating melt under debris (e.g. Carenzo et al., 2016; Fujita and Sakai, 2014; Nicholson and Benn, 2006; Soncini et al., 2016), this sensitivity study is carried out by altering the exponential function of the debris-reduction curve, such that melt beneath 50 cm debris is 50 % (original curve, based on Nicholson & Benn, 2006; 2013), 20 % (reduced curve) and 80 % (enhanced curve) of surface melt rates (Figure 8.3). The results of this experiment at Khumbu, shown in Figure 8.3, clearly indicate that altering the amount of melt supressed under debris has a significant influence on future glacier volume, particularly when melt under 50 cm of debris is 20 % of surface melt. Specifically, the remaining ice volume in 2100 ranges from 6 % to 29 % to 38 % for a reduction in melt beneath 50 cm debris of 20 %, 50 % and 80 %, respectively.

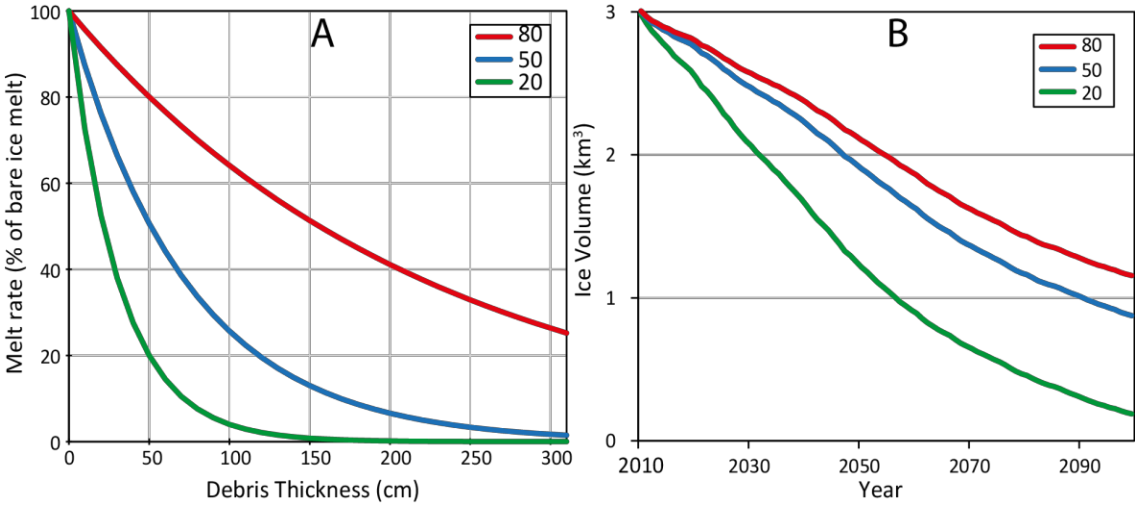

Figure 8.3: (A) The shape of the exponential debris-reduction curves, used in GERM to reduce melt rates depending on debris thickness. The "50" curve was used on all Khumbu simulations. (B) The impact of using the different melt reduction curves on glacier evolution. Results are based on one GCM-RCM combination: EC-EARTH RCA4 RCP 4.5.

There has been some recent discussion of the shape of the melt-reduction curve, with Anderson and Anderson (2015) suggesting that a hyperbolic function may better describe the shape of the Østrem curve, since the shape of the exponential curve decreases more rapidly to zero, as shown in Figure 3 in Anderson and Anderson (2015). Although this point is valid, the impact of making this adjustment on glacier-scale changes is likely to be minimal, since this only affects the thickest debris, for which melt rates are already very low, with Nicholson & Benn (2012) showing that ablation rates beneath thin debris (<50 cm) are the most sensitive. Therefore, altering the shape of the melt-reduction curve was not tested in this thesis, but it is encouraged to be included in future studies.

A limitation of the method proposed here that requires further development is the lack of spatially expanding debris, as discussed in Section 7.3.3.3. Firstly, although the method can

parameterise for the effect of thickening debris over time, the debris-surface does not spatially evolve in the methodology proposed, therefore the proportion of glacier covered with debris decreases as the glacier recedes. At Khumbu, this is a justified method because areas above the ice-fall are unlikely to become debris-covered (see Section 7.3.3 for discussion). However, to make GERM portable to other Himalayan catchments, debris expansion should be implemented using a simple scheme such as that proposed in Jouvet et al. (2011) whereby the existing debris surface expands according to the rate of glacier retreat.

Until the level of understanding of debris thickness and its relation to melt on the glacier scale is improved, it is concluded that simple methods of estimating melt beneath debris, such that exponential decrease in melt rates, are appropriate.

8.1.3.2 Capturing the Dynamics of Downwasting Glaciers.

A novel modification was made to GERM in order to capture the downwasting nature of debris-covered Himalayan glaciers. Specifically, the Δh parameterisation was calibrated to the observed pattern of mass loss at Khumbu Glacier (Nuimura et al., 2012).

The Δh retreat parameterisation in GERM was originally designed for 'typical' alpine glaciers that were not debris-covered and responded to climate changes through frontal recession (e.g. WGMS, 2015). However, many Himalayan glaciers lose mass through downwasting with minimal frontal recession (Bolch et al., 2008; Scherler et al., 2011). Although using a dynamical glacier model to simulate mass loss may also reproduce the downwasting that occurs under debris cover (e.g. Soncini et al., 2016), it is important to retain the simple, portable design of GERM such that it can easily be applied to other, data-poor, catchments. The data and computationally intensive requirements of dynamical models would have prevented this.

The results (Section 7.3.3.1) show that the modification to the Δh parameterisation successfully reduced frontal recession and allowed greater loss of mass further up the glacier, mimicking the observed patterns of mass loss observed at Khumbu Glacier and other debris-covered glaciers in the Himalayan region (e.g. Bolch et al., 2011; Gardelle et al., 2013). The testing of this part of GERM, conducted in Section 7.3.3, showed that the modifications did reduce terminus recession and mass was lost through a combination of frontal recession and downwasting. Therefore, this modification to GERM has improved the ability of the model to reproduce the downwasting behaviour of debris-covered glaciers.

8.1.3.3 Incorporating Ice Cliffs in GERM.

Ice cliff features, known to locally enhance melt rates on debris-covered areas of ice, are included in GERM by removing the reduction factor for areas of the debris-covered area where

ice cliffs are observed, such that melt rates are the same as for bare-ice. Ice cliff location was based on remote-sensing derived maps of supra-glacial lakes (Watson et al., 2016). Although this simple approach is not expected to realistically reproduce the melt rates at ice cliffs, the level of understanding of ice cliffs is very limited so this provides a first-order estimation of their influence on a glacier scale. Further development of this aspect of GERM is recommended for future research. For example, once the melt rate at ice cliffs is better understood, an additional 'enhancement factor' could be applied in GERM where the melt rate at ice cliffs is set to higher than bare-ice levels (as observed in Watson et al., 2015), if this is found to be widespread.

8.2 Review and Discussion of Key Results.

This section will summarise the key findings of this thesis and relate the findings at the three sites, before discussing projections of glacier and runoff evolution produced by this study in the context of previous research.

8.2.1 Future Glacier Changes.

8.2.1.1 Glacier Changes at Griesgletscher, Rhonegletscher and Khumbu Glacier.

Since individual chapters have already discussed the future evolution of specific glaciers (Griesgletscher and Rhonegletscher - Section 5.5, Khumbu- Section 7.3), this section will focus on synthesising the results at the three sites. To understand the significance of the future changes in glacier evolution, the mean of all GCM-RCM combinations is taken for each RCP, shown in Figure 8.4, with uncertainties accounted for in Section 8.2.2.

Although all three glaciers show considerable loss of ice, there are notable differences between the projections of future glacier changes at the three sites. For example, Griesgletscher is projected to continue rapidly losing mass and be an ice-free catchment by 2080-2100, except under RCP 2.6, whereas Rhonegletscher also loses mass but projections suggest that between 10-30 % of ice will remain in 2100. Khumbu exhibits the largest range between RCPs, in part due to the fewer number of available GCM-RCM combinations, and is likely to have the highest proportion of ice remaining in 2100 (8-41 % of initial volume). To explore the reasons behind the different rates of mass loss, it is important to consider glacier size and hypsometry (Figure 8.5). Several important characteristics of the glaciers are evident.

Firstly, the initial size differs strongly between Griesgletscher compared to Rhonegletscher and Khumbu. The faster response time of small glaciers is well documented (E.g. Hock et al., 2005; Raper and Braithwaite, 2009; Roe and Baker, 2014), partially explaining the more rapid loss of

ice at Griesgletscher. Conversely, Khumbu is considerably larger than Rhonegletscher (volume in 2010 at Khumbu: 2.99 km^3 vs. 1.86 km^3 for Rhonegletscher), partially explaining the slower rate of ice loss, although the insulating influence of debris cover is also a contributing factor.

Secondly, the hypsometry of the three sites differs in terms of the proportion of mass at high-altitudes (Figure 8.5). Griesgletscher has very little high-elevation ice, and the ELA in 2010 is already at the very upper reaches of the glacier. However, Rhonegletscher has a large accumulation zone, much of which is located above the 2010 ELA of 3000 m, therefore reducing its vulnerability to climate changes. Finally, Khumbu also has considerable high-elevation ice (over 7000 m in large areas) that is very unlikely to be affected by temperature increases before 2100. Khumbu Glacier also has a considerable expanse of debris-covered low-elevation ice, which is typical of debris-covered glaciers since the debris cover protects the ice from melting. However, the results of this thesis suggest that continued downwasting will result in considerable losses in this low elevation area by 2100. The loss of low-elevation ice is the reason for the recovery of mass balance from highly negative to less negative seen at all three sites in some projections. This recovery of mass balance is indicative of the remaining high-elevation ice mass nearing equilibrium with the warmer climate, resulting in glacier mass balance becoming less positive.

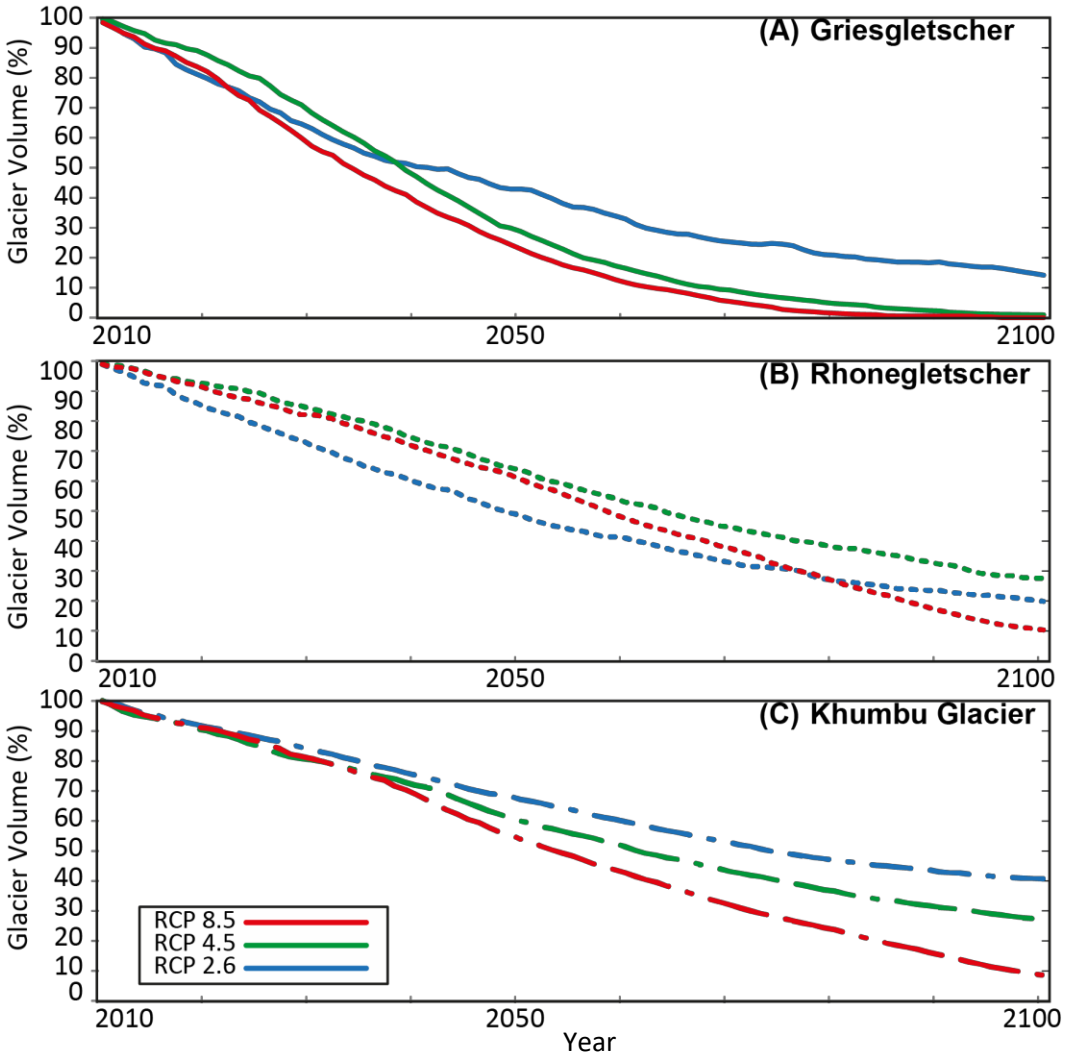

Figure 8.4: Projected glacier volume at (A) Griesgletscher, (B) Rhonegletscher, and (C) Khumbu Glacier, using the mean of all GCM-RCM combinations. Volumes converted to percentage of 2010 volume for comparison. Note that Khumbu Glacier has fewer GCM-RCM combinations and that RCP 2.6 represents only one GCM-RCM. Results for Khumbu are presented as the average of the results using the thin and thick debris layers.

A potential indicator of each glacier's individual vulnerability to climate change is the proportion of ice area above the 2010 ELA. Griesgletscher has only 13 % of ice area above the ELA; Rhonegletscher has 42 % of ice area above the ELA; and Khumbu Glacier has 70 % of ice area above the ELA in 2010. These values indicate that Griesgletscher is indeed the most vulnerable of the three to warming, and suggest that Khumbu is more resilient than Rhonegletscher. However, Khumbu and Rhonegletscher show similar mass losses in projections. This may be because ice within the Khumbu accumulation are is relatively thin (see thickness estimation in Section 6.2.2.3.2).

Topographic characteristics that are unique to each catchment are likely to influence the pattern of glacier mass loss. For example, Figure 8.5 shows the locations of overdeepenings and ice-falls

on the individual glaciers. From the distribution of ice area in the future (green profile), it is clear that Griesgletscher and Khumbu show significant thinning in the ice-fall areas, and that Rhonegletscher has an area of thinning around 2700 m. These areas of thin ice form detachments where the snout of the glacier is no longer dynamically coupled to the upper glacier. In GERM, detachment causes the Δh parameterisation to stop mass redistribution to disconnected parts of the glacier. The spatial plots in relevant chapters confirm this detachment is simulated in GERM (Griesgletscher and Rhonegletscher: Section 5.3; Khumbu Glacier: Section 7.2.2). The result of such a detachment means that there is no longer delivery of ice from the accumulation zone leading to the rapid stagnation and demise of the lower glaciers.

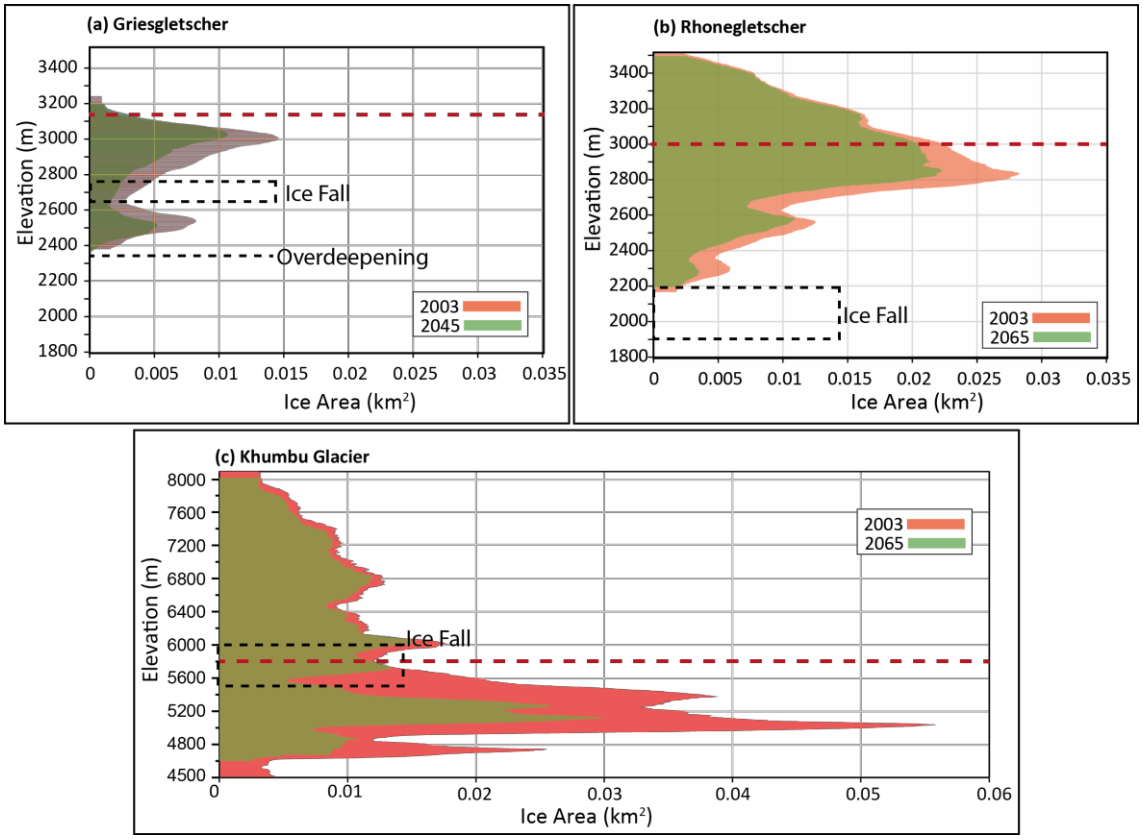

Figure 8.5: Glacier hypsometry at Griesgletscher, Rhonegletscher and Khumbu, showing the relationship between ice area and elevation in 2003 compared to the hypsometry when 50 % of ice volume is lost (2045 at Griesgletscher; 2064 at Rhonegletscher and Khumbu). Red line denotes ELA averaged over 2010-2012. Note the y-axis differs at Khumbu.

8.2.1.2 Comparison of Glacier Changes with Previous Research.

Griesgletscher. The projected glacier changes at Griesgletscher are comparable with the projected changes in Farinotti et al. (2012) who use the same glacio-hydrological model but apply the previous generation of GCMs and RCMs from ENSEMBLES with the A1B emissions

scenario (broadly halfway between RCP 4.5 and 8.5) that are downscaled using the delta-change approach. Their study shows no ice present in 2075, similar to the RCP 8.5 scenario in this thesis, but somewhat faster than RCP 4.5. Despite small differences, it is clear that both studies agree to the continual ice loss at Griesgletscher. Additionally, Farinotti et al. (2012) also projected the recovery of mass balance towards the end of the 21st century linked to the high-elevation ice mass nearing equilibrium with a warmer climate. The mass balance data was not separated for individual glaciers in Farinotti et al. (2012; Figure 8A), so Griesgletscher cannot be compared precisely, but their results suggest the mass balance recovery is widespread across the Swiss Alps.

Rhonegletscher. There are considerably more modelling studies at Rhone (e.g. Farinotti, 2013; Farinotti et al., 2012; Gabbi et al., 2014; Jouvet et al., 2009). For example, Jouvet et al. (2009) ran simulations from 2007-2100 using three climate scenarios: cold-wet; median; warm-dry, with their median scenario used for comparison (broadly similar to RCP 4.5). Their results suggest moderate mass loss by 2050 with 66 % of ice remaining, similar to the estimate of 48-65 % in this thesis. However, by 2100, Jouvet et al. (2009) simulate rapid mass loss with only 5 % of ice remaining, notably less than the mean mass loss of both RCP 4.5 and 8.5 in this thesis. This difference is likely due to the temperature projection of Jouvet et al. (2009), which suggests constant increase in temperatures whereas those applied in this thesis show a curtailing of temperature increase for RCP 4.5. Both studies do agree that Rhonegletscher in 2100 will exist as a small, high-elevation ice-field by 2100. Farinotti et al. (2012) projects a similar decline in ice mass at Rhonegletscher, but a clearer negative discharge trend than in this thesis. The discussion in Section 3.5 suggested that this difference may reflect the greater number of emissions scenarios used in this thesis (RCP 2.6, 54.5 and 8.5, vs. A1B in Farinotti et al., 2012), resulting in a wider range of temperature and precipitation projections to force GERM. Moreover, the use of delta-change downscaling in their study may not adequately adjust bias in terms of precipitation (Piani et al., 2010), improved in this thesis by using the quantile-mapping methodology.

Khumbu. Until recently, very few studies had attempted to simulate future glacier evolution at Khumbu Glacier. However, as described in Section 7.1, Shea et al. (2015) modelled the future response of all glaciers in the Everest region, using a glacier mass balance and redistribution model. They estimated that remaining ice in 2100 would be between 4 % and 27 % for RCP 8.5 and 4.5, respectively. These estimates suggest somewhat more rapid ice loss than those of this thesis. However, direct comparison is not possible because Shea et al. (2015) do not include results specific for Khumbu Glacier. Additionally, the underestimation of initial ice volume in their study may have caused more rapid glacier response to warming. Another recent study,

Soncini et al. (2016; see Section 7.1 for full description), apply a coupled ice-dynamical-hydrological model to the Khumbu catchment, forcing the model by applying statistical downscaling (delta-change for temperature; weather-generator approach for precipitation) directly to GCMs. Their data-intensive approach to model calibration is quite different to the method applied in this thesis, which intentionally calibrated the model only using satellite-derived data in order to preserve portability. A key difference in their results is their much larger estimation of initial ice volume of more than 6 km^3 which disagrees with the ice volume of 3 km^3 in this thesis and in Rowan et al. (2015). This considerable difference is potentially due to their inclusion of a larger accumulation zone than this thesis or Rowan et al. (2015), parts of which are unlikely to distribute mass to the main part of the Khumbu Glacier. Indeed, the ice thickness estimates on the main branch of Khumbu Glacier actually compare well between these studies. Their study estimates ice volume of 44-63 % of initial volume in 2050 and 32-52 % in 2100, depending on GCM and RCP. These estimates are similar to those for RCP 2.6 in this thesis, but notably higher than RCPs 4.5 and 8.5. Such differences may reflect the larger initial ice mass of their study: larger ice masses respond more slowly to climate changes (Benn & Evans, 2010). Considering both Shea et al. (2015) and Soncini et al. (2016), the projections of ice volume in this thesis fall in-between their estimates, with the lack of consensus among studies an indication of the immature nature of glacio-hydrological studies in this region. Furthermore, the lack of long-term validation data will remain a considerable limitation to all modelling studies in the Himalayan region and prevent rigorous quantification of the uncertainties associated with glacio-hydrological modelling.

To summarise the changes in glacier evolution, a dramatic loss of ice mass is projected for all sites under all GCM-RCM combinations. Only Griesgletscher is projected to be ice free in 2100, but Rhonegletscher (10-25 % remaining ice) and Khumbu Glacier (8-40 % remaining ice) will be considerably less extensive than today, resulting in high-elevation ice masses but near-complete removal of the current ice-tongue. In comparison to previous research, the future projections in the Alps are similar, although direct comparison between studies is complicated by differing climate drivers. The level of confidence in the future projections at Griesgletscher and Rhonegletscher is therefore high. At Khumbu, the results of this thesis are broadly similar to existing attempts to model future ice volume, in that they simulate considerable mass loss, however, there is a lack of consensus among the literature. This lack of consensus in the literature together combined with the importance of debris cover on glacier evolution means the projections of future glacio-hydrological changes at Khumbu are highly uncertain.

8.2.1.3 Future Runoff Evolution.

8.2.1.3.1 Annual Runoff.

The projected changes in runoff are less consistent than glacier changes in terms of trends and patterns, with considerable variability during the 21st century, resulting from the influence of precipitation changes and snow-melt. However, the detailed analysis in Chapter 5 for Griesgletscher and Rhone, and Chapter 7 for Khumbu, as well as Figure 8.6, shows that negative trends in discharge are exhibited at Griesgletscher and Khumbu, with initial increases in discharge in most projections before an overall decrease by 2100. At both Griesgletscher and Khumbu, the stronger warming and greater mass loss from RCP 2.6 to 4.5 to 8.5 results in corresponding reductions in discharge. These results suggest that, with faster mass loss of ice, peak runoff is realised earlier in the 21st century and the reduction in discharge associated with a smaller ice mass is greater. At Griesgletscher, the reduced glacier contribution to discharge is a result of minimal remaining ice mass. At Khumbu, however, the reduced glacier contribution to discharge is more likely to result from the removal of most low-elevation ice, leaving only ice at very high elevations (e.g. >6000 m) which provides only a minimal contribution to melt. At Khumbu, results are presented as the average of the thin and thick debris layers.

At Rhonegletscher, the pattern is more complex than Griesgletscher, with RCP 2.6 suggesting a strong negative trend, RCP 4.5 suggesting no trend, and RCP 8.5 suggesting a strong positive trend. The time-series show that the evolution of discharge is relatively consistent until 2060 when a divergence of the discharge projections occurs. The cause of this divergence becomes clear when considering the temperature and precipitation projections (Section 3.4.4 Figure 3.10), the ice volume projections (Figure 8.4), and the emissions scenarios associated with RCP 2.6, 4.5, and 8.5 (Section 1.3.1., Figure 1.1). In terms of temperature and precipitation, it is around 2060 that the differences between RCPs become evident, particularly in terms of temperature, which shows rapid warming from 2060-2100. For precipitation, GCM-RCM combinations B and E also show considerable increases in precipitation after 2060 for RCP 8.5. The acceleration of warming causes increased ice mass loss for RCP 8.5 and is combined with the increase in precipitation, leading to increased discharge. For RCP 2.6, the negative trends must be interpreted with knowledge that it is based on the means of only two GCM-RCM combinations and is therefore strongly influenced by the negative discharge trend of GCM-RCM combination A (see Figure 3.9 in Section 3.4.4), which reflects rapid temperature increases for RCP 2.6 in the first half of the 21st century.

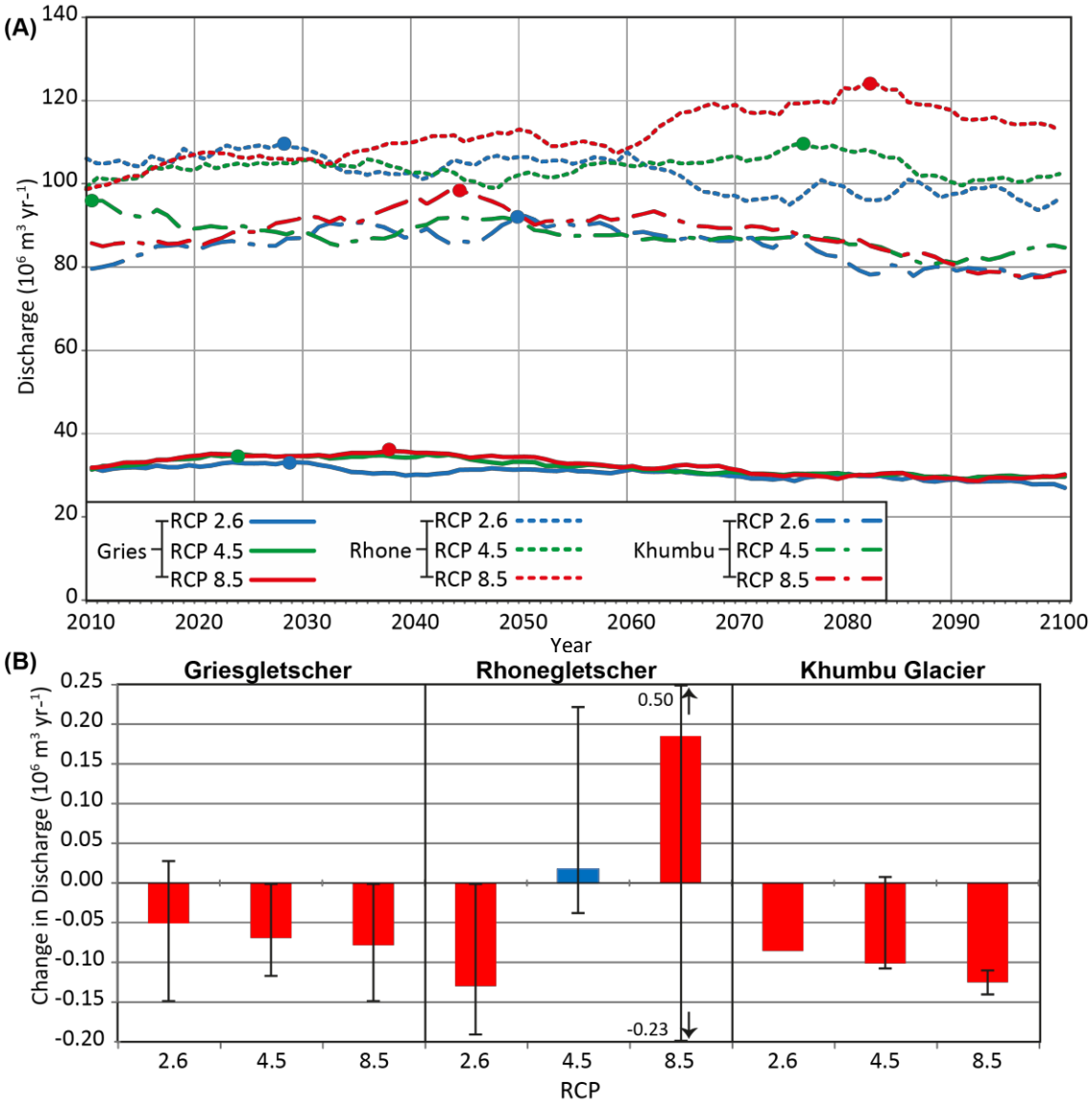

Figure 8.6: (A) Future evolution of annual discharge at the three sites, and (B) the trends associated with these time-series, calculated from 2010-2100 with red indicating significance of p<0.01. All data presented is the mean of all available GCM-RCM combinations. Circles represent year in which peak discharge occurs. Bars show maximum range across all GCM-RCMs. Results for Khumbu are presented as the average of the thin and thick debris layers.

8.2.1.3.2 Seasonal Changes in Runoff.

As shown in Chapter 5 and Chapter 7, the seasonal changes in discharge will lead to earlier onset of the melt season. Additionally, discharge in late summer appears to decrease with declining glaciation due to less available ice for melt. Finally, the overall duration of the melt season increases at all sites. At Khumbu, the notable changes in the melt season are somewhat surprising given the dominance of the Indian monsoon that coincides with the melt season.

To summarise the discharge changes, it is clear that at Griesgletscher and Khumbu the increase rates of ice mass losses result in increasingly negative discharge trends, caused by a reduction in the available ice contribution to discharge. Thus, peak discharge is reached in the first half of the 21st century, after which discharge declines. At Rhonegletscher, the increases in warming and mass loss do not result in negative discharge trends, likely because most GCM-RCM projections (B, C, D, and E) estimate considerable mass of ice remaining in the 21st century. Thus, peak discharge is reached later in the century than at Griesgletscher and Khumbu, so negative discharge trends are not projected before 2100. These conflicting result underline the importance of considering individual catchments and that future projections can vary considerably even over short distances.

8.2.1.4 Comparisons of Runoff Changes with Previous Research.

Griesgletscher and Rhonegletscher. At Griesgletscher and Rhonegletscher, the study of Farinotti provides an ideal comparison of runoff evolution, since it uses the same model but different climate inputs. Figure 8.6 shows the anticipated peak discharge at Griesgletscher in the early 21st century, which is corroborated in Farinotti et al. (2012), as is the later timing of peak discharge at Rhonegletscher. The main difference between the studies is that Farinotti et al. (2012) estimate an overall decrease in discharge at Rhonegletscher by 2100 whereas this thesis projects conflicting trends (2010-2100) depending on the RCP. Since Farinotti et al. (2012) only used one scenario (A1B), it is not possible to compare scenario uncertainty. Other studies in the Alps that assess discharge evolution at other catchments (e.g. Finger et al., 2012; Gabbi et al., 2012; Horton et al., 2006; Huss, 2008a) also show an initial peak in discharge before an eventual decrease, despite a wide range of climate inputs and scenarios. Such a consensus between results that do not use the same methods gives confidence that the results of this thesis are a good estimate of future changes, although the uncertainties remain considerable, as described in Section 8.2.2.

The seasonal changes projected at all three catchments, where the melt season begins earlier in the year and late summer discharge decreases, have been found in several studies, and are generally considered to be an accepted pattern of seasonal change (e.g. Farinotti et al., 2012; Finger et al., 2012; Horton et al., 2006; Huss et al., 2008a; Immerzeel et al., 2013; and Soncini et al., 2016, all found similar results). Therefore, the seasonal changes are not discussed further, although their impacts are considered in Section 8.4.

Khumbu Glacier. At Khumbu Glacier, there are fewer studies at the upper-catchment scale with Soncini et al. (2016) representing the only study hitherto to assess changes in discharge. Their

findings corroborate those of this thesis with an initial increase in discharge, peaking before 2050 before eventually decreasing. Another study, Immerzeel et al. (2013) modelled glacier and runoff changes at the Langtang catchment using downscaled CMIP5 climate inputs. They found a strong, consistent increase in runoff, conflicting the results presented here and in Soncini et al. (2016), which Immerzeel et al. (2013) attribute to considerable ice melt (63 - 47 % remaining ice volume in 2100) and projected increases in precipitation.

The agreement between Soncini et al. (2016) and the results of this thesis in terms of the evolution of discharge, despite the different approaches, gives some confidence that the projections are reasonable. However, as for glacier changes, glacio-hydrological modelling in this region is in its infancy and further studies are required to continue model development, obtain field-data for model validation, and perform long-term simulations.

8.2.2 Results of Long-Term Validation and Assessment of Uncertainty.

8.2.2.1 Underestimation of Glacier Volume Loss.

Validating projected glacier changes since 1874 at Rhonegletscher and 1884 at Griesgletscher against measured data showed considerable underestimation of glacier mass loss at both sites. These errors most likely reflect a change in the relationship between temperature and glacier melt. Section 4.5 provided some discussion of the stationarity of model parameters, which will be expanded upon here.

Specifically, the HTI approach to calculating melt in GERM relies on a strong relationship between temperature and the various components of the surface energy balance (e.g. net radiation, turbulent heat exchange etc.). However, several studies have noticed changes in the strength of this relationship (e.g. Gabbi et al., 2014; Huss et al., 2009; Huss et al., 2008a; Pellicciotti et al., 2014), for example, caused by strong increases in solar radiation (Huss et al., 2009b). The only accepted method to alleviate this issue is to recalibrate the model for each period where measurements are available. However, this is only possible with mass balance reconstruction of the past because period volume change observations are required to periodically re-calibrate melt parameters. Since a key aim of this thesis is to assess the uncertainties associated with estimates of future changes made by glacio-hydrological models, re-calibration was not logical, therefore the model performance is indicative of performance in the future. As such, this thesis represents one of the first attempts to quantify the error associated with changing sensitivity of glacier to climate in glacio-hydrological models.

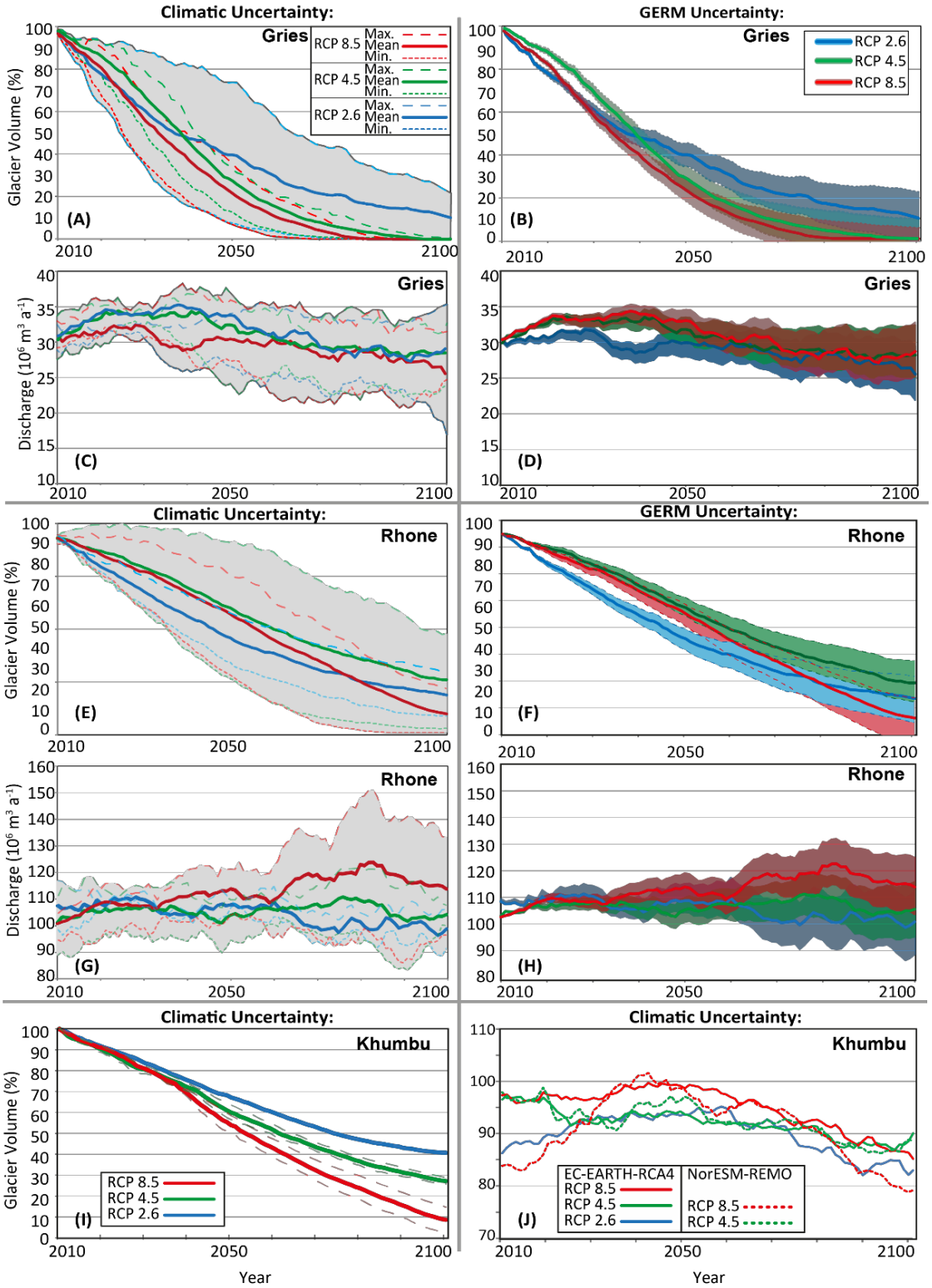

Figure 8.7: Comparison of uncertainty introduced by the range of GCM-RCM combinations and RCPs (left panel), and uncertainties associated with GERM (right panel, except for Khumbu [I-J]). Climatic Uncertainty comprises RCP uncertainty, i.e. the bold coloured lines, and GCM-RCM uncertainty, i.e. the grey area showing the range of all GCM-RCM combinations for each RCP. GERM uncertainty is shown as the uncertainty calculated on the long-term validation, applied to each RCP. Thus both panels include RCP uncertainty. Note that Khumbu shows individual model projections using the thick debris layer, and uncertainty associated with GERM is not calculated at Khumbu.

There have been several studies that have simulated the evolution of Griesgletscher and Rhonegletscher in the past (e.g. Huss et al., 2008b). However, since several of these studies recalibrated the model for each DEM-period (i.e. they reconstructed mass balance rather than forward-modelled projections), the results are not comparable. Only the study of Gabbi et al. (2014), who tested several different types of glacio-hydrological models at Rhonegletscher from 1929-2010, is comparable. Using the HTI model, similar to GERM, their study also underestimated ice loss but the magnitude of underestimation was greater in their study. Gabbi et al. (2014) employed several of the types of model in their analysis, finding that the SEB model (e.g. Oerlemans, 2001) best reproduced observed volume changes with the ETI model (e.g. Pellicciotti et al., 2005) similar in performance.

The conclusions of Gabbi et al. (2014) suggest that the ETI and SEB model parameters are more transferable in time than the HTI model, due to a reduced sensitivity to temperature changes. Their conclusions therefore agree with those of this thesis: the stationarity of melt parameters in GERM assumes a fixed relationship between temperature and glacier melt, which results in uncertainties when simulating glacier changes over very long time-scales, and these uncertainties need to be accounted for when simulating future glacier and runoff evolution. However, the results presented in Section 4.4 suggest that the extent of the error in reproducing observed volume changes is smaller than in Gabbi et al. (2014) and that some of this error is due to DEM uncertainties. The accuracy of the DEMs used in volume change observations (Bauder et al., 2007) was discussed in Section 4.5 so further discussion is not included here.

8.2.2.2 Uncertainty of Future Glacio-Hydrological Changes.

Comparing the sources of uncertainty in this thesis to the literature is difficult because no other studies have quantified glacio-hydrological modelling uncertainty using long-term validation. Therefore, the following discussion only relates to climatic sources of uncertainty.

When applying GERM to project future changes, the uncertainties associated with GERM itself, calculated using the aforementioned long-term validation, were applied alongside two other sources of uncertainty: GCM/RCM uncertainty and scenario (RCP) uncertainty. Figure 8.7 shows a comparison of these three sources of uncertainty on glacier and discharge evolution at sites in the Alps. Khumbu cannot be included in terms of the uncertainty associated with GERM due to the lack of long-term validation data, but the uncertainty associated with different RCPs and different GCM-RCM combinations is presented.

The comparison of the different components of uncertainty in the Alps clearly shows that all three sources are considerable. At Griesgletscher, the uncertainty associated with GERM (B) is larger than at Rhonegletscher (F) in terms of glacier changes due to the worse performance

during the long-term validation. However, the larger errors in discharge simulation at Rhonegletscher (H) produce slightly larger uncertainty compared to Griesgletscher (D). In terms of climatic (GCM-RCM and scenario) uncertainty, the magnitude is similar at Griesgletscher and Rhonegletscher (A, C, E, G), with the exception of discharge at Rhonegletscher (G) which shows large uncertainties after 2060, as discussed in Section 8.2.1.3. At Khumbu (I and J), there are less GCM-RCM combinations thus uncertainty cannot be directly compared. However, it is clear that the uncertainty associated with different RCPs has a considerable influence on glacier evolution.

Farinotti et al. (2012) assessed the uncertainty associated with 10 different GCM-RCM combinations, all forced with the same A1B scenario, therefore only assessing GCM-RCM uncertainty. In Farinotti et al. (2012), Figure 10 (pp.1916) shows how the future discharge evolution of Rhonegletscher and Griesgletscher is highly uncertain, with a large range between the various model simulations. The other catchments studied show similar patterns with the exception of Silvretta and Morteratsch. Interestingly, these catchments have the lowest degree of glaciation in their study, suggesting the uncertainty of future projections is reduced for less glaciated catchments. The results of this thesis would need to be repeated in more catchments in order to assess the influence of catchment glaciation on future runoff, since Griesgletscher is 50 % glaciated and Rhonegletscher and Khumbu are both 32 % glaciated. However, the large range of uncertainty shown in GCM-RCM combinations in Farinotti et al. (2012) corroborates the findings of this thesis.

The study of Soncini et al. (2016), when simulating the future evolution of Khumbu Glacier, assessed the uncertainty from three GCMs, each with RCPs 2.6, 4.5, and 8.5. Their findings indicate that the ECHAM6 GCM produces considerably different volume projections depending on the RCP, whereas the EC-AARTH GCM and CCSM4 GCM have smaller differences between RCPs. Such variability highlights the importance of selecting a large enough range of GCMs and RCMs in order to properly capture uncertainty, something that was not possible in this thesis at Khumbu.

8.3 Wider Implications.

8.3.1 Summary of Key Findings.

The key results of this thesis can be summarised as:

- Griesgletscher, Rhonegletscher and Khumbu Glacier are all projected to lose considerable mass (remaining ice of: Griesgletscher: 0-15 %; Rhonegletscher: 10-27 %; Khumbu Glacier: 8-41 %) over the coming century. Griesgletscher will lose the most mass due primarily to its small size and lack of high-elevation accumulation zone.

Rhonegletscher and Khumbu are both projected to lose similar proportions of mass. Of the glaciers in this thesis, Rhonegletscher appears to be the least vulnerable to warming due to the large volume of high-elevation ice.

- Runoff changes are less clear with considerable variation between different emissions scenarios, different GCM-RCM combinations, and different catchments. At Griesgletscher and Khumbu, it is likely that discharge will increase but will reach peak discharge before 2050, and then decline to below current levels. Rhonegletscher is expected to reach peak discharge later in the century with no decline before 2100.
- The uncertainty assessment includes RCP, GCM-RCM combination, and GERM uncertainty, showing highly uncertain projections at each catchment. The uncertainty relating to the glacio-hydrological model itself has been quantified for the first time showing that the future glacier evolution and runoff are moderately impacted by GERM uncertainty, but this remains a smaller source of uncertainty compared to the choice of RCP scenario, and the range of GCM-RCM combinations. The differences between GCM-RCM combinations are considerable and, when combined with the different RCPs, the future evolution of these catchments appears highly uncertain.

8.3.2 Relationship between Glacier Ice Loss and Runoff.

The results of this thesis project an initial increase in catchment discharge before an eventual decrease at all three catchments, although the results at Khumbu are uncertain. The period of elevated annual discharge represents the removal of water from the ice reservoir and also suggests that the current levels of discharge are elevated above non-glacial levels due to the negative mass balances widely observed in recent decades. By taking the average of all simulations separately for each three sites, it is possible to assess the relationship between ice loss and discharge (Figure 8.8). At Griesgletscher, peak discharge is reached around 2020, before a gradual decline. At Rhonegletscher, peak discharge is not reached until 2075, after which there is a decline but negative discharge is not reached before 2100. At Khumbu, peak discharge occurs around 2045 before declining, with rapid decline after 2075.

8.3.3 Implications of Future Glacier and Runoff Changes.

The projections of future glacier and runoff evolution in this thesis will have implications downstream. This section will briefly summarise the key physical impacts of glacio-hydrological changes with reference to impact-specific studies. This section will focus on hydropower and agriculture, although changing water resources are also likely to impact upon drinking water, floods, and aquatic and terrestrial ecosystems. The societal impact of these physical impacts will not be discussed.

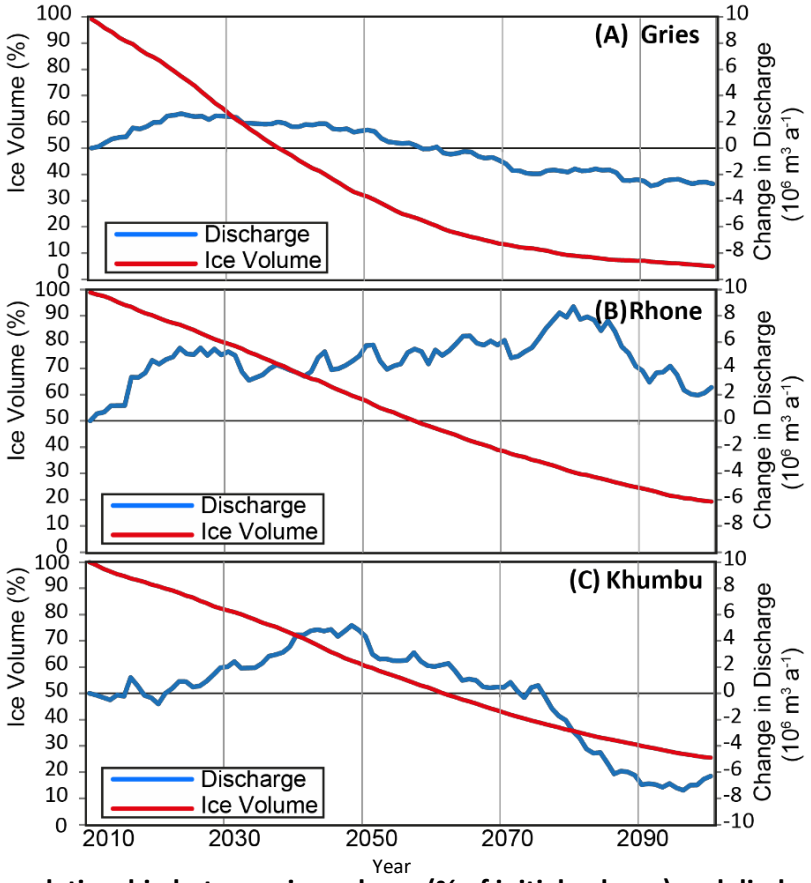

Figure 8.8: The relationship between ice volume (% of initial volume) and discharge (departure from 2010 average), averaged over all simulations at all sites.

8.3.3.1 Runoff Changes.

From the results presented in this thesis, the changes in catchment discharge can be summarised as an eventual decrease in overall runoff as well as lengthening of the melt season, the impacts of which will be discussed here. The impacts of changing water resources are elevation, location, and scale dependent. For example, Miller et al. (2012) stated that the impacts of changes to glacier runoff in the Ganges basin (to which Khumbu contributes) are high near the upper-catchments but likely to be negligible further downstream. This is because precipitation will continue to occur at similar rates to today, surpassing the effect of reduced runoff from upper catchments, and the coincident timing of peak runoff with the monsoon suppresses changes in glacier contribution (Miller et al., 2012; Immerzeel et al., 2012). However, there remains considerable debate on the contribution of upper catchment ice and snow melt to the larger catchment scale (e.g. Collins et al., 2013; Siderius et al., 2013), and there are considerable regional variations. For example, the Indus River basin drains the Western Himalaya, which receives less rainfall than central and Eastern Himalaya, leading to a stronger contribution of ice melt to downstream discharge (Lutz et al., 2014). What is clear is that the main impacts of changes in runoff are felt within the mountains, with changes in the seasonal timing of runoff just as significant as changes in overall runoff (e.g. Akhtar et al., 2008). However,

if the projections in this thesis are indicative of changes in other catchments, the aggregate effect may be considerable.

One industry particularly interested in the future changes in alpine runoff is the hydropower industry. This is centred in alpine regions with countries such as Switzerland, Norway and Sweden generating 56 %, 36 %, and 53 % of their respective electricity from this renewable source (Energy, 2013). Hydropower resources currently represent an estimated 20 % of global electricity production (Sternberg, 2010; Finger et al., 2012), a figure that is expected to rise in coming decades (IHA, 2013) with increasing concern over climate changes combined with depleting fossil fuel resources. Thus, estimating the impact that climate change will have on catchment runoff regimes will form an essential part of future energy policy. At Griesgletscher, in particular, hydropower is clearly important due to the hydropower scheme operating from the Griessee Lake. Therefore, snow and ice runoff is currently the primary water supply into the reservoir and changes in the seasonal delivery of water, for example increased spring discharge and reduced later summer discharge, will alter the management of the reservoir to ensure water is available when required for energy generation (e.g. in winter). Moreover, the eventual decrease in runoff will lead to a decrease in energy generation from the hydropower station. Finger et al. (2012) agrees with these conclusions, stating that the hydropower industry will be required to adjust the timing of energy generation to compensate for hydrological changes, and that the Mattmarksee Reservoir will not be filled to capacity after 2050 due to reduced discharge. Additionally, small run-of-river hydropower stations, which do not have the storage capacity to compensate for changes in runoff, will be strongly impacted by changes in discharge (Beniston & Stoffel, 2014). Another interesting study, Farinotti et al. (2016), assessed the potential for reservoirs to be constructed as replacements for glaciers, therefore alleviating some of the issues of changing seasonal discharge by storing runoff for use when use when it was required. They suggest that such a strategy could offset up to 65 % of expected summer-runoff changes. However, their study neglected environmental, ecological and economic considerations, thus represents a first order assessment.

In addition to hydropower, changes to the total and seasonal runoff regime will have impacts on agriculture. For example, it has been shown that elevated temperatures reduce the productivity of both arable and pastoral agriculture (Smith et al., 2012) and that the raised temperatures will increase water demand by up to 10 % in the Rhone valley, due to greater evapotranspiration (Fuhrer et al., 2014). Therefore, it is clear that reduced water delivery coupled with increased demand will place stresses on the agricultural industry (Mathison et al., 2013; Beniston & Stoffel, 2014). In particular, agriculture in the Himalaya is already under pressure due to rapid population growth, which is expected to accelerate (United Nations,

2013). In the most water-scarce regions, groundwater extraction is already relied upon but is reported to be overexploited (Tiwari et al., 2009). Moreover, Mathison et al. (2013) found that, for the period 2011-2040, reductions of up to 43 % in rice and wheat yield potential will occur in the upper Ganges basin due to reduced water resources for irrigation (Moors & Stoffel, 2013).

To summarise, it is clear that reduced runoff could be significant in terms of the impacts on hydropower and agriculture. The clear message from impact studies is that mitigation and adaptation will be required in order to minimise the negative impacts of reduced water supplies in mountain regions.

8.3.3.2 Glacier Changes.

The most significant impacts of this thesis relate to water resources. However, glacier changes have impacts themselves. For example, Glacier Lake Outburst Floods (GLOFs) are particularly prevalent on Himalayan glaciers due to debris cover and ice stagnation: debris cover thickens towards the terminus, which is therefore more insulated from warming than up-glacier, causing a reversal of the mass balance gradient, promoting a decrease in the ice gradient (Benn et al., 2012; Hambrey et al., 2009). The flatter ice surface, combined with large moraines caused by relatively stationary termini, promote the storage of supraglacial water dammed by typically fragile moraine-dams, which have been seen to lead to catastrophic outburst floods (e.g. ICIMOD, 2007; Mool, 1995; Somos-Valenzuela et al., 2015; Watanabe et al., 2009). The continued mass loss projected in this thesis will increase the supply of ice melt water, potentially increasing the danger of GLOFs, a conclusion supported by Benn et al. (2012); Thakuri et al. (2015); and Worni et al. (2013), unless adaptive measures are applied. Secondly, glaciers can be popular tourist attractions (e.g. Hall and Higham, 2005) bringing economic advantages to otherwise remote mountain regions. The considerable reduction in glacier mass projected in this thesis will reduce the potential for tourism.

8.4 Potential Areas for Future Research.

This thesis has made several methodological advances and uncovered important findings that provide potential opportunities for further investigation. This section will briefly outline where future research could focus in order to further develop and support the conclusions of this thesis.

8.4.1 Climate Model Processing.

The treatment of climate data in this thesis made every effort to ensure that state-of-the-art GCM and RCM simulations, and sophisticated statistical downscaling methodologies, were

employed. Therefore, the methods and findings of Chapter 3 identified several advances and findings that should be encompassed in future studies and further developed:

- The findings of this thesis indicate that the uncertainty associated with GCM-RCM combinations, and emissions scenarios, is larger than glacio-hydrological modelling uncertainty. Therefore, future studies should aim to incorporate the full range of climate models and emissions scenarios, as more CORDEX simulations are made available. If more CORDEX simulations were available at Khumbu for this thesis, it would have allowed greater separation of GCM uncertainty from RCM uncertainty and would more thoroughly encompass scenario and GCM-RCM uncertainty.
- The quantile-mapping bias correction methodology applied in this thesis is typical of climate projections and *non-glacial* hydrological studies, but has not previously been implemented in glacio-hydrological modelling. Therefore, it is encouraged that glaciological modelling studies should pay increased attention to climate data downscaling, and should build upon the approaches detailed in this thesis.
- Further consideration of the seasonality of the projected temperature and precipitation changes for each model combination, and the extent to which these changes are linked to projected changes in the monsoon, should also be assessed. This will enhance understanding of how climate processes are influencing the projected climate and glacier changes. To consider the uncertainty associated with the statistical downscaling methodology, the bias correction applied here should be compared to the simpler methodologies that have commonly been applied in glacier modelling studies (e.g. delta-change: Farinotti et al., 2012).

8.4.2 Assessment of GERM Uncertainty.

The assessment of the uncertainty associated with GERM, carried out by testing the skill of GERM over 120 years in a way that encompassed all aspects of the model, is unprecedented in existing studies, and is far more appropriate for long-term (e.g. 100 year) future projections than short-term validation periods.

- The findings of this thesis show that modelling uncertainty is substantive, even if the climate-uncertainty remains larger. Therefore, future studies should aim to carry out a similarly rigorous assessment of model performance, particularly in the Alps where long-term data are readily available. These uncertainty assessments should then be applied to future projections, which will contextualise and increase the transparency of projections that are used for impact and adaptation studies.

8.4.3 Modelling Debris-Covered Glaciers: Further Development and Application.

The modifications made to GERM in this thesis represent a first step to incorporating debris cover in glacio-hydrological models and there are several areas where future research could build-upon the work of this thesis.

- The method to calculate melt beneath debris in this thesis should be compared to alternative approaches. For example, an approach similar to that of Ragettli et al. (2016) could be tested, where melt rates beneath debris are calculated according to the heat conduction through the debris, using surface temperature (e.g. from Landsat or ASTER remote-sensing data) and the assumption of 0°C at the debris-ice interface. Although this method can be done without field-data, assuming the heat conduction through the debris layer remains highly uncertain. Nonetheless, this would form an interesting comparison to the method employed in this thesis.
- Since the portable nature of GERM has been maintained in the methodological developments of this thesis, testing the modified form of GERM at other debris-covered glaciers is required. For example, in the Alps, Miage Glacier would allow a thorough validation of GERM due to the long-term data available (e.g. Diolaiuti et al., 2005).
- Model validation in this thesis was necessarily based on discharge data from 2012-2014; however, the recent study of Soncini et al. (2016) conducted mass balance stake measurements that could be used to validate melt rates, and debris thickness measurements that could be used to validate remote-sensing estimates of debris thickness.
- The incorporation of ice cliffs in GERM represents a first-order attempt to assess their influence on glacier evolution that should be further developed. For example, although the evolution of ice cliffs in time is not well-understood (Reid & Brock, 2014), their number is expected to increase with continued ice stagnation (e.g. Iwata et al., 2000), which could be parameterised in GERM if observations of ice cliff expansion over time were available.
- At Himalayan sites, additional data on which to validate the model would be beneficial, thus future studies are encouraged to develop and maintain discharge monitoring stations in Himalayan catchments that could be used, in combination with geodetic mass balance surveys, for model calibration or validation. These data would enable greater awareness of the uncertainties associated with glacio-hydrological modelling in the Himalaya.

- The final suggestion for future work builds upon those aforementioned suggestions and involves applying GERM on a larger scale in Himalayan catchments, therefore building upon this thesis by estimating future glacio-hydrological changes on the regional scale. For example, applying GERM to the Greater Khumbu region, incorporating the Khumbu, Ngozumpa, Nuptse, Lhotse, and Imja Glaciers, will allow estimation of the discharge trends over a wide area, thus providing estimations that are more suited to studies assessing the impacts of glacio-hydrological changes in terms of water resources.

9. CONCLUSIONS.

This thesis has endeavoured to further the understanding of how climate changes will influence glacier evolution and runoff in mountain regions, using GERM to simulate the glacio-hydrological evolution of three catchments in the past and future.

Three novel aims have been addressed:

1) A robust assessment of the modelling uncertainty associated with projected glacier and runoff changes from alpine catchments was carried out by challenging GERM to reproduce historic changes in glacier volume and evolution over 120 year periods, and comparing projected and measured glacier and runoff changes. This represents a more comprehensive uncertainty assessment than any previous studies.
2) This assessment of uncertainty was used to contextualise and understand the precision of future (to 2100 AD) runoff projections for alpine catchments under a wide range of possible climate change scenarios.
3) GERM was developed so that it can now be applied to debris-covered, downwasting glaciers in the Himalayas.

Two further novel aspects of this thesis were the development of a more systematic and robust calibration procedure for GERM, and the application of climate data downscaling techniques that are more sophisticated than have hitherto been applied in glacio-hydrological modelling studies.

9.1 The Assessment of Model Uncertainty.

To achieve aim 1, GERM was used to forward model glacier volume and runoff for the Griesgletscher and Rhonegletscher catchments in the European Alps from 1884-2004, providing the longest assessment of any such glacio-hydrological model yet conducted. GERM was first calibrated to each catchment using contemporary glacier volume and catchment runoff measurements. Improvements to the calibration procedure were made by developing an automated calibration which systematically adjusts the parameters and calculates a combined goodness-of-fit statistic that allows comparison to observations of glacier volume and runoff. The results of model runs from 1884-2004 showed a consistent underestimation of volume losses at Griesgletscher (±0.16 % yr^{-1}) and Rhonegletscher (±0.13 % yr^{-1}), indicative of a changing relationship between temperature and melt that is not incorporated in any glacio-hydrological models, and demonstrating the importance of long term validation to quantify these errors. In terms of discharge, the annual error during the validation period was ±0.04 10^6 m^3 yr^{-1}

(±0.15 % yr^{-1}) at Griesgletscher and ±0.16 10^6 m^3 yr^{-1} (±0.2 % yr^{-1}) at Rhonegletscher. This uncertainty was then applied to the results of future projections.

9.2 The Projections of Future Glacier and Runoff Evolution.

9.2.1 Downscaling of Climate Data.

To achieve aim 2, climate model data was required to drive GERM to conduct future projections. A key novelty of this thesis relates to the downscaling of climate model data in order to address the scale difference between GCM grid box resolution and catchment scale. Specifically, this thesis used the most recently available CMIP5 GCMs that have been dynamically downscaled as part of the CORDEX project. This thesis then further statistically downscaled these simulations using an advanced quantile mapping methodology, thus representing the state-of-the art in dynamical-statistical downscaling. The investigation and testing of quantile mapping identified an 'offset' between historical and evaluation RCM simulations which would lead to a discrepancy when downscaling future RCM data if not accounted for using the 'hybrid' correction approach outlined in this thesis.

These climate data were used to drive simulations of GERM from 2010-2100, with the range of scenarios (RCPs) and range of GCM-RCM combinations providing several projections of future temperature and precipitation. In the Alps, the range of five GCM-RCM combinations and the advanced downscaling methodology provides a wide range of projections of future climate changes, thus providing a comprehensive set of possible future glacio-hydrological estimates that can be utilised by stakeholders. At Khumbu Glacier, this work has shown that the more limited GCM-RCM combinations and the imperfect representation of the influential Indian Monsoon in climate models, leads to less confidence in future climate projections and subsequent future glacio-hydrological projections.

These bias-corrected climate model outputs were used to conduct simulations of future glacier and runoff evolution at Griesgletscher and Rhonegletscher and the glacier and runoff uncertainty calculated from model performance in the past (aim 1), applied to future projections. The combination of these two sources of uncertainty (GERM and climate) provides future projections with greater awareness and better quantification of uncertainties than previous studies. At Khumbu, a smaller range of climate model outputs were available, and the limited data availability prevented assessment of the uncertainty associated with GERM.

9.2.2 Simulating Future Glacier Evolution.

The projections of future glacier evolution in 2100 show considerable ice losses of 87-100 % at Griesgletscher, 70-90 % at Rhonegletscher, and 61-92 % at Khumbu, depending on the RCP scenario, which broadly agree with existing literature. Despite the widespread mass losses, there are notable differences due to the initial size of the glacier and the proportion of ice above the current ELA (e.g. Griesgletscher has only 13 % of current ice above the ELA so cannot sustain ice masses with even a small increase in temperature).

9.2.3 Simulating Future Runoff Evolution.

The projections of future changes in discharge are less consistent than glacier volume changes due to the complicating influence of liquid precipitation and snow-melt. All three sites exhibit an increase in annual runoff that coincides with the loss of glacier mass from the catchment, before reaching peak runoff after which there is a subsequent decline in runoff. However, the timing of peak runoff varies considerably: at Griesgletscher it occurs around 2020; at Rhonegletscher it occurs around 2075; and at Khumbu Glacier it occurs around 2045. Furthermore, both Griesgletscher and Khumbu project an eventual decrease in discharge to below current levels, whereas Rhonegletscher shows no clear trend, indicating that runoff at Rhonegletscher is still decreasing from peak-runoff and is likely to become negative after 2100. The differing response of discharge at Rhonegletscher is indicative of the more stable nature of the glacier, with a large area of high-elevation accumulation area, which delays peak runoff. The seasonality of runoff is also projected to change with earlier onset and longer duration of the melt season accompanied by a reduction in later summer discharge at all sites. In the simulations in the Alps, a key finding is that the main sources of future uncertainty relate to climate inputs, which includes emissions scenarios (RCPs) and GCM-RCM combinations, which lead to variations in projected runoff of ±36 % at Griesgletscher and ±20 % at Rhonegletscher.

9.3 Modifying GERM for Debris-Covered Glaciers.

To achieve aim 3, the mass redistribution process of GERM (Δh-parameterisation) was adjusted to reflect the downwasting behaviour of the debris-covered glacier tongue, based on observed thinning rates at Khumbu Glacier. To account for the insulating effect of debris on ice, the modelled melt rate was reduced in proportion to debris thickness on a fully spatially distributed basis, using observations of reduced melt at glaciers close to Khumbu. These modifications allow GERM to be applied to debris-covered glaciers. Crucially, these modifications can be applied without considerably increasing the data requirements of GERM, needing only geodetic mass

balance (for calibration) and estimations of debris thickness that can be derived from remote-sensing techniques, albeit with uncertainty. Initial testing of these modifications over the period 1999-2010 showed reasonable reproduction of discharge (NSE=0.85). However, due to very limited long-term data in the region, it was not possible to fully assess model performance over long timescales in the same way as the Alps. Thus, further testing of these components and validation against long-term data are strongly recommended.

9.4 Future Contributions.

The three aims of this thesis have contributed several novel additions to knowledge in the fields of glacio-hydrological modelling and downscaling of climate models.

9.4.1 Uncertainty Assessment.

The more rigorous quantification of modelling uncertainty in this thesis represents a more robust assessment of overall uncertainty than any previous glacio-hydrological modelling study. This contextualises future projections and allows mitigation studies to fully understand the results. Therefore, it is encouraged that future modelling studies should seek to incorporate a similarly thorough uncertainty analysis where long term data are available (e.g. in the Alps).

9.4.2 Future Projections and Climate Downscaling.

The future projections of glacier and runoff evolution at Griesgletscher, Rhonegletscher, and Khumbu Glacier provide useful projections of future water resources to a variety of stakeholders. By forcing GERM with a wide range of climate models, downscaled using a sophisticated bias correction methodology, future policy and adaptation studies can use the results as a tool to assess future hydrological responses under differing RCP scenarios.

Moreover, the quantile mapping bias correction methodology applied throughout this thesis, or an equivalent methodology, should be implemented in future glacio-hydrological studies to ensure that the climate inputs used to drive future runoff projections are as good as possible.

9.4.3 Debris-Covered Glaciers.

As a result of the more limited state of Himalayan glacio-hydrological modelling, this is an area where future work could focus. The developments made in this thesis should be further tested and compared to other approaches to estimate melt beneath debris. It is also recommended that the model is validated at debris-covered glacier in the Alps for which long-term data are available. Because GERM has retained its portable nature, despite modifications, a potential

future study could apply GERM in an assessment of regional-scale Himalayan glacio-hydrological response, therefore estimating changes in future water resources on a larger scale.

REFERENCES.

Akhtar, M., Ahmad, N. & Booij, M.J., 2008. The impact of climate change on the water resources of Hindukush{\textemdash}Karakorum{\textemdash}Himalaya region under different glacier coverage scenarios. *Journal of Hydrology*, 355(1-4), pp.148–163.

Akhtar, M., Ahmad, N. & Booij, M.J., 2009. Use of regional climate model simulations as input for hydrological models for the Hindukush-Karakorum-Himalaya region. *Hydrology and Earth System Sciences*, 13(7), pp.1075–1089.

Andermann, C., Bonnet, S. & Gloaguen, R., 2011. Evaluation of precipitation data sets along the Himalayan front. *Geochemistry, Geophysics, Geosystems*, 12(7).

Anderson, L.S. & Anderson, R.S., 2015. Modeling debris-covered glaciers: extension due to steady debris input. *The Cryosphere Discussions*, 9(6), pp.6423–6470.

Anderson, R.S., 2000. A model of ablation-dominated medial moraines and the generation of debris-mantled glacier snouts. *Journal of Glaciology*, 46(154), pp.459–469.

Andréasson, J. et al., 2004. Hydrological change - Climate change impact simulations for Sweden. *Ambio*, 33(4-5), pp.228–234.

Andreassen, L.M. et al., 2015. Ice thickness measurements and volume estimates for glaciers in Norway. *Journal of Glaciology*, 61(228), pp.763–775.

Arnell, N.W., 1999. Climate change and global water resources. In *Global Environmental Change*.

Auer, I. et al., 2007. HISTALP - Historical instrumental climatological surface time series of the Greater Alpine Region. *International Journal of Climatology*, 27(1), pp.17–46.

Baker, D. & Oerter, H., 1982. A glacier discharge model based on results from field studies of energy balance , water storage and flow. *Hydrological Aspects of Alpine and High Mountain Areas*, (138), pp.103–112.

Barnett, T.P., Adam, J.C. & Lettenmaier, D.P., 2005. Potential impacts of a warming climate on water availability in snow-dominated regions. *Nature*, 438(7066), pp.303–309.

Barry, R.G., 1992. *Mountain Weather and Climate* 2nd ed., Taylor & Francis Ltd , Routledge.

Bauder, A., Funk, M. & Huss, M., 2007. Ice-volume changes of selected glaciers in the Swiss Alps since the end of the 19th century. *Annals of Glaciology*, 46, pp.145–149.

Begert, M., Schlegel, T. & Kirchhofer, W., 2005. Homogeneous temperature and precipitation series of Switzerland from 1864 to 2000. *International Journal of Climatology*, 25(1), pp.65–80.

Behera, S.K. & Yamagata, T., 2015. *Indo-Pacific Climate Variability and Predictability: Volume 7 of World Scientific Series on Asia-Pacific Weather and Climate*, World Scientific, 2015.

Beniston, M. & Stoffel, M., 2014. Assessing the impacts of climatic change on mountain water resources. *Science of the Total Environment*, 493, pp.1129–1137.

Benn, D.I. & Lehmkuhl, F., 2000. Mass balance and equilibrium-line altitudes of glaciers in high-mountain environments. *Quaternary International*, 65-66, pp.15–29.

Benn, D.I. & Evans, D.J.A., 2010. Glaciers and Glaciation. In *Glaciers and Glaciation*. p. 816.

Benn, D.I. et al., 2012. Response of debris-covered glaciers in the Mount Everest region to recent warming, and implications for outburst flood hazards. *Earth-Science Reviews*, 114(1-2), pp.156–174.

Bennett, J.C. et al., 2011. Performance of quantile-quantile bias-correction for use in hydroclimatological projections. *19th International Congress on Modelling and Simulation*, (December), pp.12–16

Bergstrom, S., 1955. *The HBV Model*, Water Resources Publications: Highlands Ranch, Colorado, USA.

Bergstroem, S., 1976. Development and Application of a conceptual runoff model fro Scandinavian catchment. , (January), p.153.

Bernath, A., 1991. *Zum Wasserhaushalt im Einzugsgebiet der Rhone bis Gletsch. Untersuchungen zu Niederschlag, Verdunstung und Abfluss in einem teilweise vergletscherten Einzugsgebiet.*,

Bernhardt, M. & Schulz, K., 2010. SnowSlide: A simple routine for calculating gravitational snow

transport. *Geophysical Research Letters*, 37(11), pp.1–6.
Berthier, E. et al., 2007. Remote sensing estimates of glacier mass balances in the Himachal Pradesh (Western Himalaya, India). *Remote Sensing of Environment*, 108(3), pp.327–338.
Birsan, M.V. et al., 2005. Streamflow trends in Switzerland. *Journal of Hydrology*, 314(1-4), pp.312–329.
Blöschl, G., Kirnbauer, R. & Gutknecht, D., 1991. Distributed Snowmelt Simulations in an Alpine Catchment: 1. Model Evaluation on the Basis of Snow Cover Patterns. *Water Resources Research*, 27(12), pp.3171–3179.
Boberg, F. et al., 2007. *Danish Climate Centre Report 07-03 Analysis of temporal changes in precipitation intensities using PRUDENCE data*,
Boé, J. et al., 2007. Statistical and dynamical downscaling of the Seine basin climate for hydro-meteorological studies. *International Journal of Climatology*, 27(12), pp.1643–1655.
Bolch, T. et al., 2008. Planimetric and volumetric glacier changes in the Khumbu Himal, Nepal, since 1962 using Corona, Landsat TM and ASTER data. *Journal of Glaciology*, 54(187), pp.592–600.
Bolch, T., Pieczonka, T. & Benn, D.I., 2011. Multi-decadal mass loss of glaciers in the Everest area (Nepal Himalaya) derived from stereo imagery. *The Cryosphere*, 5(2), pp.349–358.
Bolch, T. et al., 2012. The State and Fate of Himalayan Glaciers. *Science*, 336(6079), pp.310–314.
Bookhagen, B. & Burbank, D.W., 2010. Toward a complete Himalayan hydrological budget: Spatiotemporal distribution of snowmelt and rainfall and their impact on river discharge. *Journal of Geophysical Research: Earth Surface*, 115(3).
Box, G.E.P., & Draper, N.R., 2014, Evolutionary Operation (EVOP), *Wiley StatsRef: Statistics Reference Online.*
Bradley, R.S., Keimig, F.T. & Diaz, H.F., 2004. Projected temperature changes along the American cordillera and the planned GCOS network. *Geophysical Research Letters*, 31(16).
Bradley, R.S. et al., 2006. Threats to Water Supplies in the Tropical Andes. *Science*, 312(5781), pp.1755–1756.
Bradley, R.S. et al., 2009. Recent changes in freezing level heights in the Tropics with implications for the deglacierization of high mountain regions. *Geophysical Research Letters*, 36(17), pp.2–5.
Braithwaite, R.J., 1995. Positive degree-day factors for ablation on the Greenland Ice-sheet studied by energy balance modeling. *Journal of Glaciology*, 41(137), pp.153–160.
Braithwaite, R.J. & Zhang, Y., 2000. Sensitivity of mass balance of five Swiss glaciers to temperature changes assessed by tuning a degree-day model. *Journal of Glaciology*, 46(152), pp.7–14.
Braun, L.N., Grabs, W. & Rana, B., 1993. Application of a Conceptual Precipitation- Runoff Model in the Langtang Khola Basin , Nepal Himalaya. *Iahs*, 218(218), pp.221–237.
Braun, L.N. et al., 1994. Measurements and simulation of high alpine water balance components in the Linth-Limmern head watershed (north-eastern Switzerland). *Zeitschrift für Gletscherkunde und Glazialgeologie*, 30(1994), pp.161–185.
Braun, L.N., Weber, M. & Schulz, M., 2000. Consequences of climate change for runoff from Alpine regions. *Annals of Glaciology*, 31, pp.19–25.
Bruce, J.P. & Clark, R.H., 1981. *Inctoruction to Hydrometeorology* P. O. Press, ed.,
Cannone, N. et al., 2008. Accelerating climate change impacts on alpine glacier forefield ecosystems in the European Alps. *Ecological Applications*, 18(3), pp.637–648.
Carenzo, M. et al., 2009. Assessing the transferability and robustness of an enhanced temperature-index glacier-melt model. *Journal of Glaciology*, 55(190), pp.258–274.
Carenzo, M. et al., 2016. An enhanced debris temperature index model accounting for thickness effect. *Advances in Water Resources*, 94, pp.457–469.
Carenzo, M., 2012. *Distributed modelling of changes in glacier mass balance and runoff*. ETH.
Casey, K.A., Kaab, A. & Benn, D.I., 2012. Geochemical characterization of supraglacial debris via in situ and optical remote sensing methods: A case study in Khumbu Himalaya, Nepal. *Cryosphere*, 6(1), pp.85–100.

Chaturvedi, R.K. et al., 2012. Multi-model climate change projections for India under representative concentration pathways. *Current Science*, 103(7), pp.791–802.

Chen, J. et al., 2011. Overall uncertainty study of the hydrological impacts of climate change for a Canadian watershed. *Water Resources Research*, 47(12).

Chen, J. et al., 2013. Performance and uncertainty evaluation of empirical downscaling methods in quantifying the climate change impacts on hydrology over two North American river basins. *Journal of Hydrology*, 479, pp.200–214.

Christensen, J.H., Carter, T.R. & Giorgi, F., 2002. PRUDENCE employs new methods to assess European climate change. *Eos, Transactions American Geophysical Union*, 83(13), p.147.

Christensen, J.H. et al., 2013. Climate Phenomena and their Relevance for Future Regional Climate Change Supplementary Material. *Climate Change 2013: The Physical Science Basis. Contribution of Working Group I to the Fifth Assessment Report of the Intergovernmental Panel on Climate Change*, p.62.

Collier, E. et al., 2015. Impact of debris cover on glacier ablation and atmosphere–glacier feedbacks in the Karakoram. *The Cryosphere*, 9(4), pp.1617–1632.

Collins, D.N., Davenport, J.L. & Stoffel, M., 2013. Climatic variation and runoff from partially-glacierised Himalayan tributary basins of the Ganges. *Science of the Total Environment*, 468-469.

Collins, M. et al., 2013. Long-term Climate Change: Projections, Commitments and Irreversibility. In *Climate Change 2013: The Physical Science Basis. Contribution of Working Group I to the Fifth Assessment Report of the Intergovernmental Panel on Climate Change*. pp. 1029–1136.

Cuffey, K.M. & Paterson, W.S.. B., 2010. *Physics of Glaciers, Fourth Edition*, Academic Press.

Daly, C., Neilson, R.P. & Phillips, D.L., 1994. A Statistical-Topographic Model for Mapping Climatological Precipitation over Mountainous Terrain. *Journal of Applied Meteorology*, 33, pp.140–158.

Dawson, C.W. & Wilby, R.L., 2001. Hydrological modelling using artificial neural networks. *Progress in Physical Geography*, 25(1), pp.80–108.

Dee, D.P. et al., 2011. The ERA-Interim reanalysis: Configuration and performance of the data assimilation system. *Quarterly Journal of the Royal Meteorological Society*, 137(656), pp.553–597.

Déqué, M., 2007. Frequency of precipitation and temperature extremes over France in an anthropogenic scenario: Model results and statistical correction according to observed values. *Global and Planetary Change*, 57(1-2), pp.16–26.

Deser, C. et al., 2012. Uncertainty in climate change projections: The role of internal variability. *Climate Dynamics*, 38(3-4), pp.527–546.

Dettinger, M.D. et al., 2004. Simulated hydrologic responses to climate variations and change in the Merced, Carson, and American River basins, Sierra Nevada, California, 1900-2099. *Climatic Change*, 62(1-3), pp.283–317.

Diaz, H.F. et al., 2006. The Impact of Climate Change in the American Cordillera. *EOS Trans*, 87(32), p.315.

Diolaiuti, G. et al., 2005. Calving processes and lake evolution at Miage glacier, Mont Blanc, Italian Alps. *Annals of Glaciology*, 40, pp.207–214.

Doblas-Reyes, F.J., Pavan, V. & Stephenson, D.B., 2003. The skill of multi-model seasonal forecasts of the wintertime North Atlantic Oscillation. *Climate Dynamics*, 21(5-6), pp.501–514.

Dowdeswell, J.A. et al., 2002. Form and flow of the Academy of Sciences Ice Cap, Severnaya Zemlya, Russian High Arctic. *Journal of Geophysical Research-Solid Earth*, 107(B4).

Dubrovský, M., Buchtele, J. & Žalud, Z., 2004. High-frequency and low-frequency variability in stochastic daily weather generator and its effect on agricultural and hydrologic modelling. *Climatic Change*, 63(1-2), pp.145–179.

Eden, J.M. et al., 2014. Comparison of GCM- and RCM-simulated precipitation following stochastic postprocessing. *Journal of Geophysical Research: Atmospheres*, 119(19),

pp.11040–11053.
EEA, 2009. Regional climate changes and adaptation: The Alps facing the challenge of changing water resources. Journal of Glaciology, 8, pp.143.
Elsasser, H. & Bürki, R., 2002. Climate change as a threat to tourism in the Alps. *Climate Research*, 20(3), pp.253–257.
Energy, S.F.O. of, 2013. Energy Statistics. Available at: http://www.bfe.admin.ch/themen/00526/00541/00542/index.html?lang=en.
Farinotti, D., Huss, M., Bauder, A., Funk, M., et al., 2009a. A method to estimate the ice volume and ice-thickness distribution of alpine glaciers. *Journal of Glaciology*, 55(191), pp.422–430.
Farinotti, D., Huss, M., Bauder, A. & Funk, M., 2009b. An estimate of the glacier ice volume in the Swiss Alps. *Global and Planetary Change*, 68(3), pp.225–231.
Farinotti, D., 2010. Simple methods for inferring glacier ice-thickness and snow-accumulation distributio. *Methods*, (19268), p.101.
Farinotti, D. et al., 2012. Runoff evolution in the Swiss Alps: projections for selected high-alpine catchments based on ENSEMBLES scenarios. *Hydrological Processes*, 26(13), pp.1909–1924.
Farinotti, D., 2013. On the effect of short-term climate variability on mountain glaciers: Insights from a case study. *Journal of Glaciology*, 59(217), pp.992–1006.
Farinotti, D., Pistocchi, A. & Huss, M., 2016. From dwindling ice to headwater lakes: could dams replace glaciers in the European Alps? *Environmental Research Letters*, 11(5), p.054022.
Finger, D. et al., 2012. Projections of future water resources and their uncertainty in a glacierized catchment in the Swiss Alps and the subsequent effects on hydropower production during the 21st century. *Water Resources Research*, 48(2), pp.1–20.
Finger, D. et al., 2013. Identification of glacial meltwater runoff in a karstic environment and its implication for present and future water availability. *Hydrology and Earth System Sciences*, 17(8), pp.3261–3277.
Finger, D. et al., 2015. The value of multiple dataset calibration versus model complexity for improving the performance of hydrological models in mountain catchments. Water Resources Research, 51(4).
Forster, P. et al., 2007. Changes in Atmospheric Constituents and in Radiative Forcing. In *Climate Change 2007: The Physical Science Basis. Contribution of Working Group I to the Fourth Assessment Report of the Intergovernmental Panel on Climate Change*. pp.129–234.
Foster, L.A. et al., 2012. A physically based method for estimating supraglacial debris thickness from thermal band remote-sensing data. *Journal of Glaciology*, 58(210), pp.677–691.
Fowler, H.J., Kilsby, C.G. & O'Connell, P.E., 2000. A stochastic rainfall model for the assessment of regional water resource systems under changed climatic conditions. *Hydrology and Earth System Sciences*, 4, pp.263–282.
Fowler, H.J. et al., 2005. A weather-type conditioned multi-site stochastic rainfall model for the generation of scenarios of climatic variability and change. *Journal of Hydrology*, 308(1-4), pp.50–66.
Fowler, H.J., Blenkinsop, S. & Tebaldi, C., 2007. Linking climate change modelling to impacts studies: Recent advances in downscaling techniques for hydrological modelling. *International Journal of Climatology*, 27(12), pp.1547–1578.
Francou, B. et al., 2003. Tropical climate change recorded by a glacier in the central Andes during the last decades of the twentieth century: Chacaltaya, Bolivia, 16°S. *Journal of Geophysical Research*, 108(D5), pp.1–12.
Frei, C., 2007. Die Klimazukunft der Schweiz. Klimaänderung und die Schweiz 2050 - Erwartete Auswirkungen auf Umwelt, Gesellschaft und Wirtschaft. Beratendes Organ für Fragen der Klimaänderung. , 12-16.
Frei, C. & Schar, C., 1998. A precipitation climatology of the Alps from high-resolution rain-gauge observations. *International Journal of Climatology*, 18(8), pp.873–900.
Frey, S. & Holzmann, H., 2015. A conceptual, distributed snow redistribution model. *Hydrology*

and Earth System Sciences, 19(11), pp.4517–4530.
Fuhrer, J., Smith, P. & Gobiet, A., 2014. Implications of climate change scenarios for agriculture in alpine regions - A case study in the Swiss Rhone catchment. *Science of the Total Environment*, 493, pp.1232–1241.
Fujita, K. et al., 2008. Performance of ASTER and SRTM DEMs, and their potential for assessing glacial lakes in the Lunana region, Bhutan Himalaya. *Journal of Glaciology*, 54(185), pp.220–228.
Fujita, K. & Sakai, A., 2014. Modelling runoff from a Himalayan debris-covered glacier. *Hydrology and Earth System Sciences*, 18(7), pp.2679–2694.
Fyffe, C.L. et al., 2014. A distributed energy-balance melt model of an alpine debris-covered glacier. *Journal of Glaciology*, 60(221), pp.587–602.
Gabbi, J. et al., 2012. Ice volume distribution and implications on runoff projections in a glacierized catchment. *Hydrology and Earth System Sciences*, 16(12), pp.4543–4556.
Gabbi, J. et al., 2014. A comparison of empirical and physically based glacier surface melt models for long-term simulations of glacier response. *Journal of Glaciology*, 60(224), pp.1140–1154.
Gades, A. et al., 2000. Radio echo-sounding through supraglacial debris on Lirung and Khumbu Glaciers, Nepal Himalayas. *IAHS Publication*, 264(264), pp.13–22.
Gardelle, J. et al., 2013. Region-wide glacier mass balances over the Pamir-Karakoram-Himalaya during 1999–2011. *The Cryosphere*, 7(4), pp.1263–1286.
Gardner, A.S. et al., 2013. A reconciled estimate of glacier contributions to sea level rise: 2003 to 2009. *Science (New York, N.Y.)*, 340(6134), pp.852–7.
Ghimire, S., Choudhary, A. & Dimri, A.P., 2015. Assessment of the performance of CORDEX-South Asia experiments for monsoonal precipitation over the Himalayan region during present climate: part I. *Climate Dynamics*, pp.1–24.
Giorgi, F., Jones, C. & Asrar, G.R., 2009. Addressing climate information needs at the regional level: the CORDEX framework. *Bulletin - World Meteorological Organization*, 58(3), pp.175–183.
Glen, J.W., 1955. The creep of polycrystalline ice. *Proceedings of the Royal Society A*, 228(1175), pp.519–538.
Golubev, V.S., Groisman, R.G.Q., 1992. An Evaluation of the United States Standard 8-in. Nonrecording Raingage at the Valdai Polygon, Russia. *Journal of Atmospheric and Oceanic Technology*, 49(5), pp.624–629.
Graham, L.P., Hagemann, S., et al., 2007a. On interpreting hydrological change from regional climate models. *Climatic Change*, 81(S1), pp.97–122.
Graham, L.P., Andréasson, J. & Carlsson, B., 2007b. Assessing climate change impacts on hydrology from an ensemble of regional climate models, model scales and linking methods – a case study on the Lule River basin. *Climatic Change*, 81(S1), pp.293–307.
Grayson, R.B. et al., 2002. Advances in the use of observed spatial patterns of catchment hydrological response. *Advances in Water Resources,* 25, 1313–1334.
Greuell, W. & Genthon, C., 2004. Modelling land-ice surface mass balance. In *Mass Balance of the Cryosphere*. pp. 117–168.
Gurtz, J., Baltensweiler, A. & Lang, H., 1999. Spatially distributed hydrotope-based modelling of evapotranspiration and runoff in mountainous basins. *Hydrological Processes*, 13(17), pp.2751–2768.
Guyennon, N. et al., 2013. Benefits from using combined dynamical-statistical downscaling approaches – lessons from a case study in the Mediterranean region. *Hydrology and Earth System Sciences*, 17(2), pp.705–720.
Hagg, W. et al., 2007. Modelling of hydrological response to climate change in glacierized Central Asian catchments. *Journal of Hydrology*, 332(1-2), pp.40–53.
Hagg, W. et al., 2006. Runoff modelling in glacierized Central Asian catchments for present-day and future climate. *Nordic Hydrology*, 37, pp.93–105.
Hagg, W. et al., 2008. Sub-debris melt rates on southern Inylchek Glacier, central Tian Shan. *Geografiska Annaler, Series A: Physical Geography*, 90 A(1), pp.55–63.

Hall, C.M. & Higham, J.E.S., 2005. *Tourism, recreation and climate change*.

Hambrey, M.J., 1977. Structures In Ice Cliffs At The Snouts Swiss Glaciers. *Journal of Glaciology*, 18(80), pp.407–414.

Hambrey, M.J. & Milnes, A.G., 1977. Structural geology of an Alpine glacier Structural geology of an Alpine glacier. *Eclogae Geologicae Helvetiae*, 70(3), pp.667–684.

Hambrey, M.J., Milnes, A.G. & Siegenthaler, H., 1980. Dynamics and structure of Griesgletscher, Switzerland. *Journal of Glaciology*, 25(92), pp.215–228.

Hambrey, M.J. et al., 2009. Sedimentological, geomorphological and dynamic context of debris-mantled glaciers, Mount Everest (Sagarmatha) region, Nepal. *Quaternary Science Reviews*, 28(25-26), p.1084.

Hamon, W.R., 1960. Estimating potential evapotranspiration. *Doctoral dissertation, Massachusetts Institute of Technology*, 87, pp.107–120.

Harrold, T.I. & Jones, R., 2003. Downscaling of GCM rainfall: A refinement of the perturbation method. In *EGS - AGU - EUG Joint Assembly*.

Hauenstein, W., 2005. Hydropower and Climate Change—A Reciprocal Relation: Institutional Energy Issues in Switzerland. *Mountain Research and Development*, 25(4), pp.321–325.

Hay, L.E., Wilby, R.L. & Leavesley, G.H., 2000. A Comparison of Delta Change and Downscaled Gcm Scenarios for Three Mounfainous Basins in the United States1. *JAWRA Journal of the American Water Resources Association*, 36(2), pp.387–397.

Hock, R., 1999. A distributed temperature-index ice-and snowmelt model including potential direct solar radiation. *Journal of Glaciology*, 45(149), pp.101–111.

Hock, R., 2003. Temperature index melt modelling in mountain areas. *Journal of Hydrology*, 282(1-4), pp.104–115.

Hock, R., 2005. Glacier melt: a review of processes and their modelling. *Progress in Physical Geography*, 29(3), pp.362–391.

Hock, R., Jansson, P. & Braun, L., 2005. Modelling the response of mountain glacier discharge to climate warming. *Global Change and Mountain Regions*, (Ipcc 2001), pp.243–252.

Hock, R. & Noetzli, C., 1997. Areal melt and discharge modelling of Storglaci??ren, Sweden. *Annals of Glaciology*, 24, pp.211–216.

Horton, P. et al., 2006. Assessment of climate-change impacts on alpine discharge regimes with climate model uncertainty. *Hydrological Processes*, 20(10), pp.2091–2109.

Houghton, J., 2009. Global warming: the complete briefing. *Eos, Transactions American Geophysical Union*, p.454.

Humlum, O., 1998. The climatic significance of rock glaciers. *Permafrost and Periglacial Processes*, 9(4), pp.375–395.

Huss, M., 2011. Present and future contribution of glacier storage change to runoff from macroscale drainage basins in Europe. *Water Resources Research*, 47(7), p.n/a–n/a

Huss, M. & Farinotti, D., 2014. A high-resolution bedrock map for the Antarctic Peninsula. *Cryosphere*, 8(4), pp.1261–1273.

Huss, M., Hock, R., et al., 2010. 100-year mass changes in the Swiss Alps linked to the Atlantic Multidecadal Oscillation. *Geophysical Research Letters*, 37(10).

Huss, M. & Farinotti, D., 2012. Distributed ice thickness and volume of all glaciers around the globe. *Journal of Geophysical Research*, 117(F4), p.F04010.

Huss, M. & Hock, R., 2015. A new model for global glacier change and sea-level rise. *Frontiers in Earth Science*, 3, pp.1–22.

Huss, M., Bauder, A. & Funk, M., 2009a. Homogenization of long-term mass-balance time series. *Annals of Glaciology*, 50(50), pp.198–206.

Huss, M., Funk, M. & Ohmura, a., 2009b. Strong Alpine glacier melt in the 1940s due to enhanced solar radiation. *Geophysical Research Letters*, 36(November), pp.1–5.

Huss, M. et al., 2008a. Modelling runoff from highly glacierized alpine drainage basins in a changing climate. *Hydrological Processes*, 22(19), pp.3888–3902.

Huss, M. et al., 2008b. Determination of the seasonal mass balance of four Alpine glaciers since 1865. *Journal of Geophysical Research*, 113(F1), p.F01015.

Huss, M. et al., 2010a. Future high-mountain hydrology: a new parameterization of glacier retreat. *Hydrology and Earth System Sciences*, 14(5), pp.815–829.

Huss, M., et al., 2010b. Glacier mass balance in the south-eastern Swiss Alps since 1900 and perspectives for the future. *Erdkunde*, 2010(2), pp.119–140.

Huss, M., 2012. Extrapolating glacier mass balance to the mountain-range scale: The European Alps 1900-2100. *Cryosphere*, 6(4), pp.713–727.

Huss, M. et al., 2014. High uncertainty in 21st century runoff projections from glacierized basins. *Journal of Hydrology*, 510, pp.35–48.

Huss, M. et al., 2017. Toward mountains without permanent snow and ice. Earth's Future, 5, pp.418-435.

Hutter et al., 2011. Sequential model-based optimization for general algorithm configuration. *Proceedings of the 5th international conference on Learning and Intelligent Optimization.* Pp.507-523.

Ichiyanagi, K. et al., 2007. Precipitation in Nepal between 1987 and 1996. *International Journal of Climatology*, 27(13), pp.1753–1762.

ICIMOD, 2007. Impact of climate change on himalayan glaciers and glacial lakes - Case studies on GLOF and associated hazards in Nepal and Bhutan. *Rapport final*, pp.1–127.

IHA, 2013. *International Hydropower Assiciation Annual Hydropower Report*.

Immerzeel, W., 2008. Historical trends and future predictions of climate variability in the Brahmaputra basin. *International Journal of Climatology*, 28(2), pp.243–254.

Immerzeel, W.W., van Beek, L.P.H. & Bierkens, M.F.P., 2010. Climate Change Will Affect the Asian Water Towers. *Science*, 328(5984), pp.1382–1385.

Immerzeel, W.W. et al., 2012. Hydrological response to climate change in a glacierized catchment in the Himalayas. *Climatic change*, 110(3-4), pp.721–736.

Immerzeel, W.W., Pellicciotti, F. & Bierkens, M.F.P., 2013. Rising river flows throughout the twenty-first century in two Himalayan glacierized watersheds. *Nature Geoscience*, 6(9), pp.742–745.

Immerzeel, W.W. et al., 2015. Reconciling high-altitude precipitation in the upper Indus basin with glacier mass balances and runoff. *Hydrology and Earth System Sciences*, 19(11), pp.4673–4687.

Ines, A.V.M. & Hansen, J.W., 2006. Bias correction of daily GCM rainfall for crop simulation studies. *Agricultural and Forest Meteorology*, 138(1-4), pp.44–53.

Inoue, J., 1977. Mass budget of Khumbu Glacier. *Seppyo1*, 39, pp.15–19.

Inoue, J. & Yoshida, M., 1980. Ablation and Heat Exchange over the Khumbu Glacier. *Journal of the Japanese Society of Snow and Ice*, 41(Special), pp.26–33.

IPCC5 WGII, 2014. *Climate Change 2013*,

Irvine-Fynn, T.D.L., 2008. *Modelling runoff from the maritime arctic cryosphere: Water storage and routing at Midtre Lovenbreen*. Sheffield.

Isotta, F.A. et al., 2014. The climate of daily precipitation in the Alps: Development and analysis of a high-resolution grid dataset from pan-Alpine rain-gauge data. *International Journal of Climatology*, 34(5), pp.1657–1675.

Iwata, S. et al., 2000. Morphological evolution of the debris cover on Khumbu Glacier, Nepal, between 1978 and 1995. In *IAHS Publication*. pp. 3–11.

Jain, S.K., 2008. Impact of retreat of Gangotri glacier on the flow of Ganga River. *Current Science*, 95(8), pp.1012–1014.

Jakob Themeßl, M., Gobiet, A. & Leuprecht, A., 2011. Empirical-statistical downscaling and error correction of daily precipitation from regional climate models. *International Journal of Climatology*, 31(10), pp.1530–1544.

Jansson, P., Hock, R. & Schneider, T., 2003. The concept of glacier storage: A review. *Journal of Hydrology*, 282(1-4), pp.116–129.

Jarvis, A. et al., 2008. Hole-filled SRTM for the globe version 4. Available at: srtm.csi.cgiar.org.

Johannesson, T., 1997. The response of two Icelandic glaciers to climatic warming computed with a degree-day glacier mass-balance model coupled to a dynamic glacier model. *Journal of Glaciology*, 43(144), pp.321–327.

Jouvet, G. et al., 2009. Numerical simulation of Rhonegletscher from 1874 to 2100. *Journal ofComputational Physics*, 228(17), pp.6426–6439.

Jouvet, G. et al., 2011a. Modelling and Numerical Simulation of the Dynamics of Glaciers Including Local Damage Effects. *Mathematical Modelling of Natural Phenomena*, 6(5), pp.263–280.

Jouvet, G. et al., 2011b. Modelling the retreat of Grosser Aletschgletscher, Switzerland, in a changing climate. *Journal of Glaciology*, 57(206), pp.1033–1045.

Junghans, N., Cullmann, J. & Huss, M., 2015. Evaluating the effect of snow and ice melt in an Alpine headwater catchment and further downstream in the River Rhine catchment and further downstream in the River Rhine, 6667.

Kaab, a et al., 2002. Glacier monitoring from ASTER imagery: accuracy and applications. *Proceedings of EARSeL-LISSIG-Workshop Observing our Cryosphere from Space*, (2), pp.43–53.

Kääb, A. et al., 2012. Contrasting patterns of early twenty-first-century glacier mass change in the Himalayas. *Nature*, 488(7412), pp.495–8.

Kayastha, R.B. et al., 2000. Practical prediction of ice melting beneath various thickness of debris cover on Khumbu Glacier, Nepal, using a positive degree-day factor. *Debris-Covered Glaciers*, (264), pp.71–81.

Kehrwald, N.M. et al., 2008. Mass loss on Himalayan glacier endangers water resources. *Geophysical Research Letters*, 35(22), p.L22503.

Kirkbride, M.P. & Deline, P., 2013. The formation of supraglacial debris covers by primary dispersal from transverse englacial debris bands. *Earth Surface Processes and Landforms*, 38(15), pp.1779–1792.

Klok, E.J. et al., 2001. Distributed hydrological modelling of a heavily glaciated Alpine river basin. *Hydrological Sciences Journal*, 46(August 2001), pp.553–570.

Knutson, T.R. et al., 2006. Assessment of twentieth-century regional surface temperature trends using the GFDL CM2 coupled models. *Journal of Climate*, 19(9), pp.1624–1651.

Kobierska, F. et al., 2013. Future runoff from a partly glacierized watershed in Central Switzerland: A two-model approach. *Advances in Water Resources*, 55, pp.204–214.

Koboltschnig, G.R., Schöner, W., et al., 2008a. Glaciermelt of a small basin contributing to runoff under the extreme climate conditions in the summer of 2003. *Hydroogical Processes*, 23(7), pp.1010–1018.

Koboltschnig, G.R., Scherner, W., et al., 2008b. Runoff modelling of the glacierized Alpine Upper Salzach basin (Austria): Multi-criteria result validation. In *Hydrological Processes*. pp. 3950–3964.

Koenig, U. & Abegg, B., 1997. Impacts of Climate Change on Winter Tourism in the Swiss Alps. *Journal of Sustainable Tourism*, 5(May 2015), pp.46–58.

Konrad, S.K. & Humphrey, N.F., 2000. Steady-state flow model of debris-covered glaciers (rock glaciers). *Iahs Publication*, (264), pp.255–266.

Konya, K., Matsumoto, T. & Naruse, R., 2004. Surface heat balance and spatially distributed ablation modelling at Koryto Glacier, Kamchatka peninsula, Russia. *Geografiska Annaler: Series …*, (2000), pp.337–348.

Konz, M. et al., 2006. Regionalization of a distributed catchment model for highly glacierized Nepalese headwater catchments. *Iahs Publication*, (308), pp.454–459.

Konz, M. et al., 2007. Implementation of a process-based catchment model in a poorly gauged, highly glacierized Himalayan headwater. *Hydrology and Earth System Sciences*, 11(4), pp.1323–1339.

Kotlarski, S., Paul, F. & Jacob, D., 2010. Forcing a distributed glacier mass balance model with the regional climate model REMO. Part I: climate model evaluation. *Journal of Climate*, 23(6), pp.1589–1606.

Kotlarski, S. et al., 2014. Regional climate modeling on European scales: a joint standard evaluation of the EURO-CORDEX RCM ensemble. *Geoscientific Model Development*, 7(4), pp.1297–1333.

Krause, P., Boyle, D.P. & Bäse, F., 2005. Comparison of different efficiency criteria for

hydrological model assessment. *Advances in Geosciences*, 5, pp.89–97.
Laghari., J.R., 2013. Melting glaciers bring energy uncertainty. *Nature*, 502, pp.617–8.
Lal, M., 2011. Implications of climate change in sustained agricultural productivity in South Asia. *Regional Environmental Change*, 11(SUPPL. 1), pp.79–94.
Lal, M. & Harasawa, H., 2001. Future climate change scenarios for Asia as inferred from selected coupled atmosphere-ocean global climate models. *Journal of the Meteorological Society of Japan. Ser. II*, 79(1), pp.219–227.
Lang, H., Schadler B., Davidson, G., 1977. Hydrological Investigations on the Ewigschneefeld - Gr. Aletschgletscher. *Glazialgeol*, 12, pp.109–124.
Langbein, W.B., 1958. Queuing Theory and Water Storage. *Journal of the Hydraulics Division*, 84(5), pp.1–24.
Legates, D.R. & McCabe Jr., G.J., 1999. Evaluating the use of “goodness-of-fit” Measures in hydrologic and hydroclimatic model validation. *Water Resour. Res.*, 35(1), pp.233–241.
Lehning, M. et al., 2008. Inhomogeneous precipitation distribution and snow transport in steep terrain. *Water Resources Research*, 44(7).
Li, H. et al., 2015. Integrating a glacier retreat model into a hydrological model – Case studies of three glacierised catchments in Norway and Himalayan region. , 527, pp.656–667.
Li, H. et al., 2016. Water Resources Under Climate Change in Himalayan Basins. , pp.843–859.
Van der Linden, P. & Mitchell, J.F.B.F.B., 2009. *ENSEMBLES: Climate Change and its Impacts: Summary of research and results from the ENSEMBLES project*.
Liston, G.E. et al., 1999. Below-surface ice melt on the coastal Antarctic ice sheet. *Journal of Glaciology*, 45(150), pp.273–285.
Liu, Z. & Todini, E., 2002. Towards a comprehensive physically-based rainfall-runoff model. *Hydrology and Earth System Sciences*, 6(5), pp.859–881.
Lutz, A.F. et al., 2013. Comparison of climate change signals in CMIP3 and CMIP5 multi-model ensembles and implications for Central Asian glaciers. *Hydrology and Earth System Sciences*, 17(9), pp.3661–3677.
Lutz, a. F. et al., 2014. Consistent increase in High Asia's runoff due to increasing glacier melt and precipitation. *Nature Climate Change*, 4(7), pp.587–592.
Machguth, H. et al., 2009. Calculating distributed glacier mass balance for the Swiss Alps from regional climate model output: A methodical description and interpretation of the results. *Journal of Geophysical Research Atmospheres*, 114(19).
Machguth, H., Haeberli, W. & Paul, F., 2012. Mass-balance parameters derived from a synthetic network of mass-balance glaciers. *Journal of Glaciology*, 58(211), pp.965–979.
Mackintosh, B. M. et al., 2017. Regional cooling caused recent New Zealand glacier advances in a period of global warming. *Nature Communications*, 8,14202, doi: 10.1038/ncomms14202.
Maraun, D. et al., 2010. Precipitation downscaling under climate change: Recent developments to bridge the gap between dynamical models and the end user. *Reviews of Geophysics*, 48(3).
Martinec, J. & Rango, A., 1986. Parameter values for snowmelt runoff modelling. *Journal of Hydrology*, 84(3-4), pp.197–219.
Mathison, C. et al., 2013. Regional projections of North Indian climate for adaptation studies. *Science of the Total Environment*, 468-469.
Mathworks, Inc., 2018a, MATLAB and Statistics Toolbox Release 2015a, Statistics and Machine Learning Toolbox, The MathWorks, Inc., Natick, Massachusetts, United States. https://uk.mathworks.com/help/stats/gamfit.html [accessed 25/03/2018]
Mathworks, Inc., 2018b, MATLAB and Statistics Toolbox Release 2015a, Statistics and Machine Learning Toolbox, The MathWorks, Inc., Natick, Massachusetts, United States. https://uk.mathworks.com/help/stats/normfit.html [accessed 25/03/2018]
Mayr, E. et al., 2013. Calibrating a spatially distributed conceptual hydrological model using runoff, annual mass balance and winter mass balance. *Journal of Hydrology*, 478, pp.40–

49.
McGuffie, K., & Henderson-Sellers, A., 2005. *A Climate Modelling Primer*.
Mihalcea, C., Mayer, C., et al., 2008. Spatial distribution of debris thickness and melting from remote-sensing and meteorological data, at debris-covered Baltoro glacier, Karakoram, Pakistan. In *Annals of Glaciology*. pp. 49–57.
Mihalcea, C., Brock, B.W., et al., 2008. Using ASTER satellite and ground-based surface temperature measurements to derive supraglacial debris cover and thickness patterns on Miage Glacier (Mont Blanc Massif, Italy). *Cold Regions Science and Technology*, 52(3), pp.341–354.
Miles, E.S. et al., 2016. Refined energy-balance modelling of a supraglacial pond, Langtang Khola, Nepal. *Annals of Glaciology*, 57(71), pp.29–40.
Miller, J.D., Immerzeel, W.W. & Rees, G., 2012. Climate Change Impacts on Glacier Hydrology and River Discharge in the Hindu Kush–Himalayas. *Mountain Research and Development*, 32(4), pp.461–467.
Mool, P.K., 1995. Glacier lake outburst floods in Nepal. *Journal of Nepal Geological Society*, 11, pp.273–280.
Moors, E.J. & Stoffel, M., 2013. Changing monsoon patterns, snow and glacial melt, its impacts and adaptation options in Northern India: Synthesis. *Science of the Total Environment*, 468-469, pp.S162–S167.
Moribayashi, S., 1978. Transverse profiles of Khumbu Glacier obtained by gravity observation: glaciological expedition of Nepal. *Seppyo*, 46(40), pp.21–25.
Moss, R.H. et al., 2010. The next generation of scenarios for climate change research and assessment. *Nature*, 463(7282), pp.747–56.
Mott, R. et al., 2008. Simulation of seasonal snow-cover distribution for glacierized sites on Sonnblick, Austria, with the Alpine3D model. *Annals of Glaciology*, 49, pp.155–160.
Munro, D.S., 1989. Surface roughness and bulk heat transfer on a glacier: comparison with eddy correlation. *Journal of Glaciology*, 35(121), pp.343–348.
Nash, J.E. & Sutcliffe, J.V., 1970. River flow forecasting through conceptual models part I — A discussion of principles. *Journal of Hydrology*, 10(3), pp.282–290.
Nicholson, L. & Benn, D.I., 2006. Calculating ice melt beneath a debris layer using meteorological data. *Journal of Glaciology*, 52(178), pp.463–470.
Nicholson, L. & Benn, D.I., 2013. Properties of natural supraglacial debris in relation to modelling sub-debris ice ablation. *Earth Surface Processes and Landforms*, 38(5), pp.490–501.
Nolan, M. et al., 1995. Ice-thickness measurements of Taku Glacier, Alaska, USA, and their relevance to its recent behavior. *Journal of Glaciology*, 41(139), pp.541–553.
Nuimura, T. et al., 2012. Elevation changes of glaciers revealed by multitemporal digital elevation models calibrated by GPS survey in the Khumbu region, Nepal Himalaya, 1992–2008. *Journal of Glaciology*, 58(210), pp.648–656.
Oerlemans, I.M., 1997. A flowline model for Nigardsbreen, Norway; projection of future glacier length based on dynamic calibration with the historic record Papers from the International symposium on Changing glaciers. *International symposium on Changing glaciers*, 24, pp.382–389.
Oerlemans, J., 2001. *Glaciers and Climate Change*, CRC Press.
Oerlemans, J. et al., 1998. Modelling the response of glaciers to climate warming. *Climate Dynamics*, 14(4), pp.267–274.
Ohmura, A., 2001. Physical Basis for the Temperature-Based Melt-Index Method. *Journal of Applied Meteorology*, 40, pp.753–761.
Oki, T. and S.K., 2006. Global Hydrological Cycles and World Water Resources. *Science*, 313, pp.1068–1072.
Olsson, J., Yang, W. & Bosshard, T., 2013. Climate model precipitation in hydrological impact studies : limitations and possibilities. *VATTEN - Journal of Water Management and Research*, 69, pp.221–230.
Østrem, G., 1959. Ice Melting under a Thin Layer of Moraine, and the Existence of Ice Cores in

Moraine Ridges. *Geografiska Annaler*, 41(4), pp.228–230. Ageta, Y., Fujita, K., 1996. Characteristics of mass balance of summeraccumulation type glaciers in the Himalayas and Tibetan Plateau. *Gletscherkd, Glazialgeol*, 32, pp. 61-65.

Palazzi, E., et al.,., 2013. Precipitation in the hindu-kush karakoram himalaya: Observations and future scenarios. *Journal of Geophysical Research Atmospheres*, 118(1), pp. 85-100.

Palmer, T.N. et al., 2005. Probabilistic prediction of climate using multi-model ensembles: from basics to applications. *Philosophical transactions of the Royal Society of London. Series B, Biological sciences*, 360(1463), pp.1991–1998.

Parajuli, a. et al., 2015. Modified temperature index model for estimating the melt water discharge from debris-covered Lirung Glacier, Nepal. *Proceedings of the International Association of Hydrological Sciences*, 368(August 2014), pp.409–414.

Paul, F., Kotlarski, S. & Hoelzle, M., 2003. Forcing of a distributed glacier mass balance model with the regional climate model REMO : Down-scaling strategy and first results Energy Balance Mass Balance. , 719, p.105214.

Paul, F. et al., 2004. Rapid disintegration of Alpine glaciers observed with satellite data. *Geophysical Research Letters*, 31(21), pp.12–15.

Paul, F. et al., 2007. Calculation and visualisation of future glacier extent in the Swiss Alps by means of hypsographic modelling. *Global and Planetary Change*, 55(4), pp.343–357.

Paul, F. & Kotlarski, S., 2010. Forcing a distributed glacier mass balance model with the regional climate model REMO. Part II: Downscaling strategy and results for two swiss glaciers. *Journal of Climate*, 23(6), pp.1607–1620.

Peck, E.L. & Brown, M.J., 1962. An Approach to the Development of Isohyetal Maps for Mountainous Areas. *Journal of Geophysical Research*, 67(2), pp.681–694.

Pellicciotti, F. et al., 2005. An enhanced temperature-index glacier melt model including the shortwave radiation balance: development and testing for Haut Glacier d'Arolla, Switzerland. *Journal of Glaciology*, 51(175), pp.573–587.

Pellicciotti, F. et al., 2011. Transmission of solar radiation through clouds on melting glaciers: A comparison of parameterizations and their impact on melt modelling. *Journal of Glaciology*, 57(202), pp.367–381.

Pellicciotti, F. et al., 2012. Challenges and Uncertainties in Hydrological Modeling of Remote Hindu Kush–Karakoram–Himalayan (HKH) Basins: Suggestions for Calibration Strategies. *Mountain Research and Development*, 32(1), pp.39–50.

Pellicciotti, F. et al., 2014. Changes in glaciers in the Swiss Alps and impact on basin hydrology: Current state of the art and future research. *Science of the Total Environment*, 493, pp.1152–1170.

Pfeffer, W.T. et al., 2014. The Randolph Glacier Inventory: a globally complete inventory of glaciers. *Journal of Glaciology*, 60(221), pp.537–552.

Piani, C., Haerter, J.O. & Coppola, E., 2010. Statistical bias correction for daily precipitation in regional climate models over Europe. *Theoretical and Applied Climatology*, 99(1-2), pp.187–192.

Piao, S. et al., 2010. The impacts of climate change on water resources and agriculture in China. *Nature*, 467(7311), pp.43–51.

Picasso, M. et al., 2004. Numerical simulation of the motion of a two-dimensional glacier. *International Journal for Numerical Methods in Engineering*, 60(5), pp.995–1009.

Pidwirny, M., 2006. *Fundamentals of Physical Geography* 2nd ed.

Plewes, L.A. & Hubbard, B., 2001. A review of the use of radio-echo sounding in glaciology. *Progress in Physical Geography*, 25(2), pp.203–236.

Porter, S.C., 1975. Equilibrium-line altitudes of late Quaternary glaciers in the Southern Alps, New Zealand. *Quaternary Research*, 5(1), pp.27–47.

Pratap, B. et al., 2015. Influence of debris cover and altitude on glacier surface melting: a case study on Dokriani Glacier, central Himalaya, India. *Annals of Glaciology*, 56(70), pp.9–16.

Quick, M.C. & Pipes, a, 1977. U.B.C. WATERSHED MODEL M.C. QUICK and A. PIPES Department of Civil Engineering, University of British Columbia, Vancouver 8, B.C., Canada. *Hydrological*

Sciences Journal, pp.153–162.

Quincey, D.J., Luckman, A. & Benn, D., 2009. Quantification of Everest region glacier velocities between 1992 and 2002, using satellite radar interferometry and feature tracking. *Journal of Glaciology*, 55(192), pp.596–606.

Rabatel, A., et al. (2017) Annual and Seasonal Glacier-Wide Surface Mass Balance Quantified from Changes in Glacier Surface State: A Review on Existing Methods Using Optical Satellite Imagery. *Remote Sensing*, 9(5), 507.

Radić, V. & Hock, R., 2011. Regionally differentiated contribution of mountain glaciers and ice caps to future sea-level rise. *Nature Geoscience*, 4(2), pp.91–94.

Ragettli, S. & Pellicciotti, F., 2012. Calibration of a physically based, spatially distributed hydrological model in a glacierized basin: On the use of knowledge from glaciometeorological processes to constrain model parameters. *Water Resources Research*, 48(3), p.n/a–n/a.

Ragettli, S. et al., 2013. Sources of uncertainty in modeling the glaciohydrological response of a Karakoram watershed to climate change. *Water Resources Research*, 49(9), pp.6048–6066.

Ragettli, S. et al., 2015. Unraveling the hydrology of a Himalayan catchment through integration of high resolution in situ data and remote sensing with an advanced simulation model. *Advances in Water Resources*, 78, pp.94–111.

Ragettli, S. et al., 2016. Contrasting climate change impact on river flows from high-altitude catchments in the Himalayan and Andes Mountains Contrasting climate change impact on river flows from high-altitude catchments in the Himalayan and Andes Mountains. *Proceedings of the National Academy of Sciences*, (August).

Rajczak, J., Pall, P. & Schär, C., 2013. Projections of extreme precipitation events in regional climate simulations for Europe and the Alpine Region. *Journal of Geophysical Research Atmospheres*, 118(9), pp.3610–3626.

Raper, S.C.B. & Braithwaite, R.J., 2009. Glacier volume response time and its links to climate and topography based on a conceptual model of glacier hypsometry. *The Cryosphere*, 3, pp.183–194.

Rebetez, M., 2004. Summer 2003 maximum and minimum daily\ntemperatures over a 3300 m altitudinal range in the Alps\n. *Climate Research*, 27, pp.45–50.

Rees, H.G. & Collins, D.N., 2006. Regional differences in response of flow in glacier-fed Himalayan rivers to climatic warming. In *Hydrological Processes*. pp. 2157–2169.

Reid, T.D. & Brock, B.W., 2010. An energy-balance model for debris-covered glaciers including heat conduction through the debris layer. *Journal of Glaciology*, 56(199), pp.903–916.

Reid, T.D. & Brock, B.W., 2014. Assessing ice-cliff backwasting and its contribution to total ablation of debris-covered Miage glacier, Mont Blanc massif, Italy. *Journal of Glaciology*, 60(219), pp.3–13.

Riahi, K. et al., 2011. RCP 8.5-A scenario of comparatively high greenhouse gas emissions. *Climatic Change*, 109(1), pp.33–57.

Robertson, A.W., Ines, A.V.M. & Hansen, J.W., 2007. Downscaling of seasonal precipitation for crop simulation. *Journal of Applied Meteorology and Climatology*, 46(6), pp.677–693.

Roe, G.H. & Baker, M.B., 2014. Glacier response to climate perturbations: An accurate linear geometric model. *Journal of Glaciology*, 60(222), pp.670–684.

Rounce, D.R. & McKinney, D.C., 2014. Debris thickness of glaciers in the Everest area (Nepal Himalaya) derived from satellite imagery using a nonlinear energy balance model. *The Cryosphere*, 8(4), pp.1317–1329.

Rounce, D.R., Quincey, D.J. & McKinney, D.C., 2015. Debris-covered glacier energy balance model for Imja–Lhotse Shar Glacier in the Everest region of Nepal. *The Cryosphere*, 9(6), pp.2295–2310.

Rowan, A. V et al., 2015. Modelling the feedbacks between mass balance , ice flow and debris transport to predict the response to climate change of debris-covered glaciers in the Himalaya. *Earth and Planetary Science Letters*, 430, pp.427–438.

Sailer, R. et al., 2008. Snow avalanche mass-balance calculation and simulation-model

verification. In *Annals of Glaciology*. pp. 183–192.
Sakai, A., 2012. Glacial Lakes in the Himalayas : A Review on Formation and Expansion Processes. *Global Environmental Research*, 16(2011), pp.23–30.
Sakai, A., Nakawo, M. & Fujita, K., 1998. Melt rate of ice cliffs on the Lirung Glacier, Nepal Himalayas, 1996. *Bulletin of Glacier Research*, 16(October), pp.57–66.
Sakai, A. et al., 2000. Role of supraglacial ponds in the ablation process of a debris-covered glacier in the Nepal Himalayas. *IAHS Publication*, (265), pp.119–130.
Sakai, A., Nakawo, M. & Fujita, K., 2002. Distribution Characteristics and Energy Balance of Ice Cliffs on Debris-covered Glaciers, Nepal Himalaya. *Arctic, Antarctic, and Alpine Researc*, 34(1), pp.12–19.
Salathe, E.P., Mote, P.W. & Wiley, M.W., 2007. Review of scenario selection and downscaling methods for the assessment of climate change impacts on hydrology in the United States pacific northwest. *International Journal of Climatology*, 27(12), pp.1611–1621.
Salerno, F. et al., 2015. Weak precipitation, warm winters and springs impact glaciers of south slopes of Mt. Everest (central Himalaya) in the last 2 decades (1994–2013). *The Cryosphere*, 9(3), pp.1229–1247.
Salzmann, N., Machguth, H. & Linsbauer, A., 2012. The Swiss Alpine glaciers' response to the global "2 oC air temperature target." *Environmental Research Letters*, 7(4), p.44001.
San-Martin, D., et al., 2017. Reassessing Model Uncertainty for Regional Projections of Previpitation with an Ensemble of Statistical Downscaling Methods. *Journal of Climate.* 30, pp.203-223.
Schaefli, B. et al., 2005. A conceptual glacio-hydrological model for high mountainous catchments. *Hydrology and Earth System Sciences Discussions*, 2(1), pp.73–117.
Schaefli, B., Hingray, B. & Musy, a., 2007. Climate change and hydropower production in the Swiss Alps: quantification of potential impacts and related modelling uncertainties. *Hydrology and Earth System Sciences*, 11(3), pp.1191–1205.
Schäefli, B. & Huss, M., 2011. Integrating point glacier mass balance observations into hydrologic model identification. *Hydrology and Earth System Sciences*, 15(4), pp.1227–1241.
Schafer et al., 2015. Dynamic modelling of future glacier changes: mass-balance/elevation feedback in projections for the Vestfonna ice cap, Nordaustlandet, Svalbard. Journal of Glaciology. 61(230), 1121-1136.
Scherler, D., Bookhagen, B. & Strecker, M.R., 2011. Spatially variable response of Himalayan glaciers to climate change affected by debris cover. *Nature Geoscience*, 4(3), pp.156–159.
Schneeberger, C. et al., 2001. Modelling the response of glaciers to a doubling in atmospheric CO2: A case study of storglaciaren, northern Sweden. *Climate Dynamics*, 17(11), pp.825-834.
Schwarb, M. et al., 2001. Mean annual precipitation in the European Alps 1971-1990. *Hydrological Atlas of Switzerland, Landeshydrologie und Geologie*, 2.6.
Sevruk, B., 1982. Methods of correction for systematic error in point precipitation measurement for operational use. *World Meteorological Organisation*, 589, p.91.
Shabalova, M. V., van Deursen, W.P.A. & Buishand, T.A., 2003. Assessing future discharge of the river Rhine using regional climate model integrations and a hydrological model. *Climate Research*, 23(3), pp.233–246.
Sharma, D., Gupta, A. Das & Babel, M.S., 2007. Spatial disaggregation of bias-corrected GCM precipitation for improved hydrologic simulation: Ping River Basin, Thailand. *Hydrology and Earth System Sciences*, 11(4), pp.1373–1390.
Shea, J.M. et al., 2015. Modelling glacier change in the Everest region, Nepal Himalaya. *The Cryosphere*, 9(3), pp.1105–1128.
Shrestha, A.B. & Aryal, R., 2011. Climate change in Nepal and its impact on Himalayan glaciers. Reg. Environ. Change., 11.
Shrestha, A.B. et al., 2000. Precipitation fluctuations in the Nepal Himalaya and its vicinity and relationship with some large scale climatological parameters. *International Journal of Climatology*, 20(3), pp.317–327.

Siderius, C. et al., 2013. Snowmelt contributions to discharge of the Ganges. *Science of the Total Environment*, 468-469.

Singh, P. & Kumar, N., 1997. Impact assessment of climate change on the hydrological response of a snow and glacier melt runoff dominated Himalayan river. *Journal of Hydrology*, 193(1-4), pp.316–350.

Singh, P., Arora, M. & Goel, N.K., 2006. Effect of climate change on runoff of a glacierized Himalayan basin. *Hydrological Processes*, 20(9), pp.1979–1992.

Singh, P., Haritashya, U.K. & Kumar, N., 2008. Modelling and estimation of different components of streamflow for Gangotri Glacier basin , Himalayas / Modélisation et estimation des différentes composantes de l ' écoulement fluviatile du bassin du Glacier Gangotri , Himalaya Modelling and estimation o. *Hydrological Sciences Journal*, 53(2), pp.309–322.

Smith, P.C., Calanca, P. & Fuhrer, J., 2012. A simple scheme for modeling irrigation water requirements at the regional scale applied to an Alpine river catchment. *Water (Switzerland)*, 4(4), pp.869–886.

Somos-Valenzuela, M.A. et al., 2015. Assessing downstream flood impacts due to a potential GLOF from Imja Tsho in Nepal. *Hydrology and Earth System Sciences*, 19(3), pp.1401–1412.

Soncini, A. et al., 2016. Future hydrological regimes and glacier cover in the Everest region: The case study of the upper Dudh Koshi basin. *Science of The Total Environment*, 565, pp.1084–1101.

Sorg, A. et al., 2014. The days of plenty might soon be over in glacierized Central Asian catchments. *Environmental Research Letters*, 9(10), p.104018.

Sperber, K.R. et al., 2013. *The Asian summer monsoon: An intercomparison of CMIP5 vs. CMIP3 simulations of the late 20th century*,

Stahl, K. & Moore, R.D., 2006. Influence of watershed glacier coverage on summer streamflow in British Columbia, Canada. *Water Resources Research*, 42(6), pp.2–6.

Stahl, K. et al., 2008. Coupled modelling of glacier and streamflow response to future climate scenarios. *Water Resources Research*, 44(2).

Steiner, J.F. et al., 2015. Modelling ice-cliff backwasting on a debris-covered glacier in the Nepalese Himalaya. *Journal of Glaciology*, 61(229), pp.889–907.

Sternberg, R., 2008. Hydropower: Dimensions of social and environmental coexistence. *Renewable and Sustainable Energy Reviews*, 12(6), pp.1588–1621.

Sternberg, R., 2010. Hydropower's future, the environment, and global electricity systems. *Renewable and Sustainable Energy Reviews*, 14(2), pp.713–723.

Sugiyama, S. et al., 2007. Evolution of Rhonegletscher, Switzerland, over the past 125 years and in the future: Application of an improved flowline model. *Annals of Glaciology*, 46, pp.268–274.

Sutton, R.T., Dong, B. & Gregory, J.M., 2007. Land/sea warming ratio in response to climate change: IPCC AR4 model results and comparison with observations. *Geophysical Research Letters*, 34(2).

Tangborn, W. V, 1984. Prediction of Glacier Derived Runoff for Hydroelectric Development. *Geografiska Annaler. Series A, Physical Geography*, 66(3), pp.257–265.

Taylor, K.E., Stouffer, R.J. & Meehl, G. a, 2007. A Summary of the CMIP5 Experiment Design. *World*, 4(January 2011), pp.1–33.

Tebaldi, C. & Knutti, R., 2007. The use of the multi-model ensemble in probabilistic climate projections. *Philosophical Transactions of the Royal Society A: Mathematical, Physical and Engineering Sciences*, 365(1857), pp.2053–2075.

Teutschbein, C. & Seibert, J., 2012. Bias correction of regional climate model simulations for hydrological climate-change impact studies: Review and evaluation of different methods. *Journal of Hydrology*, 456-457, pp.12–29.

Thakuri, S. et al., 2014. Tracing glacier changes since the 1960s on the south slope of Mt. Everest (central Southern Himalaya) using optical satellite imagery. *The Cryosphere*, 8(4), pp.1297–1315.

Thakuri, S. et al., 2015. Factors controlling the accelerated expansion of Imja Lake, Mount

Everest region, Nepal. *Annals of Glaciology*, 57(71), pp.245–257.
Thayyen, R.J., Gergan, J.T. & Dobhal, D.P., 2007. Role of glaciers and snow cover on headwater river hydrology in monsoon regime - Micro-scale study of Din Gad catchment, Garhwal Himalaya, India. *Current Science*, 92(3), pp.376–382.
Themeßl, M.J., Gobiet, A. & Heinrich, G., 2012. Empirical-statistical downscaling and error correction of regional climate models and its impact on the climate change signal. *Climatic Change*, 112(2), pp.449–468.
Theurillat, J. & Guisan, A., 2001. Potential Impact of Climate Change on Vegetation in the European Alps : A Review. *Climate Change*, pp.77–109.
Thomson, A.M. et al., 2011. RCP4.5: A pathway for stabilization of radiative forcing by 2100. *Climatic Change*, 109(1), pp.77–94.
Tiwari, V.M., Wahr, J. & Swenson, S., 2009. Dwindling groundwater resources in northern India, from satellite gravity observations. *Geophysical Research Letters*, 36(18).
Todini, E., 2007. Hydrological catchment modelling: past, present and future. *Hydrol. Earth Syst. Sci.*, 11(1), pp.468–482.
Todini, E., 2011. History and perspectives of hydrological catchment modelling. *Journal of Hydrology*, 100(1-3), pp.341–352.
Trenberth, K.E. & Josey, S.A., 2007. Observations: surface and atmospheric climate change. *Changes*, 164(236 - 336), pp.235–336.
Turner, A.G. & Annamalai, H., 2012. Climate change and the South Asian summer monsoon. *Nature Climate Change*, 2(8), pp.587–595.
Uhlmann, B., Jordan, F. & Beniston, M., 2013a. Modelling runoff in a Swiss glacierized catchment-part I: Methodology and application in the Findelen basin under a long-lasting stable climate. *International Journal of Climatology*, 33(5), pp.1293–1300.
Uhlmann, B., Jordan, F. & Beniston, M., 2013b. Modelling runoff in a Swiss glacierized catchment-Part II: Daily discharge and glacier evolution in the Findelen basin in a progressively warmer climate. *International Journal of Climatology*, 33(5), pp.1301–1307. United Nations, 2013. World Population Prospects: The 2012 Revision. Highlights and Advance
Tables. *Population and development review*, 36, pp.775–801.
Verbunt, M. et al., 2003. The hydrological role of snow and glaciers in alpine river basins and their distributed modeling. *Journal of Hydrology*, 282(1-4), pp.36–55.
Vergara, W. et al., 2007. Economic Impacts of Rapid Glacier Retreat in the Andes. *Eos, Transactions American Geophysical Union*, 88(25), p.261.
Vincent, C. et al., 2016. Reduced melt on debris-covered glaciers: investigations from Changri Nup Glacier, Nepal. *The Cryosphere Discussions*, 2016(May), pp.1–28.
Vischer, 1979. Calving waves due to the breaking of a submerged glacer tongue. *[No source information available]*, 1(1), p.1.
Viviroli, D. et al., 2007. Mountains of the world, water towers for humanity: Typology, mapping, and global significance. *Water Resources Research*, 43(7).
Viviroli, D. et al., 2011. Climate change and mountain water resources: overview and recommendations for research, management and policy. *Hydrology and Earth System Sciences*, 15(2), pp.471–504.
Viviroli, D. & Messerli, B., 2003. Assessing the Hydrological Significance of the World's Mountains. *Mountain Research and Development*, 23(4), pp.369–375.
Vrac, M. et al., 2012. Dynamical and statistical downscaling of the French Mediterranean climate: Uncertainty assessment. *Natural Hazards and Earth System Science*, 12(9), pp.2769–2784.
Vuille, M. et al., 2008. Climate change and tropical Andean glaciers: Past, present and future. *Earth-Science Reviews*, 89(3-4), pp.79–96.
van Vuuren, D.P. et al., 2011a. RCP2.6: exploring the possibility to keep global mean temperature increase below 2 degrees C. *Climatic Change*, 109(1-2), pp.95–116.
van Vuuren, D.P. et al., 2011b. The representative concentration pathways: An overview. *Climatic Change*, 109(1), pp.5–31.

Wang, S., He, Y. & Song, X., 2010. Impacts of climate warming on Alpine glacier tourism and adaptive measures: A case study of Baishui Glacier No. 1 in Yulong Snow Mountain, Southwestern China. *Journal of Earth Science*, 21(2), pp.166–178.

Watanabe, T., Lamsal, D. & Ives, J.D., 2009. Evaluating the growth characteristics of a glacial lake and its degree of danger of outburst flooding: Imja Glacier, Khumbu Himal, Nepal. *Norsk Geografisk Tidsskrift - Norwegian Journal of Geography*, 63(4), pp.255–267.

Watson, C.S. et al., 2016. The dynamics of supraglacial ponds in the Everest region, central Himalaya. *Global and Planetary Change*, 142, pp.14–27.

WGMS, 2015. Global Glacier Change Bulletin. *World Glacier Monitoring Service*, 1(1), p.230.

Whiteman, C.D., 2000. *Mountain Meteorology: Fundamentals and Applications*,

Wild, M. & Schmucki, E., 2011. Assessment of global dimming and brightening in IPCC-AR4/CMIP3 models and ERA40. *Climate Dynamics*, 37(7-8), pp.1671–1688.

Willmott, C.J., Matsuura, K. & Robeson, S.M., 2009. Ambiguities inherent in sums-of-squares-based error statistics. *Atmospheric Environment*, 43(3), pp.749–752.

Wohlfarth, B. et al., 2008. Rapid ecosystem response to abrupt climate changes during the last glacial period in western Europe, 40-16 ka. *Geology*, 36(5), pp.407–410.

Wood, A.W. et al., 2004. Hydrologic implications of dynamical and statistical approaches to downscaling climate model outputs. *Climatic Change*, 62(1-3), pp.189–216.

Worni, R., Huggel, C. & Stoffel, M., 2013. Glacial lakes in the Indian Himalayas--from an area-wide glacial lake inventory to on-site and modeling based risk assessment of critical glacial lakes. *The Science of the total environment*, 468-469 Su, pp.S71–84.

Xu, J. et al., 2009. The melting Himalayas: cascading effects of climate change on water, biodiversity, and livelihoods. *Conservation biology : the journal of the Society for Conservation Biology*, 23(3), pp.520–30.

Yang, D.Q. et al., 1998. Adjustment of daily precipitation data at 10 climate stations in Alaska: Application of World Meteorological Organization intercomparison results. *Water Resources Research*, 34(2), pp.241–256.

Yoon, J.H., Ruby Leung, L. & Correia, J., 2012. Comparison of dynamically and statistically downscaled seasonal climate forecasts for the cold season over the United States. *Journal of Geophysical Research Atmospheres*, 117(21).

Yun, W.T., Stefanova, L. & Krishnamurti, T.N., 2003. Improvement of the multimodel superensemble technique for seasonal forecasts. *Journal of Climate*, 16(22), pp.3834–3840.

Zemp, M., Hoelzle, M. & Haeberli, W., 2009. Six decades of glacier mass-balance observations: A review of the worldwide monitoring network. *Annals of Glaciology*, 50(50), pp.101–111.

Zhang, Y. et al., 2011. Distribution of debris thickness and its effect on ice melt at Hailuogou glacier, southeastern Tibetan Plateau, using in situ surveys and ASTER imagery. *Journal of*
Glaciology, 57(206), pp.1147–1157.

Zhang, Y. et al., 2016. Using glacier area ratio to quantify effects of melt water on runoff. *Journal of Hydrology*, 538, pp.269-277.

Zierl, B. & Bugmann, H., 2005. Global change impacts on hydrological processes in Alpine catchments. *Water Resources Research*, 41(2), pp.1–13.

APPENDIX.

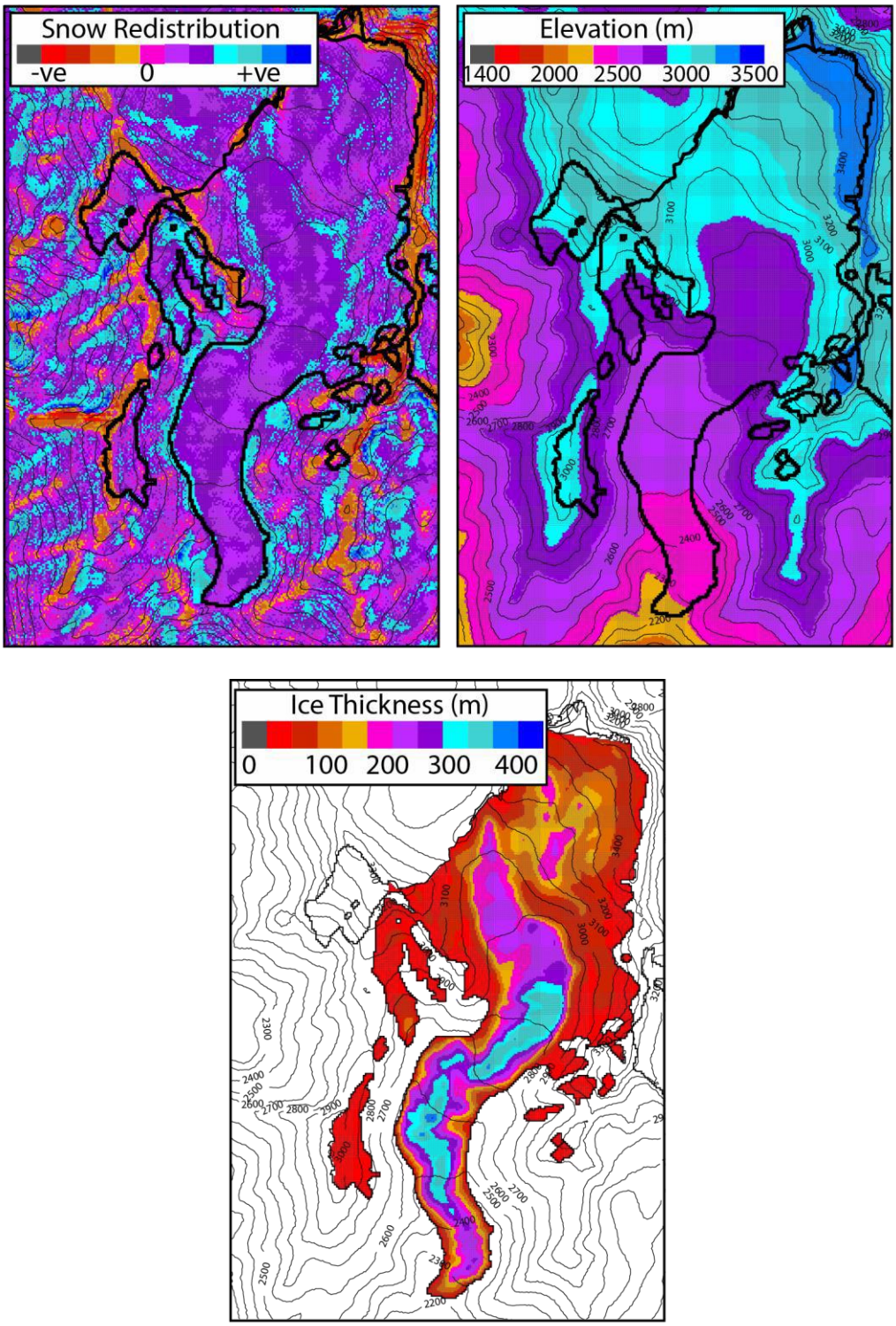

Figure A.1: Top panel (left) shows the outputs of the snow-redistribution module at Rhonegletscher with +ve areas receiving accumulation preferentially whereas –ve areas will lose accumulation. Top-right panel shows the elevation of the catchment will glacier mask superimposed. Lower panel shows the ice thickness estimation at Rhonegletscher.

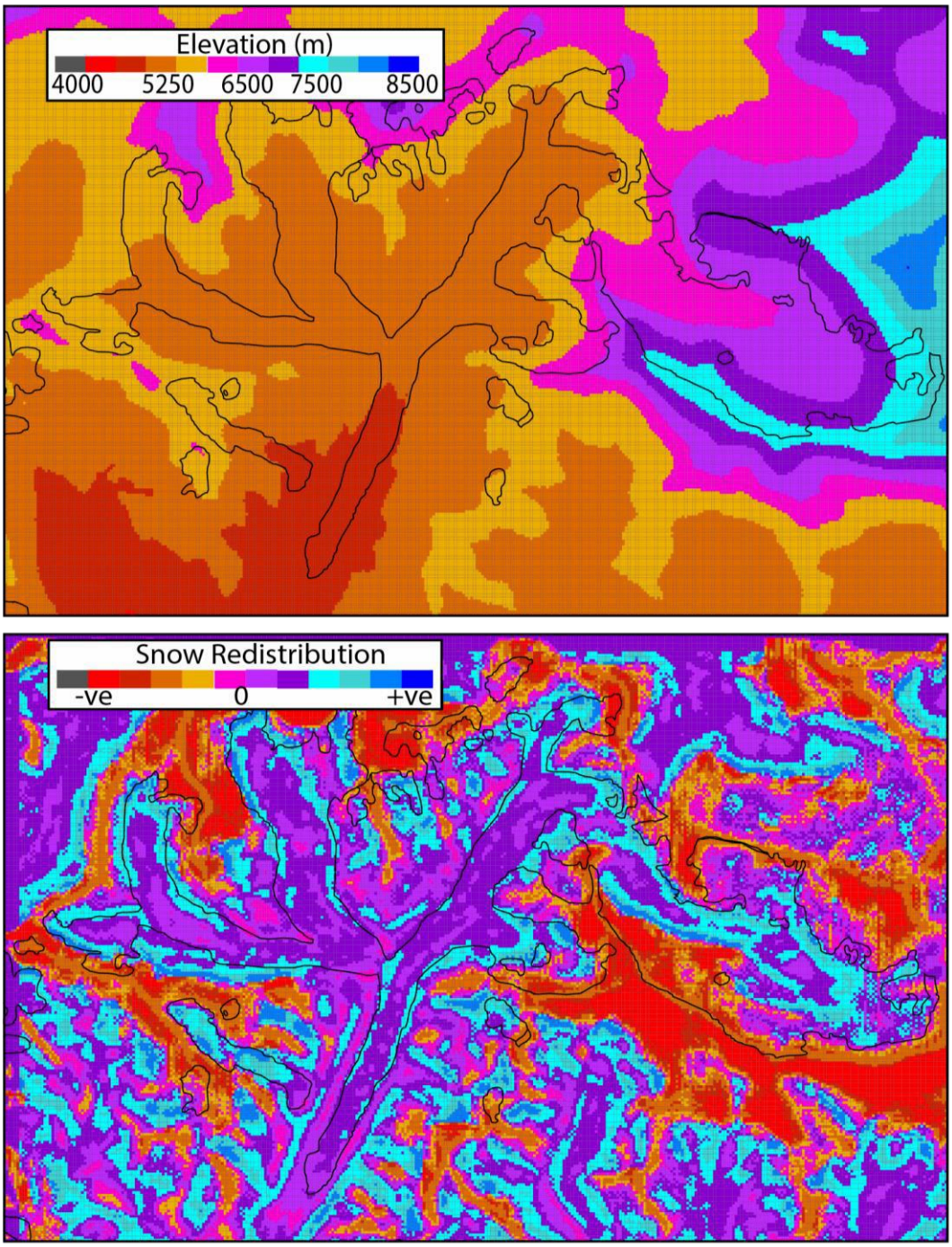

Figure A.2: Top panel shows digital elevation of the Khumbu catchment and lower panel shows the outputs of the snow-redistribution module. +ve areas will receive accumulation preferentially whereas –ve areas will lose accumulation.

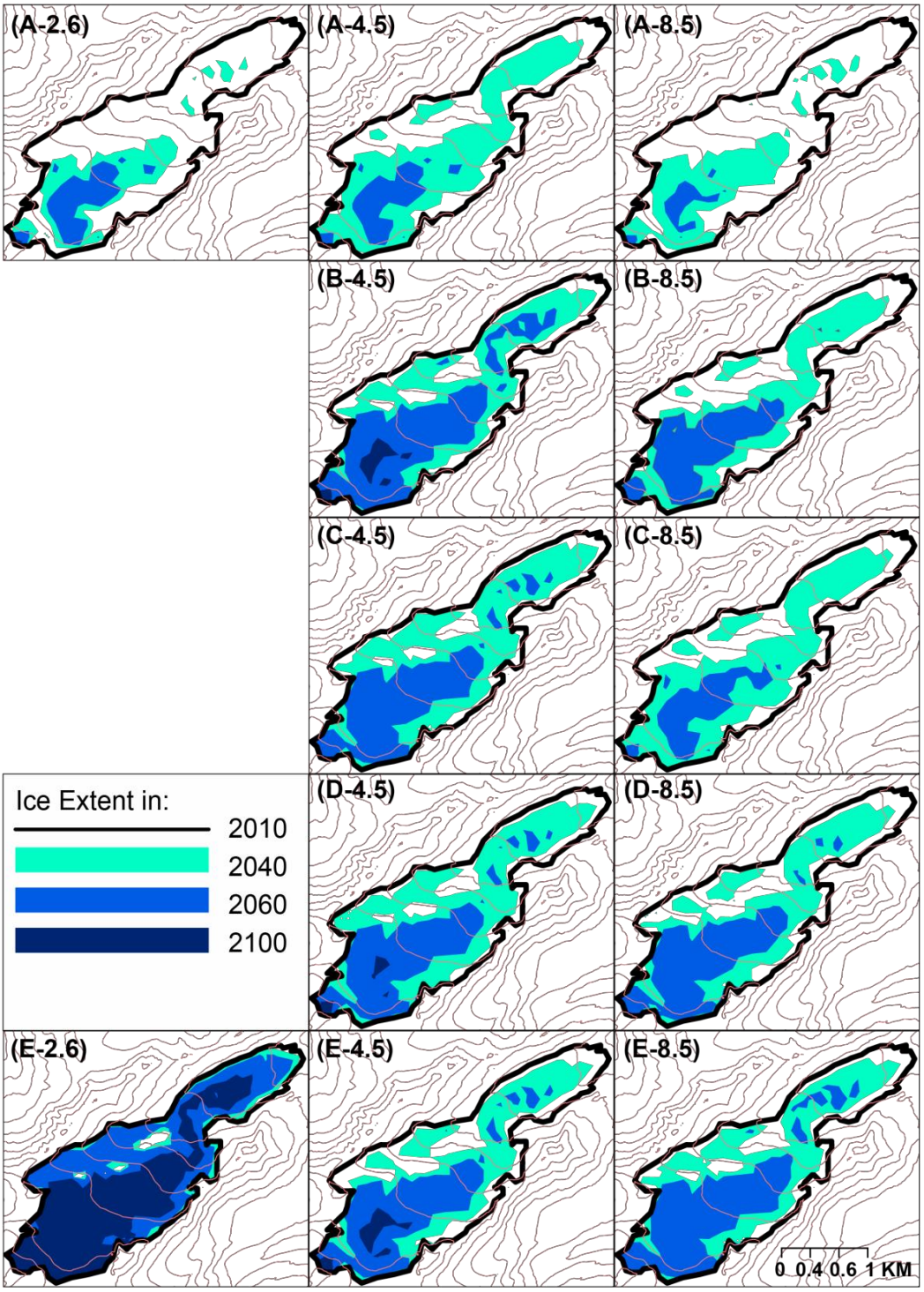

Figure A.3: Spatial plots of mass loss for all GERM simulations at Griesgletscher. Brackets refer to climate input, and contours are 100 m elevation bands.

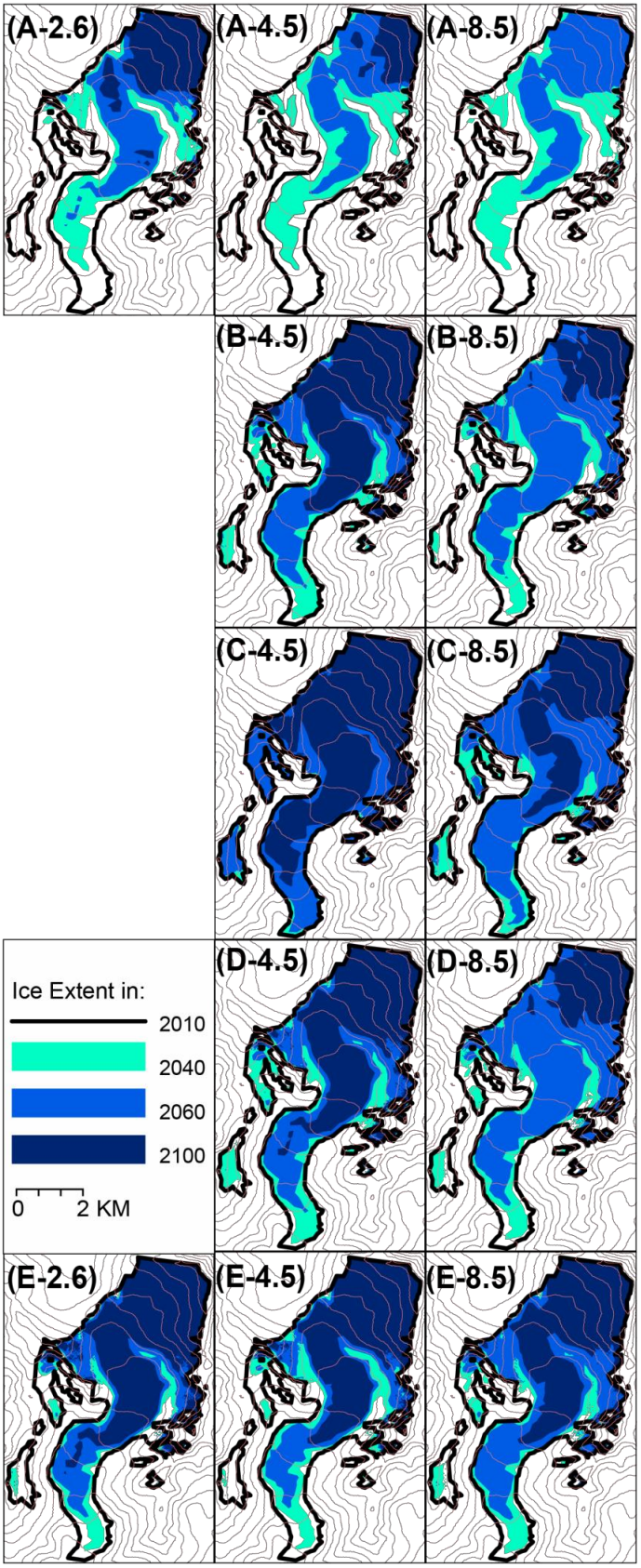

Figure A.4: Spatial plots of mass loss for all GERM simulations at Rhonegletscher. Brackets refer to climate input, and contours are 100 m elevation bands.